REPORT NO. USCG-D-122-76

ADA035599

A CRITICAL TECHNICAL REVIEW OF SIX HAZARD ASSESSMENT MODELS

N. A. Eisenberg
C. J. Lynch
R. M. Kumar
R. J. Breeding
M. N. Durrani

DOT-CG-33[illegible]-A

912-420-Shoot AS
MARKED

DDC
RECEIVED
FEB 15 1977
C

Document is available to the U.S. Public through the
National Technical Information Service,
Springfield, Virginia 22161

DECEMBER 1975

FINAL REPORT

PREPARED FOR

U.S. DEPARTMENT OF TRANSPORTATION
UNITED STATES COAST GUARD
OFFICE OF RESEARCH AND DEVELOPMENT
WASHINGTON, D.C. 20590

Technical Report Documentation Page

1. Report No	2. Government Accession No.	3. Recipient's Catalog No.
CG-D-122-76		

4. Title and Subtitle	5. Report Date
A Critical Technical Review of Six Hazard Assessment Models	December 1975
	6. Performing Organization Code
7. Author(s) N. A. Eisenberg, C. J. Lynch, R. M. Kumar, R. J. Breedina and M. N. Durrani	8. Performing Organization Report No.
9. Performing Organization Name and Address Enviro Control, Inc. One Central Plaza 1130 Rockville Pike Rockville, MD 20852	10. Work Unit No (TRAIS) 3142 11. Contract or Grant No. DOT-CG-33,377-A
12. Sponsoring Agency Name and Address Commandant (G-DSA/TP44) U. S. Coast Guard Headquarters Washington, D. C. 20590	13. Type of Report and Period Covered Final Report 14. Sponsoring Agency Code G-DSA/TP44

15. Supplementary Notes
The U. S. Coast Guard Office of Research and Development's technical representative for the work reported on herein was Dr. Michael C. Parnarouskis.

16. Abstract

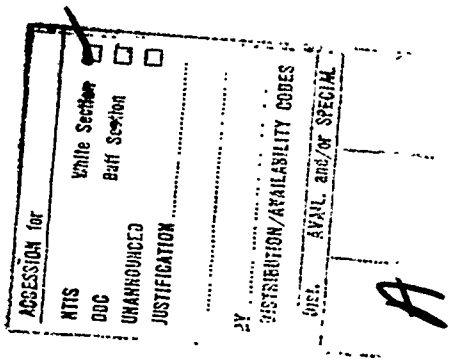
This report presents a critical technical review of six simulation models currently being used by the U. S. Coast Guard. The models were developed to describe, in a predictive manner, the behavior of maritime spills of hazardous chemicals and the damages that may result from such spills.

17. Key Words	18. Distribution Statement
Review, Hazard Assessment, Models	Document is available to the U. S. public through the National Technical Information Service, Springfield, Virginia 22161.

19. Security Classif. (of this report)	20. Security Classif. (of this page)	21. No. of Pages	22. Price
Unclassified	Unclassified	395	

Form DOT F 1700.7 (8-72) Reproduction of completed page authorized

108375



DOT USCG A CRITICAL TECHNICAL REVIEW OF SIX HAZARD ASSESSMENT MODELS DECEMBER 1975

Spine

NOTICE

This document is disseminated under the sponsorship of the U. S. Department of Transportation in the interest of information exchange. The United States Government assumes no liability for the contents or use thereof.

The United States Government does not endorse products or manufacturers. Trade or manufacturers' names appear herein solely because they are considered essential to the object of this report.

C.2

ACKNOWLEDGEMENTS

The authors express their appreciation to Dr. Michael C. Parnarouskis, the U. S. Coast Guard Project Officer, who encouraged the pursuit of promising technical avenues of approach directed towards fulfilling the USCG objectives. The authors also recognize the contributions made to this effort by Lieutenant Commander Michael W. Taylor, Dr. John S. Gardenier, and Dr. John M. Cece, all of the USCG.

In addition, significant technical contributions were made by the Enviro Control, Inc. staff members, especially Mr. Richard M. Rowley.

1068078

A CRITICAL TECHNICAL REVIEW
OF SIX HAZARD ASSESSMENT MODELS

TABLE OF CONTENTS

		page
CHAPTER 1	INTRODUCTION, SUMMARY, AND RECOMMENDATIONS	1-1
	Introduction	1
	Scope	5
	Sensitivity Analysis	7
	Results	11
	Recommendations	14
	References	17
CHAPTER 2	VENTING RATE MODEL	2-1
	Introduction	1
	Assumptions and Approximations	5
	Errors and Inconsistencies	10
	Accuracy Assessment	22
	Sensitivity Analysis	30
	Conclusions	55
	Summary and Recommendations	56
	Appendix 2A. Input Variables	59
	Appendix 2B. Energy Equations - Liquid Discharge	63
	Appendix 2C. Energy Equations - Gas Venting	69
	Appendix 2D. Properties	73
	Appendix 2E. Sensitivity Analysis	79
	List of Symbols	91
	References	93
CHAPTER 3	MIXING AND DILUTION MODEL	3-1
	Introduction	1
	Assumptions and Approximations	3
	Errors and Inconsistencies	8
	Accuracy Assessment	26
	Sensitivity Analysis	32
	Summary and Recommendations	50
	Appendix 3A. Diffusion Equation	53
	Appendix 3B. Image Sources	61
	Appendix 3C. Pollutant Concentration	69
	Appendix 3D. Computer Programs	73
	Appendix 3E. Sensitivity Coefficients	87
	List of Symbols	99
	References	101

PRECEDING PAGE BLANK-NOT FILMED

CHAPTER 4	FLAME GEOMETRY MODEL	4-1
	Introduction	1
	Assumptions and Approximations	1
	Errors and Inconsistencies	6
	Accuracy Assessment	6
	Sensitivity Analysis	29
	Summary and Recommendations	37
	Appendix 4A. Typographical Errors	39
	Appendix 4B. Coding Errors	41
	Appendix 4C. Derivation of Equivalent Cylinder	43
	Appendix 4D. Comparison of the Flame Height Model to Field Data	47
	List of Symbols	51
	References	55
CHAPTER 5	THERMAL RADIATION FROM FLAMES MODEL	5-1
	Introduction	1
	Assumptions and Approximations	1
	Errors and Inconsistencies	8
	Accuracy Assessment	12
	Sensitivity Analysis	21
	Summary and Recommendations	23
	Appendix 5A. Typographical Errors	25
	Appendix 5B. Tables	27
	Appendix 5C. Relative Damage Criteria	35
	List of Symbols	37
	References	39
CHAPTER 6	MIXING AND EVAPORATION MODEL	6-1
	Introduction	1
	Assumptions and Approximations	2
	Errors and Inconsistencies	5
	Accuracy Assessment	5
	Sensitivity Analysis	24
	Summary and Recommendations	24
	Appendix 6A. Typographical Errors	27
	Appencix 6B. Computer Programs	29
	List of Symbols	37
	References	39
CHAPTER 7	RADIATION VIEW FACTOR MODEL	7-1
	Introduction	1
	Assumptions and Approximations	2
	Errors and Inconsistencies	3
	Accuracy Assessment	4
	Sensitivity Analysis	9
	Summary and Recommendations	10
	Appendix 7A. Tables	11
	Appendix 7B. Effect of Top End of Flame	13
	Appendix 7C. Subroutine SVIEW	21
	Appendix 7C. Typographical Errors	37
	List of Symbols	41
	References	43

CHAPTER 1

INTRODUCTION, SUMMARY, AND RECOMMENDATIONS

INTRODUCTION

This report presents a critical technical review of six simulation models currently being used in connection with the following U.S. Coast Guard research programs: the Vulnerability Model, a simulation system for assessing damage resulting from spills of hazardous materials [1]; the Chemical Hazards Response Information System, CHRIS, as described in the Assessment Models in Support of the Hazard Assessment Handbook (AMSHAH) [2]; and the Hazard Assessment Computer System, HACS [3]. These research programs are concerned with describing, in a predictive manner, the behavior of maritime spills of hazardous materials and the damages that may result from such spills.

AMSHAH describes twelve models that are among those used in the above research programs; however, only six of these are addressed in this report. It is anticipated that the remaining models will be subjected to a critical review at a later date. The models addressed in this report are listed in Table 1-1.

The primary objective of this review is to evaluate the validity of the models. This evaluation was carried out as follows:

1. Assumptions stated explicitly or made implicitly in the derivation of each model were documentated.

2. The errors introduced by the departure from underlying assumptions in actual situations were defined.

---

[1] Eisenberg, N. A., C. J. Lynch, and R. J. Breeding, Vulnerability Model: A Simulation System for Assessing Damage Resulting from Marine Spills, CG-D-136-75, NTIS AD-A015245, Department of Transportation, U.S. Coast Guard, June 1975.

[2] Department of Transportation, U.S. Coast Guard, Assessment Models in Support of the Hazard Assessment Handbook (CG-446-3), CG-D-65-74, January 1974.

[3] Arthur D. Little, Inc., Hazard Assessment Computer System, User Manual (HACS), Cambridge, Mass., December 1974.

TABLE 1-1 Organization of This Report and Corresponding Entities in AMSHAH (Assessment Models in Support of the Hazard Assessment Handbook [2]) and HACS (Hazard Assessment Computer System [3])

Topic	This Report	AMSHAH	HACS	
			Executive Subroutine*	Computational Subroutine
Overview	Chapter 1	-	-	-
Venting Rate Model	Chapter 2	Chapter 2	MODA	RLJVI RLJTC RLJLQ VENTR
Mixing and Dilution Model	Chapter 3	Chapter 4	MODP	DILUN DLIN DISP CNSPL
Flame Geometry	Chapter 4	Chapter 6	MODB1 MODE1 MODE2	FLJET FLMHT FLMAN
Thermal Radiation from Flames	Chapter 5	Chapter 7	MODB2	JHHRF
Mixing, Dilution, and Evaporation	Chapter 6	Chapter 11	MODR	EVAMX DISP QSF VAPPR HMTC
View Factor	Chapter 7	Chapter 13	MODB2	SVIEW

*These subroutines acquire the necessary data and call the required computational subroutines.

3. The sensitivity of the results of each model to estimates of input variables and input parameters were determined.

4. The errors introduced by sequential simulation of processes that actually occur simultaneously were defined.

5. Errors in analysis, documentation, and computer coding were defined and rectified.

6. Inconsistencies between written documentation and computer programming were defined and resolved.

Table 1-1 shows the correspondence between chapters in this report, those in AMSHAH, and the subroutines in HACS. Each chapter in this report treats one of the models described in AMSHAH; however, one model may correspond to several computer programs or subroutines. Because of the self-contained nature of the material covered, each chapter contains its own appendices, list of symbols, and list of references.

For some of the models reviewed, substantial problems were discovered in their derivations, formulae, or assumptions. Two of the models, those describing flame geometry and thermal radiation from flames, were found to be quite satisfactory with respect to both the assumptions upon which they are based and the analyses and derivations performed. At least two of the models, the Venting Rate Model and the Mixing and Dilution Model, contain what are apparently substantial errors in analyses. In order to perform the required sensitivity analysis, these models were changed to what is believed to be the correct form and the corrected models were then tested for sensitivity to input variables and parameters. The Mixing, Dilution, and Evaporation Model is perhaps the most disappointing of the six models analyzed. The assumptions upon which it is based require that the model be developed along lines which, in addition to producing nonphysical results, give a picture of the physical processes which is a significant departure from reality. The remaining model analyzed, the View Factor Model, appears to be correct. However, the HACS computerized counterpart of the View Factor Model departs significantly from the model described in AMSHAH. The model programmed in HACS has certain restrictions and limitations which are not included in the AMSHAH model. These restrictions and limitations indicate that conservative damage estimates may not always be obtained with the use of this model. Because of the problems that were encountered, sensitivity analyses were performed for only four of the models, namely: the Venting Rate Model (as corrected), the Mixing and Dilution Model (as corrected), the Flame Geometry Model, and the Thermal Radiation from Flames Model. Table 1-2 is a summary of the conclusions and characterizations of the various models as determined by this study.

TABLE 1-2

Summary of Results of This Review; Characterization and Descriptions of the Six Models

	Chapter	Apparent Significant Errors in Analysis	Sensitivity Analysis Performed	Computer Program Corrected Before Sensitivity Analysis	Major Problems with Underlying Assumptions	Realistic Results*
Venting Rate	2	yes	yes	yes	some	2
Mixing and Dilution	3	yes	yes	yes	yes	3
Flame Geometry	4	no	yes	no	no	1
Thermal Radiation from Flames	5	no	yes	no	no	1
Mixing, Dilution and Evaporation	6	unknown	no	--	yes (significant)	4
View Factor	7	no	no	--	no	2**

*Key to code:

1 - very good
2 - better than average
3 - less than average
4 - very poor

**but not necessarily resulting in conservative damage estimates as stated.

SCOPE

The ultimate purpose of this effort is to provide the information required to plan further research efforts in the area of hazardous material spills. Of primary interest is the determination of areas in which research would yield the greatest benefits in terms of improving model accuracy. Although the models analyzed describe physical occurrences resulting from spills of hazardous materials, the immediate objective is not to improve the description of spill development, but rather to determine which areas of research will yield the greatest improvements in the capability of the models to estimate damages to people, property, and the environment. Improvements to damage assessment techniques may be achieved by further research in two distinct but related areas, namely: parameter estimation and model development. For example, if it is determined that changing a particular parameter by 10% does not substantially affect the hazard assessment, the research effort to establish a precise value of that parameter is unnecessary. Similarly, if it is determined that one model gives estimates good to say 10% of experimental or field values, while another model yields estimates which are good only to an order of magnitude, the direction for further research is clear. As stated above, the models that are analyzed are those documented in AMSHAH and used in several USCG efforts including the Vulnerability Model, HACS, and CHRIS.

In order to obtain a quantitative evaluation of the damage assessment model, the initial scope of work included the following four tasks:

Task 1. Document the assumptions and approximations inherent in each model. For each model, document the assumptions and approximations inherent in it. Identify the parametric estimations made in each model and identify frequently estimated chemical property values that are used by each model.

Task 2. Assess the errors introduced when the assumptions of the model are violated. Quantitatively assess the ability of each model to represent accurately the physical phenomena being modeled under a range of conditions expected to be encountered in actual spill situations.

Task 3. Determine the sensitivity of computed results to estimated model parameters and chemical property estimates. Determine the sensitivity of each model's output to changes in the estimated parametric values identified in Task 1. This includes placing maximum errors bounds on model parameters and chemical property data. The possible variance of the computed results should then be determined for a range of parametric inputs within the error bounds.

Task 4. Assess the errors introduced by sequentially simulating physical processes which occur simultaneously. For those models whose inputs are computed by preceding models, determine the limitations on the accuracy of

their results based on the possible errors on the inputs. Determine the possible degree of error of those sequentially executed groups of hazard assessment models representing simultaneously occurring physical phenomena.

As work began on this initial scope, it became apparent that certain problems would prevent the timely and successful completion of the tasks as originally stated. Among the unforeseen problems that arose were the following:

1. The HACS computer programs contained more coding errors than were expected or acceptable for the sensitivity and error analyses.

2. Frequently, critical equations, and in more than one case the entire model structure, have one form in AMSHAH and a different form in HACS.

3. Frequently, the models as programmed in HACS indicate that certain assumptions were made but not stated explicitly in AMSHAH.

4. In several cases the equations presented in AMSHAH do not follow from the stated assumptions; it appears that occasionally either the assumptions or the resulting equations were improperly stated.

5. In some instances it appears that the assumptions made in AMSHAH are grossly unrealistic.

Because of the existence of these unexpected problems, the original scope of work was revised; the objectives of the revised program were the same as those in the original program. However, it was obvious that additional effort would be required because of the problems that had arisen. The scope of work was enlarged to include the following tasks.

Task 5. Document coding errors and make necessary corrections. For the computerized version of each submodel, document any coding errors and the suggested correction; upon approval of the USCG, the corrections will be made and the corrected programs used for Tasks 3 and 4.

Task 6. Document inconsistencies between AMSHAH and HACS. Document any discrepancies between AMSHAH and HACS, indicate which version is judged to be preferable, and upon approval of the USCG, change either AMSHAH or HACS or both to reconcile the two.

Task 7. Document implicit assumptions. Document any assumptions implicit in HACS that are not stated explicitly in AMSHAH.

Task 8. Document and correct errors in analysis. Document any suspected errors in AMSHAH manifested as formulas not following from the stated assumptions. Upon approval of the Project Officer, change AMSHAH, HACS, or both to correspond to the physically and mathematically correct form.

Task 9. Perform a sensitivity analysis only on those models for which such an analysis is deemed worthwhile. In the event that the assumptions stated in AMSHAH appear to be unrealistic, the USCG will determine whether it is worthwhile to perform Tasks 3 and 4 on the model as is or whether it is feasible to modify the model to a more correct form with the time and resources available.

Because of the additional effort required to perform all nine tasks rather than the initial four, it was determined that only six (out of twelve models originally considered) would be analyzed. The models chosen to be analyzed in depth are (also see Table 1-1):

- Venting Rate Model
- Mixing and Dilution Model
- Flame Geometry Model
- Thermal Radiation from Flames Model
- Mixing, Dilution, and Evaporation Model
- View Factor Model

The nine tasks listed above were performed on each of these six models and the results of the analyses are reported in the chapters that follow.

SENSITIVITY ANALYSIS

For all the models for which it was deemed suitable, a sensitivity analysis was performed. Specifically, sensitivity analyses have been performed for the models described in chapters 2, 3, 4, and 5 of this report. Table 1-1 indicates the entities in AMSHAH and HACS corresponding to these chapters. Since the sensitivity analysis has been performed for so many different models, it seems appropriate to discuss in this introductory chapter the general approach to the sensitivity analysis, the methods used, and the results expected.

The concept of sensitivity analysis has been extensively discussed in the literature related to control systems and other physical systems [4,5].

---

[4] Radanovic, L. (ed), Sensitivity Methods in Control Theory, Pergamon Press, New York, 1966.

[5] Tomovic, R., Sensitivity Analysis of Dynamic Systems, McGraw-Hill, New York, 1963.

Although the theoretical concepts considered are relatively sophisticated, simplification can be made in order to apply these methods to a sensitivity analysis of models describing the behavior of hazardous material spills.

Typically, the literature considers a system with n output variables, Y_i, $i = 1, 2, \ldots, n$, and with m input variables, X_j, $j = 1, 2, \ldots, m$. Then we may write

$$Y_i = f_i (X_j) \qquad j = 1, 2, \ldots, m \qquad i = 1, 2, \ldots, n$$

to represent the functional dependence of the n output variables on the m input variables. For present purposes, the "system" is a model of spill behavior. For example, in the case of the model describing cargo venting, the output variables (Y_1, Y_2, and Y_3) are total mass venting, time for venting, and average venting rate. The input variables (X_1, X_2, X_3, ...) include such items as total mass in the tank, location of venting hole, diameter of venting hole, etc.

Consider now the differential change in one of the output variables, dY_i. By the chain rule we have

$$dY_i = \frac{\partial f_i}{\partial X_1} \, dX_1 + \frac{\partial f_i}{\partial X_2} \, dX_2 + \ldots + \frac{\partial f_i}{\partial X_m} \, dX_m$$

The factors, $\partial f_i / \partial X_j$ are usually termed the sensitivity coefficients and give, for small changes in the input variables, a measure of the effect on the output variable. The entire set of sensitivity coefficients forms an $n \times m$ matrix.

For a detailed sensitivity analysis, each of the sensitivity coefficients must be considered and its variation over the range of the several variables must be determined. One way to summarize the output variation is to consider functions such as

$$g_j = \sum_{i=1}^{n} \left(\frac{\partial f_i}{\partial X_j} \right)^2$$

which gives the "change in arc length" generated in the n dimensional space of output variables by incremental changes in the j^{th} input variable.

For the purposes of this study it was considered too costly and time consuming to investigate sensitivity in a global sense in the m dimensional space of input variables. Instead sensitivity was investigated locally. That is, the matrix of sensitivity coefficients

$$S_{ij} = \frac{\partial f_i}{\partial X_j} \qquad i = 1, 2, \ldots, n \qquad j = 1, 2, \ldots, m$$

was determined at a single point in input variable space, namely:

$$X_0 = \left(X_{0_1}, X_{0_2}, \ldots, X_{0_m}\right)$$

Examining sensitivity at a single selected point cannot yield as clear a picture as does a global sensitivity analysis; however, the points in input variable space at which sensitivity analyses are performed were selected to be representative of the typical usage of the model. For example, in the case of the Venting Rate Model, the sensitivity of model output to various inputs would be quite different for a tank that is nearly empty than for a tank that is nearly full; but the case of the nearly full tank is of considerable interest, while that of the nearly empty tank is not. Thus, although the sensitivity analyses performed do not give all the information that could possibly be derived from the models, they do provide information in areas of primary interest.

Since the models are all implemented as computer programs, it was decided to compute the sensitivity coefficients numerically. In order to exclude effects of scale, the sensitivity coefficients were determined for normalized input and output variables. What is really of interest here, as is stated in the task descriptions, is the percent error induced in model outputs by a given percent error in model inputs. In order to obtain the desired result it is tempting to use logarithmic derivatives, i.e., to define

$$S_{ij} = \frac{\frac{\partial}{\partial X_j}(\ell n\ f_i)}{\frac{\partial}{\partial X_j}(\ell n\ X_j)} = \frac{X_{0j}}{f_i(X_0)} \frac{\partial f_i}{\partial X_j}$$

This approach, however, breaks down if either X_{0j} or $f_i(X_0)$ are zero. To avoid these difficulties the X_j's were normalized by values other than the X_{0j}'s. For example, in the case of tank venting a hole height of zero is a reasonably typical value and may be used to define the point, X_0; however, variations in hole height are probably best described in terms of a percent of total tank height.

Thus, the sensitivity coefficients were computed by the following procedure. A set of values, typical for the uses of a given model, were chosen for the input variables. This set of values was termed the "normal"

values and corresponds to the set $(X_{O_1}, X_{O_2}, \ldots, X_{O_m})$, in terms of the notation used previously. The set of values, X_{O_j}, was chosen so that the values of the output variables, $f_i\ (X_O)$, were nonzero. The set of values of the output variables, $f_i\ (X_O)$, corresponding to the set of normal input variables, was termed the "normal" value of the output variable. A second set of values for the input variables was defined at the "reference" value. These values $(X_{r_1}, X_{r_2}), \ldots, X_{r_m})$, were used to normalize the input variables. In general $X_{r_j} = X_{O_j}$, unless $X_{O_j} = 0$ or unless other reasons indicated that a value other than X_{O_j} was a better choice for X_{r_j}.

The sensitivity coefficient is defined for our purposes as the ratio of the percent change in output for a percent change in value of a given input variable. Define the changed set of input variables as

$$X_C^j = (X_{O_1}, X_{O_2}, \ldots, X_{O_j} + K\ X_{r_j}, \ldots X_{O_m}) \quad j = 1, 2, \ldots, m$$

where all the values of the input variables are unchanged except for X_{O_j} which is increased by a fraction, K, of the reference value, X_{r_j}. Then the sensitivity coefficient is given by

$$S_{ij} = \left[\frac{f\ (X_C^j) - f\ (X_O)}{f\ (X_O)}\right] \Big/ \left[\frac{X_{C_j} - X_{O_j}}{X_{r_j}}\right]$$

where the changed value of the j^{th} variable, X_{C_j}, is given by

$$X_{C_j} = X_{O_j} + K\ X_{r_j}$$

For this analysis the value K was fixed throughout as 0.05 (a five percent change in input variable). Consequently the quantity

$$\left[\frac{X_{C_j} - X_{O_j}}{X_{r_j}}\right] = K$$

was always 0.05. Hence the formula for the sensitivity coefficient may be rewritten in simpler form as,

$$S_{ij} = 20\ \left[F^j - 1\right]$$

where

$$F^j = f_i (X_c^j) / f_i (X_o)$$

is the ratio of changed value of the i^{th} output variable to the normal value of the i^{th} output variable.

On the computer printouts of the sensitivity analyses for each output variable the normal value of the output, normal values of the input variables, reference values of the input variables, changed values of the input variables, the fraction, F^j, and the sensitivity coefficient are all reported. The input variables have been divided into two classes, "variables" and "parameters." Those inputs to the model which are properties of the cargo are put in the class parameters. Those inputs to the model descriptive of the physical process and provided either as a user input or as a computed output of another model are put in the class variables. Model sensitivity to both classes of inputs was determined.

The values of the sensitivity coefficients may be readily interpreted. Sensitivity coefficients approximately equal to unity indicate a moderate sensitivity of output for the input variable under consideration. A one percent change (or error) in the input variable will produce about the same change (or error) in output. For sensitivity coefficients of the order of 0.1 or less, the indication is that model output is relatively insensitive to the given input. Sensitivity coefficients of the order of 10 or greater indicate that model output is greatly sensitive to the given input. Positive sensitivity coefficients mean that the output variable increases with increases in the input variable. A negative value for a sensitivity coefficient indicates that the output changes inversely to changes in the input.

RESULTS

The results of the review of the six models may be summarized very briefly as follows: two of the models appear to be acceptable, three of the models could be improved by additional development, and one of the models appears to be greatly in need of improvement. The results of this study are summarized in Table 1-2. Minor typographical errors were discovered in the writeup of virtually every model. For many models the description in AMSHAH did not correspond to the procedure in HACS. Further generalizations about the results of this study cannot be made; specific comments about each model reviewed are given below.

The Venting Rate Model discussed in Chapter 2 of this report and Chapter 2 of AMSHAH was discovered to have a significant error in analysis. The energy equation used for the calculation of adiabatic venting was discovered to have misstated and missing terms. This error was corrected and

the sensitivity analysis was based upon the corrected computer program. The sensitivity analysis revealed an undesirably high sensitivity to some of the coefficients of the vapor pressure equation. This high sensitivity coefficient does not appear to indicate a problem with the analysis but rather appears to reflect the significant influence of these coefficients. Two of the underlying assumptions used in the development of this model produce enough of a departure from reality that revision of the model to remove these assumptions may be justified. One of the objectionable assumptions is that cargo in liquid phase is in thermal equilibrium with the cargo in gas phase. It is certainly within the realm of feasibility to produce a model not requiring that this assumption be made. Furthermore, it is not expected that the more general analysis will require a significant increase in operating cost. The other undesirable assumption concerns the manner in which the cargo tanks are vented. Virtually all cargo tanks used in marine transport are vented in one way or another. Many simply have open pipes running up to the deck of the ship; the model does not treat the case of open venting at all. Again, the treatment of the venting of cargo tanks whether the venting is open, vacuum relief, or vacuum-pressure relief is well within the realm of feasibility and should not produce a significant increase in operating costs. As it stands now, the model appears to give results which are better than average (Table 1-2).

The Mixing and Dilution Model discussed in Chapter 3 of this report and Chapter 4 of AMSHAH was discovered to have several significant errors in analysis. One analytical error concerned the location of an image source used to describe the near-field approximation concentration for an instantaneous spill. For the far-field approximation to concentration for a continuous spill, an important term in the solution was defined improperly in the analysis and carried over into the computer program. Several other errors and inconsistencies in both AMSHAH and the computer programming were discovered for this model. The computer program was corrected where appropriate and the sensitivity analysis was performed on the corrected program. Two of the assumptions underlying this model were considered to be major obstacles to obtaining a realistic description of the phenomena modeled. One of these assumptions is that this spill may be treated as a point source release. This assumption requires that for times very soon after release the entire mass of the spill must be concentrated in a very small region of space. This means that the concentrations predicted for the spilled material may and indeed do exceed the normal density of the material in its pure form. This is clearly unrealistic. The way to avoid this problem is to treat the spill as something other than a point source, namely, an area or volume source. The methods for treating nonpoint source releases are well known and can be readily applied in this context. The additional operating costs for treating the spills in a more realistic manner are not expected to be excessive. The other undesirable assumption underlying this model is that the buoyancy of the cargo may be neglected. This assumption is strictly true only for neutrally buoyant cargoes. Very few, if any, cargoes carried in marine

transport are neutrally buoyant. Furthermore, even slight departures from neutral buoyancy (that is, the same density as water) may cause significant departures from the behavior described by these models. Analyses have been performed to describe the behavior of buoyant materials released into natural environments. It is not clear whether these analyses can be adapted to describe the very general conditions this model attempts to consider. Even if pre-existing analyses cannot be adapted for use in this situation, it is definitely feasible to model the effects of buoyancy on mixing and dilution. In any event, the incorporation of buoyancy effects into the model would not be a trivial task, and may result in a significant increase in operating cost of the model. In view of the limitations imposed by these assumptions, this model was judged to give results which are less than average in realism (Table 2-1).

The Flame Geometry Model described in Chapter 4 of this report and in Chapter 6 of AMSHAH appears to contain no significant errors in analysis. Furthermore, the models are semi-empirical in nature and as a consequence, have no significant problems with underlying assumptions. Much the same may be said about the Thermal Radiation from Flames Model described in Chapter 5 of this report and in Chapter 7 of AMSHAH.

The Mixing, Dilution, and Evaporation Model described in Chapter 6 of this report and in Chapter 11 of AMSHAH is based on the unrealistic assumption that the mixing and dilution proceed independently of evaporation and that evaporation has no effect on mixing and dilution. In other words, the concentration profile from which the evaporation rate is predicted is determined on the basis of zero loss of mass by evaporation of the spilled material. This assumption requires the use of an artifact, namely, assuming that evaporation is zero beyond a certain concentration contour in order to produce a finite evaporation rate. Furthermore, it is possible by changing the value of this limiting concentration contour to have more mass evaporate than was originally spilled. Such unrealistic results are clearly unacceptable. This model also suffers from the assumptions limiting the Mixing and Dilution Model, namely, the assumption that spill behaves as a point source and the assumption that the spilled material is neutrally buoyant. In addition to these problems with underlying assumptions, a few minor errors in analyses were discovered. Because of the difficulties engendered by the assumptions, no sensitivity analysis was performed on this model. It is clearly within the realm of feasibility to treat simultaneous mixing, dilution, and evaporation; therefore, the assumption which leads to such unrealistic results should definitely be removed.

The View Factor Model described in Chapter 7 of this report and in Chapter 13 of AMSHAH was not found to have any significant problems either in analysis or in underlying assumptions; however, the analysis presented in AMSHAH did not correspond to the computer program in HACS. The underlying assumptions are clearly acceptable and may be considered to be based

on geometrical rather than physical principles. Both the analysis in AMSHAH and the computer program appear to be correct even though there is not an exact correspondence between the two. In AMSHAH the View Factor Model described is quite general. The receptor of thermal radiation from flame may be placed at any location relative to the flame and may be oriented at any angle relative to the flame. On the contrary, the computer program in HACS considers the receptor to be located directly downwind from the flame, at the same level as the base of the flame, and oriented such that both the observer and the flame are parallel. It is unfortunate that the version of the model programmed is so limited, both because the analysis is available and may be readily programmed and because the results of the model programmed may not always give conservative damage estimates. Because of the inconsistencies between AMSHAH and HACS, no sensitivity analysis was performed for this model.

RECOMMENDATIONS

In view of the results presented above, the following recommendations are made.

1. The computer programs and documentation for the Vulnerability Model, CHRIS, and HACS should be modified to eliminate the errors and inconsistencies discovered in this study.

2. The Mixing, Dilution, and Evaporation Model should be rederived so that evaporation and dispersion are modeled as simultaneous processes.

3. The general model for view factor described in AMSHAH should be implemented on the computer in order to replace the current subroutine SVIEW.

4. The Mixing and Dilution Model should be modified so the finite size of the source is accounted for.

5. Considerations of buoyancy should be incorporated in the Mixing and Dilution Model.

6. The fact that most cargo tanks used in marine transport are vented should be accounted for by the Venting Rate Model.

7. The assumption that liquid and gas phases of the cargo are in thermal equilibrium throughout the venting of the cargo should be removed by a reanalysis of the Venting Rate Model.

8. Considerations of buoyancy and finite source size should be incorporated into the Mixing, Dilution, and Evaporation Model.

These recommendations have been listed in what is judged to be their order of importance. The implementation of these recommendations appears to be clearly feasible. The relative effort required to implement these models and the impact of their implementation on hazard analysis is summarized in Table 1-3.

One final overall recommendation is that some mechanism be devised whereby the originators and users of the Vulnerability Model, HACS, and CHRIS may communicate about problems with these models, inform each other of errors discovered, and where appropriate, make changes simultaneously to all versions of the models. By such a mechanism, improvements fostered by one group would benefit all and the uniformity preserved between all versions would yield considerable logistical advantages.

TABLE 1-3 Characterization of Recommendations

RECOMMENDED IMPROVEMENT	FEASIBILITY	RELATIVE EFFORT REQUIRED	IMPORTANCE TO HAZARD ANALYSIS
1. Incorporate all corrections to errors determined by this study	Definite	Low	Varied
2. Consider evaporation simultaneously with dispersion	Definite	Moderate	High
3. Implement more general View Factor Model on the computer	Definite	Low-Moderate	High-Moderate
4. Modify Mixing and Dilution Model to account for finite source size	Definite	Low	High
5. Add consideration of buoyancy to Mixing and Dilution Model	Definite	Moderate-High	Moderate
6. Modify Venting Rate Model to account for cargo tank venting	Definite	Low-Moderate	Moderate
7. Modify Venting Rate Model to allow temperature differences to exist between liquid and solid phases of the cargo	Definite	Low-Moderate	Moderate
8. Add consideration of buoyancy and finite source size to Mixing, Dilution, and Evaporation Model	Definite	Moderate-High	Moderate*

*Reduced importance because of the overriding effects of the problem to be resolved by recommendation 2.

CHAPTER 1 - REFERENCES

[1] Eisenberg, N. A., C. J. Lynch, and R. J. Breeding, Vulnerability Model: A Simulation System for Assessing Damage Resulting from Marine Spills, CG-D-136-75, NTIS AD-A015245, Department of Transportation, U.S. Coast Guard, June 1975.

[2] Department of Transportation, U.S. Coast Guard, Assessment Models in Support of the Hazard Assessment Handbook (CG-446-3), CG-D-65-74, January 1974.

[3] Arthur D. Little, Inc., Hazard Assessment Computer System, User Manual (HACS), Cambridge, Mass., December 1974.

[4] Radanovic, L. (ed), Sensitivity Methods in Control Theory, Pergamon Press, New York, 1966.

[5] Tomovic, R., Sensitivity Analysis of Dynamic Systems, McGraw-Hill, New York, 1963.

CHAPTER 2

VENTING RATE MODEL

INTRODUCTION

The Venting Rate Model computes the rate at which cargo is vented, either in liquid or gaseous form, from a cargo container if the enclosure is ruptured. This model corresponds to the documentation in Chapter 2, Venting Rate, of the Assessment Models in Support of the Hazard Assessment Handbook (AMSHAH) [1]. The corresponding computer code in the Hazard Assessment Computer System (HACS) [2] is under the executive subroutine MODA which utilizes the following computational subroutines: RLJV1, RLJTC, RLJLQ, and VENTR.

The Venting Rate Model is designed on the principles of Continuum Mechanics. The conservation equations of mass, momentum, and energy are used to describe the venting process. The model determines the mass vented as a function of time for the interval that begins with the rupture and ends when all the cargo that can vent under the given input conditions has discharged. Although the model determines the complete time-history of venting, the important outputs of the model are (1) the total venting time and (2) the average venting rate. Venting of cargo in both gas and liquid states is considered. For volatile cargoes, and especially cargoes liquefied by elevated pressure or decreased temperature in the storage container (e.g., LNG, liquid chlorine), an appreciable amount of total cargo may be vented in gas phase. In fact, if the puncture occurs above the level of a highly volatile liquid cargo and if the cargo tank is allowed to be in thermal contact with the environment, then virtually the entire cargo will vent as a gas. For punctures below the liquid level, liquid venting will occur first and will be followed by gas venting, if the vapor pressure of the cargo is sufficiently high.

Certain assumptions and approximations have been made in the development of this model. There are at least three motivations for the use of assumptions and approximations. First, the data required as input to the model will have limited accuracy. For example, hole size, an important variable affecting venting rate, is likely to be ill defined either by an accident report on a past accident or by on-scene personnel at an ongoing accident. It would appear to be wasteful for the computational model to have an accuracy too far in excess of the accuracy of the available input data.

---

[1] Department of Transportation, U.S. Coast Guard, Assessment Models in Support of the Hazard Assessment Handbook (CG-446-3), CG-D-65-74, January 1974.

[2] Arthur D. Little, Inc., Hazard Assessment Computer System, User Manual (HACS), Cambridge, Mass., December 1974.

Second, the entire computational capacity of this model is not used by models executed subsequently. For example, certain of the mixing and dilution models will use only the average release rate and total time of release, rather than the entire time-history of venting. Although subsequent improvements to other models may make fuller use of the computational capacity of the venting model, it is doubtful that the entire capacity of the model, as it now stands, will ever be used. Therefore, increases in accuracy for intermediate results or final results are unnecessary if subsequent models cannot use all the data or do not require such high accuracy in input data.

Third, the use of more realistic, less restrictive assumptions and approximations is well within the state of the art of modeling venting processes, but more precise treatments result in an unwarranted increase in modeling costs, both developmental and operational.

Consequently, certain assumptions and approximations are made and a workable model is developed to predict the venting rates of cargoes for predetermined conditions of the size, shape, position, and orientation of the rupture; the thermodynamic condition of the cargo and its vapor; and the thermodynamic condition of the external air-water environment.

Many of the assumptions made in modeling the venting process are quite conventional. For example, the vapor in the cargo container is considered to be a perfect gas. In describing the venting of liquid cargo, the flow is assumed to be incompressible. The thermodynamic processes occurring inside the venting tank are assumed to be either adiabatic (thermodynamically isolated from the environment) or isothermal (in complete thermal contact with the environment). Other assumptions made in model development are less customary and may be subject to challenge. For example, it is assumed that the liquid and gas phase portions of the cargo are always at the same temperature, even in the case of adiabatic venting. Still other assumptions that have been made appear to be unjustified or at the very least result in a model which is physically unrealistic. For example, in the case of the adiabatic venting of a cargo with a vapor pressure below atmospheric pressure, it is assumed that liquid venting will cease, even though liquid remains above the hole, provided that the head pressure is balanced by the difference between atmospheric pressure and vapor pressure. This implies that the cargo tank is completely unvented (no pressure relief valves, vacuum relief valves, or open vents) and that entrance of air through the puncture is precluded.

The calculation procedure followed by the computer coding of the model is shown in Figure 2-1. Before describing the computational procedure, it is probably advisable to describe briefly the physical events that are important to the venting process. As an example, consider the adiabatic venting of a liquid. Imagine that the amount of cargo in the tank is such that most of the tank is filled with liquid and that a small amount of saturated vapor is in the space at the top of the tank. Initially, the liquid and vapor will be in thermodynamic equilibrium with the vapor at the saturated vapor pressure. Suppose further that a puncture occurs in the liquid-filled portion of the tank and that the puncture is above the

UNCLASSIFIED

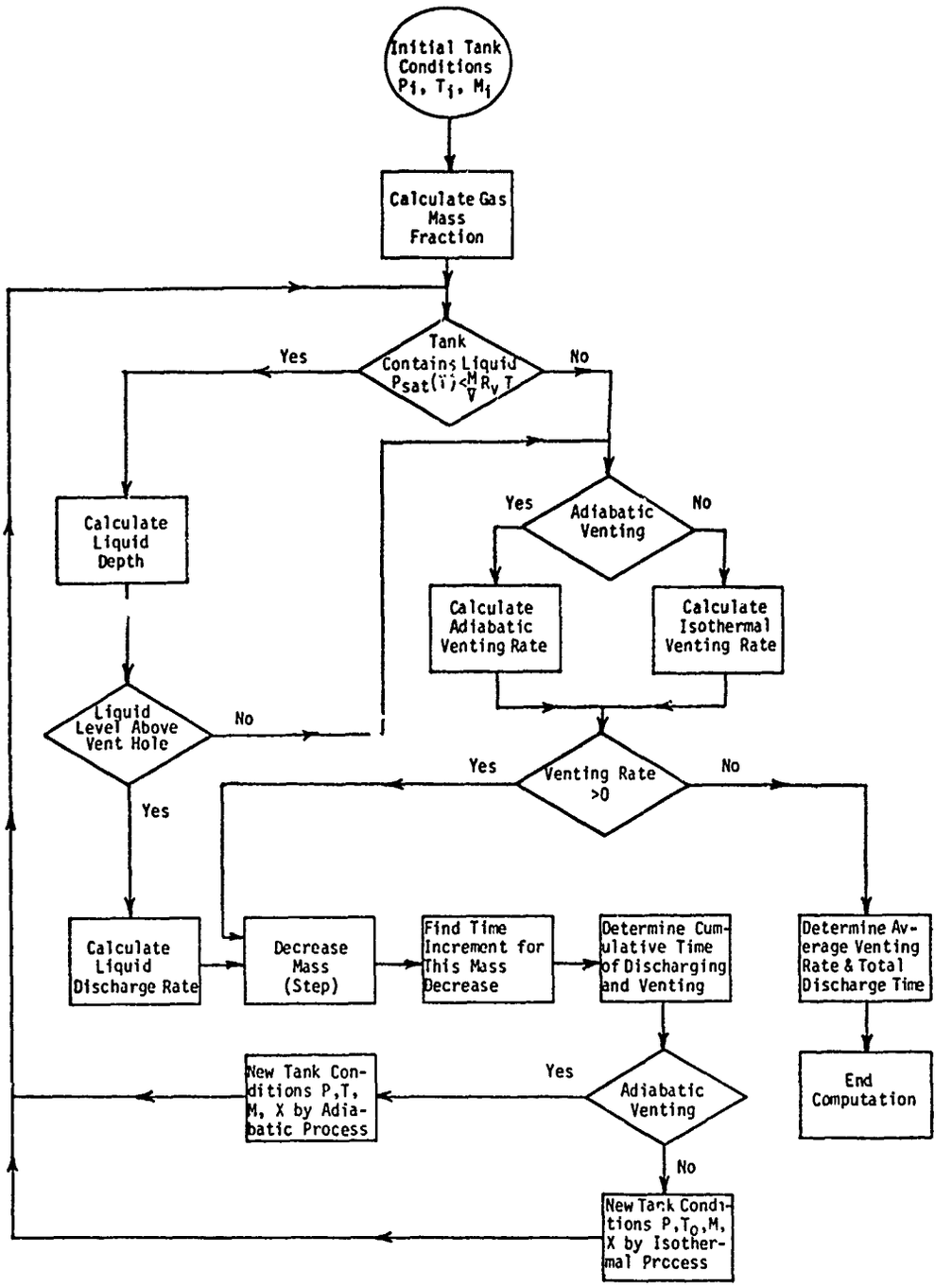


FIGURE 2-1 Flow diagram for calculation of discharge rate for venting from a tank.

waterline of the ship. Then cargo will begin to flow out of the puncture. The pressure driving the liquid from the puncture hole is the difference between the pressure inside the tank at the location of the hole (the inside pressure is the sum of the vapor pressure of the cargo and the hydrostatic head - the pressure generated by the weight of liquid cargo above the hole) and the outside atmospheric pressure. This driving pressure accelerates the fluid and causes it to flow out from the hole. The higher the driving pressure, the higher the flow rate will be. As soon as some amount of liquid, ΔM, has vented from the tank, the liquid level inside the tank will tend to fall. This means that the volume occupied by cargo vapor will increase. At this point, since the amount of cargo in vapor phase is unchanged but the vapor is occupying a larger volume, the pressure and temperature in the space above the liquid will both tend to fall. Since, at this point, the temperature of the liquid has not changed, the vapor pressure of the liquid will exceed the pressure of the gas above it, equilibrium will cease to exist and more vapor will evaporate from the upper surface of the liquid. The evaporation of liquid will (1) cool the remaining liquid, (2) further reduce the volume occupied by the liquid, and (3) tend to bring the pressure of the vapor above the liquid closer to the saturation vapor pressure. If no further venting were to occur, then evaporation and thermal equilibration by heat transfer would continue until the liquid and gas reached a state of thermodynamic equilibrium. In the adiabatic case, the equilibrium state would be cooler and consequently at a lower vapor pressure. In the venting model, it is assumed that equilibrium is indeed reached after the venting of each infinitesimal mass decrement. A further approximation is made in the computer coding by representing infinitesimal mass decrements by finite, but small mass decrements. In summary then, the venting rate is determined by certain thermodynamic conditions in the tank as well as by the remaining height of fluid above the vent hole. As venting proceeds, both the thermodynamic state and liquid level change as a result of the venting process. The computerized version of the venting model attempts to describe this reflexive (feedback) process in mathematical terms. In the isothermal case, the changes in thermodynamic state are easier to compute. In the case of gas venting, the liquid head, of course, has no influence and the equations describing flow rate in terms of pressure difference are more complex than for liquid venting.

Consider now the calculation procedure shown in the flow chart, Figure 2-1. The initial enclose conditions of pressure, temperature, and total mass content are analyzed to obtain the initial gas mass fraction. The presence of liquid in the tank is determined by comparing the saturation pressure for the liquid cargo at the initial temperature with the ideal gas pressure of vapor from the vapor mass, volume, temperature, and the ideal gas constant of the fuel vapor. If the cargo is in the liquid state, the liquid depth is computed. This liquid level is compared with the height of the rupture to determine whether liquid or vapor will discharge.

If liquid is discharging from the rupture, the liquid discharge rate is computed. Then the mass of the cargo in the enclosure is decremented by a predetermined constant fraction of the total initial mass of the cargo

in the enclosure. The time increment required to discharge this fraction of total mass is computed from the liquid discharge rate. This time increment is added to a cumulative sum to obtain the total time for discharging and venting of the cargo. After the mass discharged or vented is subtracted from the total mass of the cargo within the enclosure, the new enclosure conditions of pressure, temperature, enclosed mass, and vapor mass fraction are computed as before. The computation then proceeds by repeating the determination of presence of liquid in the enclosure, etc. During these computations, the liquid level is constantly compared with the height of the rupture. When the liquid level falls below the level of the rupture, liquid discharge stops and vapor venting commences. The computations for vapor venting are the same whether the vapor venting starts when the liquid level becomes lower than the enclosure rupture level or whether the initial state of the cargo in the enclosure is the vapor state, with no liquid present.

If vapor is venting from the rupture, the vapor venting rate is computed. Then the cumulative vapor mass vented, the time increment required for the mass decrement, and the cumulative time of venting are computed. The enclosure conditions are recomputed and calculation continues with the determination of the new vapor venting rate, etc.

The computations that are carried out in this submodel determine the intermediate discharge or venting rates, the total time of discharge and venting, and updated conditions of the cargo within the ruptured enclosure. Details of the quantities that are required by the venting rate submodel are discussed in Appendix 2A.

Several problems were encountered in the analysis of Vending Rate Model documentation of AMSHAH. One problem was a lack of full correspondence between the analysis in AMSHAH and the computer coding in HACS. There appears to be a fundamental and significant error in the energy balance equations (for the adiabatic case) stated in AMSHAH and computerized in HACS. Furthermore, other, less important errors appear to be present in the computer coding of mass decrementation, of equations for various physical constants, and of the decision to stop venting. The most significant problem concerning fundamental assumptions was the unstated assumption concerning pressure relief and purposeful venting of the cargo tanks. The symbols and references are listed at the end of this chapter.

ASSUMPTIONS AND APPROXIMATIONS

The following is a list of the assumptions and approximations made in the development of the Venting Rate Model. It should be noted that, although some assumptions are stated explicitly, many are implicit. These implicit assumptions are not documented in AMSHAH. In addition, the computer coding of HACS makes further assumptions which are not stated in AMSHAH.

10893

Explicit Assumptions

1. The cargo vapor can be treated as a perfect gas.

2. The vapor and liquid phases of cargo are in thermal equilibrium.

3. The discharge process is either adiabatic or isothermal.

4. The height of the hole does not change with respect to the water level outside the vessel.

5. The pressure of the cargo in gas phase is always less than or equal to the cargo vapor pressure.

Implicit Assumptions

6. Liquid venting is continuous with no intermittent inflow of air to relieve an internal vacuum.

7. The tank has no pressure relief valves (assumption in text; in the program the tank has a conditional vacuum relief).

8. Quasi-static analysis is applicable, or the flow is sufficiently steady state so that the (d/dt) term may be omitted in the equations of momentum and continuity.

9. The use of mass increments is an acceptable way to step through the numerical simulation.

10. The vent hole is above the waterline of the vessel.

11. The discharge coefficient is 0.80.

12. For liquid venting, the venting may be treated as ideal fluid flow of an incompressible liquid, whose density change with temperature is negligible.

These assumptions vary in their complexity, accuracy, subtlety, and effect upon the simulation. Each will be discussed in turn.

1. Perfect Gas. It is well known that the assumption that a gas behaves as a perfect gas over a wide range of temperatures and pressures is not precise. In the venting submodel, the range of temperatures and pressures encountered in not large, so the errors resulting from the approximation that the gas-vapor phase of the cargo behaves as a perfect gas are probably not significant, especially with respect to other approximations.

2. Thermal Equilibrium. This assumption is stated in a misleading fashion in AMSHAH. There the assumption is stated in terms of the applicability of "equilibrium thermodynamic relationships." Stated in these terms, the assumption is made almost universally since most analyses of fluid dynamic systems are based on this assumption. Only in very special

situations, for example in certain studies of ultrasound and biological systems, is this assumption not applicable and used. The assumption of equilibrium thermodynamics means that the relationships between variables describing the thermodynamic state of a macroscopic system in which changes occur very slowly are applicable to the description of a microscopic system (a very small fluid particle), provided infinitessimal changes in thermodynamic state occur (that is, the change in thermodynamic state may be rapid, but the change in time is infinitessimal, hence the difference between system states is infinitessimal). This assumption of the applicability of equilibrium thermodynamics relations is made in the analysis of most dynamic fluid systems including acoustic wave propagation and combustion dynamics. Obviously, thermodynamic equilibrium does not exist globally over a dynamic fluid system (e.g., an acoustical field). However, given a small enough volume and small enough time steps, each segment of the system is in thermodynamic equilibrium. That is why, in the partial differential equations that describe such systems, the inherent use of equilibrium thermodynamics is made.

The misleading statement in AMSHAH should not be allowed to obscure the fact that the model does make a significant assumption regarding thermal equilibrium. It is assumed that the portion of the cargo in gas phase is at all times in thermal equilibrium with the portion of the cargo in liquid phase. This thermal equilibrium is concerned with macroscopic systems. The assumption, albeit stated poorly if at all, introduces inaccuracies of an order consistent with those introduced by other assumptions. It is possible that some improvement in the accuracy of the results could be achieved by removing this assumption.

3. Wall Conditions. The statement of this assumption is misleading. The assumptions do not really concern the wall conditions; they refer to the process taking place inside the tank. That is, either the equations for an isothermal process or an adiabatic process are applied. Maintaining the wall of the tank at a constant temperature does not guarantee that an isothermal process is taking place inside the tank. In actuality, the tank venting can probably be described by a polytropic process: one in which none of the quantities of volume, pressure, temperature, or entropy is constant [3]. The venting rate would probably fall somewhere between that calculated with the isothermal assumption and that calculated with the adiabatic assumption, since in most fluid systems polytropic processes will yield results somewhat intermediate between the results for adiabatic and isothermal processes. Thus, the results for these cases may be considered to be the bounds for the actual result.

4. Constant Hole Height. On page 14 of AMSHAH, it is stated that they assume the height of the hole remains constant with respect to the water level. The actual assumption made is of two parts: first, that the hole remains above the water level; and second, that the height of the hole

---

[3] Short, B. E., H. L. Kent, Jr., and B. F. Treat, Engineering Thermodynamics, pp. 133 ff., Harper, New York, 1953.

above the bottom of the tank remains constant. In the situation that the vessel was damaged during the accident that caused the tank puncture and sinks in a time less than or comparable to the time it takes the tank to vent, the hole location with respect to the waterline might well change. If the event has caused the vessel to list, and this list changes as the venting proceeds, then the vertical distance between the bottom of the tank and the hole would change as the venting takes place. Further, if the list is pronounced, then the volume of liquid in the tank would not vary linearly with the height of the liquid level as the program assumes.

5. Tank Pressure Is Less Than or Equal To Cargo Vapor Pressure. This assumption has not been made in the text, but it is stated in equation (2.8), so we list it as an explicit assumption. It is true that the tank pressure will not exceed the vapor pressure of the cargo if the tank contains only the cargo being considered, and if the tank is not full of liquid. Ordinarily these conditions are met. The exception would be the case in which the tank contained an appreciable amount of air and the tank temperature was above the critical temperature for air (-140°C). Since the continued pumping of cargo into a tank containing air could lead to overpressuring of the tank with a possible safety hazard and the uneconomical use of the tank in any event, precautions are taken in actual situations to avoid this event, and this assumption is valid.

6. No Intermittent Liquid Venting. This assumption concerns the case in which the vent is above the water level and below the liquid-vapor level in the tank, no negative pressure relief is provided, and the vapor pressure of the cargo is less than ambient. In this case, as the liquid level falls due to the venting of liquid, a pressure less than the outside air pressure occurs within the tank. Since intermittent flow is not allowed, the flow would stop when the negative (relative) pressure inside the tank balanced the pressure of the head. If the vent is above the water level, however, the venting would probably go into intermittent flow similar to that which one observes when inverting a narrow-mouthed bottle full of water over the kitchen sink. This type of flow is not mentioned in the text of AMSHAH. In the isothermal portion of the program (see RLJTC), the vapor pressure is not allowed to drop below the ambient air pressure. This obviates the need for consideration of intermittent flow but tacitly assumes that the tank has a vacuum (negative pressure) relief valve, which is not mentioned. If the tank is taken to vent adiabatically, the venting will stop when the negative internal pressure balances the pressure of the liquid head.

7. Tank Venting (Intentional) or Pressure Relief. There is no mention of any pressure relief valves on the tank, so one might assume that the tank has only the one opening -- the accidentally caused puncture. In actuality, every tank used in regulated transport has some sort of pressure relief valve, although it is possible that the threshold pressure may be so high in some cases that the tank will act as if it has only the one opening. On the other hand, some cargoes which have low vapor pressure and are not highly dangerous have open, unrestricted vents. In the computer program, as discussed above, it is assumed that in the isothermal case the tank has a negative-pressure relief valve with a zero threshold, and that

in the adiabatic case the tank has no negative-pressure relief valve. The existence of a positive-pressure relief valve would be of interest in the case in which the tank is subject to heating by the burning of already spilled cargo, and in the case of a cryogenic liquid in a tank when the cargo becomes heated due to the failure of insulation or refrigeration.

8. Quasi-static Equations. This assumption amounts to dropping all the (d/dt) terms in the fluid dynamic equations. This approximation is valid when the flow is steady, but not when it is changing rapidly. Thus, this approximation is questionable when the tank vents very rapidly. A quantitative analysis of the terms omitted by using this assumption shows that for many cases of interest these terms are indeed negligible.

9. Mass Increments. It is not clear that the use of mass increments is the best way to simulate numerically the venting of the tank in the adiabatic case. As the mass approaches zero, the pressure changes may be extremely rapid in this approach, and it may be that a method of using incremental pressure changes as opposed to incremental mass changes may be more accurate.

10. Position of Puncture. The text does not say that the vent is above the waterline of the vessel, but no pressure correction is made for the depth of the vent below the waterline and no allowance is made for the entry of water into the tank, so it appears that only vents above the waterline are being considered. On the other hand, no mention is made of intermittent venting, and this would not occur for a vent below the waterline. It is further assumed that the vent is either wholly above or wholly below the liquid level in the tank. While this will probably be true for the bulk of the venting, if the venting does change from liquid to gas due to falling liquid level in the tank, there must be some period during which both vapor and liquid are vented. In the case that the puncture is a vertical gash of considerable length, as the bow of a ship might make in striking the side of another vessel, the release of both vapor and liquid might extend over a considerable period. This situation might also occur when a tank fails along a vertical seam from internal pressure or some other cause.

11. Discharge Coefficient. In RLJVI, the discharge coefficient is set equal to 0.80 for all cases. The discharge coefficient is used in the equations in R&K but is not discussed. Of the many types of accidental punctures which may occur, the discharge coefficient is unlikely to be exactly equal to 0.80 for any of them. Thus, 0.80 is probably an adequate approximation for most types of holes, and since details of the nature of the hole are liable to be difficult to come by, there are no data from which to make a better estimate.

12. Ideal Fluid Flow. A fluid process is said to be ideal if the thermal conductivity and the viscosity may be neglected. This is equivalent

to assuming that the flow is isentropic [4]. The assumption that the fluid is inviscid leads, of course, to an infinite value for the Reynolds number. Since the coefficient of discharge is a function of the Reynolds number for low values of the Reynolds number, this in turn implies an assumption about the coefficient of discharge [5]. The Reynolds number is defined to be

$$Re = uD/\nu$$

for flow through an orifice, where u is the velocity, D is the diameter for a circular hole and twice the slit width for flow through a rectangular slit, and ν is the kinematic viscosity ($\nu = \mu/\rho$). Thus, the inviscid assumption will be best for cargoes of low viscosity with large holes and rapid venting.

Of the 12 assumptions and approximations discussed above, #5 ($P_t \leq P_v$) is the only one which is obviously valid. #10 (location of vent) and #4 (constant hole height) amount to restrictions on the model which must be taken into account by the user. #1 (perfect gas), #6 (no intermittent flow), and #7 (tank venting) are assumptions which are certainly valid for some tanks and some cargoes, and are certainly invalid for others. #2 (thermal equilibrium) may not be entirely accurate, but it seems consistent with the other assumptions. The use of equilibrium thermodynamics is so common in engineering analysis that it was assumed that its listing as an assumption was a misstatement and the statement was interpreted as meaning thermal equilibrium between liquid and gaseous phases. The remaining assumptions, #3 (isothermal or adiabatic), #8 (quasi-static), #9 (mass increments), #11 (discharge coefficient), and #12 (ideal flow), appear to be valid for most situations of interest.

ERRORS AND INCONSISTENCIES

There are various analytical and typographical errors in AMSHAH and inconsistencies between the documentation of AMSHAH and the corresponding computer code of HACS. These errors and inconsistencies are listed in the following.

1. The Liquid Venting Equation

This equation has been incorrectly printed on page 4 of AMSHAH, but the programmed version (statement 5 in subroutine VENTR of HACS) is correct.

The equation of AMSHAH is

$$W_L = A_h C_d \rho_L [2g\rho_L(H_L - H_h) + 2(P - P_a)]^{1/2} \qquad \text{AMSHAH (2.2)}$$

---

[4] Landau, L. D., and E. M. Lifshitz, Fluid Mechanics, p. 4, Pergamon, London, 1959.

[5] Blackburn, J. F., G. Reethof, and J. L. Shearer, Fluid Power Control, pp. 178-184, M.I.T. Press, Cambridge, Mass., 1960.

The dimensions of the terms in this equation are not all equal. The problem of liquid venting from a tank is considered in most fluid dynamics books (e.g., [6]), and the equation should be:

$$W_L = A_h C_d \rho_L [2g(H_L - H_h) + 2(P - P_a)/\rho_L]^{1/2} \qquad (2\text{-}1a)$$

or

$$W_L = A_h C_d [2\rho_L (P - P_a + g\rho_L [H_L - H_h])]^{1/2} \qquad (2\text{-}1b)$$

Equation (2.2) of AMSHAH is wrong in that the density of the liquid (ρ_L) is multiplying ($H_L - H_h$) instead of dividing the pressure difference.

2. Gas Venting Equations

There are no errors in these equations, but the inconsistent use of different units in the text and in the program may lead to some confusion. In addition, one of the equations in AMSHAH (page 5) and both the statements in VENTR may be written in simpler forms.

Equations (2.5) are:

$$W_V = A_h C_d p [(k/(R_V T) (2/(k+1))^{(k+1)/(k-1)}]^{1/2}$$

AMSHAH (2.5a), (2-2)

$$W_V = A_h C_d [2\rho_V (P - P_a) B^{2/k} (k/(k-1)) (1 - B^{(k-1)/k})/ (1-B)]^{1/2}$$

AMSHAH (2.5b), (2-3)

where $B = P_a/P$. These equations agree with those in Owczarek [7]. However, in VENTR, statements 15 (corresponding to equation (2.5a)) and 21 (corresponding to equation (2.5b)) are different from their corresponding equations. This is due to the use of pressure in gmf/cm^2. The G which appears to be out of place is needed to convert the pressure to dynes/cm^2. Statement 15 might be rewritten for efficient computation as:

```
W = CO*PT*A* SQRT (AM*G/R/T *AK* (2./(AK+1.))**((AK+1.)/(AK-1.)))
```

(2-4)

If one wishes to have the pressures in dynes/cm^2, then statement 15 should be:

```
W = CO*PT*A* SQRT ( AK*AM/T/R* (2./(AK+1.) )**(AK+1.)/(AK-1.) ) )
```

(2-5)

---

[6] Lamb, H., Hydrodynamics, pp. 23-25, Dover, New York, 1945.

[7] Owczarek, J. A., Fundamentals of Gas Dynamics, pp. 204-205, International Textbook Co., Scranton, Pa., 1964.

with the DATA statement defining R replaced by

```
DATA R/8.3170E7/                                                    (2-6)
```

since 8.3170×10^7 is the value of R in erg/g-mole/°K

As stated previously, the factor G which appears to be extraneous in statement 21 is needed to convert the pressure from gmf/cm^2 to dynes/cm^2.

However, a simpler expression may be used. Letting $B = P_a/P$ in (2.5b), with algebra and the ideal gas relationship, we have,

$$W_v = A_h C_d \left[(2k/(k-1))\rho_v P_i (B^{2/k} - B^{(k+1)/k}\right]^{1/2} \qquad (2\text{-}7)$$

so statement 21 may be written

```
W = A*CO* SQRT ( 2.*AK/(AK-1.) *DV*PT*G* (B**(2./AK) - B**
    ((AK+1.)/AK)) ).                                                (2-8)
```

This is the expression for pressure in gmf/cm^2. If one wishes to have the pressures in dynes/cm^2, then the expression should be:

```
W = A*CO* SQRT ( 2.*AK/(AK-1.) *DV*PT* (B**(2./AK)
    - (B** ((AK+1.)/AK)) ).                                         (2-9)
```

3. Adiabatic Process Equation

Equation (2.10a) of AMSHAH (page 7) is

$$T/T_i = (P/P_i)^{k/(k-1)} \qquad \text{AMSHAH (2.10a)}$$

which is incorrect because the exponent is inverted. It should be

$$T/T_i = (P/P_i)^{(k-1)/k} \qquad (2\text{-}10)$$

as given on page 87 of Thompson [8]. The statement in subroutine RLJTS is correct.

4. Energy Equation

A detailed development of the complete energy equations is given in Appendix 2B for liquid discharge and in Appendix 2C for gas venting from a ruptured enclosure. The following is a comparison of the analytical equations in AMSHAH with the complete energy equations. The complete energy equation for gas venting (2C-10) is compared with equation (2.10b) of AMSHAH.

---

[8] Thompson, P. A., Compressible-Fluid Dynamics, McGraw-Hill, New York, 1972.

Equation (2C-10) of Appendix 2C is:

$$M_{L_2}\,\hat{C}_L\,(T_1-T_2) + \hat{C}_L\,T_1\,(M_{L_1}-M_{L_2}) + 0.5\,(M_{g_1}+M_{g_2})\,\hat{C}_{pg}\,(T_1-T_2)$$
$$- 0.5R\,(M_{g_1}+M_{g_2})\,(T_1-T_2) = 0.5\,(T_1+T_2)\,\hat{C}_{vg}\,(M_{L_1}-M_{L_2})$$
$$+ \hat{\lambda}\,(M_{L_1}-M_{L_2}) - \left\{w_o\left[\frac{P_a}{\rho_{ga}} + 0.5\,v_o^2 + Z_h g\right]\right\}_{av}(t_1-t_2) \qquad (2\text{-}11)$$

The corresponding equation in AMSHAH is:

$$m\,(T_1-T)\,(X\,\hat{C}_{pg} + (1-X)\,\hat{C}_L) = \hat{\lambda}\,[m_i\,(1-X_i) - m\,(1-X)]$$
$$+ V\,(P_i-P) \qquad \text{AMSHAH (2.10b)}$$

When rewritten in the notation of Appendix 2C, this equation becomes

$$M_{L_2}\,\hat{C}_L\,(T_1-T_2) + M_{g_2}\,\hat{C}_{pg}\,(T_1-T_2) - V_T\,(P_{T_1}-P_{T_2})$$
$$= \hat{\lambda}\,(M_{L_1}-M_{L_2}) \qquad (2\text{-}12)$$

Comparing this with (2-11), we note that the first term in (2-12) is identical to the first term in (2-11) and that the second term in (2-12) is similar to the third term in (2-11). The terms involving the heat of vaporization ($\hat{\lambda}$) are identical. At first glance, it appears that the $V_T(P_{T_1}-P_{T_2})$ term in (2-12) might be equivalent to the $0.5(M_{g_1}+M_{g_2})R(T_1-T_2)$ term in (2-11); however, a careful examination of the terms using the perfect gas law reveals two problems with this. From the perfect gas law, we have

$$P_T = \rho RT = R\,\frac{M_g T}{V_g}$$

and differentiating gives

$$\Delta P_T = \frac{RT}{V_g}\,\Delta M + \frac{RM}{V_g}\,\Delta T - \frac{RMT}{V_g^2}\,\Delta V_g$$

or

$$V_g\,\Delta P_T = RT\,\Delta M + RM\,\Delta T - P_T\,\Delta V_g$$

Using average values for nondifferentiated quantities gives

$$\frac{(V_{g_1}+V_{g_2})(P_{T_1}-P_{T_2})}{2} = \frac{R(T_1+T_2)(M_{g_1}-M_{g_2})}{2} + \frac{R(M_{g_1}+M_{g_2})(T_1-T_2)}{2}$$
$$- \frac{(P_{T_1}+P_{T_2})(V_{g_1}-V_{g_2})}{2}$$

From this result, we see first that the $V_T(P_{T_1} - P_{T_2})$ term in (2-12) equals the $0.5\,(M_{g_1} + M_{g_2})\,R\,(T_1 - T_2)$ term in (2-11) only if

$$\frac{R(T_1 + T_2)}{2}\,(M_{g_1} - M_{g_2}) = \frac{(P_{T_1} + P_{T_2})}{2}\,(V_{g_1} - V_{g_2})$$

i.e., if $\Delta\rho = 0$. Since the thermodynamic process occurring in the vapor cannot, in general, be taken to be a constant-density process, the two terms in (2-11) and (2-12) are not equivalent. Furthermore, even if

$$R(T_1 + T_2)(M_{g_1} - M_{g_2}) \simeq (P_{T_1} + P_{T_2})(V_{g_1} - V_{g_2})$$

so that

$$\frac{(V_{g_1} + V_{g_2})}{2}\quad (P_{T_1} - P_{T_2}) \simeq \frac{R(M_{g_1} + M_{g_2})}{2}\quad (T_1 - T_2)$$

a second problem arises because, in general,

$$\frac{(V_{g_1} + V_{g_2})}{2} = V_g$$

is not equal to V_T (the tank volume), which is the multiplier of the pressure difference term in (2-12). This apparently erroneous use of V_T instead of V_g in the energy balance equation could potentially create far more error than the omission of the various other terms. The rest of the terms in (2-11) are not present in equation (2.10b) of AMSHAH or in (2-12).

An intermediate form of the energy equation as obtained in equation (2C-6) of Appendix 2C is:

$$\frac{d}{dt}\,[M_L\,\hat{C}_L\,T + M_g\,\hat{C}_{vg}\,T + \hat{\lambda}\,M_g]$$
$$= (\frac{dM_L}{dt} + \frac{dM_g}{dt})\quad [\hat{C}_{vg}\,T + \hat{\lambda} + \frac{P_a}{\rho_{ga}} + 0.5\,v_0^2 + Z_h g] \qquad (2\text{-}13)$$

To see that the pressure volume term in the equation in AMSHAH does indeed correspond to the indicated term in (2-11), we go back to (2-13) and follow the derivation of the $M_g\hat{C}_{vg}$ terms in two different ways. We note that there is a term involving M_g and $\hat{C}_{vg}$ (which comes from dU/dt) on the left-hand side of (2-13) and another term involving these quantities (which comes from $w_0\hat{U}$) on the right-nand side. Gathering these two terms on the left-hand side we have

$$\frac{d}{dt}\,[M_g\,\hat{C}_{vg}\,T] - \hat{C}_{vg}\,T\,\frac{dM_g}{dt}$$

Using the fact that $\hat{C}_{vg} = \hat{C}_{pg} - P_T/(\rho_g T) = \hat{C}_{pg} - R$, we use each of these expressions in the two terms above and obtain

$$M_g \hat{C}_{pg} \frac{dT}{dt} + \hat{C}_{pg} T \frac{dM_g}{dt} - \frac{d}{dt}\left[M_g \left(\frac{P_T}{\rho_g T}\right) T\right] - \hat{C}_{pg} T \frac{dM_g}{dt}$$
$$+ \frac{P_T}{\rho_g} \cdot \frac{dM_g}{dt} = M_g \hat{C}_{pg} \frac{dT}{dt} + \hat{C}_{pg} T \frac{dM_g}{dt} - \left[\frac{dM_g}{dt} RT + M_g R \frac{dT}{dt}\right]$$
$$- \hat{C}_{pg} T \frac{dM_g}{dt} + RT \frac{dM_g}{dt} \qquad (2\text{-}14)$$

In this equation there are two terms which add out on the left side, and four which add out on the right side. Using $V_g = M_g/\rho_g$ on the left side, (2-14) becomes

$$M_g \hat{C}_{pg} \frac{dT}{dt} - \frac{d}{dt}(P_T V_g) + \frac{P_T}{\rho_g} \frac{dM_g}{dt} = M_g \hat{C}_{pg} \frac{dT}{dt} - M_g R \frac{dT}{dt} \qquad (2\text{-}15)$$

from which it follows that

$$\frac{d}{dt}(P_T V_g) - \frac{P_T}{\rho_g} \frac{dM_g}{dt} = M_g R \frac{dT}{dt} \qquad (2\text{-}16)$$

Presumably, AMSHAH has approximated the two terms on the left side of this equation by $V_T(dP_T/dt)$. In any event, the correspondence between the term just to the left of the equal sign in (2-11) and a term involving pressure and gas volume is made clear in (2-16).

The complete energy equation for liquid discharge is (2B-15):

$$\int_1^2 M_L \hat{C}_L \, dT + M_{g_2} \hat{C}_{pg} (T_2 - T_1) + \hat{C}_{pg} T_1 (M_{g_2} - M_{g_1}) + \hat{\lambda}(M_{g_2} - M_{g_1}) =$$
$$\int_1^2 \hat{C}_L T \, dM_g + \int_1^2 (-wo)\left[\frac{P_a}{\rho_L} + 0.5 v_o^2 + Zhg\right] dt + (P_T V_g)_2 - (P_g V_g)_1 \qquad (2\text{-}17)$$

and this is compared with equation (2.10c) of AMSHAH:

$$m (T_i - T)[X \hat{C}_{pg} + (1-X) C_L] = \hat{\lambda}(mX - m_i X_i) + V(P_i - P)$$
AMSHAH (2.10c), (2-18)

To facilitate comparison, we note that AMSHAH uses the subscript i to denote the previous state and the lack of a subscript to denote the present state. X denotes the fraction of the mass in the tank which is in gas phase, so Xm in AMSHAH is M_g in our notation. Likewise, (1-X)m is M_L in our notation of Appendix 2C. AMSHAH uses V to denote the volume of the

entire tank, which we denote V_T. Equation (2.10c) may now be rearranged to give

$$M_{L_2} \hat{C}_L (T_1-T_2) + M_{g_2} \hat{C}_{pg} (T_1-T_2) + \hat{\lambda} (M_{g_1}-M_{g_2}) = V_T (P_{T_1}-P_{T_2}) \quad (2\text{-}19)$$

Comparing this with equation (2-17), we see that two of the terms on the left in (2-19) are identical with terms on the left side of (2-17) but that many terms have been omitted, and that the term on the right side of (2-19) is not the same as the pressure volume term, and the omitted terms will be evaluated by means of an example in the accuracy assessment.

5. Vapor Heat Capacity Equation

The Vapor Heat Capacity, denoted C_{pg} in AMSHAH and CPG in the computer coding, gives the amount of thermal energy needed to raise a given quantity of cargo by some unit of temperature. If the quantity of cargo is in grams or kilograms, then it is called the specific heat capacity. If the quantity is one mole, it is called the molar heat capacity. The subscript p denotes that this is the heat capacity at constant pressure, which distinguishes it from the heat capacity at constant volume.

C_{pg} is a function of temperature, so the Chemical Properties File contains coefficients for a cubic equation which gives the C_{pg} as a function of temperature. These coefficients have been used to calculate the values of C_{pg} for a number of temperatures, and the results are compared with values given by standard references [9,10], (Table 2D-1 in Appendix 2D).

The coefficients given in the Chemical Properties File are for an equation which gives the molar heat capacity in Joules/kmole/°K or Joules/kmole/°C. C_{pg} is calculated for the initial tank temperature in subroutine PROP, and there it is changed to cal/mole/°C before being stored in the state file. After C_{pg} is obtained from the State File by MODA, it is divided by the molecular weight (AM) which converts it to specific heat capacity in cal/gram/°C.

In addition to the four coefficients in the cubic equation used to calculate the molar heat capacity of the vapor at constant pressure, the file contains upper and lower temperature bounds, within which the equation is applicable. For the five cargoes being considered, the temperature bounds are identical: -23°C to 327°C. The value of the vapor specific heat (C_{pg}) is calculated at the initial tank temperature. For gasoline and methyl alcohol, the tank temperature is unlikely to be below -23°C. For chlorine and ammonia, which have boiling points near -35°C, C_{pg} may be evaluated at a temperature somewhat higher than the initial tank temperature. This is because if the

---

[9] Weast, R. C. (ed.), Handbook of Chemistry and Physics, 52nd ed. (1971-1972), Chemical Rubber Co., Cleveland, Ohio, 1971.

[10] Hodgman, C. D. (ed.), Handbook of Chemistry and Physics, 41st ed. (1959-1960), Chemical Rubber Co., Cleveland, Ohio, 1959.

temperature is outside the bounds in subroutine PROP, the equation is evaluated at the appropriate bound. For chlorine or ammonia at -35°C, the value of C_{pg} would be calculated at -23°C, which is probably not a significant error. For LNG, however, which is very frequently carried in tanks near its boiling point of -151.5°C, the error could be significant.

Table 2D-1 contains values of C_{pg} from standard references and as calculated from the equation whose coefficients are stored in the Chemical Properties File. It is obvious that 0.502 will be used for LNG at -162°C, while the actual value will be considerably less than 0.450. From the values of C_{pg} for LNG from [9] in the table a quadratic equation for C_{pg} may be derived. The coefficients are:

$$\begin{aligned} A &= 0.02629 \\ B &= 0.003824 \\ C &= -7.23 \times 10^{-6} \end{aligned} \qquad (2\text{-}20)$$

These are coefficients of an equation to give C_{pg} directly in cal/gm/°K. The coefficients in the Chemical Properties File give the molar heat capacity in Joules/kmole/°K. The errors in C_{pg} for chlorine, ammonia, and methyl alcohol range from 4% to 15%.

6. Liquid Heat Capacity Equation

The values of C_{pl}, the specific heat of the liquid phase, have also been investigated. Table 2D-2 in Appendix 2D lists the values for chlorine, ammonia, methyl alcohol, and gasoline. No values were found for liquid methane, so the accuracy of the equation for C_{pl} for liquid methane cannot be assessed at this time. The coefficients in the equation for C_{pl} in the Chemical Properties File give the heat capacity in Joules/kg/°K for an input in °K. This value of the heat capacity must be divided by 4186 to get the heat capacity in cal/gm/°K.

From Table 2D-2, it is evident that the vapor heat capacity equation is accurate for ammonia and may be extended to 20°C even though the listed upper bound is 0.2°C. The equation for methyl alcohol does not do so well when extended outside its range; the lower bound for methyl alcohol is 15.2°C. This seems rather high, considering that methyl alcohol is almost always carried in tanks at ambient temperature and pressure. There seems to be a definite error in the case of chlorine. The values for C_{pl} calculated from the equation whose constants in the Chemical Properties File are nearly identical with the values for C_{pg}, and are about half the value of C_{pl} from the reference. It would appear, then, that the values for C_{pl} for chlorine are really values of C_{pg}.

7. Vapor Pressure Equation

The vapor pressure is a property of the cargo which depends markedly upon the temperature, so calculating the vapor pressure once for the initial tank temperature would be inaccurate if the tank temperature were to change significantly, as it may in the adiabatic case. Thus, the coefficients in the equation giving p_v as a function of temperature are

passed into a function RLJVP, which is used by the submodel to calculate the vapor pressure as needed. The statement there represents the equation

$$P_V = 10^{[A-(B/(T+C))]} \tag{2-21}$$

which may also be written

$$\log_{10} (P_V) = A - [B/(T+C)] \tag{2-22}$$

The accuracy of the vapor pressure equation with the coefficients from the Chemical Properties File has been examined. Table 2D-3 in Appendix 2D lists the coefficients from this file and coefficients from the Handbook of Chemistry and Physics [9]. It may be noted that the coefficients from [9] are valid over a wider range of temperatures than from this file. The accuracy of the different sets of equations is assessed in Table 2D-4. Here the temperatures at which the vapor pressure was equal to a specific value were obtained from an earlier edition of the Handbook of Chemistry and Physics [10], and P_V was calculated from the two sets of coefficients. We see that, for LNG (methane), chlorine, and methyl alcohol, the coefficients from the Chemical Properties File give more accurate results over their range, but that the coefficients from [9] give acceptable values of P_V over a wider range.

The vapor pressure of ammonia as calculated with the coefficients from the Chemical Properties File is certainly in error. While the coefficients from [9] do approximate P_V, the approximation is not particularly good between 0°C and -33.6°C. It is easy to derive a linear equation which gives a better fit to p_V in the range from +25°C to -35°C by starting with the temperatures from [10] at which p_V = 1 atm and P_V = 10 atm. The coefficients are A = 10.046 and B = 1207.3.

The coefficients from the Chemical Properties File do not appear to give accurate values for the vapor pressure of gasoline either, but the problem is made more complex by the varying composition of gasoline. The p_V values in Table 2D-4 from [9] and [10] are for n-octane. Common gasoline is very unlikely to be pure octane, but n-octane and n-heptane usually constitute the bulk of it. Using the coefficients from [9] for n-heptane (A = 9.9166, B = 1837.5), one gets P_V = .042 atm at 19.2°C and P_V = .308 atm at 65.7°C. These values are quite close to those calculated from the coefficients from the Chemical Properties File. And [10] gives the vapor pressure of n-heptane as .0526 atm at 22.3°C. So it appears that the coefficients from the Chemical Properties File give the vapor pressure of n-heptane. An unexplained inconsistency, however, is that the specific heats for gasoline were closer to those for n-octane than they were to those for n-heptane.

8. Liquid Density Equation

The accuracy of the equation by which the density of the cargo in liquid phase is calculated has been assessed, and the results are presented in Table 2D-5 in Appendix 2D. The densities for chlorine, methanol, and

gasoline are quite acceptable. The densities of liquid ammonia in the range of -20°C to +20°C are also quite acceptable, but the Chemical Properties File lists the range of validity as -78°C to -20°C, however liquid densities for liquid ammonia temperature below ~-40°C are meaningless.

9. Overspecification of Input Conditions

The venting submodel requires inputs which overspecify the conditions. Overspecification in the input conditions, in addition to being inconsistent, can cause a significant computational error. That is, the user is told that he must specify the mass in the tank, the volume of the tank, the temperature in the tank, and the pressure in the tank. But these four variables are not independent, so either the user must do a calculation beforehand to determine one of these variables from the other three, or the program will begin with an inconsistent description of the tank and its contents.

Overspecification means that more quantities have been specified than are independent. If we have $x = a + b$, we cannot specify that $x = 4$, $a = 3$, and $b = 2$, for then the equation is not satisfied. For the tank, if it contains any liquid at all, then the pressure in the tank will be the cargo vapor pressure at that temperature, so giving the tank pressure, as well as temperature, is overspecifying the problem. If the tank contains only gas, then the pressure, density, and temperature are related by the perfect gas law. Since specifying the mass and the volume amounts to determining the density, we see that all three variables in the perfect gas law have been specified, which is again overspecification.

The program calculates the pressure in the tank from the other variables for each step in the venting, and the initial pressure is not used in these steps. However, the initial pressure is used in determining the initial flow rate and thus the initial time step. Unless the user has specified a consistent set of variables, this initial step may be in error. It is possible, for example, to get a negative time for the first step.

In addition to there being no check to insure that the volume, mass, temperature, and pressure are consistent, there is no check on the mass in the tank, or that the temperature is above the critical temperature for the cargo. Thus one may specify that the tank contains more mass than it can hold at that temperature. For many cargoes the ambient temperature is unlikely to be greater than the temperature at the critical point, but for some cargoes such as LNG the critical temperatures are considerably below ambient temperatures.

10. Incrementation of the Escaped Mass

As tank conditions change during the venting process, the flow rate will change. Because it is difficult to find an analytic expression for the flow rate as a function of time when an adiabatic process is assumed, a finite-difference approach to the venting is used. In this method, the mass in the tank is divided into a number of increments, and it is assumed that the flow rate can be taken as constant for the time it takes for this mass increment to escape from the tank. This is a standard procedure, and if the increments are small enough, it provides a

good approximation to the analytic solution in those cases where an analytic solution is possible. There are two related errors:

(1) The mass in the tank at the end of a step is not the mass in the tank at the beginning of the step minus the amount which escaped. This amounts to ignoring the conservation of mass.

(2) The flow rate for a step is approximated by the flow rate at the end of that step. It is customary and more accurate to use, as a first approximation, the average of the flow rate at the beginning of the step and the flow rate at the end of the step.

The magnitude of these errors will be proportional to the change in the flow rate from step to step.

The main loop (DO 20) in which the rate of escape of the cargo is computed is in the later part of subroutine RLJVI. The quantities with which we shall be concerned are:

AMAS	=	mass increment
AMASS	=	mass in the tank at the end of the current step
AMASO	=	mass in the tank at the beginning of the current step
TML	=	total mass of liquid escaped
TMG	=	total mass of gas or vapor escaped
DT	=	time for AMAS to escape
TIME	=	time at the end of this step
FR = W	=	flow rate

The first statement in the loop is DT = AMAS/FR, and we see from statements 40 and 50 that the mass which escaped in this step is FR*DT. But in between these statements a new value of FR has been calculated in VENTR, based upon the new tank conditions computed in RLJTC. The FR at the beginning of the loop is that calculated with AMASO amount of mass in the tank, and that used in 40 and 50 is the flow rate with AMASS amount of mass in the tank. In general they will not be the same, and the mass which escaped in this step will not equal AMAS. However, when the next step begins it is assumed that AMAS has escaped, because we have AMASS = AMASS - AMAS. After a number of steps, the discrepancy between the total mass escaped, TMG + TML, and the decrease in mass in the tank, AMSSO - AMASS, could be quite large. The difference between these two quantities is mass which has simply vanished.

The changes to rectify this problem are as follows: after statement 15, the statements

```
DT   = AMAS / FR
TIME = TIME + DT
```

are removed. Between the call to VENTR and FR = W, the following statement is introduced.

```
TIME = TIME + AMAS*2. /(FR+W)
```

And then 40 and 50 are replaced by:

```
40 TML  =  TML + AMAS
50 TMG  =  TMG + AMAS
```

In order to assess the magnitude of the errors, the results as obtained by HACS are compared with the results obtained with the correction. The computer calculations for the isothermal discharge of liquid methanol in a cubic tank of height 493 meters and rupture height of 400 meters with an initial liquid level of 458.7 meters shows a 10.6% relative error for the total mass of methanol released and a 34.2% relative error for the amount of methanol discharged in the last step of discharge.

11. Tank Vents or Pressure-Relief Valves, and the Decision to Stop Venting

The problem here involves the existence of vents or pressure-relief valves on the tank. The assumed presence or absence of such valves will influence the internal tank pressure, which in turn will affect the point at which the program terminates the escape of the cargo. The program currently will seriously underestimate the amount of cargo which escapes for a low vapor pressure cargo in the adiabatic case, when the hole is below the liquid level.

A different assumption about pressure-relief valves is made in the isothermal case than that made in the adiabatic case. In the isothermal case, the assumption is made implicitly in the first portion of RLJTC that the tank has a negative-pressure relief valve with an infitesimal threshold. While this is not likely to be the case in reality, it is a good representation of the tank after an accidental puncture above the waterline, since it is difficult to imagine how a tank so punctured could sustain much of the negative relative pressure. This assumption implies that the escape of the cargo will not cease until the liquid level is below the hole. While this approximation may be valid for nearly a continuous spill, this would not be applicable to spills which have intermittent cargo venting, interspaced by air replacing the discharged cargo.

The assumption in the adiabatic case, made in RLJTS, is that there is no negative pressure relief. In RLJTS, two pressures are calculated: PV, which is the vapor pressure of the cargo at the temperature then prevailing in the tank, and PC, the pressure which would exist in the tank if all the cargo was in the gas or vapor phase. If the cargo is below its critical temperature, then the pressure cannot exceed the vapor pressure, as vapor will condense to liquid until the vapor pressure is reached. Thus, the program takes the minimum of PV and PC to be the tank pressure. This is all very well in the case where the cargo . vapor pressure is greater than the ambient pressure; but when the cargo's vapor pressure is less than ambient, a relative negative-pressure will occur within the tank. The equivalent relative pressure at the hole is [PT + G*DZ*DL - PA], where

PT = the tank pressure (absolute)
G = the acceleration due to gravity
DZ = the height of the liquid surface above the hole
DL = the density of the liquid
PA = ambient air pressure.

Now a negative relative pressure will occur when PT is less than PA, so the liquid venting will stop when DZ is positive, i.e. when G*DZ*DL = PA - PT. This condition, no escape of liquid with the liquid level above the hole, is not realistic. It is realistic if the tank is emptying through a tube with an upturn on the end, or if the puncture is underwater, but it is not realistic for any type of simple hole above the waterline. What will happen in this case is that short periods in which liquid escapes will be separated by periods in which air passes into the tank (intermittent venting) or that air will flow into the tank continuously through the top portion of the puncture and liquid will escape through the bottom portion of the puncture. In either case, the venting of liquid will not cease until the liquid level is below the hole. And the pressure inside the tank will not fall significantly below the ambient pressure.

Thus the assumption that the tank has a negative pressure relief valve with a very small threshold should apply to the adiabatic case as well as to the isothermal case. This can be done by replacing statement 10 and the following statement in RLJTS by:

```
10 PC = AMAX1 ( PV, PA )
   DV = AM *PV /R /TS
```

PV is used in the calculation of the density of the vapor, rather than PC because, if the vapor pressure PV is less than the ambient pressure, then only part of the vapor in the tank will be cargo vapor. It is the density of the cargo vapor in which we are interested, and by Dalton's law of partial pressures [3], the pressure relevant to a gas in a mixture of gases is that which each gas would exert if present alone. DV is used here to calculate the fraction of the cargo in vapor phase, and a slight error is introduced since the density of the mixture of cargo vapor and air (not the density of the cargo vapor) in the tank above the liquid is required. A relatively simple analysis will determine the desired density in terms of the amount of air drawn in to maintain atmospheric pressure.

ACCURACY ASSESSMENT

An accuracy assessment of the venting submodel is presented here with the help of two illustrative examples. The former is for the discharge of a liquid when the rupture in the enclosure is below the level of the liquid cargo and the later is for the venting of gaseous cargo when the rupture is above the level of the liquid cargo.

Example of Liquid Venting and Assessment of the Magnitude of Terms

We will compare the magnitude of the terms in equations (2-17) and (2-18) of the section on Errors and Inconsistencies for a specific example:

the venting of a tank holding 83 metric tons of LNG. The initial conditions and the properties of the cargo are approximated by:

$$M_{L_1} = 0.830 \times 10^8 \text{ g}$$

$$M_{g_1} \cong 0$$

$$T_1 = 122 \text{ °K}$$

$$\hat{\lambda} = 122 \text{ cal/g}$$

$$\hat{C}_L = 0.864 \text{ cal/(g °K)}$$

$$\hat{C}_{pg} = 0.50125 \text{ cal/(g °K)}$$

$$V_T = 0.2 \times 10^9 \text{ cm}^3$$

$$\rho_L = 0.415 \text{ g/cm}^3$$

$$R = 1.987 \text{ cal/(g-mole °K)}$$

$$\text{Molecular weight of methane} = 16 \qquad (2\text{-}23)$$

The mass of cargo in gas phase is taken to be only approximately equal to zero, since in practice it is impossible to fill a cargo tank completely with liquid. For the purposes of this analysis, this slight departure from realistic initial conditions is immaterial. For this analysis, it is assumed that the density of the liquid is independent of temperature and pressure.

Let state 2 be that state of the tank after 10 metric tons of liquid has escaped; thus $M_{L_2} \cong 0.730 \times 10^8$ g. The tank pressure will be the vapor pressure, which is a strong function of temperature. Thus, equations (2-17) and (2-18) contain the temperature implicitly in the pressure terms as well as explicitly. This makes solution of the energy equation for the temperature T_2 difficult to obtain in a straightforward manner. Instead, an iterative procedure is used. The vapor pressure for LNG is given by

$$\log_{10}(P_v) = 9.737 - 389.9/(T - 7.16)$$

where P_v is in dynes/cm^2 and T is in °K.

After several iterations one finds that AMSHAH's equation (2.10c) or (2-18) is satisfied by the following state:

$$
\begin{aligned}
T_2 &= 121.838\ ^\circ K \\
M_{L_2} &\cong 0.730 \times 10^8\ g \\
P_{T_2} &= 2.173 \times 10^6\ \text{dynes/cm}^2 \\
V_{g_2} &= V_T - \frac{M_{L_2}}{\rho_L} = 0.024096 \times 10^9\ \text{cm}^3 \\
\rho_{g_2} &= \frac{P_{T_2}}{RT_2} = 0.0034192\ \text{g/cm}^3 \\
M_{g_2} &\cong V_{g_2}\ \rho_{g_2} = 0.823 \times 10^5\ g
\end{aligned}
\qquad (2\text{-}24)
$$

where

$$
\begin{aligned}
P_{T_1}(T_1) &= P_V\ (122.0\ ^\circ K) = 2.19735 \times 10^6\ \text{dynes/cm}^2 \\
P_{T_2}(T_2) &= P_V\ (121.839\ ^\circ K) = 2.1731 \times 10^6\ \text{dynes/cm}^2
\end{aligned}
$$

and 1 atmosphere = 1.01324×10^6 dynes/cm^2.

The values of the various terms in AMSHAH's equation (2.10c) or equation (2-18) are:

$$
\begin{aligned}
(T_1-T_2)\ M_{g_2}\ \hat{C}_{pg} &= 0.00006641713 \times 10^8\ \text{cal} \\
(T_1-T_2)\ M_{L_2}\ \hat{C}_L &= 0.10154592 \times 10^8\ \text{cal} \\
\hat{\lambda}\ (M_{g_1}-M_{g_2}) &= 0.100406 \times 10^8\ \text{cal} \\
V_T\ (P_{T_1}-P_{T_2}) &= 0.00115490476 \times 10^8\ \text{cal}
\end{aligned}
\qquad (2\text{-}25)
$$

We see that the change in the internal energy of the gas in the tank is negligible, and that the pressure volume term is about one hundredth the size of the two largest terms.

To see if the values for state 2 given above satisfy the complete energy equation (2-17), we wish to substitute these values in (2-17). However, (2-17) contains explicit integrals. Let us use the average values for the arguments in these integrals; we then have

$$
\begin{aligned}
&0.5\ \hat{C}_L\ (M_{L_1}+M_{L_2})\ (T_1-T_2) + M_{g_2}\ \hat{C}_{pg}\ (T_1-T_2) + \hat{C}_{pg}\ T_1(M_{g_1}-M_{g_2}) \\
&+ \hat{\lambda}(M_{g_1}-M_{g_2}) = 0.5\ \hat{C}_L\ (T_1+T_2)\ (M_{g_1}-M_{g_2}) \\
&- \left\{ w_o \left[\frac{P_a}{\rho_L} + 0.5\ v_o^2 + Z_h\ g \right] \right\}_{av} (t_1-t_2) + P_{T_1} V_{g_1} - P_{T_2}\ V_{g_2}
\end{aligned}
\qquad (2\text{-}26)
$$

where the subscript av after the braces indicates that the quantity within is to be an average of the values at state 1 and state 2. t_2-t_1 is the

time it takes for the 10 metric tons of LNG to escape. For the values of state 2 given by (2-24), the values of the terms in (2-26) are:

$$\frac{\hat{C}_L}{2}\ (M_{L_1}+M_{L_2})\ (T_1-T_2) = 0.1090601 \cdot 10^8 \text{ cal}$$

$$M_{g_2}\ \hat{C}_{pg}\ (T_1-T_2) = 0.00006641712 \times 10^8 \text{ cal}$$

$$\hat{C}_{pg}\ T_1\ (M_{g_1}-M_{g_2}) = -0.0503285 \times 10^8 \text{ cal}$$

$$\hat{\lambda}\ (M_{g_1}-M_{g_2}) = -0.100406 \times 10^8 \text{ cal}$$

$$\frac{\hat{C}_L}{2}\ (T_1+T_2)\ (M_{g_1}-M_{g_2}) = -0.0866935 \times 10^8 \text{ cal}$$

$$\{ (-w_o) \left[\frac{P_a}{\rho_L} + 0.5\ v_o^2 + Z_h\ g\right] \}_{av} (t_1-t_2) = 0.00505268 \times 10^8 \text{ cal}$$

$$(P_{T_1}\ V_{g_1}-P_{T_2}\ V_{g_2}) = -0.0124539 \times 10^8 \text{ cal} \qquad (2\text{-}27)$$

If the above quantities are substituted in equation (2-26), the equation is not satisfied. This implies that the temperature calculated from AMSHAH equation (2.10c) is not correct.

To determine a temperature, T, which will satisfy (2-26), the iterative technique is used again. After several trials, it is found that a temperature of 121.916 °K satisfies (2-26). Thus, the values for state 2 which satisfy the complete energy equation are:

$$T_2 = 121.916 \text{ °K}$$

$$M_{L_2} = 0.730 \times 10^8 \text{ g}$$

$$P_{T_2} = 2.18447 \times 10^6 \text{ dynes/cm}^2$$

$$V_{g_2} = 0.024096 \times 10^9 \text{ cm}^3$$

$$\rho_{g_2} = 0.0034399 \text{ g/cm}^3$$

$$M_{g_2} = 0.8289 \times 10^5 \text{ g} \qquad (2\text{-}28)$$

The values for the terms in (2-26) using these new values for state 2 are:

$$\frac{\hat{C}_L}{2}\ (M_{L_1}+ M_{L_2})\ (T_1-T_2) = 0.0568115 \times 10^8 \text{ cal}$$

$$M_{g_2}\hat{C}_{pg}\ (T_1-T_2) = 0.000035025 \times 10^8 \text{ cal}$$

$$\hat{C}_{pg}\ T_1\ (M_{g_1}-M_{g_2}) = -0.0506888 \times 10^8 \text{ cal}$$

$$\hat{\lambda}\ (M_{g_1}-M_{g_2}) = -0.101124824 \times 10^8 \text{ cal}$$

$$\frac{\hat{C}_L}{2}\ (T_2+T_1)\ (M_{g_1}-M_{g_2}) = -0.08734166 \times 10^8 \text{ cal}$$

$$\left\{ (-w_o)\left[\frac{P_a}{\rho_L} + 0.5\ v_o^2 + Z_h\ g\right] \right\}_{av} (t_1-t_2) = 0.00507094 \times 10^8 \text{ cal}$$

$$(P_{T_1}\ V_{g_1}-P_{T_2}\ V_{g_2}) = -0.01253286 \times 10^8 \text{ cal}$$

(2-29)

The venting time, t_2-t_1, was found to be 6.03 seconds. We note that the largest term, which AMSHAH had correct, is the term involving the heat of vaporization. We refer the size of the other terms to this one. The only other term which AMSHAH had exactly as in (2-26) is the term giving the change in the internal energy of the gas, $M_{g_2}\hat{C}_{pg}\ (T_1-T_2)$, and we note that this term is negligible. For the first term in (2-29), AMSHAH used M_{L_2} instead of $0.5\ (M_{L_2}+ M_{L_1})$, and this term in about half the size of the largest term. The last term, which involves the pressure and gas volume and which AMSHAH had incorrect, is about one-tenth the size of the largest term. The remaining three terms do not appear in AMSHAH's equation (2.10c). While the outflow term is only about 0.5% of the largest term, the other two terms are more than half the size of the largest term. The $0.5\ \hat{C}_L\ (T_1+T_2)(M_{g_1}-M_{g_2})$, in fact, is about 87% of the largest term. Certainly it is not a valid approximation to ignore terms this large.

The value of T_2 found from (2.10c) was 121.839 °K while the value from the correct energy equation (2-26) was 121.916 °K. The temperature drop in the first case was .161 °K and in the second case was .084 °K. While the difference between the two temperatures is small, the error in the temperature change is nearly 100%.

Before leaving this example, the values calculated above will be used to show that the changes in the potential and kinetic energies are negligible with respect to the change in the internal energy. With Z_T = 500 cm and A_T = 4000,000 cm^2 we have, for the liquid phase

$$U_1 = M_{L_1} \hat{C}_L T_1 = 87.48 \times 10^8 \text{ cal}$$

$$U_2 = M_{L_2} \hat{C}_L T_2 = 76.846 \times 10^8 \text{ cal}$$

with

$$U_2 - U_1 = \hat{C}_L (M_{L_2} T_2 - M_{L_1} T_1) = 10.634 \times 10^8 \text{ cal} \quad \text{(change in internal energy)}$$

$$\Phi_1 = \frac{P_T A_T g Z_{s_1}^2}{2} = 484167 \text{ cal}$$

$$\Phi_2 = \frac{P_T A_T g Z_{s_2}^2}{2} = 374600 \text{ cal}$$

$$\Phi_2 - \Phi_1 = 109567 \text{ cal} = 0.00109657 \times 10^8 \text{ cal} \quad \text{(change in potential energy)}$$

It is obvious that the change in the potential energy is negligible since it is about 0.01% of the change in the internal energy. For the kinetic energy, the velocity of the liquid above the hole will be the same as the velocity of the liquid-gas interface:

$$v_{s_1} = \frac{w_{o_1}}{\rho_L A_T} = 10.0 \text{ cm/sec}$$

so

$$K_1 = 0.5 M_{L_1} v_{s_1}^2 = 98.8 \text{ cal}$$

It can be seen from previous calculations that the mass of liquid vaporized is less than 1% of the liquid that has vented. Therefore

$$v_{s_2} \approx \frac{w_{o_2}}{\rho_L A_T} = 9.83 \text{ cm/sec}$$

$$K_2 = 0.5 M_{L_2} v_{s_2}^2 = 83.97 \text{ cal}$$

$$K_1 - K_2 = 14.83 \text{ cal} \quad \text{(change in kinetic energy)}$$

Again, it is seen that the change in kinetic energy is insignificant with respect to the change in the internal energy. For the gas phase, it can be shown by similar calculations that the changes in kinetic and potential energy may be neglected with respect to the change in the internal energy in this case as well.

Example of Gas Venting and Assessment of Terms

For the comparison of the complete expression (2C-10) of Appendix 2C and (2.10b) from AMSHAH or equation (2-12), we will consider an example to assess the importance of the various terms in these equations. The same initial state as used above will be used here (equation 2-23). However, the loss of 10 metric tons of LNG results in too great a temperature change for some of our approximations to be valid when gas instead of liquid is being vented. In this case, therefore, we consider the case where state 2 corresponds to the initial state after the loss of one metric ton of cargo.

After a few iterations, it is found that AMSHAH equation (2.10b) or equation (2-12) is satisfied by a state 2 given by

$$T_2 = 120.263\ ^\circ K$$

$$M_{L_2} \cong 0.820 \times 10^8\ g$$

$$V_{g_2} = 0.024096 \times 10^8\ cm^3$$

$$P_{T_2} = 1.94845 \times 10^6\ dyne/cm^2$$

$$\rho_{g_2} = \frac{P_{T_2}}{RT_2} = 0.003105967\ g/cm^3$$

$$M_{g_2} = V_{g_2}\ \rho_{g_2} \cong 0.0000748425 \times 10^8\ g \qquad (2\text{-}30)$$

As before, the liquid mass does not include the small decrease caused by evaporation and is therefore an approximate value.

The values of the four terms in equation (2.10b) of AMSHAH are:

$$(T_1-T_2)\ M_{g_2}\ \hat{C}_{pg} = .0000651745 \times 10^8\ cal$$

$$(T_1-T_2)\ M_{L_2}\ \hat{C}_L = 1.23084 \times 10^8\ cal$$

$$\hat{\lambda}\ (M_{L_1}-M_{L_2}) = 1.22 \times 10^8\ cal$$

$$V_T\ (P_{T_1}-P_{T_2}) = 0.0118524\ cal \qquad (2\text{-}31)$$

and the temperature difference is 1.737 °K. It is clear that this equation is primarily a balance between the second and third terms. The first term is completely negligible and the fourth term is less than 1% the size of the two large terms.

The iterative procedure does not converge rapidly for equation (2C-10) as it has in the other cases because (2C-10) is a more complex equation than equation (2-12), and because the temperature change is much greater for gas venting than it is for liquid venting. After a few iterations a temperature of 120.759 was used to calculate P_2, ρ_{g_2}, M_{g_2} and V_{g_2}, and with these quantities equation (2C-10) was solved for a temperature of 120.787. This is sufficiently close for our purposes. We may use the average of these two temperatures to define a satisfactory state 2.

$$T_2 = 120.773\ ^\circ K$$

$$M_{L_2} = 0.820 \times 10^8\ g$$

$$P_{T_2} = 2.017155 \times 10^6\ dynes/cm^2$$

$$V_{g_2} = 0.0240964 \times 10^8\ cm^3$$

$$\rho_{g_2} = \frac{P_{T_2}}{RT_2}\ .003202278\ g$$

$$M_{g_2} = .0000771633 \times 10^8\ g/cm^3 \qquad (2\text{-}32)$$

The value of $\hat{C}_{vg}$ is needed in (2C-10) and since $\hat{C}_{pg}/\hat{C}_{vg} = 1.305$, $\hat{C}_{vg} = 0.3841\ cal/(g\ ^\circ K)$. The values of the terms in (2C-10) are:

$$M_{L_2}\ \hat{C}_L\ (T_1-T_2) = 0.8795 \times 10^8\ cal$$

$$\hat{C}_L\ T_1\ (M_{L_1}-M_{L_2}) = 1.0541 \times 10^8\ cal$$

$$0.5\ (M_{g_1}+M_{g_2})\ \hat{C}_{pg}\ (T_1-T_2) = 0.000024 \times 10^8\ cal$$

$$-0.5\ (M_{g_1}+M_{g_2})\ R\ (T_1-T_2) = -0.0000059 \times 10^8\ cal$$

$$0.5\ (T_1+T_2)\ \hat{C}_{vg}\ (M_{L_1}-M_{L_2}) = 0.4466 \times 10^8\ cal$$

$$\hat{\lambda}\ (M_{L_1}-M_{L_2}) = 1.2200 \times 10^8\ cal$$

$$\left\{ w_o \left[\frac{P_a}{\rho_{ga}} + \frac{1}{2} v_o^2 + g\ Z_h\right] \right\}_{av} (t_1-t_2) = -0.2474 \times 10^8\ cal \qquad (2\text{-}33)$$

In assessing these values it is noted that the first and sixth terms in this list are identical to terms in AMSHAH's equation (2.10b). These are both large terms. The third term above is very similar to a term in (2.10b), but this term is negligible. The fourth term in this list partially corresponds to the volume-pressure term in (2.10b), and this term is negligible as well. The second, fifth, and seventh terms in the list are omitted entirely from (2.10b). It is obvious that all three of these terms are larger than two of the terms which AMSHAH kept, and that all three of these terms are 20% or more of the magnitude of the largest term. The second term, in fact, is the second largest term and is about 80% as large as the largest term.

The temperature difference when state 2 is determined from the complete energy equation is 1.227 °K, compared with a temperature difference of 1.737 using AMSHAH's equation (2.10b). The error in using AMSHAH's equation is about 0.5 °K, or about 42%. The error is much larger in terms of degrees, here, than it is in the liquid venting example, and after a large number of steps is likely to be 10 °K or more in magnitude. In our example, AMSHAH's equation overestimated the temperature drop. This means that the temperature calculated from their equation will be less than it should be. Since the gas venting will cease when the vapor pressure drops to the ambient pressure, the use of AMSHAH's equation may seriously underestimate the amount of gas which escapes from the tank.

SENSITIVITY ANALYSIS

The sensitivity analysis of the tank venting submodel has been done for five cargoes: liquified natural gas (LNG), liquid chlorine (CL_2), liquid anhydrous ammonia (NH_3) methyl alcohol (MAL), and gasoline (GAS). For each cargo, both adiabatic and isothermal tank conditions have been used. The results are contained in tables 2-1a through 2-10b

Table 2-1a will be explained in detail as an example. The first line of the table gives the cargo in the tank, and whether the tank conditions are adiabatic or isothermal. The second line describes the output quantity used and the normal value of this quantity. Two output quantities have been used in this analysis: the total mass released and the average flow rate. The word "normal" here refers to the initial or unchanged value. To do the sensitivity analysis, normal values are selected for the variables and parameters needed to run the submodel. Those items called variables are those which the user of the model will usually select, such as tank volume. Those items which are defined to be parameters are those which the user does not ordinarily control. The parameters may be properties of the cargo such as the molecular weight which are determined once the cargo is known, or they may be quantities which are usually defined within the computer program, such as the discharge coefficient or the number of increments to be used in the numerical integration.

With the normal values of the variables and parameters specified, the model is run with these input values, and the normal output values are computed and recorded. Next the changed output values are computed. These output values are computed by changing each variable and then each parameter in turn to a changed value. The changed value is the normal value plus 5% of some reference value. For the parameters, the reference value is the absolute value of the normal value of the parameter. For the variables, the reference value is often but not always the normal value. Since the hole height could be zero, for example, the tank height has been taken as the reference value.

TABLE 2-1a Results for LNG Venting - Isothermal Case

OUTPUT IS TOTAL MASS RELEASED NORMAL VALUE IS .738E+08

INDEX	VARIABLE	SENS COEFF	V NORMAL	REFERENCE	V CHANGED	OUTPUT	FRACTION
1	INITL TEMP	.000	128.	283.	142.	.738E+08	1.000
2	INITL MASS	1.075	.746E+08	.802E+08	.786E+08	.778E+08	1.054
3	VOLUME	.000	.200E+09	.200E+09	.210E+09	.738E+08	1.000
4	TNK HEIGHT	.000	585.	585.	614.	.738E+08	1.000
5	HOL HEIGHT	.000	175.	585.	205.	.738E+08	1.000
6	HOLE DIAM	.000	58.5	58.5	61.4	.738E+08	1.000

INDEX	PARAMETER	SENS COEFF	P NORMAL	P CHANGED	OUTPUT	FRACTION
1	MOLEC WT	.000	16.0	16.8	.738E+08	1.000
2	CPG EQN C1	.000	.263E-01	.276E-01	.738E+08	1.000
3	CPG EQN C2	.000	.382E-02	.402E-02	.738E+08	1.000
4	CPG EQN C3	.000	-.723E-05	-.687E-05	.738E+08	1.000
5	CPG EQN C4	.000	.0	.0	.738E+08	1.000
6	CPL EQN C1	.000	.249E+04	.262E+04	.738E+08	1.000
7	CPL EQN C2	.000	9.21	9.67	.738E+08	1.000
8	VAP PR C1	.000	8.74	9.17	.738E+08	1.000
9	VAP PR C2	.000	390.	409.	.738E+08	1.000
10	VAP PR C3	.000	-7.16	-6.80	.738E+08	1.000
11	LIQ DEN C1	.000	580.	609.	.738E+08	1.000
12	LIQ DEN C2	.000	-1.40	-1.33	.738E+08	1.000
13	LIQ DEN C3	.000	.0	.0	.738E+08	1.000
14	HEAT VAPOR	.000	.510E+06	.535E+06	.738E+08	1.000
15	DISCH COEF	.000	.800	.840	.738E+08	1.000
16	NUMBR INCR	.010	100.	105.	.739E+08	1.000

TABLE 2-1b Results for LNG Venting - Isothermal Case

OUTPUT IS AVERAGE FLOW RATE NORMAL VALUE IS .496E+06

INDEX	VARIABLE	SENS COEFF	V NORMAL	REFERENCE	V CHANGED	OUTPUT	FRACTION
1	INITL TEMP	-0.128	128.	283.	142.	.995E+06	2.006
2	INITL MASS	1.107	.746E+08	.802E+08	.786E+08	.523E+06	1.053
3	VOLUME	-.516	.200E+09	.200E+09	.210E+09	.483E+06	.974
4	INK HEIGHT	1.091	565.	585.	614.	.523E+06	1.055
5	FUL HEIGHT	-2.280	175.	585.	205.	.439E+06	.886
6	HOLE DIAM	2.050	58.5	58.5	61.4	.547E+06	1.103

INDEX	PARAMETER	SENS COEFF	P NORMAL	P CHANGED	OUTPUT	FRACTION
1	MOLEC WT	.331	16.0	16.8	.504E+06	1.017
2	CPG EQN C1	-.005	.263E-01	.276E-01	.496E+06	1.000
3	CPG EQN C2	-.155	.382E-02	.402E-02	.492E+06	.992
4	CPG EQN C3	-.077	-.723E-05	-.687E-05	.494E+06	.996
5	CPG EQN C4	.000	.0	.0	.496E+06	1.000
6	CPL EQN C1	.000	.249E+04	.262E+04	.496E+06	1.000
7	CPL EQN C2	.000	9.21	9.67	.496E+06	1.000
8	VAP PR C1	28.428	8.74	9.17	.120E+07	2.421
9	VAP PR C2	-5.637	390.	409.	.356E+06	.718
10	VAP PR C3	.421	-7.16	-6.80	.506E+06	1.021
11	LIQ DEN C1	-.913	580.	609.	.473E+06	.954
12	LIQ DEN C2	.025	-1.40	-1.33	.496E+06	1.001
13	LIQ DEN C3	.000	.0	.0	.496E+06	1.000
14	HEAT VAPOR	.000	.510E+06	.535E+06	.496E+06	1.000
15	DISCH COEF	1.000	.800	.840	.520E+06	1.050
16	NUMBR INCR	.299	100.	105.	.503E+06	1.015

TABLE 2-2a Results for LNG Venting - Adiabatic Case

OUTPUT IS TOTAL MASS RELEASED NORMAL VALUE IS .537E+08

INDEX	VARIABLE	SENS COEFF	V NORMAL	REFERENCE	V CHANGED	OUTPUT	FRACTION
1	INITL TEMP	1.944	128.	283.	142.	.589E+08	1.097
2	INITL MASS	1.661	.746E+08	.802E+08	.786E+08	.582E+08	1.083
3	VOLUME	-.278	.200E+09	.200E+09	.210E+09	.530E+08	.986
4	LA HEIGHT	.556	585.	585.	614.	.552E+08	1.027
5	MOL HEIGHT	-1.111	175.	585.	205.	.507E+08	.944
6	HOLE DIAM	.000	58.5	58.5	61.4	.537E+08	1.000

INDEX	PARAMETER	SENS COEFF	P NORMAL	P CHANGED	OUTPUT	FRACTION
1	MOLEC WT	.000	16.0	16.8	.537E+08	1.000
2	CPG EQN C1	.000	.263E-01	.276E-01	.537E+08	1.000
3	CPG EQN C2	.000	.382E-02	.402E-02	.537E+08	1.000
4	CPG EQN C3	.000	-.723E-05	-.687E-05	.537E+08	1.000
5	CPG EQN C4	.000	.0	.0	.537E+08	1.000
6	CPL EQN C1	.000	.249E+04	.262E+04	.537E+08	1.000
7	CPL EQN C2	.000	9.21	9.67	.537E+08	1.000
8	VAP PR C1	.833	8.74	9.17	.559E+08	1.042
9	VAP PR C2	-.278	390.	409.	.530E+08	.986
10	VAP PR C3	.000	-7.16	-6.80	.537E+08	1.000
11	LIQ DEN C1	-.556	580.	609.	.522E+08	.972
12	LIQ DEN C2	.000	-1.40	-1.33	.537E+08	1.000
13	LIQ DEN C3	.000	.0	.0	.537E+08	1.000
14	HEAT VAPOR	-.278	.510E+06	.535E+06	.530E+08	.986
15	DISCH COEF	.000	.800	.840	.537E+08	1.000
16	NUMBR INCR	.106	100.	105.	.540E+08	1.005

TABLE 2-2b Results for LNG Venting - Adiabatic Case

OUTPUT IS AVERAGE FLOW RATE NORMAL VALUE IS .934E+06

INDEX	VARIABLE	SENS COEFF	V NORMAL	REFERENCE	V CHANGED	OUTPUT	FRACTION
1	INITL TEMP	-2.465	128.	283.	142.	.819E+06	.877
2	INITL MASS	-1.620	.746E+08	.802E+08	.786E+08	.859E+06	.919
3	VOLUME	.431	.200E+09	.200E+09	.210E+09	.954E+06	1.022
4	INK HEIGHT	-1.366	585.	585.	614.	.871E+06	.932
5	HOL HEIGHT	-3.311	175.	585.	205.	.780E+06	.834
6	HOLE DIAM	2.050	58.5	58.5	61.4	.103E+07	1.102

INDEX	PARAMETER	SENS COEFF	P NORMAL	P CHANGED	OUTPUT	FRACTION
1	MOLEC WT	.096	16.0	16.8	.939E+06	1.005
2	CPG EQN C1	-.048	.263E-01	.276E-01	.932E+06	.998
3	CPG EQN C2	-2.597	.382E-02	.402E-02	.813E+06	.870
4	CPG EQN C3	-.923	-.723E-05	-.687E-05	.891E+06	.954
5	CPG EQN C4	.000	.0	.0	.934E+06	1.000
6	CPL EQN C1	1.393	.249E+04	.262E+04	.999E+06	1.070
7	CPL EQN C2	.726	9.21	9.67	.968E+06	1.036
8	VAP PR C1	3.565	8.74	9.17	.110E+07	1.178
9	VAP PR C2	.670	390.	409.	.966E+06	1.034
10	VAP PR C3	.676	-7.16	-6.80	.966E+06	1.034
11	LIQ DEN C1	.989	580.	609.	.981E+06	1.049
12	LIQ DEN C2	.129	-1.40	-1.33	.940E+06	1.006
13	LIQ DEN C3	.000	.0	.0	.934E+06	1.000
14	HEAT VAPOR	4.349	.510E+06	.535E+06	.114E+07	1.217
15	DISCH COEF	1.000	.800	.840	.981E+06	1.050
16	NUMBR INCR	1.287	100.	105.	.994E+06	1.064

TABLE 2-3a Results for Cl_2 Venting - Isothermal Case

OUTPUT IS TOTAL MASS RELEASED NORMAL VALUE IS .140E+08

INDEX	VARIABLE	SENS COEFF	V NORMAL	REFERENCE	V CHANGED	OUTPUT	FRACTION
1	INITL TEMP	-.000	248.	283.	262.	.140E+08	1.000
2	INITL MASS	1.075	.142E+08	.152E+08	.149E+08	.148E+08	1.054
3	VOLUME	.000	.100E+08	.100E+08	.105E+08	.140E+08	1.000
4	TNK HEIGHT	-.000	215.	215.	226.	.140E+08	1.000
5	HOL HEIGHT	.000	64.6	215.	75.4	.140E+08	1.000
6	HOLE DIAM	.000	21.5	21.5	22.6	.140E+08	1.000

INDEX	PARAMETER	SENS COEFF	P NORMAL	P CHANGED	OUTPUT	FRACTION
1	MOLEC WT	.000	71.0	74.5	.140E+08	1.000
2	CPG EQN C1	.000	.267E+05	.281E+05	.140E+08	1.000
3	CPG EQN C2	.000	32.4	34.0	.140E+08	1.000
4	CPG EQN C3	.000	-.272E-01	-.286E-01	.140E+08	1.000
5	CPG EQN C4	.000	.0	.0	.140E+08	1.000
6	CPL EQN C1	.000	-69.4	-65.9	.140E+08	1.000
7	CPL EQN C2	.000	2.09	2.20	.140E+08	1.000
8	VAP PR C1	.000	9.54	10.0	.140E+08	1.000
9	VAP PR C2	-6.465	.109E+04	.114E+04	.950E+07	.677
10	VAP PR C3	.000	.400E-01	.420E-01	.140E+08	1.000
11	LIQ DEN C1	.000	.217E+04	.228E+04	.140E+08	1.000
12	LIQ DEN C2	.000	-2.60	-2.47	.140E+08	1.000
13	LIQ DEN C3	.000	.0	.0	.140E+08	1.000
14	HEAT VAPOR	.000	.288E+06	.302E+06	.140E+08	1.000
15	DISCH COEF	.000	.800	.840	.140E+08	1.000
16	NUMBR INCR	.010	100.	105.	.140E+08	1.000

TABLE 2-3b Results for CL_2 Venting - Isothermal Case

OUTPUT IS AVERAGE FLOW RATE NORMAL VALUE IS .468E+05

INDEX	VARIABLE	SENS COEFF	V NORMAL	REFERENCE	V CHANGED	OUTPUT	FRACTION
1	INITL TEMP	16.222	248.	283.	262.	.848E+05	1.811
2	INITL MASS	1.209	.142E+08	.152E+08	.149E+08	.497E+05	1.060
3	VOLUME	-1.077	.100E+08	.100E+08	.105E+08	.443E+05	.946
4	TNK HEIGHT	1.207	215.	215.	226.	.497E+05	1.060
5	HOL HEIGHT	-2.483	64.6	215.	75.4	.410E+05	.876
6	HOLE DIAM	2.050	21.5	21.5	22.6	.516E+05	1.103

INDEX	PARAMETER	SENS COEFF	P NORMAL	P CHANGED	OUTPUT	FRACTION
1	MOLEC WT	.450	71.0	74.5	.479E+05	1.023
2	CPG EQN C1	-.050	.267E+05	.281E+05	.467E+05	.998
3	CPG EQN C2	-.016	32.4	34.0	.468E+05	.999
4	CPG EQN C3	-.003	-.272E-01	-.258E-01	.468E+05	1.000
5	CPG EQN C4	.000	.0	.0	.468E+05	1.000
6	CPL EQN C1	.000	-69.4	-65.9	.468E+05	1.000
7	CPL EQN C2	.000	2.09	2.20	.468E+05	1.000
8	VAP PR C1	40.263	9.54	10.0	.141E+06	3.013
9	VAP PR C2	35.559	.109E+04	.114E+04	.125E+06	2.678
10	VAP PR C3	.002	.400E-01	.420E-01	.468E+05	1.000
11	LIQ DEN C1	-1.023	.217E+04	.228E+04	.444E+05	.949
12	LIQ DEN C2	-.533	-2.60	-2.47	.456E+05	.973
13	LIQ DEN C3	.000	.0	.0	.468E+05	1.000
14	HEAT VAPOR	.000	.286E+06	.302E+06	.468E+05	1.000
15	DISCH COEF	1.000	.800	.840	.492E+05	1.050
16	NUMBR INCR	-.229	100.	105.	.463E+05	.989

TABLE 2-4a Results for CL_2 Venting - Adiabatic Case

OUTPUT IS TOTAL MASS RELEASED NORMAL VALUE IS .950E+07

INDEX	VARIABLE	SENS COEFF	V NORMAL	REFERENCE	V CHANGED	OUTPUT	FRACTION
1	INITL TEMP	.597	248.	283.	262.	.978E+07	1.030
2	INITL MASS	1.704	.142E+08	.152E+08	.149E+08	.103E+08	1.085
3	VOLUME	-.597	.100E+08	.100E+08	.105E+08	.922E+07	.970
4	TNK HEIGHT	.59.	215.	215.	226.	.978E+07	1.030
5	HOL HEIGHT	-1.493	64.6	215.	75.4	.879E+07	.925
6	HOLE DIAM	.000	21.5	21.5	22.6	.950E+07	1.000

INDEX	PARAMETER	SENS COEFF	P NORMAL	P CHANGED	OUTPUT	FRACTION
1	MOLEC WT	.000	71.0	74.5	.950E+07	1.000
2	CPG EQN C1	.000	.267E+05	.281E+05	.950E+07	1.000
3	CPG EQN C2	.000	32.4	34.0	.950E+07	1.000
4	CPG EQN C3	.000	-.272E-01	-.258E-01	.950E+07	1.000
5	CPG EQN C4	.000	.0	.0	.950E+07	1.000
6	CPL EQN C1	.000	-69.4	-65.9	.950E+07	1.000
7	CPL EQN C2	.000	2.09	2.20	.950E+07	1.000
8	VAP PR C1	.299	9.54	10.0	.964E+07	1.015
9	VAP PR C2	.000	.109E+04	.114E+04	.950E+07	1.000
10	VAP PR C3	.000	.400E-01	.420E-01	.950E+07	1.000
11	LIQ DEN C1	-.597	.217E+04	.228E+04	.922E+07	.970
12	LIQ DEN C2	-.299	-2.60	-2.47	.936E+07	.985
13	LIQ DEN C3	.000	.0	.0	.950E+07	1.000
14	HEAT VAPOR	.000	.288E+06	.302E+06	.950E+07	1.000
15	DISCH COEF	.000	.800	.840	.950E+07	1.000
16	NUMBR INCR	-.100	100.	105.	.945E+07	.995

TABLE 2-4b Results for CL_2 Venting - Adiabatic Case

OUTPUT IS AVERAGE FLOW RATE NORMAL VALUE IS .357E+06

INDEX	VARIABLE	SENS COEFF	V NORMAL	REFERENCE	V CHANGED	OUTPUT	FRACTION
1	INITL TEMP	13.778	248.	283.	262.	.603E+06	1.689
2	INITL MASS	.064	.142E+08	.152E+08	.149E+08	.358E+06	1.003
3	VOLUME	-.052	.100E+08	.100E+08	.105E+08	.356E+06	.997
4	TNK HEIGHT	.056	215.	215.	226.	.356E+06	1.003
5	HOL HEIGHT	-.023	64.6	215.	75.4	.357E+06	.999
6	HOLE DIAM	2.050	21.5	21.5	22.6	.394E+06	1.1

INDEX	PARAMETER	SENS COEFF	P NORMAL	P CHANGED	OUTPUT	FRACTION
1	MOLEC WT	-.038	71.0	74.5	.356E+06	.998
2	CPG EQN C1	-.020	.267E+05	.281E+05	.357E+06	.999
3	CPG EQN C2	-.006	32.4	34.0	.357E+06	1.000
4	CPG EQN C3	-.001	-.272E-01	-.258E-01	.357E+06	1.000
5	CPG EQN C4	.000	.0	.0	.357E+06	1.000
6	CPL EQN C1	.013	-69.4	-65.9	.357E+06	1.001
7	CPL EQN C2	.094	2.09	2.20	.359E+06	1.005
8	VAP PR C1	28.994	9.54	10.0	.874E+06	2.450
9	VAP PR C2	-12.969	.109E+04	.114E+04	.125E+06	.352
10	VAP PR C3	.002	.400E-01	.420E-01	.357E+06	1.000
11	LIQ DEN C1	.772	.217E+04	.228E+04	.371E+06	1.039
12	LIQ DEN C2	.260	-2.60	-2.47	.362E+06	1.013
13	LIQ DEN C3	.000	.0	.0	.357E+06	1.000
14	HEAT VAPOR	-.061	.288E+06	.302E+06	.356E+06	.997
15	DISCH COEF	1.000	.800	.840	.375E+06	1.050
16	NUMBR INCR	.021	100.	105.	.357E+06	1.001

TABLE 2-5a Results for NH_3 Venting - Isothermal Case

OUTPUT IS TOTAL MASS RELEASED NORMAL VALUE IS .173E+09

INDEX	VARIABLE	SENS COEFF	V NORMAL	REFERENCE	V CHANGED	OUTPUT	FRACTION
1	INITL TEMP	.000	283.	283.	297.	.173E+09	1.000
2	INITL MASS	1.075	.174E+09	.187E+09	.184E+09	.182E+09	1.054
3	VOLUME	.000	.300E+09	.300E+09	.315E+09	.173E+09	1.000
4	TNK HEIGHT	.000	669.	669.	703.	.173E+09	1.000
5	HOL HEIGHT	.000	201.	669.	234.	.173E+09	1.000
6	HOLE DIAM	.000	66.9	66.9	70.3	.173E+09	1.000

INDEX	PARAMETER	SENS COEFF	P NORMAL	P CHANGED	OUTPUT	FRACTION
1	MOLEC WT	.000	17.0	17.8	.173E+09	1.000
2	CPG EQN C1	.000	.273E+05	.287E+05	.173E+09	1.000
3	CPG EQN C2	.000	23.9	25.1	.173E+09	1.000
4	CPG EQN C3	.000	.172E-01	.180E-01	.173E+09	1.000
5	CPG EQN C4	.000	.117E-04	.123E-04	.173E+09	1.000
6	CPL EQN C1	.000	.346E+04	.364E+04	.173E+09	1.000
7	CPL EQN C2	.000	4.19	4.40	.173E+09	1.000
8	VAP PR C1	.000	10.0	10.5	.173E+09	1.000
9	VAP PR C2	.000	.121E+04	.127E+04	.173E+09	1.000
10	VAP PR C3	.000	.0	.0	.173E+09	1.000
11	LIQ DEN C1	.000	-20.7	-19.6	.173E+09	1.000
12	LIQ DEN C2	.000	6.13	6.44	.173E+09	1.000
13	LIQ DEN C3	.000	-.136E-01	-.129E-01	.173E+09	1.000
14	HEAT VAPOR	.000	.137E+07	.144E+07	.173E+09	1.000
15	DISCH COEF	.000	.800	.840	.173E+09	1.000
16	NUMBR INCR	.010	100.	105.	.173E+09	1.000

TABLE 2-5b Results for NH_3 Venting - Isothermal Case

OUTPUT IS AVERAGE FLOW RATE NORMAL VALUE IS .893E+06

INDEX	VARIABLE	SENS COEFF	V NORMAL	REFERENCE	V CHANGED	OUTPUT	FRACTION
1	INITL TEMP	11.326	283.	283.	297.	.140E+07	1.566
2	INITL MASS	.582	.174E+09	.187E+09	.184E+09	.919E+06	1.029
3	VOLUME	-1.069	.300E+09	.300E+09	.315E+09	.846E+06	.947
4	INK HEIGHT	.582	669.	669.	703.	.919E+06	1.029
5	HOL HEIGHT	-2.895	201.	669.	234.	.764E+06	.855
6	HOLE DIAM	2.050	66.9	66.9	70.3	.985E+06	1.102

INDEX	PARAMETER	SENS COEFF	P NORMAL	P CHANGED	OUTPUT	FRACTION
1	MOLEC WT	.450	17.0	17.8	.913E+06	1.023
2	CPG EQN C1	-.073	.273E+05	.287E+05	.890E+06	.996
3	CPG EQN C2	-.019	23.9	25.1	.892E+06	.999
4	CPG EQN C3	-.004	.172E-01	.180E-01	.893E+06	1.000
5	CPG EQN C4	.000	.117E-04	.123E-04	.893E+06	1.000
6	CPL EQN C1	.000	.346E+04	.364E+04	.893E+06	1.000
7	CPL EQN C2	.000	4.19	4.40	.893E+06	1.000
8	VAP PR C1	37.433	10.0	10.5	.257E+07	2.872
9	VAP PR C2	-7.573	.121E+04	.127E+04	.555E+06	.621
10	VAP PR C3	.000	.0	.0	.893E+06	1.000
11	LIQ DEN C1	.001	-20.7	-19.6	.893E+06	1.000
12	LIQ DEN C2	-2.394	6.13	6.44	.786E+06	.880
13	LIQ DEN C3	-1.502	-.136E-01	-.129E-01	.826E+06	.925
14	HEAT VAPOR	.000	.137E+07	.144E+07	.893E+06	1.000
15	DISCH COEF	1.000	.800	.840	.938E+06	1.050
16	NUMBR INCR	-.229	100.	105.	.883E+06	.989

TABLE 2-6a Results for NH_3 Venting - Adiabatic Case

OUTPUT IS TOTAL MASS RELEASED NORMAL VALUE IS .132E+09

INDEX	VARIABLE	SENS COEFF	V NORMAL	REFERENCE	V CHANGED	OUTPUT	FRACTION
1	INITL TEMP	1.053	283.	283.	297.	.139E+09	1.053
2	INITL MASS	1.353	.174E+09	.187E+09	.184E+09	.141E+09	1.066
3	VOLUME	-.263	.300E+09	.300E+09	.315E+09	.131E+09	.987
4	TNK HEIGHT	.263	669.	669.	703.	.134E+09	1.013
5	HOL HEIGHT	-1.053	201.	669.	234.	.125E+09	.947
6	HOLE DIAM	.000	66.9	66.9	70.3	.132E+09	1.000

INDEX	PARAMETER	SENS COEFF	P NORMAL	P CHANGED	OUTPUT	FRACTION
1	MOLEC WT	.000	17.0	17.8	.132E+09	1.000
2	CPG EQN C1	.000	.273E+05	.287E+05	.132E+09	1.000
3	CPG EQN C2	.000	23.9	25.1	.132E+09	1.000
4	CPG EQN C3	.000	.172E-01	.180E-01	.132E+09	1.000
5	CPG EQN C4	.000	.117E-04	.123E-04	.132E+09	1.000
6	CPL EQN C1	.263	.346E+04	.364E+04	.134E+09	1.013
7	CPL EQN C2	.000	4.19	4.40	.132E+09	1.000
8	VAP PR C1	.789	10.0	10.5	.136E+09	1.039
9	VAP PR C2	-.526	.121E+04	.127E+04	.129E+09	.974
10	VAP PR C3	.000	.0	.0	.132E+09	1.000
11	LIQ DEN C1	.000	-20.7	-19.6	.132E+09	1.000
12	LIQ DEN C2	-.789	6.13	6.44	.127E+09	.961
13	LIQ DEN C3	-.526	-.136E-01	-.129E-01	.129E+09	.974
14	HEAT VAPOR	-.263	.137E+07	.144E+07	.131E+09	.987
15	DISCH COEF	.000	.800	.840	.132E+09	1.000
16	NUMBR INCR	.050	100.	105.	.133E+09	1.003

TABLE 2-6b Results for NH_3 Venting - Adiabatic Case

OUTPUT IS AVERAGE FLOW RATE NORMAL VALUE IS .105E+07

INDEX	VARIABLE	SENS COEFF	V NORMAL	REFERENCE	V CHANGED	OUTPUT	FRACTION
1	INITL TEMP	-.457	283.	283.	297.	.103E+07	.977
2	INITL MASS	-1.012	.174E+09	.187E+09	.184E+09	.100E+07	.949
3	VOLUME	-3.768	.300E+09	.300E+09	.315E+09	.856E+06	.812
4	TNK HEIGHT	-.912	669.	669.	703.	.101E+07	.954
5	HOL HEIGHT	-5.264	201.	669.	234.	.777E+06	.737
6	HOLE DIAM	2.050	66.9	66.9	70.3	.116E+07	1.102

INDEX	PARAMETER	SENS COEFF	P NORMAL	P CHANGED	OUTPUT	FRACTION
1	MOLEC WT	1.413	17.0	17.8	.113E+07	1.071
2	CPG EQN C1	-1.196	.273E+05	.287E+05	.991E+06	.940
3	CPG EQN C2	-.276	23.9	25.1	.104E+07	.986
4	CPG EQN C3	-.055	.172E-01	.180E-01	.105E+07	.997
5	CPG EQN C4	.000	.117E-04	.123E-04	.105E+07	1.000
6	CPL EQN C1	-1.689	.346E+04	.364E+04	.965E+06	.916
7	CPL EQN C2	1.039	4.19	4.40	.111E+07	1.052
8	VAP PR C1	5.821	10.0	10.5	.136E+07	1.291
9	VAP PR C2	-1.993	.121E+04	.127E+04	.949E+06	.900
10	VAP PR C3	.000	.0	.0	.105E+07	1.000
11	LIQ DEN C1	.005	-20.7	-19.6	.105E+07	1.000
12	LIQ DEN C2	-6.137	6.13	6.44	.731E+06	.693
13	LIQ DEN C3	-2.662	-.136E-01	-.129E-01	.914E+06	.867
14	HEAT VAPOR	2.623	.137E+07	.144E+07	.119E+07	1.131
15	DISCH COEF	1.000	.800	.840	.111E+07	1.050
16	NUMBR INCR	-2.897	100.	105.	.902E+06	.855

TABLE 2-7a Results for MAL Venting - Isothermal Case

OUTPUT IS TOTAL MASS RELEASED NORMAL VALUE IS .595E+08

INDEX	VARIABLE	SENS COEFF	V NORMAL	REFERENCE	V CHANGED	OUTPUT	FRACTION
1	INITL TEMP	.299	288.	283.	302.	.604E+08	1.015
2	INITL MASS	1.704	.888E+08	.955E+08	.936E+08	.646E+08	1.085
3	VOLUME	-.299	.120E+09	.120E+09	.126E+09	.586E+08	.985
4	TNK HEIGHT	.597	493.	493.	518.	.613E+08	1.030
5	HOL HEIGHT	-1.493	148.	493.	173.	.551E+08	.925
6	HOLE DIAM	.000	49.3	49.3	51.8	.595E+08	1.000

INDEX	PARAMETER	SENS COEFF	P NORMAL	P CHANGED	OUTPUT	FRACTION
1	MOLEC WT	.000	32.0	33.6	.595E+08	1.000
2	CPG EQN C1	.000	.164E+06	.173E+06	.595E+08	1.000
3	CPG EQN C2	.000	74.1	77.8	.595E+08	1.000
4	CPG EQN C3	.000	.335E-01	.352E-01	.595E+08	1.000
5	CPG EQN C4	.000	.0	.0	.595E+08	1.000
6	CPL EQN C1	.000	-.146E+04	-.138E+04	.595E+08	1.000
7	CPL EQN C2	.000	13.4	14.1	.595E+08	1.000
8	VAP PR C1	.000	10.9	11.5	.595E+08	1.000
9	VAP PR C2	.000	.200E+04	.210E+04	.595E+08	1.000
10	VAP PR C3	.000	.400E-01	.420E-01	.595E+08	1.000
11	LIQ DEN C1	-.597	.106E+04	.111E+04	.577E+08	.970
12	LIQ DEN C2	.000	-.920	-.874	.595E+08	1.000
13	LIQ DEN C3	.000	.0	.0	.595E+08	1.000
14	HEAT VAPOR	.000	.110E+07	.115E+07	.595E+08	1.000
15	DISCH COEF	.000	.800	.840	.595E+08	1.000
16	NUMBR INCR	.185	100.	105.	.601E+08	1.009

TABLE 2-7b Results for MAL Venting - Isothermal Case

OUTPUT IS AVERAGE FLOW RATE NORMAL VALUE IS .524E+06

INDEX	VARIABLE	SENS COEFF	V NORMAL	REFERENCE	V CHANGED	OUTPUT	FRACTION
1	INITL TEMP	-.878	288.	283.	302.	.501E+06	.956
2	INITL MASS	.211	.888E+08	.955E+08	.936E+08	.530E+06	1.011
3	VOLUME	-1.797	.120E+09	.120E+09	.126E+09	.477E+06	.910
4	TNK HEIGHT	-.061	493.	493.	518.	.523E+06	.997
5	HOL HEIGHT	-1.304	148.	493.	173.	.490E+06	.933
6	HOLE DIAM	2.050	49.3	49.3	51.8	.578E+06	1.102

INDEX	PARAMETER	SENS COEFF	P NORMAL	P CHANGED	OUTPUT	FRACTION
1	MOLEC WT	-.001	32.0	33.6	.524E+06	1.000
2	CPG EQN C1	.000	.164E+06	.173E+06	.524E+06	1.000
3	CPG EQN C2	.000	74.1	77.8	.524E+06	1.000
4	CPG EQN C3	.000	.335E-01	.352E-01	.524E+06	1.000
5	CPG EQN C4	.000	.0	.0	.524E+06	1.000
6	CPL EQN C1	.000	-.146E+04	-.138E+04	.524E+06	1.000
7	CPL EQN C2	.000	13.4	14.1	.524E+06	1.000
8	VAP PR C1	-.040	10.9	11.5	.523E+06	.998
9	VAP PR C2	.009	.200E+04	.210E+04	.524E+06	1.000
10	VAP PR C3	-.000	.400E-01	.420E-01	.524E+06	1.000
11	LIQ DEN C1	.145	.106E+04	.111E+04	.528E+06	1.007
12	LIQ DEN C2	-.829	-.920	-.874	.502E+06	.959
13	LIQ DEN C3	.000	.0	.0	.524E+06	1.000
14	HEAT VAPOR	.000	.110E+07	.115E+07	.524E+06	1.000
15	DISCH COEF	1.000	.800	.840	.550E+06	1.050
16	NUMBR INCR	-1.148	100.	105.	.494E+06	.943

TABLE 2-8a Results for MAL Venting - Adiabatic Case

OUTPUT IS TOTAL MASS RELEASED NORMAL VALUE IS .595E+08

INDEX	VARIABLE	SENS COEFF	V NORMAL	REFERENCE	V CHANGED	OUTPUT	FRACTION
1	INITL TEMP	.299	288.	283.	302.	.604E+08	1.013
2	INITL MASS	1.704	.988E+08	.955E+08	.936E+08	.646E+08	1.085
3	VOLUME	-.299	.120E+09	.120E+09	.126E+09	.586E+08	.985
4	TNK HEIGHT	.597	493.	493.	518.	.613E+08	1.030
5	HOL HEIGHT	-1.493	148.	493.	173.	.551E+08	.925
6	HOLE DIAM	.000	49.3	49.3	51.8	.595E+08	1.000

INDEX	PARAMETER	SENS COEFF	P NORMAL	P CHANGED	OUTPUT	FRACTION
1	MOLEC WT	.000	32.0	33.6	.595E+08	1.000
2	CPG EQN C1	.000	.164E+06	.173E+06	.595E+08	1.000
3	CPG EQN C2	.000	74.1	77.8	.595E+08	1.000
4	CPG EQN C3	.000	.335E-01	.352E-01	.595E+08	1.000
5	CPG EQN C4	.000	.0	.0	.595E+08	1.000
6	CPL EQN C1	.000	-.146E+04	-.138E+04	.595E+08	1.000
7	CPL EQN C2	.000	13.4	14.1	.595E+08	1.000
8	VAP PR C1	.000	10.9	11.5	.595E+08	1.000
9	VAP PR C2	.000	.200E+04	.210E+04	.595E+08	1.000
10	VAP PR C3	.000	.400E-01	.420E-01	.595E+08	1.000
11	LIQ DEN C1	-.597	.106E+04	.111E+04	.577E+08	.970
12	LIQ DEN C2	.000	-.920	-.874	.595E+08	1.000
13	LIQ DEN C3	.000	.0	.0	.595E+08	1.000
14	HEAT VAPOR	.000	.110E+07	.115E+07	.595E+08	1.000
15	DISCH COEF	.000	.800	.840	.595E+08	1.000
16	NUMBR INCR	.185	100.	105.	.601E+08	1.009

TABLE 2-8b Results for MAL Venting - Adiabatic Case

OUTPUT IS AVERAGE FLOW RATE NORMAL VALUE IS .524E+06

INDEX	VARIABLE	SENS COEFF	V NORMAL	DIFFERENCE	V CHANGED	OUTPUT	FRACTION
1	INITL TEMP	-.878	288.	283.	302.	.501E+06	.956
2	INITL MASS	.211	.688E+08	.955E+08	.936E+08	.530E+06	1.011
3	VOLUME	-1.797	.120E+09	.120E+09	.126E+09	.477E+06	.910
4	TNK HEIGHT	-.061	493.	493.	518.	.523E+06	.997
5	HOL HEIGHT	-1.304	148.	493.	173.	.490E+06	.935
6	HOLE DIAM	2.050	49.3	49.3	51.8	.578E+06	1.102

INDEX	PARAMETER	SENS COEFF	P NORMAL	P CHANGED	OUTPUT	FRACTION
1	MOLEC WT	-.001	32.0	33.6	.524E+06	1.000
2	CPG EQN C1	.000	.164E+06	.173E+06	.524E+06	1.000
3	CPG EQN C2	.000	74.1	77.8	.524E+06	1.000
4	CPG EQN C3	.000	.335E-01	.352E-01	.524E+06	1.000
5	CPG EQN C4	.000	.0	.0	.524E+06	1.000
6	CPL EQN C1	-.000	-.146E+04	-.138E+04	.524E+06	1.000
7	CPL EQN C2	-.000	13.4	14.1	.524E+06	1.000
8	VAP PR C1	-.039	10.9	11.5	.523E+06	.998
9	VAP PR C2	.009	.200E+04	.210E+04	.524E+06	1.000
10	VAP PR C3	-.000	.400E-01	.420E-01	.524E+06	1.000
11	LIQ DEN C1	.145	.106E+04	.111E+04	.528E+06	1.007
12	LIQ DEN C2	-.829	-.920	-.874	.502E+06	.959
13	LIQ DEN C3	.000	.0	.0	.524E+06	1.000
14	HEAT VAPOR	.000	.110E+07	.115E+07	.524E+06	1.000
15	DISCH COEF	1.000	.800	.840	.550E+06	1.050
16	NUMBR INCR	-1.148	100.	105.	.494E+06	.943

TABLE 2-9a Results for Gas Venting - Isothermal Case

OUTPUT IS TOTAL MASS RELEASED NORMAL VALUE IS .428E+08

INDEX	VARIABLE	SENS COEFF	V NORMAL	REFERENCE	V CHANGED	OUTPUT	FRACTION
1	INITL TEMP	.299	288.	283.	302.	.435E+08	1.015
2	INITL MASS	1.704	.640E+08	.688E+08	.674E+08	.465E+08	1.085
3	VOLUME	-.299	.100E+09	.100E+09	.105E+09	.422E+08	.985
4	INK HEIGHT	.597	464.	464.	487.	.441E+08	1.030
5	HOL HEIGHT	-1.493	139.	464.	162.	.397E+08	.925
6	HOLE DIAM	.000	46.4	46.4	48.7	.428E+08	1.000

INDEX	PARAMETER	SENS COEFF	P NORMAL	P CHANGED	OUTPUT	FRACTION
1	MOLEC WT	.000	106.	111.	.428E+08	1.000
2	CPG EQN C1	.000	-29.7	-28.2	.428E+08	1.000
3	CPG EQN C2	.000	647.	679.	.428E+08	1.000
4	CPG EQN C3	.000	-.270	-.256	.428E+08	1.000
5	CPG EQN C4	.000	.0	.0	.428E+08	1.000
6	CPL EQN C1	.000	.123E+04	.129E+04	.428E+08	1.000
7	CPL EQN C2	.000	3.35	3.52	.428E+08	1.000
8	VAP PR C1	.000	9.03	9.48	.428E+08	1.000
9	VAP PR C2	.000	.127E+04	.133E+04	.428E+08	1.000
10	VAP PR C3	.000	-56.1	-53.3	.428E+08	1.000
11	LIQ DEN C1	-.597	947.	994.	.416E+08	.970
12	LIQ DEN C2	.000	-.900	-.855	.428E+08	1.000
13	LIQ DEN C3	.000	.0	.0	.428E+08	1.000
14	HEAT VAPOR	.000	.297E+06	.312E+06	.428E+08	1.000
15	DISCH COEF	.000	.800	.840	.428E+08	1.000
16	NUMBR INCR	.185	100.	105.	.432E+08	1.009

TABLE 2-9b Results for Gas Venting - Isothermal Case

OUTPUT IS AVERAGE FLOW RATE NORMAL VALUE IS .389E+06

INDEX	VARIABLE	SENS COEFF	V NORMAL	REFERENCE	V CHANGED	OUTPUT	FRACTION
1	INITL TEMP	-.759	288.	283.	302.	.374E+06	.962
2	INITL MASS	.208	.640E+08	.668E+08	.674E+08	.393E+06	1.013
3	VOLUME	-1.809	.100E+09	.100E+09	.105E+09	.354E+06	.910
4	TNK HEIGHT	-.067	464.	464.	487.	.388E+06	.997
5	HOL HEIGHT	-1.307	139.	464.	162.	.364E+06	.933
6	HOLE DIAM	2.050	46.4	46.4	48.7	.429E+06	1.102

INDEX	PARAMETER	SENS COEFF	P NORMAL	P CHANGED	OUTPUT	FRACTION
1	MOLEC WT	-.001	106.	111.	.389E+06	1.000
2	CPG EQN C1	.000	-29.7	-28.2	.389E+06	1.000
3	CPG EQN C2	.000	647.	679.	.389E+06	1.000
4	CPG EQN C3	.000	-.270	-.256	.389E+06	1.000
5	CPG EQN C4	.000	.0	.0	.389E+06	1.000
6	CPL EQN C1	.000	.123E+04	.129E+04	.389E+06	1.000
7	CPL EQN C2	.000	3.35	3.52	.389E+06	1.000
8	VAP PR C1	-.042	9.03	9.48	.388E+06	.998
9	VAP PR C2	.011	.127E+04	.133E+04	.389E+06	1.001
10	VAP PR C3	-.004	-50.1	-53.3	.389E+06	1.000
11	LIQ DEN C1	.044	947.	994.	.390E+06	1.002
12	LIQ DEN C2	-1.030	-.900	-.855	.369E+06	.949
13	LIQ DEN C3	.000	.0	.0	.389E+06	1.000
14	HEAT VAPOR	.000	.297E+06	.312E+06	.389E+06	1.000
15	DISCH COEF	1.000	.600	.840	.408E+06	1.050
16	NUMBR INCR	-1.160	100.	105.	.366E+06	.942

TABLE 2-10a Results for Gas Venting - Adiabatic Case

OUTPUT IS TOTAL MASS RELEASED NORMAL VALUE IS .428E+08

INDEX	VARIABLE	SENS COEFF	V NORMAL	REFERENCE	V CHANGED	OUTPUT	FRACTION
1	INITL TEMP	.299	288.	283.	302.	.435E+08	1.015
2	INITL MASS	1.704	.640E+06	.688E+06	.674E+06	.465E+08	1.085
3	VOLUME	-.299	.100E+09	.100E+09	.105E+09	.422E+08	.985
4	TNK HEIGHT	.597	464.	464.	487.	.441E+08	1.030
5	HOL HEIGHT	-1.493	139.	464.	162.	.397E+08	.925
6	HOLE DIAM	.000	46.4	46.4	48.7	.428E+08	1.000

INDEX	PARAMETER	SENS COEFF	P NORMAL	P CHANGED	OUTPUT	FRACTION
1	MOLEC WT	.000	100.	111.	.428E+08	1.000
2	CPG EQN C1	.000	-29.7	-24.2	.428E+08	1.000
3	CPG EQN C2	.000	647.	679.	.428E+08	1.000
4	CPG EQN C3	.000	-.270	-.256	.428E+08	1.000
5	CPG EQN C4	.000	.0	.0	.428E+08	1.000
6	CPL EQN C1	.000	.123E+04	.129E+04	.428E+08	1.000
7	CPL EQN C2	.000	3.35	3.52	.428E+08	1.000
8	VAP PR C1	.000	9.03	9.48	.428E+08	1.000
9	VAP PR C2	.000	.127E+04	.133E+04	.428E+08	1.000
10	VAP PR C3	.000	-56.1	-53.3	.428E+08	1.000
11	LIQ DEN C1	-.597	947.	994.	.416E+08	.970
12	LIQ DEN C2	.000	-.900	-.855	.428E+08	1.000
13	LIQ DEN C3	.000	.0	.0	.428E+08	1.000
14	HEAT VAPOR	.000	.297E+06	.312E+06	.428E+08	1.000
15	DISCH COEF	.000	.600	.649	.428E+08	1.000
16	NUMBR INCR	.185	100.	105.	.432E+08	1.009

TABLE 2-10b Results for Gas Venting - Adiabatic Case

OUTPUT IS AVERAGE FLOW RATE NORMAL VALUE IS .389E+06

INDEX	VARIABLE	SENS COEFF	V NORMAL	REFERENCE	V CHANGED	OUTPUT	FRACTION
1	INITL TEMP	-.759	288.	283.	302.	.374E+06	.962
2	INITL MASS	.208	.640E+08	.688E+08	.674E+08	.393E+06	1.010
3	VOLUME	-1.409	.100E+09	.100E+09	.105E+09	.354E+06	.911
4	[illegible] HEIGHT	-.037	464.	464.	487.	.388E+06	.997
5	HOL HEIGHT	-1.307	139.	464.	102.	.363E+06	.933
6	HOLE DIAM	2.050	46.4	46.4	48.7	.429E+06	1.102

INDEX	PARAMETER	SENS COEFF	P NORMAL	P CHANGED	OUTPUT	FRACTION
1	MOLEC WT	-.001	106.	111.	.389E+06	1.000
2	CPG EQN C1	-.000	-29.7	-28.2	.389E+06	1.000
3	CPG EQN C2	-.000	647.	679.	.389E+06	1.000
4	CPG EQN C3	-.000	-.270	-.256	.389E+06	1.000
5	CPG EQN C4	.000	.0	.0	.389E+06	1.000
6	CPL EQN C1	.000	.123E+04	.129E+04	.389E+06	1.000
7	CPL EQN C2	.000	3.35	3.52	.389E+06	1.000
8	VAP PR C1	-.042	9.03	9.48	.388E+06	.998
9	VAP PR C2	.011	.127E+04	.133E+04	.389E+06	1.001
10	VAP PR C3	-.004	-56.1	-53.3	.389E+06	1.000
11	LIQ DEN C1	.044	947.	994.	.390E+06	1.002
12	LIQ DEN C2	-1.030	-.900	-.855	.384E+06	.949
13	LIQ DEN C3	.090	.0	.0	.389E+06	1.000
14	HEAT VAPOR	-.009	.297E+06	.312E+06	.389E+06	1.000
15	DISCH COEF	1.009	.800	.840	.408E+06	1.050
16	[illegible] INCR	-1.150	100.	105.	.366E+06	.942

To obtain the sensitivity coefficient for the initial tank temperature, the model is run with the changed value for the initial temperature (the first variable), and this changed output is compared with the normal output. The sensitivity coefficient is defined by the following equation:

$$S = [(\phi_c - \phi_n)/\phi_n]/[(x_c - x_n)/x_r] \qquad (2\text{-}34)$$

where S is the sensitivity coefficient, ϕ_c is the changed output value, ϕ_n is the normal output value, x_c is the changed input value, x_n is the normal input value, and x_r is the reference input value. The output values are all required to be positive and greater than zero, so the output change may be normalized by the normal output value. An input value, however, may be zero or negative, so the input change is normalized by the reference value, which is chosen to be greater than zero. Now x_c is defined by

$$x_c = x_n + Ax_r \qquad (2\text{-}35)$$

so (2-34) becomes

$$S = \frac{1}{A}\left(\frac{\phi_c}{\phi_n} - 1\right) \qquad (2\text{-}36)$$

A has been chosen to be 0.05 for this analysis.

The first variable in Table 2-1a is the initial temperature in the tank. It may be seen that the normal value for this variable is 128 °K, the reference value is 283 °K, and the changed value is 142 °K. The output when all the variables except the initial temperature had their normal values, when the initial temperature had its changed value, and when all the parameters had their normal values was 0.738×10^8 grams for the total mass released. This is identical to the normal output value, so the fractional output (ϕ_c/ϕ_n) is 1.0 and the sensitivity coefficient is zero. The reason for this is that the initial temperature is above the boiling point of LNG at atmospheric pressure. Since the tank conditions are assumed to be isothermal, after the liquid level has fallen to the hole height the tank will vent gas and, as the temperature will remain above the boiling point, the tank pressure will be equal to the vapor pressure of methane, which will be greater than atmospheric pressure. Thus the tank will keep venting methane gas until it is empty. Actually, there is a check in the program to prevent the tank from containing zero or negative mass. This means that the last step will not be carried through. Thus if there are N steps specified, the computation will stop with 1/N of the cargo remaining. In this case, N = 100, so 99% of the mass vents in each case. Thus the initial temperature, as long as it is above the normal boiling point of LNG will have no effect on the total mass released.

The initial temperature does have an effect on the rate of venting, however. In fact, Table 2-1b shows that it has a very large effect. This is due to the way in which the average flow rate is calculated, and the strong dependence of the vapor pressure on the temperature. Since the hole is one-third of the way up the tank wall, and the tank is almost full, approximately two-thirds of the mass will vent in liquid phase, and the venting rate of the liquid is not very sensitive to the vapor pressure. The remaining one-third of the cargo will vent in vapor phase, and the gas venting is much slower (in terms of grams/second, not in terms of cm/second) than the liquid venting. The venting of this third of the cargo in gas phase will take much longer than the preceding venting of two-thirds of the cargo in liquid phase. Since the average flow rate is just the total mass vented divided by the total venting time, the average flow rate will be very sensitive to the vapor pressure and thus to the temperature, even though the vapor pressure has little effect upon the venting of two-thirds of the mass in liquid phase.

Sensitivity of the Tank Venting Submodel to the Six Variables

1. Initial Temperature. The initial temperature enters the computations in a number of ways. Its most pronounced influence is through the vapor pressure for those cargoes which have boiling points below ambient temperature at normal atmospheric pressure. Thus the venting of LNG, chlorine, or ammonia is quite sensitive to the initial temperature. The effect is greatest for the average flow rate for the isothermal case. In the adiabatic case, increasing the temperature will increase the amount of mass vented since the temperature will have farther to fall before it reaches the normal boiling point. Increasing the initial temperature may increase or decrease the average flow rate. Two competing effects are at work. Increasing the initial temperature increases the initial flow rate because the cargo vapor pressure is raised. At the same time, the liquid density is lowered so the mass flow rate is decreased for liquids. The gas density (saturated vapor density) will be increased. Depending upon which effects predominate, the average flow rate will either increase or decrease.

For methanol and gasoline, which are liquid at ambient temperatures and pressures, the initial tank temperature is not so important. The dependence here is not dominated by any single effect. The liquid density and specific heats are all functions of temperature, so changing the initial temperature will affect the venting simulation in many ways.

2. Initial Mass. The normal initial mass is taken to be 93% of the mass that the tank can hold at the normal initial temperature. The tank cannot be 100% full, for if it were, then increasing the mass in the tank by 5% or increasing the initial temperature by 5% would cause the tank to overflow. Of course both the total mass released and the flow rate are sensitive to the initial amount of cargo in the tank, and the mass released is more sensitive to this variable than the flow rate as one might expect. There is no pronounced difference in sensitivity between the isothermal and adiabatic cases.

3. Tank Volume. Since the tank height is specified, changing the tank volume effectively changes the cross-sectional area of the tank. The submodel is not particularly sensitive to this variable insofar as the total mass released is concerned, but the tank volume does affect the average flow rate.

4. Tank Height. The height of the tank has some effect on the output values except that the total mass released in the isothermal case for cargoes which have normal boiling points below ambient temperature is independent of the tank height. This submodel is less sensitive to the height of the tank than it is to most other variables.

5. Hole Height. The effect of changing the hole height is fairly straightforward as one might expect. There is no effect on the total mass released in the isothermal case for cargoes which have normal boiling points below ambient temperature as might be expected. In these cases, increasing the hole height increases the portion of the cargo which escapes in gas phase, and thus decreases the average flow rate. For adiabatic venting for these cargoes, the venting ceases soon after gas venting starts because the tank temperature decreases to the normal boiling point. Thus both the mass released and the flow rate decrease when the hole height is increased. For the cargoes which are liquid at ambient conditions, the venting ceases when the liquid level drops to the height of the hole, and the dependence of the output variables on the hole height is straightforward.

6. Hole Diameter. The size of the hole or puncture in the tank has no effect upon the total mass released, but of course it has a direct effect upon the flow rate. The sensitivity coefficient for the average flow rate is 2.05 in all cases.

Sensitivity of the Tank Venting Submodel to the Sixteen Parameters

1. Molecular Weight. The submodel is most sensitive to the molecular weight of the cargo for the adiabatic venting of ammonia, and for this case only the average flow rate is affected. On the whole, the molecular weight of the cargo has little effect on the results of the submodel.

2. Specific Heat of the Gas. The equation for calculating the specific heat as a function of temperature has provisions for four parameters, but only the first three are non-zero for most of the cargoes in the Chemical Properties File. Except for the average flow rates for the adiabatic venting of ammonia and LNG, the submodel is nearly insensitive to the constants in the equation for the specific heat of the cargo in gas phase.

3. Specific Heat of the Liquid. The equation for calculating the specific heat of the cargo in liquid phase as a function of temperature has provisions for two parameters. For the average flow rates for the adiabatic venting of LNG and ammonia, the submodel is fairly sensitive to the values of these constants. Otherwise, the values of these constants do not have a large effect upon the results.

4. Vapor Pressure. The equation for the vapor pressure as a function of temperature has three parameters, but only the first two are important except for LNG. Even for LNG, the results are much less sensitive to the changes in the third constant than they are to changes in the first two constants. As might be expected, the values of the constants in the vapor pressure equation affect only the three cargoes which have normal boiling points below ambient temperatures. The effect is larger for the flow rate than it is for the mass of cargo escaped. The results of this submodel are more sensitive to the values of the constants in the vapor pressure equation than they are to any other parameters if the cargo is a gas at ambient conditions. If the cargo is a liquid at ambient conditions, the results of the submodel are nearly insensitive to the vapor pressure.

5. Liquid Density. Except for the total mass released in the case of isothermal venting of a cargo which is transported in the liquid state but which is a gas at ambient conditions, all the output values are somewhat sensitive to the values of the constants in the liquid density equation. The effect of changing the values of these constants is largest for the average flow rate during adiabatic venting of ammonia.

6. Specific Heat of Vaporization. As might be expected, the value of the heat of vaporization matters only in the case where the tank conditions are adiabatic and the escaping cargo was originally a liquid in the tank and is a gas at ambient conditions.

7. Discharge Coefficient. As might be deduced from the equations used, the mass released is completely independent of the discharge coefficient, and the flow rate is proportional to the discharge coefficient.

8. Number of Increments. The escape of the cargo from the tank is considered in steps, and the number of steps may be represented by N. After each step, the amount of mass remaining in the tank is decremented by (1/N) of the initial mass, and the amount which has escaped is incremented by (1/N) of the initial mass. Thus N may be considered to be the number of increments or the number of decrements. While the amount of mass which escapes during each step is constant, the time it takes to escape and the flow rate are not constant. The value of N has little effect upon the amount of mass which escapes. The average flow rate is somewhat sensitive to the value of N, and the tables show that increasing N may cause the flow rate to decrease in some cases and increase in others. N = 100 has been used here; the submodel from HACS had N = 200.

Appendix 2E gives details of the various subroutines that were updated for use in the sensitivity analysis.

CONCLUSIONS

The sensitivity of the model depends strongly upon the tank conditions and whether the cargo is liquid or gas at ambient conditions.

A. Isothermal Conditions - Cargo in Gaseous State at Ambient Conditions. This case applies to the venting of LNG, CL_2, and NH_3. In this case all of the cargo will escape as long as the initial temperature is above the boiling point of the cargo at ambient atmospheric pressure. Thus the total mass released is independent of all the variables and all the parameters. The sole exception to this is for chlorine, where the changed value of the second constant in the vapor pressure reduced the vapor pressure in the tank at the initial temperature to a value less than the atmospheric pressure. Therefore, venting continued only until the liquid level was below the hole, and then stopped; no gas venting taking place.

As mentioned above, the average flow rate is sensitive to the vapor pressure during the gas venting stage for this case. Therefore, the flow rate is sensitive to changes in the initial temperature and to changes in the parameters in the vapor pressure equation.

B. Isothermal Conditions - Cargo in Liquid State at Ambient Conditions. In this case the venting stops when the liquid level falls below the hole, since the vapor pressure of the cargo is too small to cause any gas venting. For methyl alcohol and gasoline, then, the submodel is primarily sensitive to the initial mass and to the hole height. It is also sensitive to the parameters in the liquid density equation and to the height of the tank.

C. Adiabatic Conditions - Cargo in Gaseous State at Ambient Conditions. For adiabatic tank conditions, the situation is more complicated. The tank will cool somewhat as the liquid vents. After the liquid level drops below the hole, gas vents and the temperature falls more rapidly. Soon the temperature has dropped to the boiling point at atmospheric pressure and the venting ceases. The total mass released is independent of the hole size, but depends at least to some degree on the other variables. The average flow rate is sensitive to all the variables. The total mass released is not particularly sensitive to any of the parameters and is independent of some of them. The flow rate may be quite sensitive to the values of the parameters in the vapor pressure equation. The sensitivity differences between chlorine and ammonia are largely due to the fact that the chlorine tank was refrigerated and the vapor pressure was only about 1.5 atmospheres, whereas the ammonia tank was not refrigerated and the pressure inside it was about 6.0 atmospheres. Thus the different sensitivities for chlorine and ammonia show the different reactions of the model between a case where the cargo is maintained in the liquid state by low temperatures in one case and by high pressure in the other case.

D. Adiabatic Conditions - Cargo in Liquid State at Ambient Conditions. In this case, the venting ceases when the liquid level falls below the hole because the vapor pressure of the cargo is too low to cause gas venting after the liquid venting stops. Thus the only way that the adiabatic case differs from the isothermal case is that the decrease in the tank temperature may change the liquid density slightly. However, the liquid density is considered to be a constant at the initial temperature, so for both methyl alcohol and gasoline, the results for the adiabatic case are identical to the results for the isothermal case. The computed temperature drop is just over 1.2 °C for the gasoline venting, and about 15.5 °C for methanol which has a much higher vapor pressure than gasoline.

On the whole, the models which follow this one (and the results of the Vulnerability Model) are more dependent upon the total mass released from the punctured tank than they are on the average rate of flow from the tank. For these five cargoes, for both adiabatic and isothermal conditions, the total mass released is fairly insensitive to all the parameters. The amount of the cargo which escapes is sensitive to the initial tank conditions such as the amount of cargo in the tank and the hole height, but this is to be expected.

For the average flow rate, for those cargoes which are gases at ambient pressure and temperature, the submodel is quite sensitive to the initial temperature and to changes in the constants in the vapor pressure equation. This is due to the fact that the rate of release is much slower when the cargo is escaping as a gas rather than as a liquid, and the gas flow rate depends strongly upon the internal tank pressure which will be the vapor pressure, and the vapor pressure, in turn, is a strong function of the tank temperature.

SUMMARY AND RECOMMENDATIONS

The Venting Rate Submodel, in its original form, appears to have a significant error in the formulation and corresponding computer coding of the energy equation. Other minor problems have also been detected. When the energy balance equation is reformulated, the model appears to be satisfactory provided it is utilized by persons cognizant of the inherent limitations of the model. Perhaps the most serious limitation of the model is its neglect or incomplete treatment of the venting arrangements common on most bulk cargo tanks. This, in some situations, may produce unrealistic results, which unfortunately may not always err in a manner producing conservative estimates of damage. It is recommended that this limitation on model realism be removed. Other less pressing improvements that might be made include:

(1) in the case of adiabatic venting when the cargo temperature drops below its freezing temperature, put in a test so that (a) different vapor pressure equation is used in the case of gas venting or (b) venting is stopped in the case of liquid venting;

(2) rederive the energy equation by assuming that the liquid and gas phases of the cargo are not in thermal equilibrium with each other, but that each can be characterized by a single temperature;

(3) analyze the case of intermittent venting;

(4) explore the advantages (if any) of numerical methods other than decrementing mass;

(5) restructure the program so that overspecification of input conditions is no longer a problem.

In summary, the Venting Rate Submodel as corrected gives results reasonably close to reality considering the economy with which the results are obtained.

APPENDIX 2A

INPUT VARIABLES TO VENTING RATE MODEL

There are between one and two dozen quantities whose values must be known before the Venting Rate Model can be run successfully. The quantities are divided into four categories:

A. Spill definition variables such as the volume of the tank

B. Model internal parameters such as the number of iterations used in the venting subroutine

C. Properties of the cargo such as density and specific heat

D. Constants for which a fixed value is assigned in the subroutine such as the acceleration due to gravity.

The type A quantities may vary over some range which is determined by such things as the sizes of the ships or barges now in use or under construction. The type C quantities have only one correct value for the conditions which exist at any given time and place, but these values may not be known accurately, or the specified conditions may differ from those which actually occur.

A. Spill Definition Variables

Some of these variables are dependent upon the type of cargo being considered. For example, some cargoes are not carried in as large quantities as others, so the maximum tank size would depend on the cargo; some cargoes are carried in pressurized tanks, so the initial tank pressure would depend upon the type of cargo. The type A quantities used in the Venting Rate Model are listed in Table 2A-1. They are all real, continuously-variable quantities except IADBT which is a flag indicating whether the conditions in the tank are assumed to be isothermal or adiabatic during the venting process.

B. Model Parameters

There is only one quantity in this class for the Venting Rate Model; it is INC which is the maximum number of incremental steps to be used in calculating the venting rate as a function of time and mass remaining in the tank. The maximum value of INC is currently 200, due to the dimensioned size of the storage arrays.

C. Cargo Properties

Six properties of the substance in the tank are used in the Venting Rate Model. They are listed in Table 2A-2. The density in liquid phase, molecular weight, and heat of vaporization are simple properties which do not

TABLE 2A-1 List of Type A (Spill Definition) Quantities Used in the Venting Rate Model (MODA)

Name	Number	Value is Cargo Dependent	Suggested			Units Used in this Table	Description	Units Used in Programs
			Lower Bound	Upper Bound	Normalization Value			
VOL	2001	yes			Upper Bound	cm^3	volume of tank	cm^3
HT	2002	yes*	$\frac{1}{5}(VOL)^{1/3}$	$2(VOL)^{1/3}$	$(VOL)^{1/3}$	cm	height of tank	cm
HH	2003	no	0	HT	HT	cm	height of tank above tank bottom	cm
HOLED	2008	no	20	$\frac{1}{2}(\frac{VOL}{HT})^{1/2}$	$(\frac{VOL}{HT})^{1/2}$	cm	diameter of hole in tank	cm
PTO	2005	yes			1.0	Atm	initial pressure in the tank	gmf/cm^2 and $dynes/cm^2$
IADBT	2006	no	not continuous				flag, = 0 for isothermal, = 1 for adiabatic	
TO	2004	yes			273.16	°K	initial temperature in tank	°C and °K
AMSSO	2007	yes	0.10*VOL*DL	0.98*VOL*DL	VOL*DL	g	initial s in tank	g

*Certain cargoes are traditionally carried in tanks of different shapes, but this fact may be overlooked if one wishes.

TABLE 2A-2 List of Type C (Cargo Properties) Quantities Used in the Venting Rate Model (MODA)

Name	Number	Description	Units Used in Programs
DL	1004	density of liquid	g/cm^3
AM	1002	molecular weight	
CPG	1013	specific heat* of gas	cal/g/°C
CPL	1007	specific heat of liquid	cal/g/°C
HVAP	1014	heat of vaporization	cal/g
AVP	1010	constants in vapor pressure equation	
BVP	1011		
CVP	1012		

*It is actually the molar heat at constant pressure that is obtained in MODA, but it is changed to specific heat before being passed to RLJVI.

change appreciably with temperature or pressure. Heat capacity and vapor pressure change appreciably with temperature, and equations with which to calculate appropriate values of these properties are available in the Chemical Properties File. The specific heat at constant pressure for both the gas and liquid phases have been calculated at the initial tank temperature or at the boiling point and are passed to RLJVI as simple constants For the vapor pressure, the constants in an equation are passed through RLJVI, RLJTC and RLJTS to RLJVP where they are used to calculate the vapor pressure as a function of temperature. The density of the cargo in vapor phase is used in this model, but it is calculated from the temperature and pressure by means of the ideal gas relationship.

D. Constants

This type of quantity includes all those which are treated as constants, whether or not this is entirely appropriate. R and π are absolute quantities, and there is no question about defining them to have a single value in a subroutine. This is true as well for the conversion factors needed to change units, and the standard value for one atmosphere of pressure. The case of g, the acceleration of gravity, is slightly different. There is a standard value for g which is that at sea level at a selected location, and this is commonly used without regard to the fact that the value of g varies with location. The error involved in using the standard value for g is probably small relative to other errors in this model. The final quantity in this class for the Venting Rate Model is CO, the discharge coefficient. Strictly speaking, CO depends upon the shape of the hole, and how far the bent pieces of metal extend into the tank (or out from the original plane of the tank wall if the puncture is due to forces from within the tank). From theoretical considerations, CO is known to lie between 0.5 and 1.0. For round holes, experimental values are available for different types of mouthpieces [6]. While measurements of CO for the jagged types of holes to be expected in accidents may have been made, even if these data are available, the shapes of actual accidental punctures of cargo tanks are not known. CO is set equal to 0.80 in RLJVI for all holes in the program. (In this discussion of the discharge coefficient it has been assumed that the inviscid approximation is valid.)

APPENDIX 2B

ENERGY EQUATIONS - LIQUID DISCHARGE

Derivation of the Energy Equation for Liquid Discharge

The conservation of mass is expressed by

$$\frac{dM_L}{dt} = -w_o - w_e \tag{2B-1}$$

$$\frac{dM_g}{dt} = +w_e \tag{2B-2}$$

where M_L and M_g are the masses of liquid and gas in the tank, respectively, w_o is the rate of mass flow out the hole in the tank, and w_e is the rate of mass flow from the liquid to the gas due to evaporation.

The general energy balance equation as given in Bird, Stewart and Lightfoot [11] is

$$\frac{dE_{tot}}{dt} = -\Delta \left[\left(\hat{U} + P\hat{V} + \frac{1}{2} \frac{\langle v \rangle^3}{\langle v \rangle} + \hat{\Phi} \right) w \right] + Q - W \tag{2B-3}$$

where

$$E_{tot} = U_{tot} - K_{tot} + \Phi_{tot} \tag{2B-4}$$

denotes the total energy in the system.

U, K, and Φ denote, internal, kinetic and potential energies, respectively. The circumflex indicates that the quantity is given per unit mass: $\hat{U}$ is the kinetic energy per unit mass. Q is the rate of heat flow into the system, which will be zero here since adiabatic conditions are assumed. W is the rate at which mechanical work is done by the system on its surroundings.

---

[11] Bird, R.B., W.E. Stewart, and E.N. Lightfoot, Transport Phenomena, Ch. 15, Wiley, New York, 1960.

v is the velocity of the material, and V is the volume. <v> indicates that the average is taken over the cross-section. Pressure is denoted by p. The Δ indicates that the quantity following it in brackets should be evaluated for the flow into and out of the system; the inflow term is to be subtracted from the outflow term.

To proceed further, we make the following assumptions:

1. Thermodynamic equilibrium exists between the gas and liquid in the tank at all times. This implies that the gas pressure in the tank is the vapor pressure of the cargo, and that the temperatures in the gas and the liquid are the same.

2. The cargo gas may be treated as a perfect gas.

3. The cargo liquid may be treated as an incompressible liquid, whose density change with temperature is negligible.

4. Changes in kinetic energy and potential energy of both the liquid and the gas phase are negligible as compared to the changes in internal energy. (This assumption is shown to be valid by the case study below.)

5. Changes in cargo properties like the specific heat with the temperature may be neglected or their mean values may be used.

Since

$$\hat{U} = \hat{U}(T,V)$$

we have,

$$d\hat{U} = \left(\frac{\delta\hat{U}}{\delta T}\right)_V dT + \left(\frac{\delta\hat{U}}{\delta V}\right)_T dV$$

For perfect gases and incompressible liquids,

$$\left(\frac{\delta\hat{U}}{\delta V}\right)_T = 0$$

so

$$d\hat{U} = \left(\frac{\delta\hat{U}}{\delta T}\right)_V dT = \hat{C}_V dT \qquad (2B\text{-}5)$$

We take $\hat{U} = 0$ for the cargo material in the liquid state at a temperature of absolute zero. Then

$$\hat{U} = \int_0^T \hat{C}_v \, dT = \hat{C}_v \, T \tag{2B-6}$$

where $\hat{C}_v$ is the specific heat at constant volume, for the liquid phase.

Thus,

$$U_{tot} = \int_V \rho \, \hat{U} \, dV; \; K_{tot} = \int_V \frac{1}{2} \rho \, v^2 \, dV; \; \Phi_{tot} = \int_V \rho \, \hat{\Phi} \, dV$$

where ρ is the density.

If ρ and $\hat{U}$ are independent of the volume,

$$U_{tot} = M\hat{U} = M \, \hat{C}_v \, T$$

and if ρ and v are independent of position,

$$K_{tot} = \int_V \frac{1}{2} \rho \, v^2 \, dV = \frac{1}{2} M \, v^2$$

$$\Phi_{tot} = \int_V \rho \, \hat{\Phi} \, dV = \int_0^{Z_S} \rho \, A_T \, g \, Z \, dZ$$

In the expression for Φ_{tot}, A_T is the cross-sectional area of the tank (which is assumed to be independent of z), and g is the acceleration due to gravity. The positive z axis is upwards, and z_s denotes the height of the liquid surface in the tank. (z = 0 at the bottom of the tank.)

We may now write the energy equation for that portion of the tank occupied by liquid. From equation (2B-3) we have

$$\frac{d}{dt}\left[M_L \, \hat{C}_L \, T + 0.5 \, M \, v_s^2 + \int_0^{Z_S} \rho_L \, A_T \, g \, Z \, dZ \right] =$$

$$- w_o \left[\hat{C}_L \, T + \frac{P_a}{\rho_L} + 0.5 \, v_o^2 + Z_h \, g \right] - w_e \left[\hat{C}_{vg} \, T + \hat{\lambda} + \frac{P_T}{\rho_g} + 0.5 \, v_e^2 + Z_S \, g \right]$$

$$- A_T \, P_T \frac{dZ_S}{dt} \tag{2B-7}$$

where the subscript g refers to the gas, the subscript L refers to the liquid, and the subscript a refers to ambient conditions outside the tank, v_s is the velocity at which the liquid surface is falling, v_o is the velocity at which the liquid is passing out of the hole, and Z_h is the height of the hole. v_e is the velocity at which the evaporating mass leaves the liquid surface. $\hat{\lambda}$ represents the heat of evaporation (per unit mass) of the cargo.

By the fourth assumption above we may neglect the change of kinetic and potential energy within the liquid so (2B-7) may be written

$$\frac{d}{dt}\left[M_L\ \hat{C}_L\ T\right] = -\ w_o\left[\hat{C}_L\ T + \frac{P_a}{\rho_L} + 0.5\ v_o^2 + Z_h\ g\right]$$
$$-\ w_e\left[\hat{C}_{vg}\ T + \hat{\lambda} + \frac{P_T}{\rho_g} + 0.5\ v_e^2 + Z_s\ g\right] - A_T\ P_T\ \frac{dZ_s}{dt} \qquad (2B\text{-}8)$$

For the portion of the tank occupied by gas, from equation (2B-3) we have

$$\frac{d}{dt}\left[M_g\ \hat{C}_{vg}\ T + M_g\ \hat{\lambda} + 0.5\ M_g\ v_s^2 + \int_{Z_s}^{Z_T} \rho_g\ A_T\ g\ Z\ dZ\right] =$$
$$w_e\left[\hat{C}_{vg}\ T + \hat{\lambda} + \frac{P_T}{\rho_g} + 0.5\ v_e^2 + Z_s\ g\right] + A_T\ P_T\ \frac{dZ_s}{dt} \qquad (2B\text{-}9)$$

The $M_g\ \hat{\lambda}$ term on the left-hand side is required because we have taken U to be zero at a temperature of absolute zero in the liquid state. Since we wish to use the same reference for the internal energy of the cargo in both the liquid and gas phases, the specific heat of evaporation must be explicitly included in the internal energy of the cargo in the gas phase. By neglecting the kinetic and potential energy of the material in the tank, equation (2B-9) may be simplified to

$$\frac{d}{dt}\left[M_g\ \hat{C}_{vg}\ T + M_g\ \hat{\lambda}\right] = w_e\left[\hat{C}_{vg}\ T + \hat{\lambda} + \frac{P_T}{\rho_g} + 0.5\ v_e^2 + Z_h\ g\right] + A_T\ P_T\ \frac{dZ_s}{dt} \qquad (2B\text{-}10)$$

To obtain an equation for the entire tank, we add the energy equation for the liquid portion (2B-8) to that for the gas portion (2B-10):

$$\frac{d}{dt}\left[M_L\ \hat{C}_L\ T + M_g\ \hat{C}_{vg}\ T + M_g\ \hat{\lambda}\right] = -w_o\left[\hat{C}_L\ T + \frac{P_a}{\rho_L} + 0.5\ v_o^2 + Z_h\ g\right] \qquad (2B\text{-}11)$$

It may be noted that the w_e terms add out since they concern only the transfer of energy from one part of the tank to another. Some terms may be eliminated

from this equation by noting that the equations (2B-1) and (2C-2) for the conservation of mass allow one to write

$$+w_o = - \frac{dM_L}{dt} - \frac{dM_g}{dt}$$

With this expression one may eliminate the w_o in the $w_o C_L T$ term, so (2B-11) becomes

$$\hat{C}_L T \frac{dM_L}{dt} + \hat{C}_L M_L \frac{dT}{dt} + \frac{d}{dt} (M_g \hat{C}_{vg} T) + \hat{\lambda} \frac{dM_g}{dt} =$$
$$\hat{C}_L T \frac{dM_L}{dt} + \hat{C}_L T \frac{dM_g}{dt} - w_o \left[\frac{P_a}{\rho_L} + 0.5 v_o^2 + Z_h g \right] \qquad (2B\text{-}12)$$

It may be seen that there is now an identical term on each side of the above equation and these terms may be eliminated. Since

$$\hat{C}_{pg} = \hat{C}_{vg} + R$$

for a perfect gas where R is the universal gas constant in terms of mass and the perfect gas law is

$$P = \rho R T$$

$\therefore$ we have

$$\hat{C}_{vg} = \hat{C}_{pg} - P_T/(\rho_g T)$$

Thus equation (2B-12) becomes

$$M_L \hat{C}_L \frac{dT}{dt} + \frac{d}{dt} (M_g \hat{C}_{pg} T) - \frac{d}{dt} \frac{(M_g P_T)}{\rho_g} + \hat{\lambda} \frac{dM_g}{dt} =$$
$$\hat{C}_L T \frac{dM_g}{dt} - w_o \left[\frac{P_a}{\rho_L} + 0.5 v_o^2 + Z_h g \right] \qquad (2B\text{-}13)$$

We now integrate this equation over the time which it takes the system to go from state 1 to state 2. Those terms which are total differential terms may be integrated directly, so we obtain

$$\int_1^2 M_L\ \hat{C}_L\ dT + (M_g\ \hat{C}_{pg}\ T)_2 - (M_g\ \hat{C}_{pg}\ T)_1 + \hat{\lambda}\ (M_{g_2}-M_{g_1}) = \int_1^2 \hat{C}_L\ T\ dM_g +$$

$$\int_1^2 (-w_o) \left[\frac{P_a}{\rho_L} + 0.5\ v_o^2 + Z_h\ g\right] + \left(\frac{P_T\ M_g}{\rho_g}\right)_2 - \left(\frac{P_T\ M_g}{\rho_g}\right)_1 \qquad \text{(2B-14)}$$

Now $V_g = M_g/\rho_g$, where V_g is the volume occupied by the gas. And by adding and subtracting the quantity $M_{g_2}\ C_{pg} T_1$ we see that

$$(M_g\ \hat{C}_{pg}\ T)_2 - (M_g\ \hat{C}_{pg}\ T)_1 = M_{g_2}\ \hat{C}_{pg}\ (T_2-T_1) + \hat{C}_{pg}\ T_1\ (M_{g_2}-M_{g_1})$$

So we arrive at a final form for our energy equation in the case where the tank is venting liquid:

$$\int_1^2 M_L\ \hat{C}_L\ dT + M_{g_2}\ \hat{C}_{pg}\ (T_2-T_1) + \hat{C}_{pg}\ T_1\ (M_{g_2}-M_{g_1}) + \hat{\lambda}\ (M_{g_2}-M_{g_1}) =$$

$$\int_1^2 \hat{C}_L\ T\ dM_g + \int_1^2 (-w_o) \left[\frac{P_a}{\rho_L} + 0.5\ v_o^2 + Z_h\ g\right] dt + (P_T\ V_g)_2 - (P_g\ V_g)_1$$

(2B-15)

APPENDIX 2C

ENERGY EQUATIONS - GAS VENTING

Derivation of the Energy Equation When Gas is Being Vented

If the hole in the tank is above the surface of the liquid, gas will be vented from the tank as long as the tank pressure P_T is greater than the ambient atmospheric pressure, P_a. As discussed above, the tank pressure will be the vapor pressure of the cargo at the temperature inside the tank, and the temperature of the gas and liquid phases in the tank may be considered to be the same. The mass balance or mass conservation equations are

$$\frac{dM_L}{d_t} = - w_e \qquad (2C\text{-}1)$$

$$\frac{dM_g}{d_t} = w_e - w_o \qquad (2C\text{-}2)$$

where w_o is now the flow of mass in gas phase out of the tank.

The energy equations are similar in nature to those for the case where liquid was venting. Neglecting the change in potential and kinetic energy within the tank, for the portion of the tank containing liquid the energy equation is

$$\frac{d}{dt}\left[M_L \hat{C}_L T\right] = -w_e \left[\hat{C}_{vg}T + \hat{\lambda} + \frac{P_T}{\rho_g} + 0.5\ v_e^2 + Z_s\ g\right] - A_T\ P_T \frac{dZ_s}{dt} \qquad (2C\text{-}3)$$

The change of potential and kinetic energy in the portion of the tank containing gas is also neglected, and the energy equation for this part of the tank is

$$\frac{d}{dt}\left[M_g \hat{C}_{vg} T + \hat{\lambda} M_g\right] = w_e \left[\hat{C}_{vg} T + \hat{\lambda} + \frac{P_T}{\rho_g} + 0.5\ v_e^2 + Z_s\ g\right] - w_o \left[\hat{C}_{vg} T + \hat{\lambda} + \frac{P_a}{\rho_{ga}} + 0.5\ v_o^2 + Z_h\ g\right] + A_T\ P_T \frac{dZ_s}{dt} \qquad (2C\text{-}4)$$

In this equation, ρ_{ga} is the density of the cargo gas at ambient atmospheric pressure, and at the tank temperature. Adding these two equations, the energy equation for the entire tank may be obtained:

$$\frac{d}{dt}\left[M_L \hat{C}_L T + M_g \hat{C}_{vg} T + \hat{\lambda} M_g\right] = -w_o\left[\hat{C}_{vg} T + \hat{\lambda} + \frac{P_a}{\rho_{ga}} + 0.5\ v_o^2 + Z_h\ g\right] \quad (2C\text{-}5)$$

Eliminating w_o by the use of equations (2C-1) and (2C-2).

$$\frac{d}{dt}\left[M_L\ \hat{C}_L\ T + M_g\ \hat{C}_{vg}\ T + \hat{\lambda}\ M_g\right] =$$
$$\left(\frac{dM_L}{dt} + \frac{dM_g}{dt}\right)\left[\hat{C}_{vg}\ T + \hat{\lambda} + \frac{P_a}{\rho_{ga}} + 0.5\ v_o^2 + Z_h\ g\right] \quad (2C\text{-}6)$$

Expanding the terms, (2C-6) becomes

$$\frac{d}{dt}\ (M_L\ \hat{C}_L\ T) + M_g\ \hat{C}_{vg}\ \frac{dT}{dt} + \hat{C}_{vg}\ T\ \frac{dM_g}{dt} + \hat{\lambda}\ \frac{dM_g}{dt} =$$
$$\hat{C}_{vg}\ T\ \frac{dM_L}{dt} + \hat{C}_{vg}\ T\ \frac{dM_g}{dt} + \hat{\lambda}\ \frac{dM_L}{dt} + \hat{\lambda}\ \frac{dM_g}{dt} + (-w_o)\left[\frac{P_a}{\rho_{ga}} + 0.5\ v_o^2 + Z_h\ g\right] \quad (2C\text{-}7)$$

There are now two identical dM_g/dt terms on each side of the equation, and these terms may be eliminated.

$$\frac{d}{dt}\ (M_L\ \hat{C}_L\ T) + M_g\ \hat{C}_{pg}\ \frac{dT}{dt} - R\ M_g\ \frac{dT}{dt} =$$
$$\hat{C}_{vg}\ T\ \frac{dM_L}{dt} + \hat{\lambda}\ \frac{dM_L}{dt} + (-w_o)\left[\frac{P_a}{\rho_{ga}} + 0.5\ v_o^2 + Z_h\ g\right] \quad (2C\text{-}8)$$

Integrating this equation between the states 1 and 2 as was done for liquid venting:

$$(M_L\ \hat{C}_L\ T)_2 - (M_L\ \hat{C}_L\ T)_1 + \int_1^2 M_g\ \hat{C}_{pg}\ dT - \int_1^2 R\ M_g\ dT =$$

$$\int_1^2 \hat{C}_{vg}\ T\ dM_L + \hat{\lambda}\ (M_{L_2}-M_{L_1}) + \int_1^2 (-w_o) \left[\frac{P_a}{\rho_{ga}} + 0.5\ v_o^2 + Z_h\ g\right] dt \qquad (2C\text{-}9)$$

This is the complete, rigorous energy equation for a tank which is venting gas. For use in finite-difference schemes, where the difference between states 1 and 2 are small, we write the arguments of the integrals as the average of the arguments at the end points as was done for the liquid venting case. Then (2C-9) becomes

$$M_{L_2}\ \hat{C}_L\ (T_1-T_2) + \hat{C}_L\ T_1\ (M_{L_1}-M_{L_2}) + 0.5\ (M_{g_1}+M_{g_2})\ \hat{C}_{pg}\ (T_1-T_2) -$$

$$0.5\ R\ (M_{g_1}+M_{g_2})\ (T_1-T_2) = 0.5\ (T_1+T_2)\ \hat{C}_{vg}\ (M_{L_1}-M_{L_2}) +$$

$$\hat{\lambda}\ (M_{L_1}-M_{L_2}) - \left\{ w_o \left[\frac{P_a}{\rho_{ga}} + 0.5\ v_o^2 + Z_h\ g\right] \right\}_{av} (t_1-t_2) \qquad (2C\text{-}10)$$

APPENDIX 2D

PROPERTIES

TABLE 2D-1 Values of C_{pg} at Different Temperatures

C_{pg} is the heat capacity of the substance in vapor phase at constant pressure. C P Eqn stands for the equation used in HACS with the coefficients from the Chemical Properties File. Since this equation gives the molar heat capacity, the molecular weight of the cargo must be used to get the specific heat. A molecular weight of 16 has been used for LNG, and a molecular weight of 114 for gasoline. 114 corresponds to octane, and the specific heat from [9] listed under gasoline is the specific heat for n-octane. LNG is assumed to be pure methane [10].

Cargo	Temperature (°C)	C_{pg} (cal/g/°K)	Source
LNG	-115	.450	[10, p.2289]
	-75	.500	[10, p.2289]
	15	.528	[10, p.2289]
	-23	.502	C P Eqn
	15	.527	C P Eqn
Chlorine	15	.115	[10, p.2288]
	25	.114	[9, p.D-135]
	15	.129	C P Eqn
	25	.131	C P Eqn
Ammonia	15	.523	[10, p.2288]
	15	.504	C P Eqn
Methyl Alcohol	77	.390	[10, p.2288]
	25	.328	[9, p.D-130]
	77	.347	C P Eqn
	25	.310	C P Eqn
Gasoline	25	.396	[9, p.D-130]
	25	.348	C P Eqn

TABLE 2D-2 Values of C_{pl} at Different Temperatures

C_{pl} is the specific heat capacity of the cargo in liquid phase. An asterisk (*) indicates that the temperature is outside the range given in the Chemical Properties File; the equation has been evaluated at this temperature nevertheless. The value of C_{pl} for gasoline from [9] is the value for n-octane.

Cargo	Temperature (°C)	C_{pl} (cal/g/°K)	Source
Chlorine	0-24	.226	[10, p.2266]
	0	.120	C P Eqn
	25*	.132	C P Eqn
Ammonia	-60	1.047	[10, p.2274]
	0	1.098	[10, p.2274]
	20	1.125	[10, p.2274]
	-60	1.040	C P Eqn
	0	1.100	C P Eqn
	20*	1.120	C P Eqn
Methyl Alcohol	0	.566	[10, p.2282]
	20	.600	[10, p.2282]
	25	.609	[9, p.D-130]
	0*	.526	C P Eqn
	20	.590	C P Eqn
	25	.606	C P Eqn
Gasoline	25	.532	[9, p.D-130]
	25	.532	C P Eqn

TABLE 2D-3 Coefficients in Equation for Vapor Pressure as a Function of Temperature

The columns headed CP have the coefficients from the Chemical Properties File, and those headed [9] have the coefficients from [9, p.D-151 to D-177]. These are the coefficients in the equation

$$\text{Log}_{10}(p_V) = A - B/(T+C) \qquad P_V \text{ in } N/m^2,\ T \text{ in } °K$$

LTB and UTB are the lower and upper temperature bounds (°C) over which these coefficients are given to be valid. The values [9] for LNG are methane values; those for gasoline are octane values.

	LNG		Chlorine		Ammonia		Methyl Alcohol		Gasoline	
	CP	[9]	CP	[9]	CP	[9]	CP	[9]	CP	[9]
A	8.737	9.153	9.543	9.675	10.61	10.40	10.93	10.76	9.027	10.02
B	389.9	465.1	1086	1132	1674	1311	2002	1962	1268	2015
C	-7.160		.04		0.0		.04		-56.1	
LTB	-180	-206	-50	-118	-13	-109	-10	-44	-20	-14
UTB	-150	-86	10	127	27	98	80	224	130	281

TABLE 2D-4 Values for p_V for Different Temperatures

The temperature column contains the temperatures at which the vapor pressure of the substance is given to be equal to the value in the column headed [10]. These values are to be found on pages 2335-2424 of [10]. The values of P_V in the other two columns are calculated from the equations given in Table 2D-3. LNG has been assumed to be pure methane and gasoline has been assumed to be pure octane. An asterisk (*) denotes values for which the temperature is outside the bounds listed for the coefficients.

Cargo	Temperature (°C)	P_V (ATM)		
		[10]	C P Eqn	Eqn from [9]
LNG	-181.4	.132	.132	.119
	-161.5	1.0	1.001	.958
	-152.3	2.0	2.005	1.987
	-138.3	5.0	4.765*	4.987
	-108.5	20.0	18.019*	20.991
Chlorine	-71.7	.132	.140*	.113
	-47.3	.526	.537	.455
	-33.8	1.0	1.003	.873
	10.3	5.0	5.088	4.748
	35.6	10.0	10.482*	10.083
Ammonia	-68.4	.132	.003*	.097
	-45.4	.526	.018*	.428
	-33.6	1.0	.041	.823
	-18.7	2.0	.106	1.721
	4.7	5.0	.379	4.676
	25.7	10.0	1.007	10.035
Methyl Alcohol	-16.2	.013	.013*	.013
	21.2	.132	.132	.124
	64.7	1.0	.997	.896
	112.5	5.0	5.410	4.697
Gasoline	-14.0	.001	.006	.002
	19.2	.013	.045	.013
	65.7	.132	.344	.117
	125.6	1.0	2.093	1.123

TABLE 2D-5 Liquid Densities

The densities of the five priority cargoes calculated from the equation whose constants are in the Chemical Properties File are compared with values from references.

Cargo	Temperature (°C)	ρ_l (g/cm^3)	Source
LNG	-164	0.415	[9, p.C-365] (methane)
	-164	0.428	C P Eqn
Clorine	-33.6	1.56	[9, p.B-10]
	-33.6	1.55	C P Eqn
Ammonia	-20	0.665	[9, p.E-21]
	-20	0.660	C P Eqn
	0	0.639	[9, p.E-21]
	0	0.639	C P Eqn
	20	0.610	[9, p.E-21]
	20	0.608	C P Eqn
Methyl Alcohol	20	0.791	[9, p.C-370]
	20	0.791	C P Eqn
Gasoline	20	0.702	[9, p.C-399] (octane)
	20	0.684	[9, p.C-321] (heptane)
	20	0.683	C P Eqn

APPENDIX 2E

SENSITIVITY ANALYSIS FOR MODA

The sensitivity analysis on the Venting Rate Model is described in the following pages.

1. The total mass released and the average flow rate are used as the output variables.

2. All five cargoes which were priority cargoes during the first year of development of the Vulnerability Model are used for the analysis. The analysis is done for both isothermal tank conditions and adiabatic tank conditions. The "medium-sized" amounts of each cargo are used. The initial conditions are given in Table 2E-1.

3. The cargo properties are contained in the Chemical Properties File. In a few cases the coefficients in an equation which is used to calculate a specific property have been changed. For example, the coefficients used in the equation to calculate the vapor pressure of ammonia have been replaced by more accurate values. The discharge coefficient and the number of increments of mass to be considered are also needed. These two quantities and the properties of the cargo are included in the class denoted parameters. The items listed in Table 2E-1 are denoted variables. A discharge coefficient of 0.80 is to be used, and the number of increments has been set at 100.

4. The subroutines shown in the figures are used. A number of problems have been encountered with the original Venting Rate Model. The changes required to upgrade the treatment of the adiabatic cases were so substantial that it seemed preferable to rewrite the subroutines involved rather than to modify the existing subroutines. Therefore, some of the subroutines discussed are considerably different from those subroutines contained in HACS. The names of the subroutines have been changed to prevent the confusion which might result from having two substantially different subroutines with the same name.

TABLE 2E-1 Initial conditions to be used in the sensitivity analysis of the Venting Rate Model. The tank volumes for the five cargoes are those designated "medium" in the VM. The mass is calculated by assuming that the tank is 93% full. The height of the tank is taken to be cube root of the volume, and the hole is assumed to be one-third of the way up the tank. The tank hole is assumed to have a diameter which is one-tenth of the tank height. The initial tank temperatures were taken to be typical for the type of transport vessel which is most commonly used.

Variable	Unit	LNG	Cl_2	NH_3	CH_3OH	Gasoline
Mass	grams	74.6×10^6	14.2×10^6	174×10^6	88.8×10^6	68.8×10^6
Volume	cm^3	200×10^6	10×10^6	300×10^6	120×10^6	100×10^6
Temperature	°C	-145	-25	+10	+15	+15
Height of Tank	cm	585	215	669	493	464
Height of Hole	cm	175	64.6	201	148	139
Diameter of Hole	cm	58.5	21.5	66.9	49.3	46.4

MODA Subroutines

The correspondence between the original subroutines in HACS and the new subroutines developed for this sensitivity analysis is shown in Table 2E-2.

VENTING (Figure 2E-1) replaces RLJVI, and performs many of the same functions, but very few statements are the same in both subroutines. The arguments are now passed in labeled COMMON statements instead of by argument lists; and the constants are now defined in DATA statements rather than in replacement statements. The nomenclature has been revised to be more consistent. Pressure is no longer included as an input because of the over-specification problem. Generally, the pressure will be the ambient atmospheric pressure if the tank has pressure relief valves.

The FORMAT statements 9001, 9003, and 9039, and the associated PRINT statements are included only for testing and for the sensitivity analyses. They will be removed before the subroutine is made a part of the VM.

The main loop in VENTING extends from statement number 11 to the statement above statement number 50. In this loop the mass in the tank is decremented, and the tank conditions and the flow rate at the end of the escape of this mass decrement are calculated by means of the call to TANK. The procedure here is straightforward - the amount of mass in the tank is decreased by the size of the decrement, and the time for this amount of mass to escape is computed using a flow rate which is the average of the rate at the beginning of the escape of the decrement and of the rate at the end of the escape of this decrement. In RLJVI, a time for the escape of the decrement was calculated based on the beginning flow rate, and then this time period was multiplied by the final flow rate to give the amount which escaped.

Subroutine TANK is shown in Figure 2E-2. This subroutine performs the functions which were previously divided between RLJTC and RLJTS. There are four different cases to be considered, depending upon whether the tank conditions are taken to be isothermal or adiabatic, and whether there is both liquid and gas in the tank, or only gas. The isothermal cases are quite simple, and are easily computed.

In RLJTC and RLJTS, the iteration loop for the adiabatic case was contained in RLJTC, and the equations were evaluated in RLJTS. It turns out that the case in which there is only gas in the tank may be solved analytically, hence an iterative procedure in this case is not required. The thermodynamics of the case when there is both liquid and gas in the tank depend upon whether the cargo is escaping in liquid or vapor phase. Thus the two subcases for an adiabatic tank containing both liquid and gas make up the greater part of this subroutine. The computations when gas is escaping are covered in the section that starts ten cards below statement 31, and the computations when liquid is escaping begin at statement 41.

In RLJTC and RLJTS the procedure was to assume that the temperature at the end of the decrement was 10°K below the temperature at the beginning of

TABLE 2E-2 Correspondence of the subroutines in the new version of the Venting Rate Model with the subroutines in the old version. TANK replaces both RLJTC and RLJTS. The calling sequence is somewhat different, because the flow rate must be known at the new step in order to calculate the tank conditions for this step. Thus FLOW is called from TANK, whereas VENTR was called from RLJVI.

New Name	Old Name	Comments
VENTING	RLJVI	Main Calculational Subroutine, called by MODA.
TANK	RLJTC, RLJTS	Computes the tank conditions.
FLOW	VENTR	Calculates the rate at which mass escapes.
LIQLEV	RLJLQ	Computes the height of the liquid in the tank.
VAPPR	RLJVP	Computes the vapor pressure for a given temperature.

```
      SUBROUTINE  VENTING
C  THIS SUBROUTINE DECREMENTS THE AMOUNT OF MASS IN THE TANK, AT EACH
C  STEP THE OUTFLOW RATE, TIME, AND TANK CONDITIONS ARE COMPUTED.
C
C **** INPUTS
C      VOL      VOLUME OF TANK                                  CM**3
C      HT       HEIGHT OF TANK                                  CM
C      HH       HEIGHT OF HOLE                                  CM
C      HOLED    DIAMETER OF THE HOLE                            CM
C      DL       LIQUID DENSITY                                  GM/CM**3
C      TO       INITIAL TEMPERATURE OF TANK                     DEG K
C      AMSO     INITIAL MASS OF CARGO IN TANK                   GRAMS
C      AM       MOLECULAR WEIGHT OF THE CARGO
C      CPG      HEAT CAPACITY OF VAPOR                          CAL/GM-DEG C
C      CPL      HEAT CAPACITY OF LIQUID                         CAL/GM-DEG C
C      IADBT    HEAT TRANSFER FLAG (IF POSITIVE, TANK IS ADIABATIC,
C                  OTHERWISE IT IS ISOTHERMAL
C      HVAP     HEAT OF VAPORIZATION                            CAL/GM
C      INC      NUMBER OF MASS INCREMENTS TO BE USED     MAX = 200
C      AVP,BVP,CVP    CONSTANTS IN VAPOR PRESSURE EQUATION
C      CO   DISCHARGE COEFFICIENT

      COMMON /MAP/ AVP,BVP,CVP, R,RS,G,A,CO,ACO, AM,AK,CPG,CVG,CL, HVAP,
     1 IADBT,INC,INS, HT,HH,HOLED, VOL,VOLVP,VOLVN, AMSO,AMSP,AMSN,DELMS
     2 ,TMS,TMSL,TMSG, XP,XN,DVP,DVN,DL, WP,WN,AVFLOW, TIMP,TIMN,DZP,DZN
     3 ,PO,PP,PN,PV,PA, TO,TP,TN,TT,TA
      COMMON / FLOCON / BTEST, CHOK, CN1,CN2,CN3

C **** OUTPUTS
C      INS      NUMBER OF INCREMENTS RELEASED
C      TMS      TOTAL MASS RELEASED                             GRAMS
C      TMSL     TOTAL MASS OF LIQUID RELEASED                   GRAMS
C      TMSG     TOTAL MASS OF GAS RELEASED                      GRAMS
C      TIMP     TIME TO COMPLETE VENTING                        SECONDS
C      AVFLOW   AVERAGE FLOW RATE                               GRAMS/SEC
C      FRMSV    FRACTION OF ORIGINAL MASS VENTED

      DATA  R/8.317E7/, G/980.665/, PA/1013250./

C **** CALCULATED VARIABLES
C      THE LAST LETTER USUALLY INDICATES A TIME OR STATE
C              O FOR INITIAL
C              P FOR PRESENT OR PREVIOUS STEP
C              N FOR NEW OR NEXT STEP
C              A FOR AMBIENT CONDITIONS OUTSIDE THE TANK
C              THUS PP = PRESENT PRESSURE, PN = NEW PRESSURE, ETC
C      P     PRESSURE            DYNES/CM**2
C      T     TEMPERATURE         DEGREES K
C      W     OUTFLOW             GRAMS/SECOND
C      X     FRACTION OF MASS IN GAS(VAPOR) PHASE
C      DZ    HEIGHT OF LIQUID SURFACE ABOVE HOLE               CM
C      DV    DENSITY OF VAPOR    GRAMS/CM**3
C      AMS   MASS                GRAMS
C      TIM   TIME                SECONDS
C      VOLV     VOLUME OCCUPIED BY VAPOR                       CM**3
C
C **** MISCELLANEOUS ITEMS  -  CONSTANTS, ETC.
C      A     AREA OF HOLE        CM**2
C      R     UNIVERSAL GAS CONSTANT          ERGS/MOLE/DEG K
C      RS    SPECIFIC  GAS CONSTANT          ERGS/GRAM/DEG K
C      AK    RATIO OF SPECIFIC HEATS

      AK = 1./ ( 1. - ( 1.986 / AM / CPG ) )
      A = 3.14159 * HOLED * HOLED / 4.
      ACO = A * CO
      RS = R / AM
C     R AND RS IN ERGS, CPG,CVG, AND CL IN CALORIES
      CVG = CPG - 1.986/AM
      PRINT 9001,AK,A,ACO,AM,RS,CVG
```

FIGURE 2E-1 Venting.

```
9001 FORMAT(* VENTING  AK A ACO AM RS CVG *,6G12.4)

     AKP = AK + 1.
     AKM = AK - 1.
     BTEST = ( 2. / AKP ) ** ( AK / AKM )
     CHOK = AK / RS * ( 2./ AKP ) ** ( AKP / AKM )
     CN1 = 2.* AK / AKM
     CN2 = 2. / AK
     CN3 = AKP / AK
     PRINT  9003,   BTEST, CHOK, CN1,CN2,CN3
9003 FORMAT      (* BTEST, CHOK, CN1,CN2,CN3 *, 5G12.4 ;

     TMSG = 0.0
     TMSL = 0.0
     TIMN = 0.0
     AMSN = AMSO
     INC = MIN0( 200, INC )
     DELMS = AMSO / FLOAT( INC )
     TN = TO
     PP = AMSN * RS * TN / VOL
     PO = AMIN1( PP, VAPPR( TN, AVP,BVP,CVP ) )
     PN = AMAX1( PO, PA )
     PO = PN
     DVN = PN / RS / TN
     XN = ( VOL * DL * DVN / AMSN - DVN ) / ( DL - DVN )
     CALL  FLOW
     INS = -1
     GO TO 44

  11 AMSN = AMSP - DELMS
     IF ( AMSN .LT. 0.004*AMSO )   GO TO 55
     CALL  TANK
     IF ( PN + DZN*DL*G .LE. PA ) GO TO 55
     IF ( DZN .GE. 0.0 )   TMSL = TMSL + DELMS
     IF ( DZN .LT. 0.0 )   TMSG = TMSG + DELMS
     TIMN = TIMP + 2.* DELMS / ( WN + WP )

  44 PP = PN
     TP = TN
     XP = XN
     WP = WN
     DZP = DZN
     DVP = DVN
     AMSP = AMSN
     VOLVP = VOLVN
     TIMP = TIMN
     INS = INS + 1
     IF ( INS .LE. INC )   GO TO 11

  55 TMS = TMSL + TMSG
     IF ( TIMP .LE. 0.0 ) GO TO 56
     AVFLOW = TMS / TIMP
     GO TO 57
 56  AVFLOW = 0.0
 57  FRMSV = TMS / AMSO
     PRINT  9039, INS, TMSG,TMSL,TMS,FRMSV, AVFLOW,TIMP,DZP,PP,XP,TP
9039 FORMAT (*0VENTING    INS*,I4,3X,*MASS VENTED  GAS LIQ TOT FRACTION
    1*,3E10.4,F6.3, 5X,*AVG RATE =*,E10.4 / * TIME =*,F7.2,* SEC
    2 DZ =*,F7.2, 3X,*PT =*,E10.4, 3X,*X =*,F7.4, 3X,*T =*,F7.2 // )
     RETURN
     END
```

FIGURE 2E-1 (continued) Venting.

```
      SUBROUTINE  TANK
C  COMPUTES TANK CONDITIONS - PN,TN,DVN, XN, ETC
      COMMON /MAP/ AVP,BVP,CVP, R,RS,G,A,CO,ACO, AM,AK,CPG,CVG,CL, HVAP,
     1 IADBT,INC,INS; HT,HH,HOLED, VOL,VOLVP,VOLVN, AMSO,AMSP,AMSN,DELMS
     2 ,TMS,TMSL,TMSG, XP,XN,DVP,DVN,DL, WP,WN,AVFLOW, TIMP,TIMN,DZP,DZN
     3 ,PO,PP,PN,PV,PA, TO,TP,TN,TT,TA
C     ERGCAL     NUMBER OF ERGS IN ONE CALORIE (GRAM-CALORIE)
      DATA  ERGCAL/4.184E7/

      IF ( IADBT .GT. 0 )   GO TO 21

C  ISOTHERMAL CASE
      TN = TP
      PN = AMSN * RS * TN / VOL
      PV = VAPPR ( TN, AVP,BVP,CVP )
      IF ( PN .LT. PV )   GO TO 15
C  BOTH LIQUID AND VAPOR(GAS) IN THE TANK
      PN = AMAX1 ( PV, PA )
      DVN = PV / RS / TN
      XN = ( VOL * DL * DVN / AMSN - DVN ) / ( DL - DVN )
      GO TO 99
C  ONLY GAS IS IN THE TANK
   15 DVN = AMSN / VOL
      XN = 1.0
      PN = AMAX1 ( PN, PA )
      GO TO 99

C ADIABATIC TANK CONDITIONS
C FIND NEW TEMP (TN) AND NEW PRESSURE (PN) IF ONLY GAS IS IN THE TANK
   21 F1 = AMSN * RS / VOL
      TN = ( F1 / PP ) ** (AK-1.) * TP ** AK
      PN = F1 * TN
C     IF LIQUID IS IN TANK, NEW TEMP WILL BE CLOSE TO OLD TEMP
      PV = VAPPR ( TP, AVP,BVP,CVP )
      IF ( PV .LT. PN )   GO TO 31
C  ONLY GAS IS IN THE TANK
      GO TO 15

C  BOTH GAS AND LIQUID ARE IN THE TANK
   31 PN = PP
      TN = TP
C  FOR FIRST ESTIMATE, ASSUME THAT PN=PP, TN=TP
      DVN = DVP
      XN = ( VOL * DL * DVN / AMSN - DVN ) / ( DL - DVN )
      CALL  LIQLEV
      AMSLP = AMSP * ( 1.- XP )
      AMSGP = AMSP * XP
      L = 0
      IF ( DZN .GT. 0.0 )   GO TO 41

C GAS IS ESCAPING    ENERGY EQUATION IS IN CALORIES
C FOR A FIRST APPROXIMATION USE DELMS FOR DELMSL
      F1 = 0.5 * CVG * DELMS
      CMSLP = CL * AMSLP
      VOP = WP / ACO / DVP
      POT = RS * TA + G * HH
      PEET = WP * ( POT + 0.5*VOP*VOP )
C  USING THE 4 LARGEST TERMS, GET FIRST ESTIMATE OF TN
      TN = ( (CMSLP - F1)*TP - HVAP * DELMS )/ ( AMSN*(1.-XN)*CL + F1 )
```

FIGURE 2E-2 Tank.

```
C  START ITERATION LOOP
   33 L = L + 1
      PN = VAPPR ( TN, AVP,BVP,CVP )
      IF ( PN .LE. PA )   GO TO 38
      DVN = PN / RS / TN
      XN = ( VOL * DL * DVN / AMSN - DVN ) / ( DL - DVN )
      CALL  FLOW
      VON = WN / ACO / DVN
      F3 = WN * ( POT + 0.5*VON*VON )
      DELTIM = DELMS * 2.0 / ( WP + WN )
      F4 = 0.5 * ( F3 + PEET ) * DELTIM / ERGCAL
C  ENERGY OF ESCAPING CARGO IS INDETERMINATE DURING THE STEP IN WHICH
C  THE VENTING CHANGES FROM LIQUID VENTING TO GAS VENTING
      IF ( DZP .GT. 0.0 )   F4 = 0.0
      DELMSL = AMSLP - AMSN * ( 1.- XN )
      F2 = 0.5 * CVG * DELMSL
      F1 = 0.5 * ( AMSGP + AMSN * XN ) * CVG
      TT = ( ( CMSLP + F1 - F2 ) *TP - HVAP * DELMSL - F4 ) /
     1   ( AMSN * (1.- XN) * CL + F1 + F2 )
      TN = 0.2 * ( 4.*TT + TN )
      IF ( L .LT. 2 ) GO TO 33
      IF ( L .GT. 10 )   GO TO 99
      IF ( ABS ( TT - TN ) .GT. 0.01 )   GO TO 33
      GO TO 99

   38 PN = PA
      PRINT  9038,   INS,L,TN,PN
 9038 FORMAT(*0L INS *,2I4,*    TN PN *,F10.4,G12.4,* END GAS VENTING *,
     1      *     PV .LE. PA* / )
      RETURN

C LIQUID IS ESCAPING     ENERGY EQUATION IS IN (GRAM) CALORIES
   41 CMSGP = CPG * AMSGP
      VOP = WP / ACO / DL
      POT = PA / DL + G * HH
      PEET = WP * ( POT + 0.5*VOP*VOP )
C  FIRST APPROXIMATION, ASSUME GAS FILLS VOL LEFT BY VENTING LIQUID
C     DELMSG = AMSGP-AMSGN = NEGATIVE IF MASS OF GAS IS INCREASING
      DELMSG = - DVN * DELMS / DL
      CMSLAV = CL  *0.5 *( AMSLP + AMSN*(1.-XN) )
      F2 = 0.5 * CL * DELMSG
      TN = ( TP*(CMSLAV-F2) + (CPG*TP + HVAP) *DELMSG )/( CMSLAV + F2 )

C  START ITERATION LOOP
   44 L = L + 1
      PV = VAPPR ( TN, AVP,BVP,CVP )
      PN = AMAX1 ( PV, PA )
      DVN = PV / RS / TN
      XN = ( VOL * DL * DVN / AMSN - DVN ) / ( DL - DVN )
      CALL  FLOW
      VON = WN / ACO / DL
      F3 = WN * ( POT + 0.5*VON*VON )
      DELTIM = DELMS * 2.0 / ( WP + WN )
      F4 = 0.5 * ( F3 + PEET ) * DELTIM
      F3 = ( F4 + ( VOLVP * PP - VOLVN * PN ) ) / ERGCAL
      DELMSG = AMSGP - AMSN * XN
      CMSLAV = CL  *0.5 *( AMSLP + AMSN*(1.-XN) )
      F2 = 0.5 * CL  * DELMSG
      F1 = CMSLAV + AMSN * XN * CPG
      TT = (TP*(CMSLAV+CMSGP-F2) + HVAP * DELMSG - F3 ) / ( F1 + F2 )
      TN = 0.2 * ( 4.*TT + TN )
      IF ( L .LT. 2 ) GO TO 44
      IF ( L .GT. 10 )   GO TO 99
      IF ( ABS ( TT - TN ) .GT. 0.03 )   GO TO 44

   99 CALL  FLOW
      RETURN
      END
```

FIGURE 2E-2 (continued) Tank.

the decrement for the first iteration, and then to come successively closer to the final temperature by the method of halving the interval. The procedure here is to estimate the final temperature for the first iteration by using just the largest terms in the energy equation. The size of the terms and the equations used in TANK are discussed in the text of this chapter. This scheme requires fewer iterations than the earlier method. In the case of liquid venting, the temperature drop is usually a small fraction of a degree for each mass decrement, and two iterations are usually sufficient to find the temperature to within a few hundredths of a degree. Two or three iterations are usually sufficient for gas venting as well, even though the temperature drop in these cases is usually a few degrees.

The energy equation given in Appendices 2B and 2C contains the temperature both explicitly and implicitly through the vapor pressure and the vapor density. Ignoring the implicit dependence on temperature, the energy equation is solved for temperature at the end of the mass decrement. The temperature so obtained is denoted TT in TANK. The temperature used to obtain the vapor pressure and gas density is denoted TN. When the value of TT is found to be very close to the value of TN used in obtaining TT, the equation is satisfied. In examining the results of individual iterations, it was found that the final value of the temperature was closer to TT and to TN after each step, so the value of TT is weighted more heavily than the old value of TN when calculating the new TN.

The step during which the liquid level falls below the height of the hole presents special problems. It has been assumed here that the vertical dimension of the hole or puncture is small enough so that the escape of both liquid and gas simultaneously will not be very long compared to the time required for the complete venting. While it is possible to do a detailed analysis of the amounts of liquid and gas vented during the period in which the liquid level falls from the top of the hole to the bottom of the hole, this does not seem to be worthwhile. The level of effort required is not consistent with the detail of approximations made elsewhere in this submodel and in other submodels. Further, the exact configuration and dimensions of the puncture would be needed, and these are unlikely to be available for actual accidents. This problem has been treated by assuming that the tank vents liquid as long as the liquid level at the end of the time decrement step is above the hole height. Otherwise that venting of gas is assumed. The program compares the hole height and the liquid level at each step to determine which phase is being vented, and switches to gas venting from liquid venting when appropriate. The first step in which gas venting is assumed presents a small problem, however. In calculating the energy which the escaping fluid takes with it, the flow rate at the beginning of the decrement and the end of the decrement is needed. For this one step, the escaping mass was liquid at the beginning of the step and gas at the end of the step. Rather than go through a long procedure to determine the amount of energy carried away in this special case, because this term is not a particularly large one in the energy equation, this term is ignored for this one step.

Subroutine FLOW (Figure 2E-3) performs the same calculations that VENTR did, but there are many differences between the two. In the first place, the

arguments have been placed in COMMON/MAP/. Secondly, since the outflow rate is evaluated many times, the combinations of constants are evaluated once in VENTING, and passed into FLOW in COMMON/FLOCON/. Finally, the pressures here are in dynes/cm^2 whereas the pressures were in grams-force/cm^2 in the original version of VENTR.

```
      SUBROUTINE  FLOW
      COMMON /MAP/ AVP,BVP,CVP, R,RS,G,A,CO,ACO, AM,AK,CPG,CVG,CL, HVAP,
     1 IADBT,INC,INS, MT,MH,MOLED, VOL,VOLVP,VOLVN, AMSO,AMSP,AMSN,DELMS
     2 ,TMS,TMSL,TMSG, XP,XN,DVP,DVN,DL, WP,WN,AVFLOW, TIMP,TIMN,DZP,DZN
     3 ,PO,PP,PN,PV,PA, TO,TP,TN,TT,TA
      COMMON / FLOCON / BTEST, CHOK, CN1,CN2,CN3

      CALL  LIQLEV
      IF ( DZN .LE. 0.0 )   GO TO 11

C LIQUID VENTING
      WN = ACO * SQRT ( 2.*DL *(PN - PA + G* DL * DZN ) )
      RETURN

C GAS VENTING
   11 B = PA / PN
      IF ( B .LT. 1.0 )   GO TO 13
      WN = 0.0
      RETURN
   13 IF ( B .GE. BTEST )   GO TO 17
C CHOKED FLOW
      WN = ACO * PN * SQRT ( CHOK / TN )
      RETURN
C NON-CHOKED FLOW
   17 WN = ACO * SQRT ( CN1 * DVN * PN * ( B**CN2 - B**CN3 ) )

      RETURN
      END
```

FIGURE 2E-3 Flow.

LIQLEV (Figure 2E-4) computes the distance of the liquid-gas interface above the hole. If the liquid surface is below the hole, a value of -0.01 cm is returned. This allows the test for the cessation of venting to be one simple test (third statement below statement 11 in VENTING) rather than the more complicated procedure used in RLJVI. Figure 2E-4 also contains the function VAPPR, which computes the vapor pressure in dynes/cm^2 for the given temperature.

```
      SUBROUTINE  LIQLEV
      COMMON /MAP/ AVP,BVP,CVP, R,RS,G,A,CO,ACO, AM,AK,CPG,CVG,CL, HVAP,
     1 IADBT,INC,INS, HT,HH,HOLED, VOL,VOLVP,VOLVN, AMSO,AMSP,AMSN,DELMS
     2 ,TMS,TMSL,TMSG, XP,XN,DVP,DVN,DL, WP,WN,AVFLOW, TIMP,TIMN,DZP,DZN
     3 ,PO,PP,PN,PV,PA, TO,TP,TN,TT,TA
      VOLLN = ( 1.- XN ) * AMSN / DL
      VOLVN = VOL - VOLLN
      DZN = HT * VOLLN / VOL - HH
      IF ( DZN .LT. 0.0 )   DZN = -0.01
      RETURN
      END



      FUNCTION VAPPR ( T, A,B,C )
C  GIVES VAPOR PRESSURE IN DYNES/CM**2  FOR T IN DEG K
C  THE +1 CONVERTS FROM NEWTONS/M**2
      X    = A - B / ( T + C )
      VAPPR = 10. ** ( X + 1. )
      RETURN
      END
```

FIGURE 2E-4 LIQLEV and VAPPR.

CHAPTER 2 - LIST OF SYMBOLS

A_h = area of the hole or puncture in the tank (cm^2)

A_T = cross-sectional area (xy plane) of the tank (cm^2)

$\hat{C}_L$ = specific heat of the liquid phase of the cargo (cal/g °C)

$\hat{C}_{pg}$ = specific heat at constant pressure of the gas phase of the cargo (cal/g °C)

$\hat{C}_{vg}$ = specific heat at constant volume of the gas phase of the cargo (cal/g °C)

E = energy of the cargo as defined by the equation (2C-4) (erg or cal)

g = acceleration due to gravity (cm/s^2)

K = kinetic energy of the cargo with respect to the tank (erg or cal)

M = mass of the cargo at any time (g)

P = pressure (variously $dyne/cm^2$, gmf/cm^2, atm)

R = gas constant (cal/g-mole °K)

T = absolute temperature (°K)

t = time (s)

U = internal energy (cal or erg)

V = volume (cm^3)

v = velocity (cm/s)

W = rate at which work is done by the system (dyne/s or cal/s)

w = mass flow rate (g/s)

X = mass fraction of the gas phase in the tank

z = vertical coordinate, z=0 at the bottom of the tank and increases in the upward direction (cm)

ρ = density (g/cm^3)

λ = heat of vaporization (cal/g)

Φ = potential energy of the cargo (cal or erg)

PRECEDING PAGE BLANK-NOT FILMED

Δ = change between outflow and inflow

$< >$ = average value of a quantity over the area through which the material is flowing

SUBSCRIPTS:

e refers to the evaporating mass

g refers to the gas phase

h refers to the hole

L refers to the liquid phase

o refers to the outflow through the hole

s refers to the surface between the liquid and the gas in the tank

T refers to the tank as a whole

tot refers to the value of a property for the entire system

1 refers to the initial state

2 refers to the final state

A circumflex (^) indicates that the quantity is given per unit mass

CHAPTER 2 - REFERENCES

[1] Department of Transportation, U.S. Coast Guard, Assessment Models in Support of the Hazard Assessment Handbook (CG-446-3), CG-D-65-74, January 1974.

[2] Arthur D. Little, Inc., Hazard Assessment Computer System, User Manual (HACS), Cambridge, Mass., December 1974.

[3] Short, B. E., H. L. Kent, Jr., and B. F. Treat, Engineering Thermodynamics, pp. 133 ff., Harper, New York, 1953.

[4] Landau, L. D., and E. M. Lifshitz, Fluid Mechanics, p. 4, Pergamon, London, 1959.

[5] Blackburn, J. F., G. Reethof, and J. L. Shearer, Fluid Power Control, pp. 178-184, M.I.T. Press, Cambridge, Mass., 1960.

[6] Lamb, H., Hydrodynamics, pp. 23-25, Dover, New York, 1945.

[7] Owczarek, J. A., Fundamentals of Gas Dynamics, pp. 204-205, International Textbook Co., Scranton, Pa., 1964.

[8] Thompson, P. A., Compressible-Fluid Dynamics, McGraw-Hill, New York, 1972.

[9] Weast, R. C. (ed.), Handbook of Chemistry and Physics, 52nd ed. (1971-1972), Chemical Rubber Co., Cleveland, Ohio, 1971.

[10] Hodgman, C. D. (ed.), Handbook of Chemistry and Physics, 49th ed. (1959-1960), Chemical Rubber Co., Cleveland, Ohio, 1959.

[11] Bird, R. B., W. E. Stewart, and E. N. Lightfoot, Transport Phenomena, ch. 15, Wiley, New York, 1960.

CHAPTER 3

MIXING AND DILUTION MODEL

INTRODUCTION

The Mixing and Dilution Model is designed to compute the concentrations of a spilled cargo in water. The concentration is computed for locations on and below the water surface as a function of time from the beginning of the spill. This model corresponds to the documentation in Chapter 4, Mixing and Dilution, of the Assessment Models in Support of the Hazard Assessment Handbook (AMSHAH) [1]. The corresponding computer code in the Hazard Assessment Computer System (HACS) [2] is under the executive subroutine MODP which utilizes the following computational subroutines: DILUN, DLIN, DISP, and CNSPL.

AMSHAH originally considers five basic types of environmental settings in which a spill may occur. These are lakes (still water), non-tidal rivers, tidal rivers, estuaries, and open sea. Of these five, only three are analyzed in AMSHAH, namely, non-tidal rivers, tidal rivers, and estuaries, and only three are computer coded in HACS: non-tidal rivers, tidal rive[illegible]rd still water (Table 3-1). The solutions of the partial differen[illegible]ations governing the mixing and dilution of the spills are obta[illegible]the form of a "near-field" approximation (when the location of the concentration to be computed is "near" the spill) or a "far-field" approximation (when the location of the concentration is "far" from the spill). The spill itself is modeled as either a "continuous" spill or an "instantaneous" spill, depending upon whether the spill is best characterized as continuous or instantaneous in nature given the time of observation of the spilling-mixing process. When the length of time is greater than five times the total venting time of a continuous spill, the computations are based on the analysis of "instantaneous" spills.

Some of the major problems encountered in the Mixing and Dilution Model developed in AMSHAH and the corresponding coding in HACS are: the complete neglect of buoyancy forces in the modeling of the dispersion of the spill; an artificial "jump" in the concentration predictions when the model switches from a near-field approximation to a far-field approximation, because of a lack of matching of the asymtotic behavior when the switching occurs; lack of an accurate analysis for the near-field region when the spill is in a tidal river; predicted concentration of the spilled cargo that

---

[1] Department of Transportation, U.S. Coast Guard, Assessment Models in Support of the Hazard Assessment Handbook (CG-446-3), CG-D-65-74, January 74.

[2] Arthur D. Little, Inc., Hazard Assessment Computer System, User Manual (HACS), Cambridge, Mass., December 1974.

TABLE 3-1 Types of Receiving Bodies for Spilled Cargo

	AMSHAH Discussion	AMSHAH Analysis	HACS Computer Coding
Lakes	*		
Non-tidal rivers	*	*	*
Tidal rivers	*	*	*
Estuaries	*	*	
Open sea	*		
Still water			*

becomes greater than the density of the cargo in the liquid state for many hours after an instantaneous spill, when in reality the concentration of the spilled cargo cannot be greater than the density of the cargo in the liquid state; no documentation in AMSHAH for the computer coding in HACS for the analysis of dispersion in still water; various typographical errors in AMSHAH and coding errors in HACS. The symbols and references are listed at the end of this chapter.

ASSUMPTIONS AND APPROXIMATIONS

The following is a list of the assumptions and approximations which were made either explicitly or implicitly in the modeling of the Mixing and Dilution Model.

1. There are no heat sources or heat sinks, no chemical reaction or phase change in either the spill or in the water in which the spill occurs.

2. The effect of buoyancy on the dissemination of the spilled cargo is negligible.

3. Density stratification within the receiving water bodies has negligible effect on the dissemination of the spilled cargo.

4. The velocity distribution across a river is assumed to be uniform in all cases.

5. The river is modeled as a rectangular channel.

6. Image sources of the first order are assumed sufficiently accurate to satisfy the boundary conditions on the sides of the river.

7. In the computer coding of HACS, for the Mixing and Dilution Model, the spill rate (venting rate) is assumed to be constant for the entire duration of continuous spills.

8. The longitudinal dispersion is considered vanishingly small for the near-field approximation of continuous spills.

9. When the concentration of the pollutant is nearly uniform across a river, the far-field approximation can be used.

10. The river velocity of tidal rivers is treated as a constant velocity on which is superimposed a sinusoidal variation which is dependent on the tides at sea.

The following is a brief discussion of the implications of the assumptions and approximations.

1. No heat sources, heat sinks, chemical reaction or phase changes influence the dispersion. The Mixing and Dilution Model does not consider any heat sources or sinks in the spill of the cargo into the water. Initial differences of temperature between the spilled cargo and the receiving water bodies are not considered. It is assumed that the cargo is instantaneously brought to the temperature of the water without affecting in any way the mixing and dilution of the cargo. However, changes in cargo properties caused by bringing the cargo to the temperature of the receiving water are considered by the model. Chemical reactions of the spill with water are not considered by this model, nor is a phase change of the spill considered. Some phase changes, from liquid to vapor, if they occur, would be analyzed by the mixing and evaporation model. The assumptions stated here are valid for a large number of cargoes and any exceptional cargoes would require additional analysis.

2. Effect of buoyancy on the dissemination of the spilled cargo is negligible. The amount of dispersion or movement of the pollutant that is caused by buoyancy is assumed to be negligible compared to the amount of dispersion or movement of the pollutant that is caused by diffusion and convection. While this assumption may give acceptable predictions of concentrations of spills for cargoes which are neutrally buoyant in the receiving water body, the model is not applicable to cargoes denser or lighter than water. The mechanism of mixing and dilution for spills that are denser than water (and hence sink) is quite different from the mechanism of mixing and dilution for spills nearly equal in density to that of water. In order to consider the effects of buoyancy analytically, it is necessary to solve the system of partial differential equations comprised of the continuity equation, momentum equation, and diffusion equation; this task is considerably more difficult than the analysis given in AMSHAH in which only the diffusion equation is considered.

3. Density stratification within the receiving water body has negligible effect on the dissemination of the spilled cargo. The assumption of negligible effect on dissemination of spilled cargo by density stratification is a limiting assumption. Density stratification can form one or more inversion floors and ceilings and hence affect the dissemination of the spilled cargo. Even for neutrally buoyant cargo spills, the inversion layers may affect the dissemination of the pollutant with a possibility of the formation of inverted mushroom spill envelopes.

4. The velocity of the river is uniform. In both AMSHAH and HACS an implicit assumption is that the river velocity is uniform, i.e., the flow does not vary with time (for the non-tidal river - a time variation is considered for tidal rivers) or changes of position in either the streamwise, cross-stream, or depthwise directions. In fact the river velocity does change with changes in any of these variables. For non-tidal rivers, the time variation of flow may occur at a sufficiently slow rate so that negligible changes occur over the time of observation of the spill; for such cases the time invariance of flow is an acceptable assumption.

Since the river velocity is always zero at solid boundaries, viz. the sidewalls and bottom, it is known a priori that the assumption of velocity invariance with depth and cross-stream distance is, strictly speaking, invalid. However, since the rivers of interest generally contain turbulent flow, the velocity profiles will tend to be blunt and in many cases may be accurately modeled by slug flow. Variations in flow velocity with distance downstream will generally occur, caused both by changes in the geometry of the riverbed and by inflow of additional water from tributaries. Whether these variations may be successfully neglected depends upon how rapidly the flow varies with distance downstream and for how long a distance downstream the spill is to be observed.

5. River is modeled as a rectangular channel. The cross sections of rivers are such as to have either sharp banks and approximately flat beds (rectangular) or sloping banks and irregular inclined beds. For the purpose of modeling, the river has been modeled as having sharp banks and a flat bed and the rectangular area of the model is set equal to the irregular cross-sectional area of the actual river. The depth or width is specified and equating the areas thereby determines the remaining geometrical parameter. Both the river depth and width are then specified as user inputs to the model. Modeling the river as a rectangular channel seems to be an adequate assumption for the type of accuracy desired. The details of the configuration of the river are not as important as the gross depth and width of the river. The modeled rectangular channel is shown in Figure 3-1.

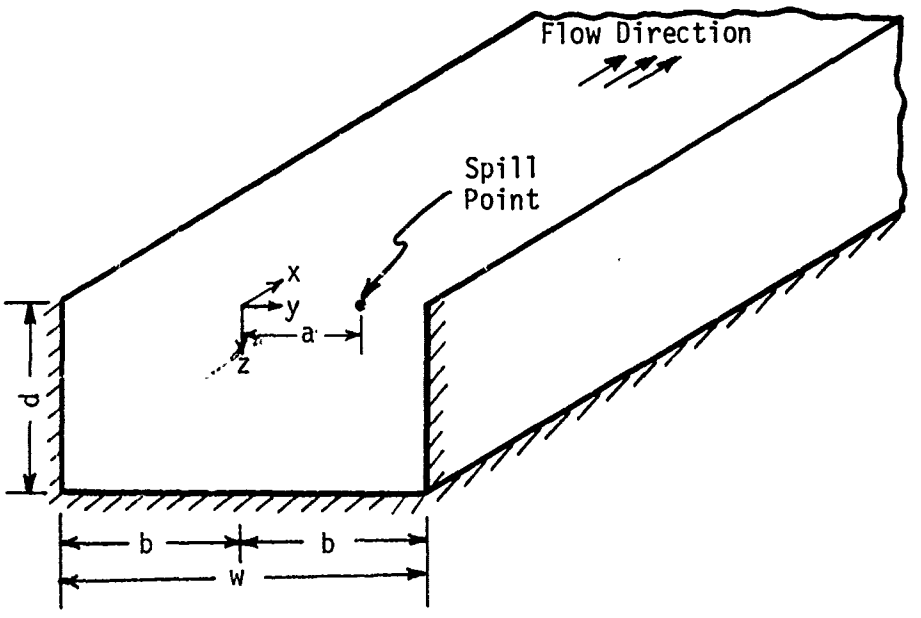
6. First order image sources are sufficient for river bank boundary conditions. It is implicitly assumed that there is no loss of the spilled cargo by either adhesion to the river banks or by absorption into the river banks. In order to predict the concentrations of the spill at various locations, the model first utilizes the solution of the equations in an infinite region and then utilizes the superimposed solutions from first-order image sources to "confine" the spill within the banks of the river. For an "exact" confinement, an infinite number of image sources would be necessary. The first-order images (one reflected about each bank) gives an acceptable prediction of the concentrations only if the solution is applied for time durations after the spill which are smaller than the horizontal dispersion time given by

$$T_c = b^2/(e_y) \qquad \text{AMSHAH (4.4a), (3-1)}$$

or the vertical dispersion time given by

$$T_{cz} = d^2/(e_z) \qquad (3\text{-}2)$$

where b = half-width of the river
d = depth of the river
e_y, e_z = turbulent diffusion coefficients in the y and z directions.



a = distance of spill point from center of channel

b = half-width of the channel

d = depth of the channel

w = width of the channel

x,y,z = coordinate axes

FIGURE 3-1 Rectangular channel model.

7. Constant spill rate. The model as developed incorporates continuous spills. Some of the analysis in AMSHAH considers available spill rate for continuous spills. The computer program DILUN of HACS assumes the spill rate "ZMDOT" is a constant. In the HACS model, MODP, the rate of spill is set equal to a constant averaged spill rate which is obtained by dividing the total mass of the spill by the total time of spilling. This averaged spill rate may give acceptable predictions when the instantaneous spill rate is approximately constant throughout most of the spilling process. (The total simulated mass spilled is set equal to the total cargo actually spilled.)

8. Longitudinal dispersion is negligible in the near-field treatment for continuous spills. The additional longitudinal travel of a spill due to dispersion in the direction of the river is assumed negligible in comparison to the travel of the spill by the river velocity, for the near-field analysis of continuous spills. This assumption is applicable to rivers in which the rate of longitudinal diffusion is small compared to the rate of advection by the river velocity; all but very slowly flowing rivers fall into this category.

9. Far-field concentration of a spilled material can be obtained from a one-dimensional analysis of the diffusion process. After a spill occurs in a river - the spill being either continuous or instantaneous - as the spill travels downstream, the mixing and dilution process distributes the pollutant throughout the cross section of the river. When the concentration of the pollutant is nearly uniform throughout the cross section of the river, a one-dimensional diffusion model is used for modeling this far-field location. This approximation gives concentration of the pollutant at downstream locations but assumes that the concentration across the river is uniform. The far-field approximation appears to be adequate, but care should be used to assure appropriate matching to the near-field solution.

10. Variations in the tidal river velocity are sinusoidal. The velocity of water in tidal rivers is dependent on the rate of discharge of the water in the river and the superimposed effect of rising and falling tides. The velocity of the current is denoted by U_f and the amplitude of the sinusoidal superimposed tidal flow velocity is denoted by U_T. Since the superimposed tidal flow velocity, U_T, of a river is both along the direction of flow velocity of the river, U_f, during falling tide and opposite to the direction of the flow of the river during rising tide, the total flow velocity $U(t)$ of the river can be represented by

$$U(t) = U_f + U_T \sin [\sigma (t - \delta)] \qquad (3\text{-}3)$$

where σ is 2π divided by the tidal period, δ represents the time until the next high-water stack, and $t = 0$ is the time of occurrence of the spill. This is a reasonable assumption, but time variations in river velocity

caused by winds, storms, runoff, and the effect of the sun on tides are not described by this formula.

ERRORS AND INCONSISTENCIES

This section summarizes inconsistencies and errors in documentation in the computer programming and in the analyses for the Mixing and Dilution Model.

In developing the Mixing and Dilution Model, Figure 4.1 in AMSHAH presents the following environmental settings in which a spill may occur: lakes, non-tidal rivers, tidal rivers, estuaries, and open sea. Of these five settings AMSHAH analyses only the following three: non-tidal rivers, tidal rivers, and estuaries. On the other hand, the computer coding in HACS includes non-tidal rivers, tidal rivers, and still water settings. The last setting of still water is not analyzed in AMSHAH. This is shown in Table 3-1. AMSHAH considers variable and constant spill rates but HACS is restricted to constant spill rates of cargoes. AMSHAH limits its analysis to the mixing and dilution of the cargo while the cargo is being spilled and does not consider the mixing and dilution after the spill stops. HACS analyzes the mixing and dilution of the cargo for the duration of the spill and also after the cessation of spilling. This is shown in Table 3-2.

The following categories of navigational waters are either analyzed in AMSHAH or computer coded in HACS (cf. Table 3-1):

1. Non-tidal river
    a. Near-field approximation for an instantaneous spill
    b. Near-field approximation for a continuous spill
    c. Far-field approximation for a instantaneous spill
    d. Far-field approximation for a continuous spill
2. Tidal river
    a. Instantaneous spill
    b. Continuous spill
3. Estuaries
4. Still water
    a. Instantaneous spill
    b. Continuous spill

Errors and inconsistencies found in the modeling of these various cases are described on a case-by-case basis in the following.

TABLE 3-2 Comparison of Analyses of AMSHAH and HACS

	Type of Venting Rate Analyzed	Mixing and Dilution Analyzed During Spill	Mixing and Dilution Analyzed After Spilling Ceases
AMSHAH	variable and constant	yes	no
HACS	constant	yes	yes

1. Non-Tidal River

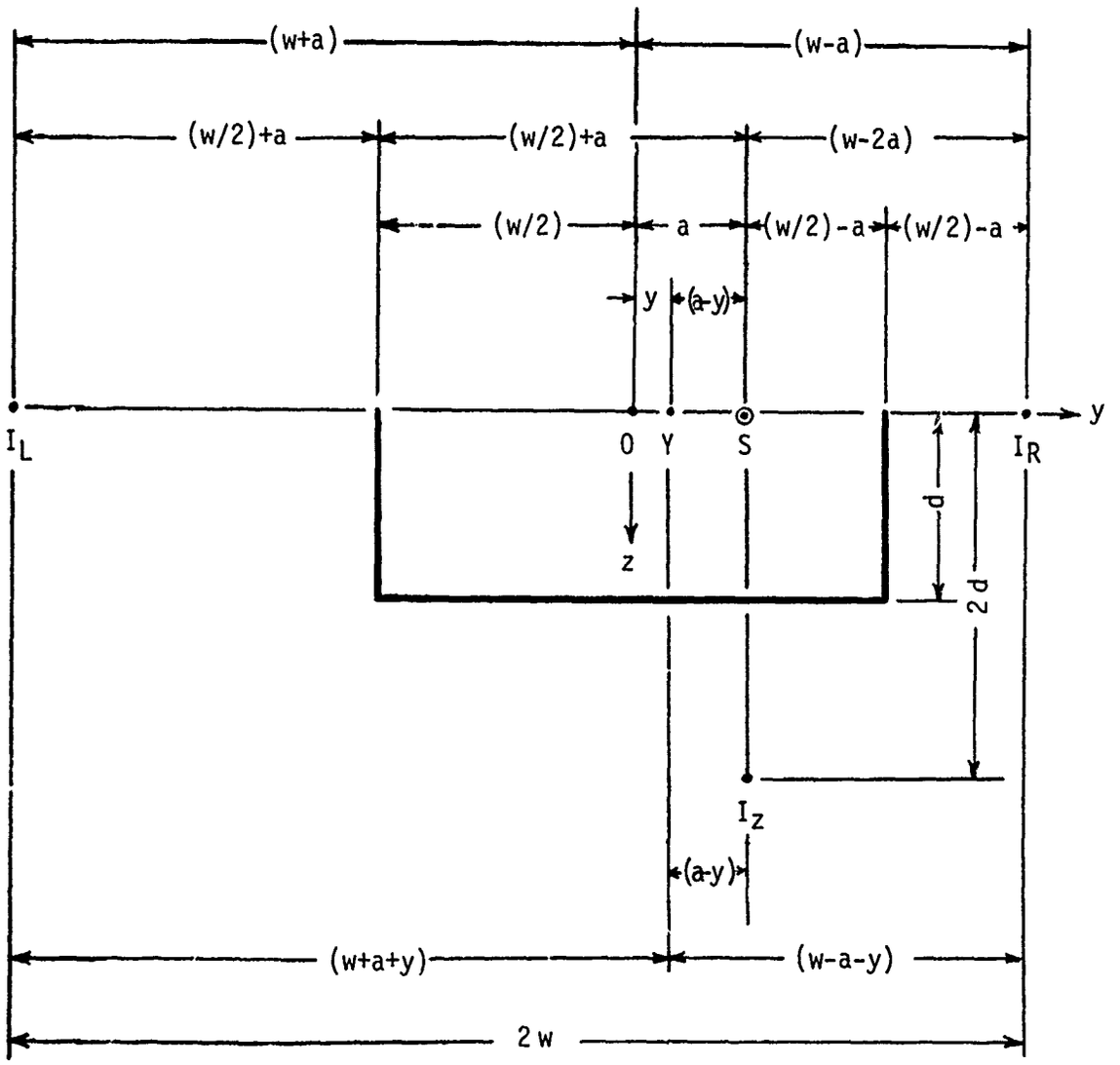
For spills of cargo into non-tidal rivers, four approximations were carried out. These approximations are analyzed in the following:

a. Near-field approximation for an instantaneous spill. In non-tidal rivers, the concentration of a pollutant is given by equation (4.1) on page 30 of AMSHAH, without a derivation, as:

$$c(x,y,z,t) = \frac{2\,M}{(4\pi t)^{3/2}\,(e_x\,e_y\,e_z)^{1/2}} \cdot \mathrm{EXP}\left[-kt - \frac{(x-Ut)^2}{4\,e_x\,t}\right]$$
$$\cdot \left\{\mathrm{EXP}\left[-\frac{(y-a)^2}{4\,e_y\,t}\right] + \mathrm{EXP}\left[-\frac{(y-a-w)^2}{4\,e_y\,t}\right] + \mathrm{EXP}\left[-\frac{(y+a-w)^2}{4\,e_y\,t}\right]\right\}$$
$$\cdot \left\{\mathrm{EXP}\left[-\frac{z^2}{4\,e_z\,t}\right] + \mathrm{EXP}\left[-\frac{(z-2d)^2}{4\,e_z\,t}\right]\right\} \qquad \text{AMSHAH(4.1), (3-4)}$$

for an instantaneous spill that occurs on the surface of the non-tidal river at the point (0, a, 0). The origin of axes is on the surface of the river, at the midpoint of its width and at the same river cross section which passes through the position of the spill. The direction of the axes of reference are such that the positive x-axis is along the downstream direction, the positive z-axis is downward, and the positive y-axis is cross-current so as to form a right-handed system of coordinate axes. Equation (4.1) of AMSHAH contains only first-order image terms, one first-order image being reflected about each of the two banks of a rectangular channel and the third first-order image being reflected about the bottom of the rectangular channel. The formula should, for consistency at least, also include a first-order image reflected in the top surface of the river. This inconsistency is discussed at length in Appendix 3B. The assumption in equation (4.1) of AMSHAH of no transport of the spill through the sides is valid everywhere only if an infinite set of higher-order images is considered, the statement in AMSHAH that equation (4.1) of AMSHAH is valid everywhere and for any time appears to be in error.

The exponent for the effect of the image source reflected about the bank at $y = -w/2$ is given as $[(y-a-w)^2/4\,e_y\,t]$ in equation (4.1) of AMSHAH. This is incorrect and should be $[(y+a+w)^2/4\,e_y\,t]$. From Figure 3-2 it can be seen that the distance of the observer y (at y from the origin) to the image source reflected about the bank at $y = -w/2$ is $[y+a+w]$. Thus the equation corrected for the correct image location is



Legend

I_L = Image source reflected about left bank
I_R = Image source reflected about right bank
I_z = Image source reflected about river bed
0 = Origin of axes
S = Source of spill
y = Observation position

FIGURE 3-2 Position of spill source and image sources.

$$c(x,y,z,t) = \frac{2\,M}{(4\pi t)^{3/2}\,(e_x\,e_y\,e_z)^{1/2}} \cdot EXP\left[-kt - \frac{(x-Ut)^2}{4\,e_x\,t}\right]$$

$$\cdot\left\{EXP\left[-\frac{(y-a)^2}{4\,e_y\,t}\right] + EXP\left[-\frac{(y+a+w)^2}{4\,e_y\,t}\right] + EXP\left[-\frac{(y+a-w)^2}{4\,e_y\,t}\right]\right\}$$

$$\cdot\left\{EXP\left[-\frac{z^2}{4\,e_z\,t}\right] + EXP\left[-\frac{(z-2d)^2}{4\,e_z\,t}\right]\right\} \qquad (3\text{-}5)$$

b. Near-field approximation for a continuous spill. In non-tidal rivers the concentration of a pollutant is given by equation (4.2a) on page 32 of AMSHAH, also without a derivation, for a spill rate $\dot{M}$ as:

$$c(x,y,z,t) = \frac{2\,\dot{M}\,(t - x/U)}{4\,\pi\,x\,\sqrt{e_y\,e_z}} \cdot EXP\left[-\frac{U}{4x}\left\{\frac{y^2}{e_y} + \frac{z^2}{e_z} + 4k\right\}\right]$$

AMSHAH (4.2a), (3-6)

When the spill rate $\dot{M}$ is constant, the expression for the concentration of the pollutant is given as:

$$c(x,y,z) = \frac{\dot{M}}{2\,\pi\,x\,\sqrt{e_y\,e_z}} \cdot EXP\left[-\frac{U}{4x}\left\{\frac{y^2}{e_y} + \frac{z^2}{e_z} + 4k\right\}\right]$$

AMSHAH (4.2b), (3-7)

Both of these expressions appear to be incorrect and incomplete. The former expression reduces to the latter since the mass flow rate for the latter is a constant and the mass flow rate of the former is evaluated at time equal to $\{ t - (x/U) \}$ where x/U is the time taken to travel from the spill point at $x = 0$ to the observation point at x when the river current in U. The error in both equations is in the decay term which is shown as $k\,U/x$ and it should be $k\,x/U$. These equations were to be derived for the spill located at $(0,a,0)$, as stated in the documentation of AMSHAH, which would give one of the exponents of the exponential term as $\{(y-a)^2/e_y\}$ instead of just $\{y^2/e_y\}$.

The image source terms are also missing in the given expression. Hence the application of the expressions (when corrected for the decay term) would be restricted to length of time less than either of the diffusion times $T_c = w^2/(4e_y)$ or $T_{cz} = d^2/e_z$. The expression is valid only for $0 < x < Ut$ and this restriction is not mentioned in the documentation of AMSHAH. As the

image sources are not included in equation (4.2) of AMSHAH, the statement in the documentation of AMSHAH seems to be in error when it states on page 33 " . . . equations (4.1) and (4.2) could be used for any length of time because of the provision of the image source terms in the equations, which assure that there is no diffusion through the boundaries." This statement in AMSHAH appears to be in contradiction to equations (4.1) and (4.2) because equation (4.1) has only first order image sources and equation (4.2) does not have any image sources.

The concentration of the pollutant, neglecting longitudinal dispersion and higher order image sources, can be expressed as

$$\begin{aligned} c(x,y,z,t) &= 0 \quad \text{for} \quad t < 0 \\ c(x,y,z,t) &= 0 \quad \text{for} \quad x < 0 \\ c(x,y,z,t) &= 0 \quad \text{for} \quad x > Ut \\ c(x,y,z,t) &= 0 \quad \text{for} \quad x < U(t-t_{MT}), \text{ if } \quad t > t_{MT} \end{aligned} \tag{3-8}$$

and for all other combinations of x and t,

$$c(x,y,z,t) = \frac{\dot{M}}{2\,\pi\,x\,(e_y\,e_z)^{1/2}} \cdot EXP\left[-\frac{U}{4x}\left\{\frac{(y-a)^2}{e_y} + \frac{z^2}{e_z}\right\} - \frac{kx}{U}\right] \tag{3-9}$$

where t_{MT} is the time when the tank is empty and the spill stops. The expressions for c given in AMSHAH have no provision for circumstances when the spill could stop and dispersion and mixing would continue with the pollutant already present in the water.

When the image sources are included, equation (3-9) becomes

$$\begin{aligned} c(x,y,z,t) = {} & \frac{\dot{M}}{2\,\pi\,x\,(e_y\,e_z)^{1/2}} \cdot EXP\left[-\frac{kx}{U}\right] \\ & \cdot \left\{EXP\left[-\frac{U(y-a)^2}{4\,e_y\,x}\right] + EXP\left[-\frac{U(y+a+w)^2}{4\,e_y\,x}\right] + EXP\left[-\frac{U(y+a-w)^2}{4\,e_y\,x}\right]\right\} \\ & \cdot \left\{EXP\left[-\frac{Uz^2}{4\,e_z\,x}\right] + EXP\left[-\frac{U(z-2d)^2}{4\,e_z\,x}\right]\right\} \end{aligned} \tag{3-10}$$

Subroutine DILUN of HACS corresponding to the Mixing and Dilution Model of AMSHAH is listed in Appendix 3D, Figure 3D-1. DILUN computer codes

equation (4.2) from statement 122 and hence the errors of equation (4.2) are also included in the computer code.

Page 33 of AMSHAH gives values for turbulent diffusion coefficients. The expression for e_y agrees with equation (31) of Holley, Harleman, and Fischer [3]. Holley et al. also state that [$e_y = 0.g3\ U^*\ R_h$] for straight wide channels. There appears to be an error in the documentation of AMSHAH where this expression for e_y is listed under narrow rivers.

c. Far-field approximation for an instantaneous spill. In non-tidal rivers the concentration of a pollutant is given by equation (4.6a) on page 34 of AMSHAH, and the expression contains decay terms involving the decay rate coefficient k. The differential equation from which the solution for the concentration of the pollutant was to be derived is equation (4.5) on page 33 of AMSHAH. The differential equation appears to be incomplete as it does not account for the decay of pollutant concentration, but the solution does take into consideration the decay of the pollutant concentration. The differential equation in AMSHAH without any boundary conditions is given as

$$\frac{\partial c}{\partial t} + U\,\frac{\partial c}{\partial x} = \frac{1}{A}\,\frac{\partial}{\partial x}\left[E\ A\ \frac{\partial c}{\partial x}\right] \qquad \text{AMSHAH (4.5), (3-11)}$$

and the differential equation including decay of pollutant concentration would be

$$\frac{\partial c}{\partial t} + U\,\frac{\partial c}{\partial x} = \frac{1}{A}\,\frac{\partial}{\partial x}\left[E\ A\ \frac{\partial c}{\partial x}\right] - kc \qquad (3\text{-}12)$$

with the boundary conditions

$$\begin{aligned} &c \to 0 \quad \text{for} \quad x \to \pm\infty \\ &c \to 0 \quad \text{for} \quad t \to \infty \\ &c = \frac{M}{A}\ \delta(x) \ \text{for} \ t = 0 \end{aligned} \qquad (3\text{-}13)$$

The solution to the differential equation (3-12) with the boundary conditions (3-13) is

$$c(x,t) = \frac{M}{A\sqrt{4\pi E t}} \cdot \text{EXP}\left[-\left\{\frac{(x-Ut)^2}{4Et} + kt\right\}\right] \text{ for } t > 0 \qquad \text{AMSHAH (4.6a), (3-14)}$$

and $c(x,t) = 0 \quad \text{for } t < 0 \qquad (3\text{-}15)$

---

[3] Holley, E. R., D. R. F. Harleman, and H. B. Fischer, "Dispersion in homogeneous estuary flow," Am. Soc. Civil Eng., J. Hydraulics Div. 96:1691-1709, 1970.

The near-field and the far-field approximations were developed so that these expressions could be utilized where appropriate and automatic switching from the near-field approximation to the far-field approximation would occur according to the conditions for each. Unfortunately, the computer coding of DILUN utilizes only the near-field approximation for instantaneous spills and does not switch to the far-field approximation.

d. Far-field approximation for a continuous spill. In non-tidal rivers the concentration of a pollutant is given on page 34 of AMSHAH as

$$c(x,t) = \frac{\dot{M}}{2\Omega A} \cdot EXP\left[\frac{xU}{2E}\right] \cdot \left[EXP\left\{\frac{x\Omega}{2E}\right\} \cdot \left\{ERF\left(\frac{x+\Omega t}{\sqrt{4Et}}\right) - 1\right\} - EXP\left\{\frac{-x\Omega}{2E}\right\} \cdot \left\{ERF\left(\frac{x-\Omega t}{\sqrt{4Et}}\right) - 1\right\}\right] \qquad \text{AMSHAH (4.6b), (3-16)}$$

where AMSHAH defines

$$\Omega = \sqrt{U^2+2kE} \qquad (3\text{-}17)$$

A complete derivation of the solution to the differential equation is given in Appendix 3A from where it can be clearly seen that the definition of Ω appears to be incorrect in AMSHAH. It should be

$$\Omega = \sqrt{U^2+4kE} \qquad (3\text{-}18)$$

The corresponding computer code for Ω in DILUN, statement 13, also appears to be in error. Statement 123 of DILUN should be

```
123   OMG = SQRT(U**2 + 4.*XK*E).
```
(3-19)

If t_{MT} is the time at which the spill ceases, the complete solution is given below:

For $t<0$, $c(x,t) = 0$ (3-20a)

for $0<t<t_{MT}$, $c(x,t) = \frac{\dot{M}}{2A\Omega} \cdot EXP\left[\frac{xU}{2E}\right] \cdot \left[EXP\left\{\frac{x\Omega}{2E}\right\} \cdot \left\{ERF\left(\frac{x+\Omega t}{\sqrt{4Et}}\right) - 1\right\} - EXP\left\{\frac{-x\Omega}{2E}\right\} \cdot \left\{ERF\left(\frac{x-\Omega t}{\sqrt{4Et}}\right) - 1\right\}\right]$ (3-20b)

and for $t>t_{MT}$,

$$c(x,t) = \frac{\dot{M}}{2A\Omega} \cdot EXP\left[\frac{xU}{2E}\right] \cdot \left[EXP\left\{\frac{x\Omega}{2E}\right\} \cdot \left\{ERF\left(\frac{x+\Omega t}{\sqrt{4Et}}\right) - ERF\left(\frac{x+\Omega(t-t_{MT})}{\sqrt{4E(t-t_{MT})}}\right)\right\}\right.$$

$$\left. - EXP\left\{\frac{-x\Omega}{2E}\right\} \cdot \left\{ERF\left(\frac{x-\Omega t}{\sqrt{4Et}}\right) - ERF\left(\frac{x-\Omega(t-t_{MT})}{\sqrt{4E(t-t_{MT})}}\right)\right\}\right] \qquad (3\text{-}20c)$$

Even though the documentation of AMSHAH gives the solution for only $0<t<t_{MT}$, the computer coding of HACS considers the solution for pollutant concentration for $0<t<t_{MT}$ and for $t>t_{MT}$. There is an error in the computer coding of equation (3-20). The error function terms must be subtracted. In DILUN the computer code multiplies the error function terms. DILUN has the following expression:

$$C = F1*F2*F3 \qquad (3\text{-}21a)$$

The documentation in AMSHAH gives further simplications for $t\to\infty$ as

$$c(x) = \frac{\dot{M}}{A\Omega} \cdot EXP\left[\frac{x(U-\Omega)}{2E}\right] \qquad \text{AMSHAH (4.6c), (3-22)}$$

and when $E << U^2/2k$,

$$c(x) = \frac{\dot{M}}{AU} \cdot EXP\left[-\frac{xk}{U}\right] \qquad \text{AMSHAH (4.6d), (3-23)}$$

These options are not computer coded in the corresponding computer program in HACS.

The computer coding does consider switching the approximate concentration solution from a near-field approximation (point source and dispersion in three dimensions) to a far-field approximation (when the pollutant is assumed to be uniformly distributed throughout the cross-section of the channel).

Since no provision has been made in the computer coding to match the concentrations from the near-field approximation to the concentrations from the far-field approximation, a jump in the predicted concentrations can occur when the computer program switches from the near-field approximation to the far-field approximation.

2. Tidal River

For spills of cargo into tidal rivers which have a sinusoidal variation in the water velocity, the differential equation governing the mixing and dilution of the pollutant concentration is given by equation (4.9) on page 35 of AMSHAH as:

$$\frac{\partial c}{\partial t} + U(t)\frac{\partial c}{\partial x} = \frac{1}{A(t)}\frac{\partial}{\partial x}\left(AE\frac{\partial c}{\partial x}\right) \qquad \text{AMSHAH (4.9), (3-24)}$$

The decay term is missing from this equation and the complete equation is:

$$\frac{\partial c}{\partial t} + U(t)\frac{\partial c}{\partial x} = \frac{1}{A(t)}\frac{\partial}{\partial x}\left(A(t)\,E\frac{\partial c}{\partial x}\right) - kc \qquad (3\text{-}25)$$

This is a one-dimensional diffusion equation and hence in the model of AMSHAH an implicit assumption of uniform distribution of the pollutant concentration throughout the cross-section of the river has been used. AMSHAH does not have any near-field solution for tidal rivers which would include dispersion in the y and z directions. The far-field solutions will be inaccurate for times soon after the spill (that is, before the diffusion is such that the pollutant is nearly uniformly distributed throughout the cross section of the river).

There are two subcategories of spills in tidal rivers that were documented in AMSHAH, instantaneous spills and continuous spills.

a. Instantaneous spills. For tidal rivers, the concentration of the pollutant is given by equation (4.10a) on page 35 of AMSHAH as:

$$c(x,t) = 0 \quad \text{where } t \le \tau$$

$$c(x,t) = \frac{M}{A\sqrt{4\pi E(t-\tau)}} \cdot EXP\left[\frac{\chi^2}{4E(t-\tau)} - k(t-\tau)\right] \quad \text{where } t > \tau \qquad \text{AMSHAH (4.10a), (3-26)}$$

where

$$\chi = x - \int_{\tau}^{t} U(t')dt' \qquad \text{AMSHAH (4.11), (3-27)}$$

with the spill occurring at time τ and position $x=0$, where the sinusoidally varying tidal current is represented by

$$U(t) = U_f + U_T \sin\sigma(t-\delta) \qquad \text{AMSHAH (4.12), (3-28)}$$

The concentration of the pollutant is given by equation (4.10b) as:

$$c(x,t) = \frac{M}{A\sqrt{4\pi Et}} \cdot EXP\left\{(-1) \cdot \left[\frac{(x-U_f t) + (U_T/\sigma)\{\cos\sigma(t-\delta)-\cos(\sigma\delta)\}}{\sqrt{4Et}}\right]^2\right\}$$

AMSHAH (4.10b), (3-29)

This solution is not a general solution but has the added implicit assumption that $k=0$ and $\tau=0$. When $k\neq 0$ and $\tau\neq 0$, the solution for the concentration of the pollutant is given by equation (3-26) with

$$\chi = x - U_f(t-\tau) + (U_T/\sigma)\cdot[\cos\{\sigma(t-\delta)\}-\cos\{\sigma(\tau-\delta)\}] \qquad (3\text{-}30)$$

b. Continuous spills. For tidal rivers the concentration of the pollutant is given by:

$$c(x,t) = \int_0^{t'} \frac{\dot{M}(\xi)\, d\xi}{\sqrt{4\pi E(t'-\xi)}} \cdot EXP\left[-\frac{\chi^2}{4E(t'-\xi)} - k(t'-\xi)\right]$$

AMSHAH (4.13a), (3-31)

where $t'=t-\tau$ is the instant at which injection starts and χ is defined in equation (3-27). This expression appears to be incorrect because the argument of the $\dot{M}$ term is not (ξ) but $(\xi+\tau)$, as shown in Appendix 3C. χ also has its limits changed from those given by AMSHAH equation (4.11) as shown in Appendix 3C.

$$c(x,t) = \int_0^{t} \frac{\dot{M}(\xi)\, d\xi}{A\sqrt{4\pi E(t-\xi)}} \cdot EXP\left[(-1) \cdot \left\{\frac{x-U_f(t-\xi) + (U_T/\sigma)[\cos(t-\xi-\delta)\sigma-\cos(\sigma\delta)]}{\sqrt{4E(t-\xi)}}\right\}^2 - k\,(t-\xi)\right]$$

AMSHAH (4.13b), (3-32)

The same type of error appears to be present in this equation (3-32) as in equation (3-31); the derivation given in Appendix 3C would apply except the sinusoidal velocity function would be substituted where appropriate. In this equation, presented on page 36 of AMSHAH, the symbol ξ is not defined. The equation has been stated for a continuous source and the possibility of the cessation of the continuous source is not considered either in AMSHAH or in the computer coding.

Consider a source with a constant rate of spill $\dot{M}$, starting at time t_a and continuing until time t_b when the spill ceases. The concentration at any time t can be determined by integrating equation (3-26) over the source time τ which is from t_a to t_c and for $t>0$ the concentration of the pollutant can be represented by:

$$c(x,t) = \int_{t_a}^{t_c} \frac{\dot{M}\, d\tau}{A\sqrt{4\pi E(t-\tau)}} \cdot \mathrm{EXP}\left[-\frac{\chi^2}{4E(t-\tau)} - k(t-\tau)\right] \qquad (3\text{-}33)$$

where χ is defined by equation (3-27),

for $t<t_b$, $t_c=t$

and for $t\geq t_b$, $t_c=t_b$.

When the river velocity U, is given as in equation (3-28), χ is obtained from equation (3-30), which is not expressed with all the terms in the documentation of AMSHAH.

The arguments of the cosine terms in equation (4.13b) of AMSHAH appear to be incorrect as can be seen from the following:

$$\int_{\tau}^{t} \sin[\sigma(t'-\delta)]dt' = [-(1/\sigma) \cdot \cos\{\sigma(t'-\delta)\}]_{\tau}^{t}$$

$$= -(1/\sigma) \cdot [\cos\{\sigma(t-\delta)\} - \cos\{\sigma(\tau-\delta)\}] \qquad (3\text{-}34)$$

The arguments of the cosine terms should be $[\sigma(t-\delta)]$ and $[\sigma(\tau-\delta)]$, and not as given in equation (4.13b) of AMSHAH.

The computer coding of DILUN which performs the integration indicated by equation (3-32) for the concentration of the pollutant utilizes the subroutine DLIN, which is an adaptation of a standard integration subroutine. DLIN in turn calls function CNSPL to obtain the value of the integrand. CNSPL is an accurate computer coding for the incorrect equation (4.13b) of AMSHAH -- because of the incorrect cosine terms -- and hence CNSPL would give incorrect values of the concentration of the pollutant in tidal rivers for continuous spills. The statement defining F2 needs to be recoded to obtain the general expression.

For the determination of the dispersion parameter E, the estimates of Holley et al. [3] are utilized and as AMSHAH has its positive z-axis downward, the expressions for T_v' and T_t' as given in AMSHAH appear to be incorrect because the same diffusivity is used in AMSHAH to define both times instead of using the diffusivity applicable to the direction of interest. More appropriate expressions appear to be:

$$T_v' = Te_z/d^2$$

and $$T_t' = Te_y/b^2$$

where T is the tidal period; e_z and e_y are the vertical and transverse mass diffusivities; d and b are the channel depth and half-width; and T_v' and T_t' are diffusion time ratios for vertical and transverse spreading.

The computer coding in subroutine DISP is for the dispersion parameters. The ratio (E_t/E_v) is given in AMSHAH as:

$$(E_t/E_v) = 0.11 \left[\frac{U_T T}{b}\right]^2 \cdot \left[\frac{\overline{U''^2}}{\{(2/\pi)U_T\}^2}\right] \qquad \text{AMSHAH (4.14), (3-36)}$$

Holley et al. [3] give the coefficient as 0.011, hence equation (4.14) of AMSHAH appears to be incorrect. The coefficient used in the computer coding of subroutine DISP is 0.011, which agrees with Holley et al. An error in the computer coding of equation (4.14) of AMSHAH is that the equation evaluates the ratio (E_t/E_v) whereas the computer code utilizes a similar expression with the coefficient 0.011 and calls it ET, instead of the ratio (E_t/E_v). The expression in HACS for ET is:

```
ET = 0.011*0.025*(UT*T/B)**2                                    (3-37)
```

The "T" of equation (3-36) is the tidal period and the "T" in the FORTRAN statement (3-37) is the time of evaluation. TP is used as the tidal period in the subroutines associated with MODP. The erroneous use of T instead of TP occurs in the statement defining TPV and TPT as well. An alternate computer coding from statement 82 can be as follows:

```
82  E = 6.*D*USTAR
    F = 0.000275*(UT*TP/B)**2
    TPV = TP*EZ/D/D
    IF(TPV.LT.1.) RETURN
    IF(F.LT.1.) RETURN
    E = E*F
    RETURN
```

In the coding shown above, TPT was not completed as it was not used in the subsequent steps.

For tidal rivers, $U_f << U_T$ is assumed by AMSHAH and the corresponding computer coding of HACS does not check to determine if this inequality is valid. Holley et al. discuss only the cases for which $T_v' > 1$ and $T_t' > 0.1$, pointing out that most tidal channels will satisfy these conditions for the normal tidal period of 12.4 hours. In the computer coding, the test to determine if $T_t < 0.1$ is not made. This test may not be required only because the concentration of the pollutant is not very sensitive to the value of E, as stated by Holley et al. They recommend using $E = E_y$ if the velocity distribution is unknown. They also mention that usually

$$0.01 < \left[\overline{(U'')^2}/(2U_T/\pi)^2\right] < 0.04;$$

AMSHAH used a value of 0.025 for this term.

3. Estuaries

For spills of cargo into estuaries, AMSHAH does not give any expressions for the concentration of the pollutant when the density gradients due to salinity are important. It states that certain quantities must be known for each estuary before a solution can be obtained. The computer program does not consider spills in estuaries where density gradients are important. Decay terms have been omitted from equations (4.15) and (4.16) on page 40 of AMSHAH. Equation (4.16) of AMSHAH applies to average concentration over a tidal period, and since the tidal period is around 12.4 hours, the equation is restricted in application; a finer time resolution is not possible from this model.

4. Still Water

This discussion is based on the computer coding of HACS since AMSHAH does not discuss spills in still water. The computer statements following statement 60 of DILUN and following statement 12 of CNSPL contain the equations for spills in still water. There are two sub-categories of instantaneous spills and continuous spills and these are discussed in the following.

a. Instantaneous spills

For spills of cargo into still water, from computer statement 60 of DILUN, the equation to compute the concentration of the pollutant in still water from an instantaneous spill is:

$$c(x,y,z,t) = \frac{2M}{\sqrt{4\pi Et}} \cdot \text{Exp}\left[-\frac{x^2+y^2+z^2}{4Et} - kt\right] \qquad (3\text{-}39)$$

where E is the diffusion coefficient. DILUN uses DIFCO for the diffusion coefficient which is represented by E in equation (3-39). This quantity E is not calculated in MODP, but is a user input. The current version of the mixing and dilution subroutines compute DIFCO from the properties of the cargo. The value of E or DIFCO computed in this way is generally between 0.010 cm^2/sec and 0.001 cm^2/sec, which is appropriate for molecular diffusion. However, the water would have to be very still for molecular diffusion to be the dominant mode of mixing; if not, turbulent mixing or any other type of mixing can easily be larger than the relatively slow molecular diffusion. The cautionary note in HACS is to be noted carefully as there is the possibility of a serious error for the physically impossible condition that the concentration of the spilled cargo is greater than the density of the cargo in the liquid state. This problem in the model can produce an unrealistic result which is quite objectionable. For the case of molecular diffusion the problem is especially acute since the model can predict that these erroneous concentrations exist for many hours after the spill.

A numerical example will be considered to demonstrate the problem of using this equation and the molecular diffusion coefficient. Consider a spill consisting of 160 metric tons or 1.6×10^8 grams of methyl alcohol - a medium sized spill. Pure methyl alcohol has a density of 0.79 gms/cm^3 and hence 160 metric tons or 1.6×10^8 grams would have a volume of 2.025×10^8 cm^3 and would form a sphere about 360 cm in radius or a cube of a side of about 590 cm. But from equation (3-39) which is computer coded, ten minutes after the spill, almost all of the methyl alcohol will be contained in a sphere of radius 2 cm. From equation (3-39), if we use 4ET = R (say), as a measure of the size of the area in which the concentration is a significant fraction of the concentration at the center of the spill, then with E = 0.002 cm^2/sec, it will take about 60,000 seconds, or over 16 hours, before R will be equal to 360 cms. Hence, we would have to wait about 16 hours after the spill, during which time the size of the equivalent sphere of the pollutant would increase to become the size of a normal density sphere. Hence for smaller time and or larger distances from the center of the spill, the concentration of the pollutant is likely to be essentially zero. Because of the use of the molecular diffusion coefficient and because the computed concentrations of the pollutant are greater than the liquid density, this equation gives unrealistic concentrations for many times and locations of interest. It is suggested that this equation be replaced by a more comprehensive expression in which the initial volume of the spill is considered and diffusion coefficient values between molecular diffusion and turbulent diffusion are utilized.

b. Continuous spill

For spills of cargo into still water, the computer coding of HACS from subroutines DILUN, DLIN, and CNSPL gives the concentration of the pollutant for continuous spills. The integrand is in computer statement 12 and the two following statements of CNSPL. DILUN and DLIN give the limits of integration.

$$c(x,y,z,t) = \int_0^t F(x,y,z,t,\tau)\, d\tau \quad , \text{ if } t \leq t_{MT}$$

$$c(x,y,z,t) = \int_0^{t_{MT}} F(x,y,z,t,\tau)\, d\tau \quad , \text{ if } t > t_{MT} \qquad (3\text{-}40)$$

where the integrand $F(x,y,z,t,\tau)$ is given by:

$$F(x,y,z,t,\tau) = \frac{2\dot{M}}{(\sqrt{4\pi E\ (t-\tau)})} \cdot \text{Exp}\left[-k\ (t-\tau) - \frac{(x^2+y^2+z^2)}{4E\ (t-\tau)}\right] \qquad (3\text{-}41)$$

The computation of the concentrations uses the same basic equation in the continuous spill as ir the instantaneous spill and hence the same error of pollutant concentration greater than liquid density of spill and other errors mentioned for the instantaneous spill are involved in the continuous spill model.

The above summarizes errors in the documentation in AMSHAH. The following is a critical evaluation of the four subroutines used in the Mixing and Dilution Model.

Subroutine DILUN

The subroutine DILUN is the main calculation subroutine: MODP merely retrieves the data from the state file and passes it to DILUN. DILUN calls DISP to obtain the turbulent dispersion coefficients and DLIN to perform the numerical integration. DLIN calls CNSPL to get the arguments in the integration.

The first two statements in DILUN (Appendix 3D, Figure 3D-1) were required previously because DLIN was originally a general purpose integration subroutine, and passing in the name of the function subprogram and the size of the array AUX allows one to write a very general integration subroutine. However, the original integration subroutine has been altered for its specific use in MODP. The use of both T and TIME to refer to the present time, t, is redundant. T does not appear to be redefined anywhere, so the need for two variables is not necessary.

Between statement 5 and statement 20, the program considers changing, the "instantaneous spill/continuous spill" flag, ICOND. For a continuous spill, ICOND = 1. The program changes the flag from continuous to instantaneous spill (ICOND = 0), if the evaluation time (t) is greater than or equal to five times the time at which the tank is empty (5.*TMT).

Other criteria for choosing between an instantaneous or continuous description of the spill may be more appropriate. In an appendix to

Chapter 3 of the Vulnerability Model Final Report [4], a discussion of scaling and the implications on switching between continuous and instantaneous descriptions of dispersion is presented. The discussion is concerned with air dispersion, rather than water dispersion, but the reasoning is valid for both cases. For the case of the flowing river it appears that the instantaneous description is more appropriate than the continuous description when the advection length of the spill (t_{MT}/u) is comparable to or smaller than the diffusion width of the spill ($\sqrt{e_y t}$ or $\sqrt{e_z t}$). The decision depends not only on release time and observation time, but also upon rates or diffusion and advection. Thus it would seem questionable to consider the spill to be instantaneous for $t > 5t_{MT}$ no matter what the values of x, U, e_y, e_z, and t_{MT}. In addition, it may be desirable to choose a switching time such that a smooth transition from the continuous to instantaneous descriptions is assured.

The section of the program beginning at statement 60 refers to an instantaneous spill in still water, and the problems arising from the use of the molecular diffusion coefficient have been discussed.

The section beginning with statement 70 concerns an instantaneous spill into a non-tidal river. It has already been mentioned that the distance to the left-hand image source is y+a+w instead of y-a-w, and that the far-field approximation has not been programmed. If this section is reprogrammed, the argument of the EXP function might be examined before evaluation to eliminate the possibility of underflows.

The section beginning at statement 80 is for an instantaneous spill into a tidal river. The equation used here agrees with equation (4.10b) of AMSHAH and is correct when the observor is far enough from the spill so that it is a good approximation that the cargo is uniformly distributed over the cross-section of the river.

For continuous spills, the cases of still water and tidal river require numerical integration and are treated by means of subroutine DLIN and function CNSPL. A continuous spill into a non-tidal river is treated in the section beginning with statement 120. For the near-field approximation, we have noted above that the expression used here assumes that a = 0 and that the image sources are omitted. Further, the decay term is K*UF/S when it should be K*X/UF, as discussed earlier. For the far-field approximation, we have a factor of 2 instead of 4 in the definition of OMG(Ω), and C = F1*F2*F3 instead of C = F1*(F2-F3).

---

[4] Eisenberg, N.A., C. J. Lynch, and R. J. Breeding, Vulnerability Model: A Simulation System for Assessing Damage Resulting from Marine Spills, CG-D-136-75, NTIS AD-A015245, Department of Transportation, U.S. Coast Guard, June 1975.

Subroutine DISP

The subroutine DISP (Appendix 3D, Figure 3D-2) calculates turbulent dispersion coefficients for tidal and non-tidal rivers. For non-tidal rivers, we note that the definition on page 49 of AMSHAH for USTAR (u*) has a coefficient of 3.115, while statement 70 has a coefficient of 6.716. This difference is due to the fact that the definition of u* was given for MKS units, while the program is working in CGS units. The fact that R_h is in meters in one case and centimeters in the other accounts for the difference. The case of the coefficient 77.0 in the definition of E for wide rivers (see statement following statement 71) is not so easily explained. On page 35 of AMSHAH, it is mentioned that

$$E = 63\ nUR_h^{5/6}$$

for narrow rivers. In this equation, E has units of m^2/s, U has units of m/s, and R_h has units of m. The Manning roughness factor, n, is dimensionless. Denoting these quantities in CGS units by a subscript c, we have

$$10^{-4}\ E_c = 63\ n(10^{-2}\ U_c)\ (10^{-2}\ R_{hc})^{5/6}$$

which gives

$$E_c = 136\ nU_cR_{hc}^{5/6}$$

where $136 = 63\ (10)^{1/3}$. It is not known why a factor of 77 is used instead of a factor of 136.

The calculation for the case of the tidal river also starts with the computation of USTAR, but the numerical coefficient is different. Statement 80 correctly uses the mean oscillating flow velocity (average of the absolute value of the velocity) which is $2U_T/\pi$. It is not known why the numerical factor is 3.9 instead of 6.7, as it was above. The three statements following statement 82 include errors as mentioned above.

It should be noted that there is no upper bound placed on F = ET/EV. The text points out that Holley et al. [3] found a maximum value of 11 for this ratio. If the tidal river case is specified with a narrow river, then F may easily become very large due to the $(UT*TP/B)^2$ factor. In this manner one may easily end up with values of E around 10^{10} which are unrealistically large. It is recommended that some upper bound be placed on F to eliminate this possibility.

Subroutine DLIN

The numerical integration subroutine DLIN (Appendix 3D, Figure 3D-3) is an adaptation of a utility routine which was written to be very general. The present DLIN seems to work correctly, but it might be made more efficient by making it more specific for its use here. For example, we might replace the dummy function FCT by CNSPL, which will save passing in CNSPL. The variable EPS in DLIN is used in testing the accuracy of the numericl approximation, and in statement 131 in DILUN, ESP is set, not EPS, so in this case an indeterminate value is used for EPS and therefore for E in DLIN.

Function CNSPL

The function subprogram CNSPL (Appendix 3D, Figure 3D-4) evaluates the argument which is being integrated by DLIN. It might be faster to pass the quantities used by DNSPL in by a common data block rather than by passing all the variables through DLIN as is done at present.

In the still water case, the equation used has been discussed earlier. The programs are due to the use of the molecular diffusion coefficient and the neglect of the finite volume occupied by the spilled liquid. For the case of a spill in a tidal river, the cosine terms are incorrect as noted above. Since the lengthy statement defining F2 must be replaced with one containing the correct cosine terms, the statements defining F1, F3, and CNSPL might also be replaced to give code which might be slightly faster.

```
F1 = XMDOT /2./W/D /SQRT ( PI*E*TT )
F2 = X - UF*TT + UT/SIG * ( COS( SIG*(T-DEL) ) - COS( SIG*(TOW - DEL) )
F3 = XK*TT + F2 **2 /4./E/TT
IF ( F3 .GT. 46. ) GO TO 31
CNSPL = F1 * EXP( -F3 )
```

ACCURACY ASSESSMENT

The following is an accuracy assessment for the Mixing and Dilution Model. The assessment is for the assumptions and approximations in AMSHAH and HACS.

Heat sources and heat sinks are neglected, and this would imply that the initial temperatures of both the spilled cargo and the water into which the spill occurs are nearly equal. Any initial unequal temperatures would ultimately come to equilibrium at a temperature very nearly equal to the temperature of the water into which the spill occurs because of the comparatively large thermal capacity of the river, lake, sea, or ocean into which a spill may occur. During the initial stages of mixing and dilution, the difference in the temperatures of the spilled cargo and the water into which the cargo is spilled could effect the rate of dispersion. This effect could be due to any of the following, depending on the cargo transported:

1. An LNG spill - or a spill of a similar liquid cryogen - could break up into small quantities and water could form ice coverings around these cold liquid cryogens. As the liquid cryogen evaporates inside the ice capsule, the pressure inside these capsules increases with the consequent explosion of the capsules. This process of encapsulation and consequent explosion of the spilled liquid cryogenic cargo could effect the turbulence level of the receiving water body with an increased rate of mixing.

2. When the temperature of the cargo is different from the temperature of the receiving water body, a thermal boundary layer forms naturally at the interface between the spill and the receiving water body. This thermal boundary layer would effect the diffusion process by changing the rates of diffusion of the cargo within the thermal boundary layer.

3. Another effect of different temperatures of the spill and the receiving water body is the formation of convection currents. Spills that are initially at a lower temperature and hence denser than the receiving water body would sink in the water. As the spill gets warmed to the temperature of the surrounding water, it could become lighter and start to rise. These movements of the spill would generate convection currents in the receiving water body. These convection currents in turn would effect the turbulence level and both these convection currents and turbulence levels would effect the rate of dispersion of the spill.

Chemical reactions between the cargo and water are also not considered, and the related effect of phase change is not analyzed. Chemical reactions between cargo and water of nearly equal temperature could be exothermic or endothermic thus creating heat sources or heat sinks for the complete duration of the chemical interaction, and thereby changing the temperature of the spill when compared to the temperature of the water into which the spill occurs. The total heat of reaction is dependent upon the reacting components and upon the quantity of the spill. The heat of reaction could also affect the dispersion rate of the spill. Phase change of cold liquefied gas cargoes could occur after a spill occurs in warmer water. In the case of a phase change, by boiling of the cold liquefied gas cargo, the spill would become a vapor cloud. The dispersion rates of the spill could be affected by any of the above. If the rate of dispersion becomes large, the spreading area of the spill would become large, and hence the consequent vaporization rate or burning rate of the cargo could increase, which in turn could affect the dispersion rate of the remaining spill.

The Mixing and Dilution Model also neglects buoyancy forces on the spill by the body of water into which a spill may occur. The buoyancy forces would be due to the difference in the density of the spill and the body of water. These density differences, for spills of density greater than the density of the body of water, would cause the spill to sink until the spill density equals the density of the body of water (for bodies of

water with density gradients). The existence of many diffusion floors inside the body of water could limit the depth to which the spill would diffuse once a neutral environment is available, the diffusion being confined between a diffusion floor and a diffusion ceiling. The formation of an inverted mushroom for a spill which would sink up to a diffusion floor is shown qualitatively in Figure 3-3.

Diffusion floors in large lakes or oceans are known to exist [5]. These are the thin horizontal layers often bounding regions of turbulent flow. There is no measurable turbulence in these thin layers on account of the stabilizing effect of the force of gravity. Because of the low molecular diffusivities, very sharp gradients develop in such stable shuts and any spill pollutant in the water appears to be confined for all practical purposes to one side. Such layers, when present, would act as confining horizontal layers which would in effect reflect and limit any of the pollutant trying to disperse beyond these layers. These floors can also be described as the density stratification which occur between the thin layers. The model for mixing and dilution does not consider any limitation in the dispersion due to these diffusion floors. However, the simulation of AMSHAH and HACS would be adequate when the diffusion process is slow and the diffusion floors are at great depths.

In modeling non-tidal rivers, AMSHAH and HACS assume that the rivers velocity is uniform throughout the cross section of the river and also uniform along locations in the direction of flow. Rivers normally have variations in their flow velocity due to any of the following: narrowing or broadening of the river; the river becoming shallow, deep; existence of obstruction in the flow in the shape of large boulders or islands; variations in the slope of the river bed; irregular additions to the water in the river by tributaries; and irregular reduction from the water in the river by distributaries, etc. When the spill observation is such that any of the above variations occur to an appreciable extent, then the model would not predict accurate concentrations of pollutant. However, most observations of interest are such that the above variations - even though they definitely occur - could be approximated to a mean constant value. This would greatly simplify the analysis and would give predictions of the same order as the predictions from the other limitations of the model.

Most rivers do not have the precise cross sectional shape of a rectangle as in Figure 3-4a. The modeling, which is based on a river of rectangular cross section, though not precise, could be improved by a trapezoidal cross section for the river as in Figure 3-4b. This would introduce an additional parameter into the model, the parameter being the inclination of the sides of the river. The original two parameters

---

[5] Csanady, G. T., Water Res. 4:79, 1970.

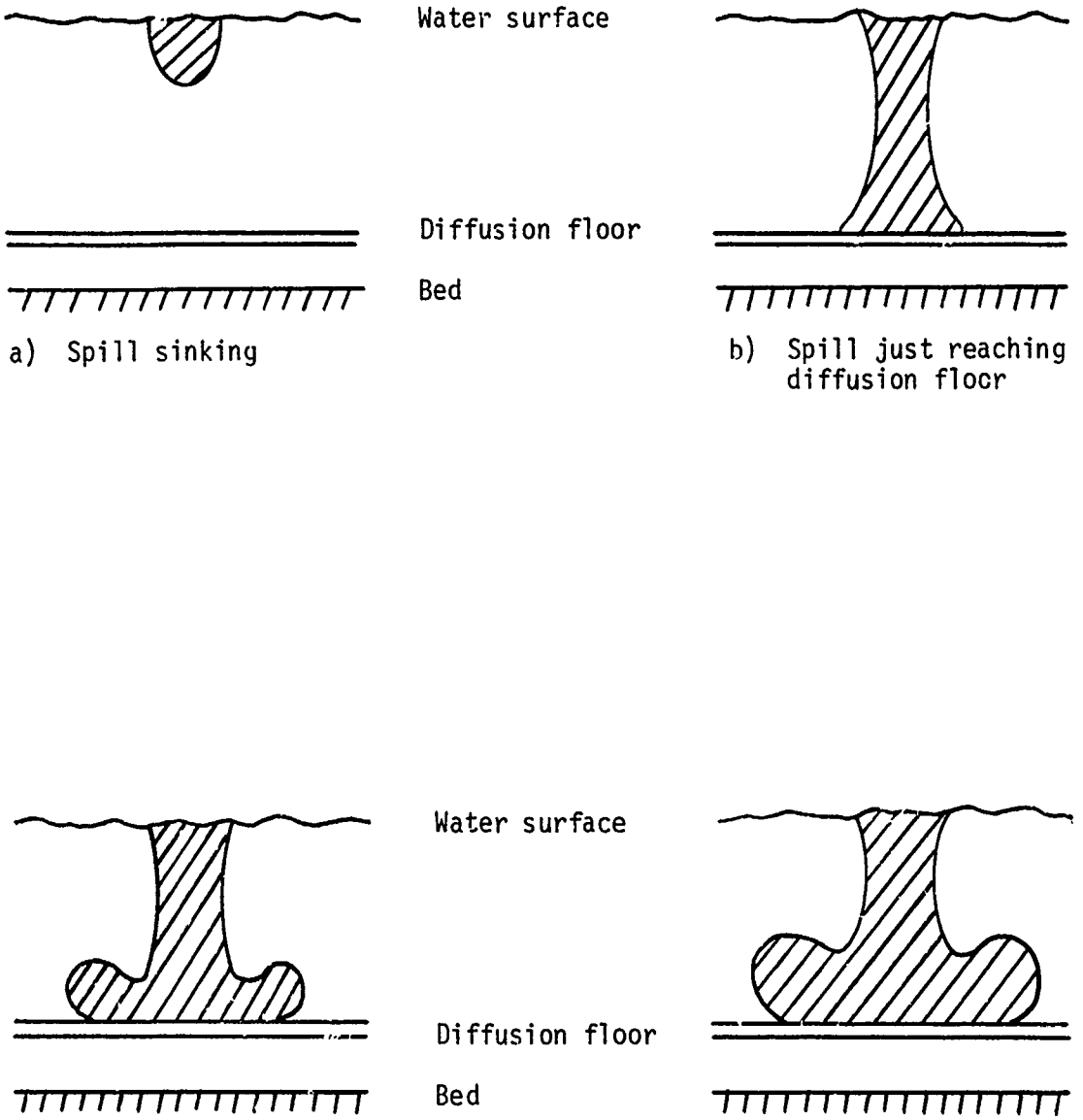


FIGURE 3-3 Formation of inverted mushroom for spills that sink to a diffusion floor.

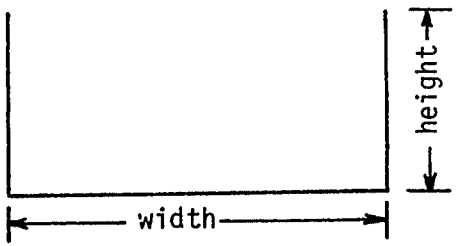
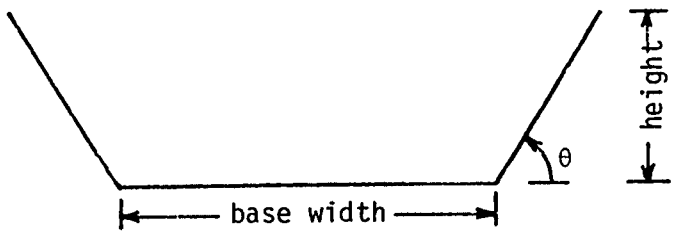


FIGURE 3-4a Rectangular channel.



θ = angle of inclination of sides of channel.

FIGURE 3-4b Trapezoidal channel.

of width and depth would also be required in the trapezoidal model. The trapezoidal model would be most effective when the mixing and dilution of cargoes which sink in the river are to be analyzed for rivers that are deep and which have slightly inclined banks (the inclination Θ of the sides of the channel being less than 45°).

Image sources are required to compensate for the apparent loss of cargo through the banks of the river. First-order images compensated for the first reflections of the original source about each of the banks and the bottom of the riverbed. The first-order image source reflected about the top surface of the river was not considered. For consistency, all the first-order image sources are to be included. This inconsistency is discussed in Appendix 3B. Any second-order image sources would be reflections of the first-order image sources, and their effect is less as compared to the effect of the first-order images because the distance of these second-order images from the point of observation is more than the distance of the first-order images from the observation point. For the present model of a rectangular channel for the river, the first-order image sources seem to be sufficient to give predictions of the same order of accuracy as the predictions as limited by the remaining assumptions.

The spill rate was assumed to be constant. The actual spill rate would be dependent on the venting rate from the cargo vessel. The venting rate is usually not uniform and could also be intermittent (venting would stop when air is entering the vessel; when the vent is below the liquid cargo level and it is inside above the level of the outside receiving water body). The predictions of spill concentrations near a spill site would be different for intermittent venting as compared to the constant rate of venting assumed in HACS because of the impulsive and discontinuous nature of intermittent venting. For example, the spurting of the cargo from the venting hole will tend to increase the mixing rate. At distances far from the spill, the intermittent spill could be approximated as a continuous spill, depending on whether the time period of the intermittent flow is small (frequency large) when compared to the time required for the cargo to reach the distant point of observation by diffusion and advection, i.e. whether the time variations in concentration at the distant point are negligible in comparison to the mean concentration of the pollutant.

The longitudinal dispersion of the spill is governed by the longitudinal dispersion coefficient which in turn is dependent on the shear velocity of the body of water in which the spill occurs. This longitudinal dispersion is usually small when compared to the bulk flow of the river, and hence neglecting the longitudinal dispersion seems valid in these environments. In some instances the flow velocity of a river may be sufficiently small while the turbulence level is sufficiently large so that the longitudinal dispersion may be comparable to advection; such cases are expected to be rare.

The uniform distribution of the pollutant in non-tidal rivers for far-field approximations seems valid because the effect of the primary source and the first-order sources becomes such that, for positions which are off-center in the river, the variation in the position seems to cause only slight variation in the concentration of the pollutant.

Tidal river velocities change because of the proximity of the river with a body of water which has tides due to the moon, and the variation in the velocity could be adequately represented by a sinusoidal variation. In addition, the sun will cause perturbations to the tides which are not accounted for by these sinusoidal variations. The sinusoidal superimposed velocity and the resultant tidal velocity of the river is shown qualitatively in Figure 3-5. In reality, changes in the water currents of the river could also change the velocity of water in tidal rivers for the period of interest after a spill occurs. These changes of the upstream river currents are not considered by the model and the tidal variation (a 12.4-hour period from high tide to high tide) is considered. Hence this model would not account for any flash floods that might occur.

The combined effects of modeling the spill as a continuous spill in a rectangular channel with only first-order image sources, with longitudinal dispersion negligible in comparison to the velocity of the river, gives a simplified model which could give predictions of the same order of accuracy as the accuracy to which the inputs to the model are readily available. The other environmental conditions of lake or sea and the near- and far-field approximations also give combined predictions of the same order of accuracy as the accuracy to which the inputs are readily available.

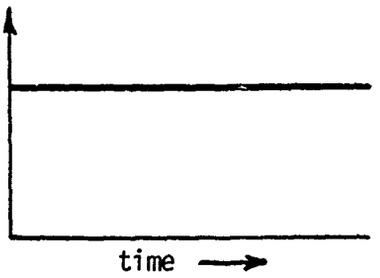
SENSITIVITY ANALYSIS

This section summarizes the sensitivity analysis for MODP.

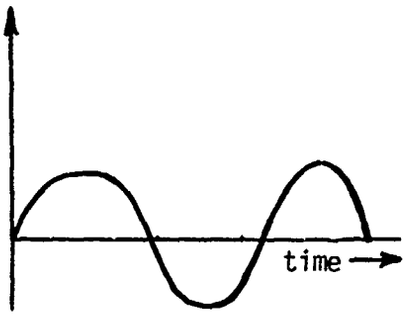
1. The output variable for the sensitivity analysis is the concentration at (x,y,z,t) where these four coordinates are given below.

2. The input variables are listed in Table 3-3. The water temperature will not be used since it is required only for the calculation of the molecular diffusion coefficient in the still water case. The values of D and W selected will give $W/D < 100$, so the narrow river options will be used in DISP for the dispersion coefficients. The difference between the narrow and wide river cases in the computation of the dispersion coefficients is discussed later.

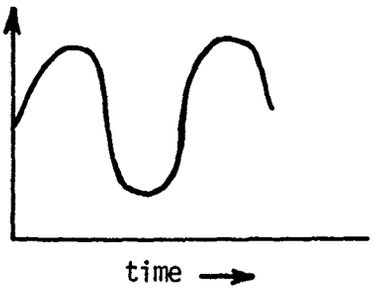
The x-coordinate for the position where the concentration is calculated must be chosen with care, otherwise the concentration may be very small. Let x be the coordinate of the point at which the concentration is calculated, and let x_0 be the x-coordinate of the present position of the water, which was at the spill site at time $t = 0$. By this definition



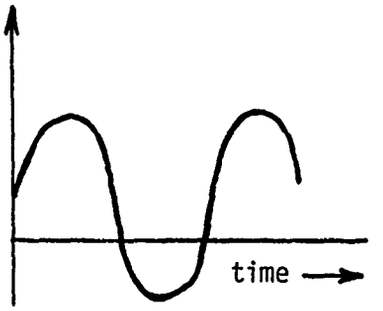
a) Non-tidal river velocity



b) Sinusoidal superimposed velocity



c) Tidal river velocity, small amplitude variations



d) Tidal river velocity, large amplitude variations

Note: River velocity could be opposite to direction of total flow for some time.

FIGURE 3-5 Tidal river velocity representation.

TABLE 3-3 Values of Variables Used in the Sensitivity Analysis of MODP

Variable	Computer Symbol	Value	Explanation
1. Spilled Mass	ZM	0.80*DL*CVOL	CVOL = 300 m^3 = 300x10^6 cm^3 for ammonia CVOL = 120 m^3 = 120x10^6 cm^3 for methyl alcohol DL = the density of the cargo in liquid phase.
2. Spilling Rate	ZMDOT	Z / 300.	300 seconds - 5 minutes
3. River Depth	D	8 m = 800 cm	
4. River Width	W	500 m = 50,000 cm	
5. Spill y	A	25 m = 2,500 cm	Distance of spill point from the center of the river
6. Point x	X	see text	
7. Point y	Y	0	
8. Point z	Z	10 cm	
9. Point time	T	600 s = 10 min	
10. Decay Coefficient	XK	0.278x10^{-3}	XK = 1/(1 hour)
11. River Flow	UF	200 cm/s	
12. Tidal Flow	UT	300 cm/s	
13. Tidal Period	TP	43,200 s	43,200 seconds = 12 hours
14. Tidal Lag,	DEL	12,960 s	DEL = TP / 3.
15. Roughness	RF	0.05	Manning Roughness Factor
16. Water Temp	TW	10°C	

$x_o = U_f t$ for the non-tidal river

$x_o = U_f t - (U_T/\sigma) [\cos (\sigma (t-\delta)) - \cos (\sigma\delta)]$ for the tidal river

The results of the tidal and non-tidal river cases can easily be compared if we let x_d be of constant value during the sensitivity analysis, where,

$x_d = x - x_o$

If we let x_d be positive, the concentration will be zero in some of the cases with continuous sources. Thus we will take $x_d = -100m = -10^4$ cm.

3. Since only two of the five priority cargoes are soluble in water, the sensitivity analysis will be done only for ammonia and methyl alcohol.

4. There are eight possible paths through this submodel:

(1) Still water, instantaneous spill
(2) Still water, continous spill
(3) Non-tidal river, instantaneous spill, near-field approximation
(4) Non-tidal river, instantaneous spill, far-field approximation
(5) Non-tidal river, continuous spill, near-field approximation
(6) Non-tidal river, continuous spill, far-field approximation
(7) Tidal river, instantaneous spill
(8) Tidal river, continuous spill

The use of the molecular diffusion coefficient in the still water cases causes the concentration to be very small for most distances and times of interest and the model also gives predictions of the concentration of the pollutant (at positions near the spill) to be higher than the normal liquid density of the cargo, which is an erroneous result. Hence the sensitivity analysis is not done for the still water cases.

5. The sensitivity analysis presented is only for tidal rivers and non-tidal rivers.

6. When MODP is called with the variables as listed above, only cases (5), (7), and (8) are executed. The program tries to execute case (3), non-tidal river, instantaneous spill, near-field approximation; but the concentrations are too small to be meaningful. This is due to the small values for EX which are calculated in DISP. The point at which the concentration is calculated will have to be within ten meters or less of the center of the cargo concentration in order to get reasonable concentrations.

The decision regarding the use of the near-field or far-field approximations for the non-tidal river is based on a comparison of the present time (t or T) with

$$TC = 0.3*B*B/EY$$

where B is half the width of the river channel. For the values given in Table 3-3, we have:

$$B = 250 \text{ m} = 25{,}000 \text{ cm}$$
$$EY = 6524 \text{ cm}^2/\text{sec}$$
$$TC = 28740 \text{ sec} = 8 \text{ hours}$$

EY depends upon the parameters describing the flow and the channel in a complex manner, hence it is not obvious as to how much W would have to be reduced in order to obtain the desired reduction in TC. Just increasing the time at which the concentration is calculated may not switch the program to the far-field approximation, because the current will have transported the spilled material over 57 km, and the model is not valid for such large distances. Thus B and W will be reduced. Decreasing the width of the channel from 500 m to 50 m gives a small value of TC:

$$B = 25 \text{ m} = 2500 \text{ cm}$$
$$EY = 4629 \text{ cm}^2/\text{sec}$$
$$TC = 405 \text{ sec}$$

Although a channel this narrow may be unrealistic, W = 50 m will be used in order to do the sensitivity analysis for the far-field approximations in the non-tidal river case.

Of the eight possible cases, then, the values used in Table 3-3 will be used to execute cases (5), (7), and (8). W will then be changed to 50 m or less in order to execute cases (4) and (6). Cases (1), (2), and (3) will not be executed as discussed above.

7. The sensitivity analyses will be performed with the subroutines presented in the following subsection.

The MODP Subroutines

The subroutines which perform the actual calculations for the submodel which calculates the mixing and dispersion of a soluble liquid in water are presented and discussed below.

The main computational subroutine is DILUN. The version of this subroutine used in the sensitivity analysis is shown in Appendix 3D, Figure 3D-5. This subroutine differs in many ways from the subroutine by the same name which is a part of HACS. The major differences will be noted here.

In DILUN all the arguments have been placed in a common statement. This facilitates the passage of variables among the subroutines. PI has been defined in a data statement rather than a replacement statement, and the definitions of CNSPL and AUX have been removed. Setting C = 0.0 in the beginning allows the program to return this value by a RETURN if the value of C is so low that underflows may be encountered in calculating the value of C. The last statement on the first page of Figure 3D-5 in Appendix 3D is to avoid calculating a very small concentration, for values of x for which the concentration will be identically zero or very close to zero.

Pages 2 and 3 of Figure 3D-5 show 6 PRINT statements and their associated FORMAT statements. These are to print useful information during the course of these sensitivity analysis runs.

The calculation for the case of an instantaneous spill in still water is the same as in the original (statement 60 and the following statements). The programming has been changed so that a value of 0.0 will be returned when the concentration is less than one part in 10^{20} of the concentration at the center of the spilled cargo. This is done to prevent underflows.

For the case of an instantaneous spill into a non-tidal river (statement 70 and the following statements), the near-field approximation has been changed by replacing [y-a-w] for the calculation of F3 (as in the original DILUN) with [y+a+w]. The computation has been reprogrammed to allow for testing to prevent underflows. XD, SI, and TC are calculated to obtain useful information.

The far-field approximation was mentioned in the text of AMSHAH but was not contained in the original version of DILUN. The equation for the far-field concentration has been programmed and is in the current version of DILUN, as the group of statements beginning with statement 75. As above, the statements defining XD, SI, and TC are for useful information.

The statements which calculate the concentration for the case of an instantaneous spill into a tidal river begin with statement 80. There is no change in the equation, but the computation has been reprogrammed to eliminate underflows.

There has been some reorganization in the section dealing with continuous spills. Since the computation of the concentration for both the still water and the tidal river cases was by the integration subroutine DLIN, these two sections of the original program have been consolidated into the section that begins after statement 100.

For a continuous spill into a non-tidal river, there are near-field and far-field cases. The near-field equation, as originally programmed, would give incorrect answers unless XK was set equal to zero. This section (starting after statement 120) has been reprogrammed with the correct expression. The section of the original program which calculated the

concentration in the far-field case was also incorrect. The definition of OMG was not correct, and the final statement was C=F1*F2*F3 instead of C-F1*(F2-F3). This section, beginning with statement 123, has been corrected and reprogrammed.

Subroutine DISP is shown in Appendix 3D, Figure 3D-6. This subroutine retains its argument list because it is called by the MODV package as well. The errors in this subroutine were in the tidal river section where the current time, T, was used in the statements defining ET, TPV, and TPT instead of the tidal period, TP. Since TPT was not used, to calculate a value for it is not necessary. This section of the program has been rewritten, and T has been dropped from the argument list. A limit has been placed on the value of F to insure that reasonable values of F are returned in the tidal river case.

It may be noted that in each section of this subroutine values are calculated for EX, EY, EZ, and E. The first two or three of these quantities are used in the near-field approximations, and E is used in the far-field approximations. Further, the values of EY and E depend on the ratio of the width to the depth (W/D) in the river. The values calculated for EY and E depend upon whether or not the ratio W/D is just over or just under the value of 100 which classifies rivers into wide rivers or narrow rivers. This in turn will have an effect upon the mixing and dilution of the cargo. Further, EX, EY, and EZ have no particular relationship to E, so that when the program switches from the near-field to the far-field approximation the distribution of the cargo will change significantly and discontinuously.

There may be no easy way around these problems, but the user should be aware of the consequences of the ways in which the dispersion coefficients are calculated. A numerical example may help to clarify the matter. Let W/D = 100 and consider the non-tidal river, both the narrow and wide river cases. The variables of interest are:

W	=	500 m = 50,000 cm	
D	=	5m = 500 cm $\therefore$ (W/D=100)	
UF	=	200 cm/sec	
RF	=	.050	
RH	=	490 cm, $(RH)^{1/6} = 2.817$	
USTAR	=	23.84 cm/sec	
EZ	=	798.7 cm^2/sec	$(4*EZ*T)^{1/2} = 1384$ cm
EX	=	79.87 cm^2/sec	$(4*EX*T)^{1/2} = 438$ cm

For the wide river

EY	=	79.87 cm^2/sec	$(4*EY*T)^{1/2} = 438$ cm
E	=	136,670 cm^2/sec	$(4*E*T)^{1/2} = 18,110$ cm

For the narrow river

EY	=	2690 cm^2/sec	$(4*EY*T)^{1/2}$ =	2540 cm
E	=	2,630,000 cm^2/sec	$(4*E*T)^{1/2}$ =	79,500 cm

Expressions of the form $(4*E*T)^{1/2}$ indicate the length of the dispersion parameter and give a rough idea of the distance over which most of the spilled cargo is concentrated. T = 600 sec has been used in calculating these values.

It can be seen from the above that the values of EY and E and their associated dispersion lengths differ in the narrow and wide river cases. The computed concentration distribution will appear to be different in the case W/D = 99.9 and when W/D = 100.1. This is not a realistic discontinuity but occurs because the model does not match the asymtotic behavior of the near-field approximation and the far-field approximation.

Further, from DILUN it can be seen that the downstream dispersion term in the near-field approximation (non-tidal river) is a function of

```
(X-UF*T)**2/(4.*EX*T)
```

whereas in the far-field approximation it is a function of

```
(X-UF*T)**2/(4.*E*T)
```

Since EX and E are different for both narrow and wide rivers, the distribution of the spilled cargo will change when the program switches from the near-field to the far-field approximation. If the river width were such that the change was made at T = 600 sec, the longitudinal dispersion length would change instantly from about 4.4 m to either 181 m or 802 m.

Subroutine DLIN was originally a very general integration routine which was modified for use in this submodel. In the current version it has been modified further by defining AUX and NDIM in DLIN itself, and replacing the dummy function name with CNSPL. DLIN is listed in Appendix 3D, Figure 3D-7.

The function subprogram CNSPL evaluates the quantity being integrated by DLIN. Both the still water and the tidal river cases have been reprogrammed to eliminate the possibility of underflows. The arguments of the cosine functions were incorrect in the original version of this function. The cosine terms are evaluated correctly in the current version of CNSPL shown in Appendix 3D, Figure 3D-8.

In the following, a few general definitions are given, followed by a description of the method for determining the sensitivity coefficients, a detailed description of one output, and finally a comparison and discussion of the conditions in which different spills may occur.

Table 3-3 gives the list of variables for which the sensitivity coefficients were determined. The choice of the variables for which the sensitivity coefficients were determined is dependent on whether the variable has an effect on the concentration predictions. These user input variables would define the spill mass (for instantaneous spills) or spill rate (for continuous spills); location of spill; river size and roughness; observation point and time; decay coefficient (different coefficients for differences in cargoes or in receiving water body conditions); water temperature; and tidal flow, period, and lag (for tidal rivers). This model did not have any parameters, that is, constants of the model which are dependent on cargo properties or quantities which are usually defined within the computer program.

The following is a description of the method used to obtain the sensitivity coefficients. A normal value, X_{ni}, is specified for each of the variables by the user. A reference value, X_{ri}, (usually equal to the normal value) is also chosen for each of the variables. The normal values are used as inputs for the Mixing and Dilution Model, which in turn gives as the normal value of output, Y_n, the concentration of the pollutant (at the position and time specified by the variables).

The variables are now changed one at a time (one variable changed to obtain the sensitivity coefficient of that variable) until all the variables have been changed. The change is five percent of the reference value of that variable. The changed variable, X_{ci}, is greater by five percent as compared to the normal variable. The changed variable can be expressed as:

$$X_{ci} = X_{ni} + 0.05\ X_{ri}$$

where "i" is the subscript denoting the variable used (first, second, third, etc.). For the Mixing and Dilution Model,

$$i = 1, 2, 3, \ldots, m = 16.$$

With all the other variables at their normal values and the one particular variable (whose sensitivity coefficient is now being determined) at its changed value, the changed output, Y_{ci}, is determined. With this changed output for the concentration of the pollutant, the sensitivity coefficient, S_i, for this particular variable is defined as:

$$S_i = \{(Y_{ci} - Y_n)/(Y_n)\} \div \{(X_{ci} - X_{ni})/(X_{ri})\}$$

Various combinations of spill situations have been considered and these are:

1. Non-tidal river or tidal river

2. Instantaneous spill or continuous spill

3. Width of the river, either 4000 cm or 5000 cm

4. Liquid ammonia spill or methyl alcohol spill

The instantaneous spill of liquid ammonia in a non-tidal river of width 4000 cm will be considered in detail in the following:

Figure 3-6 is the output for the above mentioned conditions. In Figure 3-6, the value of XN is the distance the river travels during the time of observation. For non-tidal rivers, the normal velocity of the river was chosen as 200 cm/sec (V11) and the normal time of observation was chosen as 600 seconds (V9). Hence for non-tidal rivers:

$$XN = 600 \times 200 = 120{,}000 \text{ cm}$$

X is defined by:

$$X = XN - A = 120{,}000 - 2{,}500 = 117{,}500 \text{ cm}$$

where A is the variable (V5), whose value is 2500 cm. The river width (V4) for this spill is chosen as 4000 cm. This is a narrow river. For the normal values of the variables given under the column heading "V NORMAL," the Mixing and Dilution model predicted an output normal concentration $Y_n = 0.00026$ g/cm^3. The values of the variables under the column heading "REFERENCE" are the reference values of the variables. The values of the variables under the column heading "V CHANGED" are the changed values of the variables. For example, for the spill mass (V1):

the normal value of the spill mass is $X_{n1} = 0.150 \times 10^9$ g = ZM

the reference value of the spill mass is $X_r = 0.150 \times 10^6$ g

change in spill mass = 5% of reference value

$= 0.05 \times 150 \times 10^6$ g

$= 7.5 \times 10^6$ g

changed variable = normal value of variable + (5% of reference value of the variable)

$= 150 \times 10^6 + 7.5 \times 10^6$

$= 157.5 \times 10^6$

Hence the changed value of the spill mass is $X_{C1} = 0.1575 \times 10^9$ g. With all the other variables at their normal value and the spill mass at its changed value, the Mixing and Dilution Model gives the output variable:

changed concentration of pollutant, $Y_{C1} = 0.273E\text{-}03$

XN = 120000. X = 117500.RIVER WIDTH = 4000.

OUTPUT IS POINT CONCENTRATION NORMAL VALUE IS .260E-03

INDEX	VARIABLE	SENS COEFF	V NORMAL	REFERENCE	V CHANGED	OUTPUT	FRACTION
1	SPILL MASS	1.000	.150E+09	.150E+09	.157E+09	.273E-03	1.050
2	SPILL RATE	0.000	.500E+06	.500E+06	.525E+06	0.	0.000
3	RIV DEPTH	-1.218	800.	800.	840.	.244E-03	.939
4	RIV WIDTH	-1.058	.400E+04	.400E+04	.420E+04	.246E-03	.947
5	SPILL Y	0.000	.250E+04	.250E+04	.263E+04	.260E-03	1.000
6	DELTA X	-.028	.100E+05	.100E+05	.105E+05	.260E-03	.999
7	POINT Y	0.000	0.	.200E+04	100.	.260E-03	1.000
8	POINT Z	0.000	10.0	10.0	10.5	.260E-03	1.000
9	POINT TIME	-1.027	600.	600.	630.	.247E-03	.949
10	DECAY COEF	-.166	.278E-03	.278E-03	.292E-03	.258E-03	.992
11	RIVER FLOW	-.868	200.	200.	210.	.249E-03	.957
12	TIDAL FLOW	0.000	300.	300.	315.	0.	0.000
13	TIDAL PER	0.000	.432E+05	.432E+05	.454E+05	0.	0.000
14	TIDAL LAG	0.000	.130E+05	.432E+05	.151E+05	0.	0.000
15	ROUGHNESS	0.000	.500E-01	.500E-01	.525E-01	0.	0.000
16	WATER TEMP	0.000	10.0	283.	24.2	0.	0.000

FIGURE 3-6 Sensitivity coefficients.

The ratio of the changed output to the normal output is given under the column heading "FRACTION":

$$\text{FRACTION} = Y_{c_1} \div Y_n$$

$$= (0.273 \times 10^{-3}) \div (0.260 \times 10^{-3})$$

$$= 1.050$$

The sensitivity coefficient, S_1, for the first variable is determined by:

$$S_1 = \{(Y_{c_1} - Y_n)/(Y_n)\}/\{(X_{c_1} - X_{n_1})/(X_{r_1})\}$$

$$= \{(0.273E\text{-}03)\text{-}(0.260E\text{-}03)\}/\{(0.260E\text{-}03)\}$$
$$\div \{(0.1575E09)\text{-}(0.150E09)\}/\{(0.150E09)\}$$

$$\therefore S_1 = 1.000$$

A similar procedure is carried out for each of the remaining fifteen variables. The normal values of the remaining variables are determined as in the following:

The spill rate (V2), ZMDOT, is determined by assuming that the total cargo mass is spilled at a constance rate in 5 minutes

$$\text{ZMDOT} = \text{ZM}/(5*60) = 0.150 \times 10^9/300 = 0.5 \times 10^6 \text{ g/s}$$

The characteristics of the river are given by:

river depth = (V3) = D = 800 cm

river width = (V4) = W = 4000 cm

river flow velocity = (V11) = UF = 200 cm/s

tidal flow velocity = (V12) = UT = 300 cm/s

tidal period = (V13) = TP = 43,200 s = 12 hours

tidal lag = (V14) = DEL= 12,960 s = TP/3

roughness coefficient = (V15) = RF = 0.05 = Manning Roughness Factor

river water temperature = (V16) = TW = 10°C

In the following, the remaining normal variables and the implied physical meaning of all the variables will be discussed.

1053911

The ratio of the width (V4), w, to the depth (V3), d, of the river is:

w/d = (normal value of V4)/(normal value of V3)

= 4000/800

$\therefore w/d = 5$

Because ($w/d < 100$), this river is classified as a narrow river and the narrow river formula for the dispersion coefficients is used.

The location of the sp ll is given by:

x = 0 cm

y = A (V5) = 2500 cm

z = 0 cm

The position of observation is given by:

Delta x = 10,000 cm (V6)

y = 0 cm (V7)

z = 10 cm (V8)

The time of observation is:

T = 600 S (V9)

The decay coefficient is chosen as:

$XK = 0.278 \times 10^{-3} = 1/(60 \times 60)\ S^{-1}$

= 1/(1 hour)

The overall physical picture (for the normal values) can now be stated as follows:

An instantaneous spill of 1.5×10^{8} g of liquid ammonia occurs at a location given by

x = 0 cm

y = 2500 cm

z = 0 cm

in a narrow non-tidal river, whose characteristics are:

river depth = 800 cm

river width = 4000 cm

river flow velocity = 200 cm/s

roughness coefficient of river = 0.05

river water temperature = 10°C

The concentration of the pollutant is observed at a position given by:

Delta x = 10,000 cm

y = 0 cm

z = 10 cm

at a time of 600 s after the spill occurs.

The realism of the various sensitivity coefficients will be examined in the following.

The sensitivity coefficient for the spill mass is 1.000 and this appears to be because of the direct dependence of the concentration of the pollutant on the amount of the spill. The sensitivity coefficient for the spill rate is not computed because this spill is an instantaneous spill. The river depth and the river width affect the concentration of the pollutant in a manner such that the greater the depth or the width, the smaller the turbulence level in the river. When the turbulence level in the river is small, the shear velocity u* (USTAR) is also small. At the same time, increasing the value of either the depth or width of the river increases the hydraulic radius of the river, where,

$$\text{hydraulic radius} = R_h = \left[\frac{\text{area of cross section}}{\text{perimeter of river}}\right]$$

Using the equation in AMSHAH for the relation between the values of R_h, u*, and E, the dispersion coefficient, we can determine E.

$$\frac{E}{R_h\ u^*} = 225$$

AMSHAH (4.8b)

$$\therefore E = 225\ R_h\ u^*$$

Depending upon the change in the values of R_h and u*, the value of E could increase or decrease. For this river, the value of E increased with increase in either the width or depth of the river. This value of E is

utilized in the equation for the concentration of the pollutant for a far-field approximation of an instantaneous spill,

$$c(x,t) = \frac{M}{A\sqrt{4\pi Et}} \cdot \text{Exp} - \{ \frac{(x-Ut)^2}{4Et} + kt \} \qquad \text{A}^{\text{M}}\text{SHAH (4.6a)}$$

where $c(x,t)$ = concentration of pollutant

M = mass of spill

A = cross-sectional area of river

E = dispersion coefficient

x = position of observation point

U = river velocity

t = time after spill when concentration is observed

k = decay coefficient

The increased value of E caused a decrease in the concentration of the pollutant. Hence the sensitivity coefficient for both the depth and the width of the river is negative. For the particular dimensions of the river, the depth is 800 cm and the width is 4000 cm, and variations in the depth cause greater effect on the concentration of the pollutant as compared to equal percentage variations in the width of the river. It is to be noted that a negative sensitivity coefficient indicates that the output concentration decreases when the changed input variable increases. The sensitivity coefficients are of the order of unity and hence the concentration of the pollutant is reasonably sensitive to the depth and width of the river.

The spill location (from the center of the river, in a cross-stream direction) along with the variations in the y and z directions for the point of observation do not seem to have any effect on the concentration of the pollutant. This is because the river is narrow and the point of observation is relatively distant from the location of the spill (at the time of observation) and hence the simulation adopted the far-field approximation option. The far-field approximation is a one-dimensional solution which is applicable when there is negligible variation in the concentration of the pollutant at positions cross-stream or depthwise. Hence the sensitivity coefficients for SPILL Y (V5), POINT Y (V7), and POINT Z (V8) are all zero.

The observation point DELTA X (V6) along the downstream direction effects the concentration prediction in an inverse exponential manner.

For the particular spill being analyzed, changes in the observation point seems to have a relatively small effect on changes in the concentration of the pollutant and hence the sensitivity coefficient is relatively small. Here again, increasing DELTA X decreases the concentration and hence results in a negative sensitivity coefficient.

The variable POINT TIME, t (V9) has an effect on the concentration of the pollutant comparable to that of the spill mass, river depth, and river width. Increase of the observation time decreases the concentration and hence the negative sensitivity coefficient.

The pollutant concentration seems to be less sensitive to the decay coefficient, k, (V10). This can be seen from the following:

The exponential decay of the concentration of the pollutant can be expressed simply as

$$c(k,t) = \text{Exp}\ (-kt)$$

where $c\ (k,t)$ = concentration of pollutant

k = decay coefficient

t = time

The sensitivity coefficient for the concentration of the pollutant can be analyzed qualitatively by studying the behavior of:

$$\text{sensitivity coefficient} = \left[\frac{\{(\partial c)/c\}}{\{(\partial k)/k\}}\right]$$

$$= \left[\frac{\partial c}{\partial k}\right] \cdot \left[\frac{k}{c}\right]$$

$$= \left[\frac{\partial}{\partial k}\ \{\ \text{Exp}\ (-kt)\ \}\right] \cdot \left[\frac{k}{\text{Exp}\ (-kt)}\right]$$

$$= \left[(-t) \cdot \{\ \text{Exp}\ (-kt)\}\right] \cdot \left[\frac{k}{\text{Exp}\ (-kt)}\right]$$

hence, sensitivity coefficient $\simeq [-kt]$

The choice of normal values for the variables of the cargo spill, being simulated in the computer, gives small values of the approximate sensitivity coefficient. If the decay coefficient was large, then it would have a considerable effect on the sensitivity coefficient, even for a short observation time after the spill. The negative sensitivity coefficient can also

be understood from the physical behavior of the pollutant; increasing the decay coefficient decreases the pollutant concentration.

Increase in the river velocity (V11) causes the turbulence level in the river to increase with a consequent increase in the shear velocity u* and an increase in the dispersion coefficient E, and a subsequent decrease in the concentration of the pollutant. The concentration is reasonably sensitive to the river velocity (note the negative sensitivity coefficient, as expected) and this sensitivity is less than that of the spill mass, river depth and width, and the time of observation.

For the instantaneous spill in a non-tidal river, the variables of tidal flow (V12), tidal period (V13), and tidal lag (V14) are not applicable and hence have zero sensitivity coefficients. The river roughness (V15) and river water temperature (V16) have negligible effect on the pollutant concentration and in this case have zero sensitivity coefficients.

This completes the detailed discussion of a particular spill and the associated sensitivity coefficients. Comparisons with different spills under different conditions are analyzed in the following.

Two types of cargoes were analyzed, namely, liquid ammonia and methyl alcohol. Two types of river conditions were considered, non-tidal rivers and tidal rivers. Two types of spills were used, instantaneous spills and continuous spills. Finally two river widths were employed, 4000 cm and 50,000 cm.

The sensitivity coefficients for the instantaneous spill of cargo in non-tidal rivers of 50,000 cm width are not presented because the initial normal value of pollutant concentration were so low as to cause under-flow of data in the computer simulation. The sensitivity coefficients for the remaining five cases for each of the cargoes are presented in Appendix 3E, Figures 3E-1 to 3E-10. It is to be noted that for the present sensitivity analysis, change of the cargo does not produce any changes in the sensitivity coefficients because the turbulent diffusion - as modeled in the present analysis - is independent of cargo properties. For a complete sensitivity analysis, the simulation of the mixing and dilution process would have to include the buoyancy effects of cargoes, heat sources and sinks, and the particular cargo properties involved in the mixing and dilution process (for example, the cargo heat capacity, kinematic viscosity, etc.). A summary of the sensitivity coefficients is presented in Figure 3-7.

Comparing instantaneous spill (case 1) and continuous spill (case 2), we notice the decrease in the sensitivity coefficient for the spill mass (V1), a slight increase in the sensitivity coefficient for spill rate (V2), slight decreases in the sensitivity coefficient of the river depth (V3) and width (V4), a considerable decrease in the sensitivity coefficient for the time of observation (V9), and a slight decrease in the sensitivity coefficient of the river flow (V11). The continuous spill has been going

Variable \ Case Number	1	2	3	4	5
Type of Spill	N I 4	N C 4	N C 50	T I 50	T C 50
1. Spill Mass	1.00	0.90	0.00	1.00	0.37
2. Spill Rate	0.00	0.05	1.00	0.00	0.56
3. River Depth	- 1.22	- 1.15	- 0.23	- 1.29	- 0.99
4. River Width	- 1.06	- 1.03	- 0.01	- 0.95	- 0.95
5. Spill Y	0.00	0.00	- 1.42	0.00	0.00
6. Delta X	- 0.03	0.02	0.04	- 0.13	- 0.37
7. Point Y	0.00	0.00	14.30	0.00	0.00
8. Point Z	0.00	0.00	- 0.00	0.00	0.00
9. Point Time	- 1.03	- 0.38	0.00	- 0.01	1.79
10. Decay Coefficient	- 0.17	0.15	- 0.15	- 0.17	- 0.13
11. River Flow	- 0.87	- 0.50	- 0.81	- 1.91	- 3.27
12. Tidal Flow	0.00	0.00	0.00	0.79	4.15
13. Tidal Period	0.00	0.00	0.00	0.76	1.77
14. Tidal Lag	0.00	0.00	0.00	- 9.56	-11.61
15. Roughness	0.00	0.00	0.00	- 0.42	- 0.05
16. Water Temperature	0.00	0.00	0.00	0.00	0.00

N = Non-tidal river
I = Instantaneous spill
4 = 4,000 cm river width

T = Tidal river
C = Continuous spill
50 = 50,000 cm river width

FIGURE 3-7 Sensitivity coefficients for different spills of liquid ammonia.

on for 600 seconds and variations in the time of observation do not seem to affect the pollutant concentration to a large degree. This is because the continuous pollutant has already reached the point of observation by the convection of the river and changes in the time still keep the point of observation within the convected pollutant.

When a continuous spill is in a non-tidal river of 50,000 cm width (case 3), the simulation model chooses the near-field approximation option and hence the high sensitivity to variations in the cross-current dimension (V7) of the observation point can be noticed. The moderate sensitivity to the location of the spill (V5) is also evident.

Tidal rivers (case 4 and 5), as compared with non-tidal rivers, give greater sensitivity coefficients for the velocity of the river (V11), tidal flow velocity (V12), tidal period (V13), and river roughness (V15). There is also a large sensitivity to the pollutant concentration from the tidal lag (V14), for the cases chosen. This is because any difference in the tidal lag affects the time at which the spill occurs and, consequently, whether the tide is rising or falling.

In summary, the dispersion of a spilled cargo is highly sensitive to the cross-stream observation point for continuous spills in a non-tidal river of 50,000 cm width (with normal values for the variables). The disperson is also highly sensitive to the tidal lag for spills in tidal rivers. For continuous spills in tidal rivers the dispersion is quite sensitive to the river velocity and to the tidal flow velocity. Finally the dispersion of the pollutant is moderately sensitive to the river depth and width for points of observation where the pollutant concentration can be predicted by far-field approximations.

SUMMARY AND RECOMMENDATIONS

The model as developed in AMSHAH and computer programmed in HACS has errors in the modeling and documentation of AMSHAH and in the programming of HACS. There is an apparent jump in the concentration of the pollutant when the approximation switches from a near-field to a far-field approximation, when no such jump exists physically. The predicted concentration of the pollutant is greater than the density of the spilled cargo for considerable lengths of time. No buoyancy forces were considered for all the spills.

For the modeling of the mixing and dilution phenomena to be adequate, the following recommendations are made.

- The apparent jump in the concentration of the pollutant should be resolved by adequate matching of the near-field and far-field approximations.

- The unnatural predictions of the liquid density should be eliminated by taking into account the initial size of a spill and then model the mixing and dilution of the pollutant.

- Cargoes which are heavier or lighter than the receiving water body into which the spill occurs should also be modeled because most cargoes are not neutrally buoyant.

APPENDIX 3A

We wish to solve the equation (4.5) of AMSHAH

$$\frac{\partial C}{\partial t} + U \frac{\partial C}{\partial x} = E \frac{\partial^2 C}{\partial x^2} - kC \qquad (3A\text{-}1)$$

for $C(x,t)$ with the boundary conditions

$$C(x,0) = \frac{M}{A} \delta(x) \qquad (3A\text{-}2a)$$

$$C(x \to \pm\infty) = 0 \qquad (3A\text{-}2b)$$

$$C(t \to +\infty) = 0, \; C(t<0) = 0 \qquad (3A\text{-}2c)$$

In the above, M, U, E, A, and K are constants. Let us define new variables, $\xi = x - Ut$ and $\zeta = t$, and then we have

$$\frac{\partial C}{\partial t} = \frac{\partial C}{\partial \zeta} - U \frac{\partial C}{\partial \xi}, \; \frac{\partial C}{\partial x} = \frac{\partial C}{\partial \xi}, \; \frac{\partial^2 C}{\partial x^2} = \frac{\partial^2 C}{\partial \xi^2} \qquad (3A\text{-}3)$$

Then equation (3A-1) becomes

$$\frac{\partial C}{\partial \zeta} + kC = E \frac{\partial^2 C}{\partial \xi^2} \qquad (3A\text{-}4)$$

and the boundary conditions are

$$C(\xi, 0) = \frac{M}{A} \delta(\xi) \qquad (3A\text{-}5a)$$

$$C(\xi \to \pm\infty) = 0 \qquad (3A\text{-}5b)$$

$$C(\zeta \to +\infty) = 0, \; C(\zeta<0) = 0 \qquad (3A\text{-}5c)$$

Consider the Laplace transform with respect to ζ. We know that

$$\mathcal{L}\left[\frac{\partial C}{\partial \zeta}\right] = s\hat{C} - C(\xi, +0)$$

PRECEDING PAGE BLANK-NOT FILMED

Hence, equation (3A-4) may be written in terms of $\hat{C}(\xi,s)$, the transform of $C(\xi,\zeta)$:

$$s\hat{C} - C(\xi, 0) + k\hat{C} = E \frac{\partial^2 \hat{C}}{\partial \xi^2} \tag{3A-6a}$$

and using the initial condition this is

$$(s+k)\hat{C} - \frac{M}{A} \delta(\xi) = E \frac{\partial^2 \hat{C}}{\partial \xi^2} \tag{3A-6b}$$

Now the homogeneous equation corresponding to (3A-6) is

$$(s+k)\hat{C} = E \frac{\partial^2 \hat{C}}{\partial \xi^2} \tag{3A-7}$$

to which the solution is

$$\hat{C} = a \exp\left[-\xi\left(\frac{s-k}{E}\right)^{1/2}\right] + b \exp\left[+\xi\left(\frac{s-k}{E}\right)^{1/2}\right] \tag{3A-8}$$

Since $\hat{C}$ is continuous at $\xi = 0$, and since $C \to 0$ for $\xi \to \pm \infty$, we have

$$\hat{C}(\xi, s) = a \exp\left[-\xi\left(\frac{s+k}{E}\right)^{1/2}\right] \text{ for } \xi \geq 0$$

$$\hat{C}(\xi, s) = a \exp\left[+\xi\left(\frac{s+k}{E}\right)^{1/2}\right] \text{ for } \xi \leq 0 \tag{3A-9}$$

The unknown constant a is evaluated by means of the equation

$$\left.\frac{\partial \hat{C}}{\partial \xi}\right|_{\xi = +0} - \left.\frac{\partial \hat{C}}{\partial \xi}\right|_{\xi = -0} = \frac{-M}{AE} \tag{3A-10}$$

([6], pp. 61-65). Using equation (3A-9) here on either side of zero, we have

$$a = \frac{M}{2AE} \left(\frac{E}{s+k}\right)^{1/2} = \left(\frac{M}{A}\right) (4E(s+k))^{-1/2} \tag{3A-11}$$

---

[6] Stakgold, I., Boundary Value Problems of Mathematical Physics, vol. 1, MacMillan, New York, 1967.

Thus the solution to (3A-6) can be written

$$\hat{C}(\xi, s) = \left(\frac{M}{A}\right) (4E(s+k))^{-1/2} \exp\left[-\xi\left(\frac{s+k}{E}\right)^{1/2}\right] \text{ for } \xi \geq 0$$

$$\hat{C}(\xi, s) = \left(\frac{M}{A}\right) (4E(s+k))^{-1/2} \exp\left[+\xi\left(\frac{s+k}{E}\right)^{1/2}\right] \text{ for } \xi \leq 0 \qquad \text{(3A-12)}$$

Now if $\mathcal{L}[F(t)] = f(s)$, then $\mathcal{L}[e^{at}F(t)] = f(s-a)$, and for

$$F(t) = \frac{1}{(\pi t)^{1/2}} \exp\left(-\frac{m^2}{4t}\right), \quad f(s) = \frac{1}{s^{1/2}} e^{-m s^{1/2}} \text{ for } m \geq 0 \qquad \text{(3A-13)}$$

(see, for example, #84 on p. 320 for the CRC Math tables [7]). Since $\zeta = t$, let us transform back to t instead of to ζ. We have

$$C(\xi, t) = \left(\frac{M}{A}\right) \frac{e^{-kt}}{(4\pi Et)^{1/2}} \exp\left[-\frac{\xi^2}{4Et}\right] \qquad \text{(3A-14)}$$

This is equation (4.6a) on p. 34 of AMSHAH. We now procede to derive the equation corresponding to (4.6b) of AMSHAH.

We wish to consider the case where the source is not an instantaneous one at $t = 0$, but one that continues at a constant rate from $t = 0$ to $t = t_{MT}$. We may get the solution by integrating (3A-14) with respect to the source time. We write (3A-14) for a spill which occurred at time τ :

$$C(x, t) = \frac{M}{2A} (\pi E(t-\tau))^{-1/2} \exp\left[-k(t-\tau) - \frac{(x-U(t-\tau))^2}{4E(t-\tau)}\right] \text{ for } t > \tau$$

$$C(x, t) = 0 \text{ for } t < \tau \qquad \text{(3A-15)}$$

If two successive instantaneous spills occurred, the concentration would be given by the sum of two expressions similar to (3A-15). Instead of summing for a number of discrete events, we may integrate to get the solution for a continuous spill.

Let the spill commence at $t = 0$ and continue to $t = t_{MT}$, at which time it ceases. We note that (3A-15) is written entirely in terms of the difference between the present time t and the time of the spill, τ. Let us denote this difference by y: $y = t - \tau$. The smallest value of y will be

[7] Hodgman, C. D. (ed.), C.R.C. Standard Mathematical Tables, 11th ed., Chemical Rubber Co., Cleveland, Ohio, 1957.

$$y = 0 \text{ if } t < t_{MT} \tag{3A-16a}$$

or

$$y = t - t_{MT} \text{ if } t > t_{MT} \tag{3A-16b}$$

and the largest value will be

$$y = t \text{ in either case} \tag{3A-16c}$$

Thus for a source with rate $\dot{M}$:

$$C(x, t) = 0 \text{ for } t < 0 \tag{3A-17a}$$

$$C(x, t) = \int_0^t \frac{\dot{M}}{2A} (\pi E y)^{-1/2} \exp\left[- ky - \frac{(x-Uy)^2}{4Ey}\right] dy \text{ for } 0 < t < t_{MT} \tag{3A-17b}$$

$$C(x, t) = \int_{t-t_{MT}}^t \frac{\dot{M}}{2A} (\pi E y)^{-1/2} \exp\left[- ky - \frac{(x-Uy)^2}{4Ey}\right] dy \text{ for } t > t_{MT} \tag{3A-17c}$$

Denoting the arguments of these integrals by arg, and expanding $(x-Uy)^2$, we note that one term in the exponential is not a function of y, so we have

$$\text{arg} = \left(\frac{\dot{M} dy}{2A}\right) (\pi E y)^{-1/2} \exp\left[\frac{2xU}{4E} - \frac{x^2+U^2y^2+4Eky^2}{4Ey}\right] \tag{3A-18}$$

Let us define Ω by

$$\Omega^2 = U^2 + 4Ek \tag{3A-19}$$

Then we have

$$\text{arg} = \left(\frac{\dot{M} dy}{2A}\right) (\pi E y)^{-1/2} \exp\left[\frac{2xU}{4E}\right] \exp\left[- \frac{x^2}{4Ey} - \frac{\Omega^2 y}{4E}\right] \tag{3A-20}$$

Changing variables, let $y = z^2$, $dy = 2zdz$, and

$$a^2 = \Omega^2/4E, \quad b^2 = x^2/4E \tag{3A-21}$$

we have

$$\text{arg} = \frac{\dot{M}}{A(\pi E)^{1/2}} \exp\left[\frac{xU}{2E}\right] \exp\left[-\frac{b^2}{z^2} - a^2 z^2\right]dz \qquad (3A\text{-}22)$$

For $t > t_{MT}$, from (3A-17), we have

$$C = \int_{t-t_{MT}}^{t} \text{arg}(y)dy = \int_{(t-t_{MT})^{1/2}}^{t^{1/2}} \text{arg}(z)dz \qquad (3A\text{-}23)$$

where arg(y) is given by (3A-18) or (3A-20), and arg(z) is given by (3A-22). This integral may be evaluated in closed form as shown on page 304 of Abramowitz and Stegun [8] (#7.4.33).

$$C(x, t) = \frac{\dot{M}}{A(E\pi)^{1/2}} \exp\left[\frac{xU}{2E}\right] \left(\frac{\pi^{1/2}}{4a}\right) \left[e^{2ab}\, \text{erf}\left(az+\frac{b}{z}\right) + e^{-2ab}\, \text{erf}\left(az-\frac{b}{z}\right)\right] \Bigg|_{(t-t_{MT})^{1/2}}^{t^{1/2}} \qquad (3A\text{-}24)$$

In this expression erf is an abbreviation for the error function. Evaluating this expression and using (3A-21) for a and b, we get the expression for the concentration for $t > t_{MT}$:

$$C(x, t) = \frac{\dot{M}}{2A\Omega} \exp\left[\frac{xU}{2E}\right] \left[\exp\left(\frac{x\Omega}{2E}\right) \left\{ \text{erf}\left[\frac{\Omega t^{1/2}}{2E^{1/2}} + \frac{x}{2(Et)^{1/2}}\right] - \text{erf}\left[\frac{\Omega (t-t_{MT})^{1/2}}{2E^{1/2}} + \frac{x}{2(E(t-t_{MT}))^{1/2}}\right]\right\} + \exp\left[\frac{-x\Omega}{2E}\right] \left\{ \text{erf}\left[\frac{\Omega t^{1/2}}{2E^{1/2}} - \frac{x}{2(Et)^{1/2}}\right] - \text{erf}\left[\frac{\Omega (t-t_{MT})^{1/2}}{2E^{1/2}} - \frac{x}{2(E(t-t_{MT}))^{1/2}}\right]\right\}\right] \qquad (3A\text{-}25a)$$

which may be more compactly written as

$$C(x, t) = \frac{\dot{M}}{2A\Omega} \exp\left[\frac{xU}{2E}\right] \left[\exp\left(\frac{x\Omega}{2E}\right) \left\{ \text{erf}\left[\frac{\Omega t + x}{2(Et)^{1/2}}\right] -$$

---

[8] Abramowitz, M., and I. Stegun (eds.), Handbook of Mathematical Functions, National Bureau of Standards, Applied Mathematics Series Number 55, U. S. Government Printing Office, 1964.

$$\text{erf}\left[\frac{\Omega(t-t_{MT}) + x}{2(E\,(t-t_{MT}))^{1/2}}\right] \} + \exp\left[\frac{-x\Omega}{2E}\right] \{ \text{erf}\left[\frac{\Omega t - x}{2\,(Et)^{1/2}}\right] \quad \text{(3A-25b)}$$

$$- \text{erf}\left[\frac{\Omega(t-t_{MT}) - x}{2\,(E\,(t-t_{MT}))^{1/2}}\right] \}]$$

For the case where $0 < t < t_{MT}$, we may obtain the integral by letting $t_{MT} \to t$ in (A25). Since erf $(+\infty) = 1$ and erf $(-\infty) = -1$, we have

$$C(x, t) = \frac{\dot{M}}{2A\Omega} \exp\left[\frac{xU}{2E}\right] [\exp\left(\frac{x\Omega}{2E}\right) \{ \text{erf}\left(\frac{\Omega t + x}{2\,(Et)^{1/2}}\right) - 1 \}$$

$$+ \exp\left[\frac{-x\Omega}{2E}\right] \{ \text{erf}\left(\frac{\Omega t - x}{2\,(Et)^{1/2}}\right) + 1 \}] \quad \text{(3A-26a)}$$

This equation may be compared to (4.6b) of AMSHAH:

$$C(x, t) = \frac{\dot{M}}{2\Omega A} e^{\frac{xU}{2E}} [e^{\frac{x\Omega}{2E}} (\text{erf}\left(\frac{x+\Omega t}{(4Et)^{1/2}}\right) - 1) - e^{-\frac{x\Omega}{2E}} (\text{erf}\left(\frac{x-\Omega t}{(4Et)^{1/2}}\right) - 1]$$

AMSHAH (4.6b), (3A-26b)

Using the fact that erf $(-x) = -\text{erf}\,(x)$, we see that the two expressions are identical. The text does not mention the case where $0 < t < t_{MT}$, but the computer program contains the expression for this case. Both cases are treated in DILUN between statement number 123 and statement number 126. The two error function terms are calculated correctly, but instead of subtracting them, the program multiplies them. The statement above statement number 126 is

```
C = F1*F2*F3                                    (3A-27)
```

when it should be

```
C = F1 * (F2 - F3).                             (3A-28)
```

It may be seen from the derivation above that the definition of Ω on p. 34 of AMSHAH is incorrect. It should be

$$\Omega = (U^2 + 4kE)^{1/2} \quad \text{(3A-29)}$$

The program also contains this error, and statement 123 in DILUN should be changed accordingly.

The limiting expressions (4.6c) and (4.6d) are correct for the case in which the source never ceases; i.e. when $t_{MT} \to \infty$. Neither of these expressions is used in the program.

APPENDIX 3B

IMAGE SOURCES

In the following analysis, the relative importance of the image sources to the prediction of concentration of pollutant is determined.

Consider two reflecting surfaces, L and R, as shown in Figure 3B-1, where S is any source

L (left reflecting surface), $z = 0$

R (right reflecting surface), $z = d$

S (source), $z = \ell$

where ℓ can be positive or negative. When S is reflected about the left surface, the image source has its coordinates as:

I_L (image reflected about left surface), $z = -(\ell)$

When S is reflected about the right surface, the image source has its coordinate as:

I_R (image reflected about the right surface), $z = 2d-(\ell)$

These distances are also shown in Figure 3B-1.

Hence, when a source, S, is reflected about the left surface, the coordinate of its image, I_L, is the negative quantity of the coordinate of the source; and when the source, S, is reflected about the right surface, the coordinate of this image, I_R, is the difference of twice the distance of separation of the two reflecting surfaces and the coordinate of the source. This general statement will now be used to determine multiple reflections of a source and its images about two reflecting surfaces.

The general expressions can be expressed as:

Source, S, $z = \ell$

Left Image, I_L, $z = -(\ell)$

Right Image, I_R, $z = 2d-(\ell)$

We will now consider a general source and multiple reflections about the reflecting surfaces. The initial source will have two images, one about the left surface, I_L, and the second about the right surface, I_R. The image, I_L, from the left surface, is made to reflect about the right surface to obtain the image, I_{LR}, as shown in Figure 3B-2. The image, I_R, from the right surface, is made to reflect about the left surface to obtain

PRECEDING PAGE BLANK-NOT FILMED

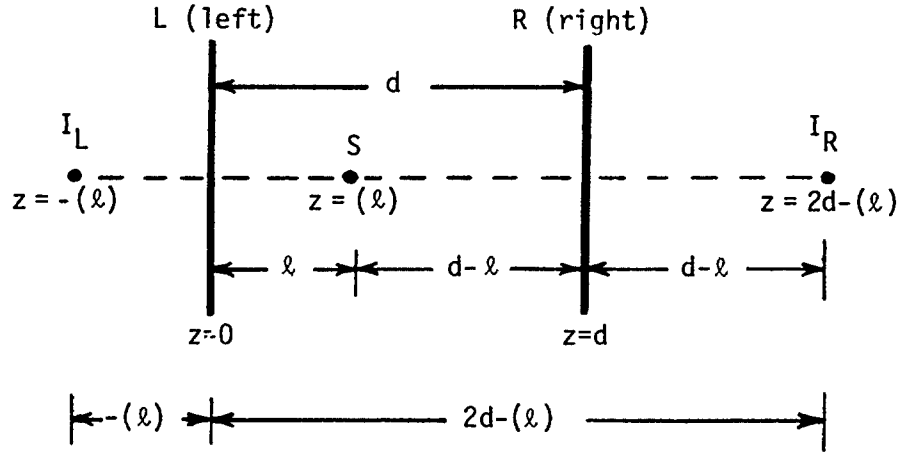


FIGURE 3B-1 Image sources.

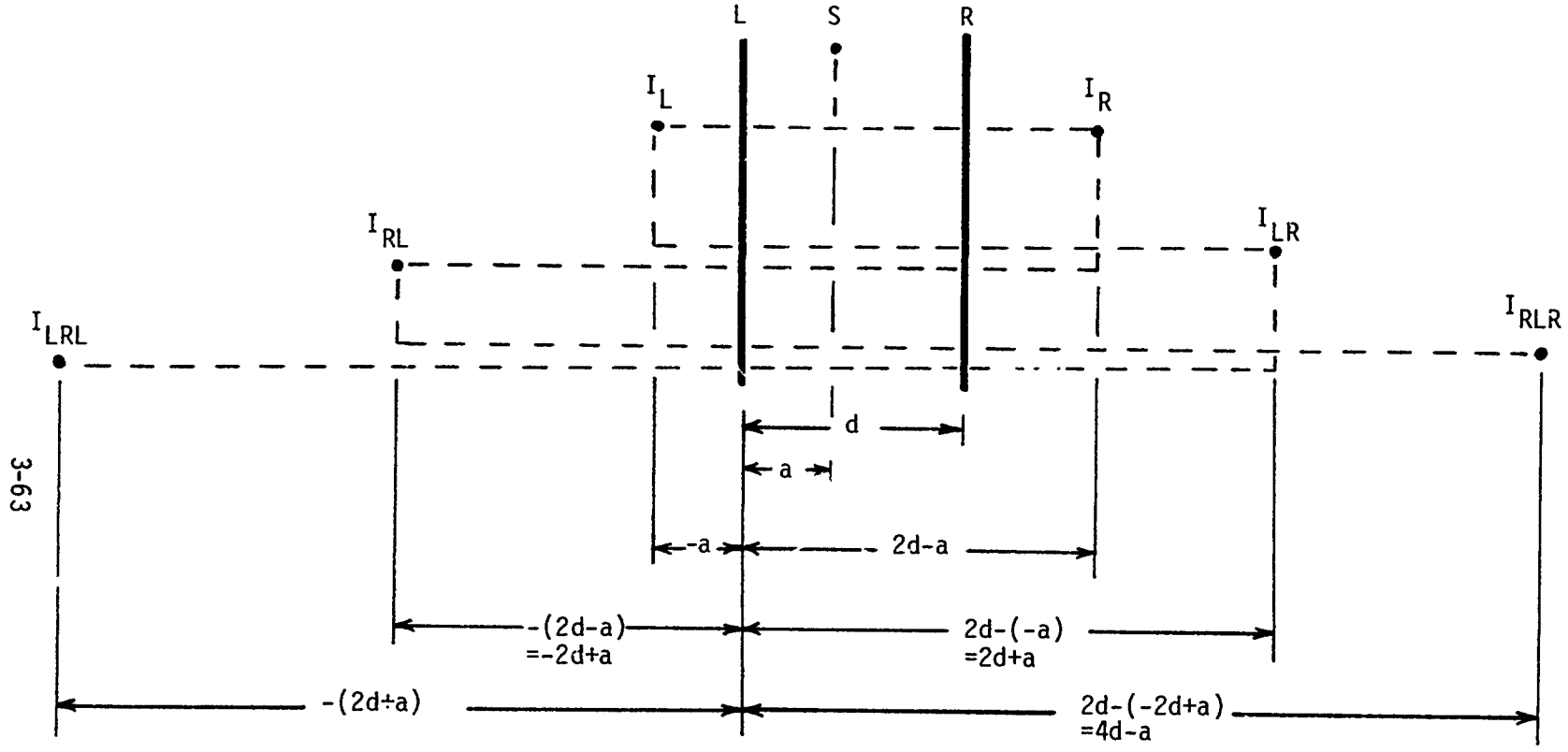


FIGURE 3B-2 Multiple reflections.

the image, I_{RL}. Similar mutiple reflections are shown in Figure 3B-2. The coordinates of the source and its multiple images are shown in Table 3B-1.

When we make [a = 0], the coordinates of the source and its multiple images become:

0 , 2d , 2d , 4d , 4d , ...

and -0 , -2d , -2d , -4d , -4d , ...

The concentration of the pollutant can now be qualitatively expressed in terms of the source and its multiple images and their z-coordinate position as:

$$c(z,t) = e^{-Az^2} + \sum_{n=1,2,3,\ldots}^{\infty} B\left[e^{-A(z-2nd)^2} + e^{-A(z+2nd)^2}\right]$$

where A and B are constants.

The variation of z is given by:

$$0 \leqslant z \leqslant d$$

where d is the depth of the rectangular channel model.

The limits of the terms in the expression for the concentration of the pollutant will be analyzed so that the relative importance of each term in the full expression can be determined.

The limits of the leading term are given by:

$$e^{-Ad^2} \leqslant e^{-Az^2} \leqslant 1$$

When n=1, the limits of the first term in the brackets are:

$$e^{-4Ad^2} \leqslant e^{-A(z-2d)^2} \leqslant e^{-Ad^2}$$

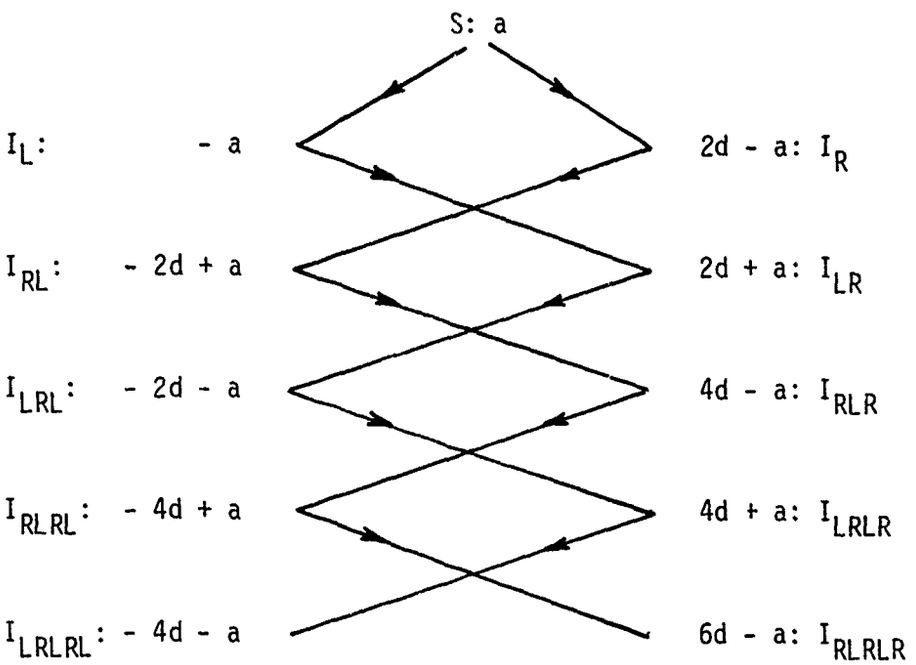
and the limits of the second term in the brackets are:

$$e^{-9Ad^2} \leqslant e^{-A(z+2d)^2} \leqslant e^{-4Ad^2}$$

If the last term is to be neglected, in comparison to the first two terms, we require that the largest value of the last term to be negligible in comparison to the other two,

TABLE 3B-1 Coordinates of Multiple Reflection Images

When there are multiple reflections and a reflection about a left reflecting surface occurs, the coordinates of the reflection are equal and opposite to that of the source. For example, when I_{LR} (coordinate: 2d+a) is reflected about the left reflecting surface, the reflection is I_{LRL} (coordinate: -2d - a). When the reflection is about a right reflecting surface the coordinate of the reflection is the difference of twice the distance of separation of the reflecting surfaces and the coordinate of the source. For example, when I_{LRL} (coordinate: -2d - a) is reflected about the right reflecting surface, the reflection is I_{LRLR} (coordinate: 2d - (-2d - a) = 4d+a).



i.e. $3^{-4Ad^2} \ll 1$

If $4Ad^2 = 5$

then $e^{-4Ad^2} = e^{-5} = 0.0067$

and $e^{-4Ad^2} = 0.0067 \ll 1$

Hence, to be able to neglect the third term, $[4Ad^2]$ should be greater than 5.

From the expression for the concentration of the pollutant given in Chapter 3, the constant A is given by:

$$A = \frac{1}{4e_z t}$$

where e_z = turbulent diffusion coefficient in the z-direction

and t = time of observation, after spill occurs.

$\therefore$ $4Ad^2 > 5$ would imply that

$$4 \cdot \frac{1}{4e_z t} \cdot d^2 > 5$$

i.e., for $t < \frac{d^2}{5e_z}$

Therefore, for time less than $[d^2/5e_z]$, the last term for the concentration of the pollutant is relatively unimportant in comparison to the other two terms. But, to be consistent and general, equation 4.1 of AMSHAH should include all the three terms discussed above. This is especially true for the important case when the position of observation is at the surface of the water (i.e., z=0).

In order to neglect the higher-order terms, we require that, for z=0,

$$e^{-A(4d)^2} \ll 1 + 2e^{-A(2d)^2}$$

i.e., when $A(4d)^2 > 5$

$$\frac{1}{4e_z t} \cdot 16d^2 > 5$$

or $$t < \frac{4}{5} \frac{d^2}{e_z}$$

APPENDIX 3C

POLLUTANT CONCENTRATION FOR SPILLS IN TIDAL RIVERS

The response to an instantaneous spill of cargo in a tidal river (without decay of pollutant), is given by:

$$c(x,t) = \begin{cases} 0 & t < \tau \\ \left[\dfrac{M}{A\sqrt{4\pi E(t-\tau)}}\right] \cdot \left[\text{Exp} - \left\{\dfrac{\chi}{4E(t-\tau)}\right\}\right] & t > \tau \end{cases}$$

where

$c(x,t)$ = pollutant concentration

M = mass of spill

$E(t-\tau)$ = dispersion coefficient

χ = $x - \int_{\tau}^{t} U(\sigma)\ d\sigma$

$U(\sigma)$ = velocity of river

σ = dummy "time" variable

τ = time at which instantaneous spill occurs

t = time

When the spill is continuous, the concentration of the pollutant is given by:

$$c(x,t) = \int_{0}^{t} M(\tau)\ f\ d\tau$$

where

$$f = \begin{cases} 0 & t < \tau \\ \left[\dfrac{1}{A\sqrt{4\pi F(t-\tau)}}\right] \cdot \left[\text{Exp} - \left\{\dfrac{\chi^2}{4E(t-\tau)}\right\}\right] & t > \tau \end{cases}$$

$$\dot{M}(\tau) = \begin{cases} 0 & t < T \\ \dot{M}(\tau) & t > T \end{cases}$$

PRECEDING PAGE BLANK-NOT FILMED

$$\dot{M}(\tau) = \begin{cases} 0 & t < T \\ \dot{M}(\tau) & t > T \end{cases}$$

T = start of continuous spill

$\dot{M}(\tau)$ = rate of spill

Therefore,

$$c(x,t) = \int_0^t \left[\frac{\dot{M}(\tau)}{A\sqrt{4\pi E(t-\tau)}}\right] \cdot \left[\text{Exp} - \left\{\frac{\chi^2}{4E(t-\tau)}\right\}\right] \cdot d\tau$$

If $t < T$ and $0 < \tau < t$, then $c(x,t) = 0$.

If $t \geq T$, then

$$c(x,t) = \int_T^t \left[\frac{\dot{M}(\tau)}{A\sqrt{4\pi E(t-\tau)}}\right] \cdot \left[\text{Exp} - \left\{\frac{\chi^2}{4E(t-\tau)}\right\}\right] \cdot d\tau$$

We shall transform the independent variables as follows:

Let $\tau = \xi + T$ and $t = t' + T$

The concentration of the pollutant becomes

$$c(x,t) = \int_0^{t'} \left[\frac{\dot{M}(\xi+T)}{A\sqrt{4\pi E(t'-\xi)}}\right] \cdot \left[\text{Exp} - \left\{\frac{\chi}{4E(t'-\xi)}\right\}\right] \cdot d\xi \qquad (3C\text{-}1)$$

and the expression for χ, which was

$$\chi = x - \int_\tau^t U(\sigma)\, d\sigma$$

will now become

$$\chi = x - \int_{\xi+T}^{t'+T} U(\sigma)\, d\sigma \qquad (3C\text{-}2)$$

Hence, comparing equation (3C-1) with equation (4.13a) of AMSHAH, the arguments for the $\bar{M}$ term in AMSHAH seem to be incorrect and the limits of integration of equation (4.11) of AMSHAH are to be changed to those shown in equation (3C-2).

APPENDIX 3D

COMPUTER PROGRAMS

The subroutines in Figure 3D-1 through Figure 3D-4 are the original subroutines of HACS. For the sensitivity analysis, certain changes were made in these subroutines which are discussed in the section Sensitivity Analysis of this chapter. The modified subroutines are listed in Figure 3D-5 through Figure 3D-8.

PRECEDING PAGE BLANK-NOT FILMED

```
      SUBROUTINE DILUN(IFLAG,ICOND,ZMAS,ZMDOT,X,Y,Z,TIME,DIFCO,D,W,A,UP,
     1U1,TP,DEL,XK,XN,C)
C
C ***************************************************************************
C***   THIS SUBROUTINE GIVES THE CONENTRATION OF A WATER MISCIBLE LIQUID
C     SPECIFIED SPATIAL POINT AND GIVEN TIME, FOR SPILL IN LAKE, RIVER O
C     ESTUARY. ALL THE LIQUID SPILLED IS ASSUMED TO TO GO INTO SOLUTION
C     WATER. THE SAME PROGRAM CAN ALSO BE USED FOR DISPERSION OF SOLIDS
C     ARE NEUTRALLY BUOYANT OR WHOSE SETTLING TIMES ARE LARGE COMPARED T
C     TIMES.
C
C     THIS SUBROUTINE CANNOT BE USED WITH ACCURACY FOR CONCENTRATION PRE
C     FOR THOSE FLUIDS WHICH REACT WITH WATER OR WHOSE BOILING POINT IS
C     THAN THAT OF THE AMBIENT TEMPERATURE.
C ***************************************************************************
C
C *********  INPUT ARGUMENTS   **********
C ***  IFLAG =  FLAG INDICATING WHERE THE SPILL OCCURS. (1 FOR SPILL IN
C                SIILL WATER ,2 FOR NON TIDAL RIVER, 3 FOR TIDAL REGIONS
C ***  ICOND =  A FLAG WHICH SPECIFIES WHETHER THE SPILL IS CONTINUOUS OR
C                OF SHORT DURATION("INSTANTANEOUS") SPILL. THE VALUE OF ICOND
C                0 FOR SHORT DURATION SPILL AND 1 FOR CONTINUOUS SPILL.
C ***  ZMAS   =  TOTAL MASS OF LIQUID SPILLED                    GMS
C ***  ZMDOT  =  RATE OF MASS SPILL (TO BE GIVEN ONLY IF ICOND=1)     GMS
C ***  X,Y,Z  =  CO ORDINATE POSITIONS AT WHICH THE CONCENTRATION IS NEEDED.
C                THE ORIGIN IS ON THE WATER SURFACE . FOR RIVER SPILLS THE
C                X-DIRECTION IS IN THE DIRECTION  OF FLOW AND Z- DIRECTION IS
C                DEPTHWISE.                                         CMS
C ***  TIME   =  TIME (COUNTED FROM INSTANT OF SPILL) AT WHICH THE CONCENTRA-
C                TION AT POINT X,Y,Z IS TO BE KNOWN.                 SEC
                                                  REAL DUMMY
C ***  DIFCO  =  DIFFUSION COEFFICIENT FOR THE LIQUID IN WATER        CM*
C ***  D      =  MEAN RIVER DEPTH                                     CMS
C ***  W      =  MEAN RIVER WIDTH                                     CMS
C ***  A      =  Y-COORDINATE OF THE POINT OF SPILL ON THE WATER SURFACE
C ***  UP     =  STREAM VELOCITY  ( TO BE GIVEN IF IFLAG =2 OR 3)     CMS
C ***  U1     =  TIDAL VELOCITY AMPLITUDE  (FOR IFLAG = 3)            CMS
C ***  TP     =  TIDAL PERIOD                                         SEC
C ***  DEL    =  PHASE LAG-- ESSENTIALLY THE TIME FOR THE NEXT HIGH WATER
C                SLACK FROM THE INSTANT OF SPILL.                    SEC
C ***  XK     =  DECAY COEFFICIENT ( TO BE GIVEN ONLY IF THE POLLUTANT DECAYS
C                AS PER THE FIRST ORDER DECAY EQUATION)              1./
C ***  XN     =  MANNING FACTOR OF ROUGHNESS FOR RIVERS          NON-DIM
C
C *************     OUTPUT ARGUMENTS     ************
C ***  C      =  CONCENTRATION OF THE POLLUTANT                       GMS
C ***************************************************************************
C
C
      EXTERNAL CNSPL
      DIMENSION AUX(25)
      PI=3.14159265
      B=W/2.
      T=TIME
      IF(ICOND) 20,20,5
5     TMT=ZMAS/ZMDOT
C ***  TMT IS THE TIME TO EMPTY "ZMAS" AT THE RATE OF "ZMDOT".
      IF(T-5.*TMT) 20,10,10
```

FIGURE 3D-1 DILUN.

```
10    ICOND=0
20    CONTINUE
      IF(ICOND)50,50,100
50    CONTINUE
C ***  INSTANTANEOUS SPILL FORMULAE  *********
      GO TO (60,70,80),IPLAG
C ***    SPILL IN CALM AND STILL WATER    *********
60    C=((2.*ZMAS)/(4.*PI*T*DIFCO)**1.5)*EXP(-(X**2+Y**2+Z**2)/(4.*DIFCO
     1*T))*EXP(-XK*T)
      RETURN
C *********   SPILL INTO A NON TIDAL RIVER    ********
70    CALL DISP(W,D,IPLAG,T,UP,UT,XN,TP,E,EX ,EY,EZ)
      TC=B**2/EY
C *** NEAR FIELD APPROXIMATION ***
74    P1=(2.*ZMAS)/((4.*PI*T)**1.5*SQRT(EX*EY*EZ))
      P2=EXP(-(XK*T+(X-UP*T)**2/(4.*EX*T)))
      P3=EXP(-(Y-A)**2/(4.*EY*T))+EXP(-(Y-A-W)**2/(4.*EY*T))
     1+EXP(-(Y-W+A)**2/(4.*EY*T))
      P4=EXP(-(Z**2/(4.*EZ*T)))+EXP(-((Z-2.*D)**2/(4.*EZ*T)))
      C=P1*P2*P3*P4
      RETURN
C  ********     SPILL INTO TIDAL REGIONS OF A RIVER   *********
80    CALL DISP(W,D,IPLAG,T,UP,UT,XN,TP,E,EX ,EY,EZ)
      SIG=2.*PI/TP
C  ****    THE CROSS SECTIONAL MEAN CONCENTRATION IS CALCULATED ASSUMING
C          THE RIVER OSCILLATION VELOCITY TO BE SUNUSOIDAL.
      P1= ZMAS /(W*D*SQRT(4.*PI*E*T))
      P2=EXP(-XK*T)
      P3=EXP(-(X-UP*T+(UT/SIG)*(COS(SIG*(T-DEL))-COS(SIG*DEL)))**2/(4.*E
     1*T))
      C=P1*P2*P3
      RETURN
C
C *******    CONTINUOUS SPILLS  ****************
C **** IN THE FOLLOWING PROGRAM ON THE CONTINUOUS SPILLS WE ASSUME THAT
C  ****RATE OF SPILL "ZMDOT" IS A CONSTANT.
100   GO TO (110,120,130),IPLAG
C ***  CONTINUOUS SPILL IN A STILL WATER REGION   *****
110   EPS=0.1
      NDIM=25
      IF(T-TMT) 112,112,113
112   CALL DLIN(IPLAG,X,Y,Z,T,UP,UT,TP,DEL,W,D,XK,DIFCO,TMT,ZMDOT,0.0,
     1T,EPS,NDIM,CNSPL,C,IER,AUX)
      RETURN
113   CALL DLIN(IPLAG,X,Y,Z,T,UP,UT,TP,DEL,W,D,XK,DIFCO,TMT,ZMDOT,0.0,
     1TMT,EPS,NDIM,CNSPL,C,IER,AUX)
      RETURN
C ***  SPILL IN A NON TIDAL RIVER  ***,  WE ASSUME THAT THE LONGITUDINAL
C       SION IS SMALL. THE CONCENTRATION GIVEN IS THE CROSS SECTIONAL AVE
120   C=0.
      IF(X-UP*T) 121,121,126
121   CALL DISP(W,D,IPLAG,T,UP,UT,XN,TP,E,EX ,EY,EZ)
      TC=B**2/EY
      IF(T-0.3*TC) 122,122,123
C  ****  NEAR FIELD APPROXIMATION
122   P1=2MDOT/(2.*PI*X*SQRT(EY*EZ))
      P2=EXP(-  (UP/(4.*X))*(Y**2/EY+Z**2/EZ+4.*XK))
      C=P1*P2
```

FIGURE 3D-1, continued DILUN.

```
      RETURN
C ***  FAR FIELD APPROXIMATION    *********
123   OMG=SQRT(UF**2+2.*XK*E)
      F1=ZMDOT/(W*D*OMG*2.)
      G1=1.
      G2=1.
      IF(T-TMT)125,125,124
124   G1=ERF((X+OMG*(T-TMT))/SQRT(4.*E*(T-TMT)))
      G2=ERF((X-OMG*(T-TMT))/SQRT(4.*E*(T-TMT)))
125   F2=(ERF((X+OMG*T)/SQRT(4.*E*T))-G1)*EXP((X*0.5/E)*(UF+OMG))
      F3=(ERF((X-OMG*T)/SQRT(4.*E*T))-G2)*EXP((X*0.5/E)*(UF-OMG))
      C=F1*F2*F3
126   RETURN
C ****    CONTINUOUS INJECTION IN TIDAL RIVERS  ********
130   CALL DISP(W,D,IFLAG,T,UF,UT,XN,TP,E,EX ,EY,EZ)
131   EPS=0.01
      NDIM=25
      IF(T-TMT) 132,132,133
132   CALL DLIN(IFLAG,X,Y,Z,T,UF,UT,TP,DEL,W,D,XK,E     ,TMT,ZMDOT,0.0,
     1T,EPS,NDIM,CNSPL,C,IER,AUX)
      RETURN
133   CALL DLIN(IFLAG,X,Y,Z,T,UF,UT,TP,DEL,W,D,XK,E     ,TMT,ZMDOT,0.0,
     1TMT,EPS,NDIM,CNSPL,C,IER,AUX)
      RETURN
      END
```

FIGURE 3D-1, continued DILUN.

```
      SUBROUTINE DISP(W,D,IFLAG,T,UP,UT,XN,TP,E,EX,EY,EZ)
C ***********************************************************************
C ****  THIS SUBROUTINE IS CALLED BY THE DILUN SUBROUTINE . DISPERSION
C       AND TURBULENT DIFFUSION COEFFICIENTS ARE RETURNED BY THIS SUBROU
C
      PI=3.14159265
      B=W/2.
      RH=W*D/(2.*D+W)
      GO TO (60,70,80),IFLAG
60    E=0.
      RETURN
C *** SPILL INTO A NON TIDAL RIVER
70    USTAR=6.716*XN*UP/RH**(1./6.)
      EZ=0.067*USTAR*RH
      EX=0.1*EZ
      IF(W/D-100.) 72,71,71
71    EY=0.1*EZ
      E=77.*XN*UP*RH**(5./6.)
      GO TO 75
72    EY=0.23*USTAR*RH
      E=225.*USTAR*RH
75    RETURN
C ***  TIDAL RIVER   ******
80    USTAR=3.9*XN*(2.*UT/PI)/RH**(1./6.)
C  ***  USTAR IS BASED ON THE MEAN OSCILLATING FLOW VELOCITY.  ***
      EZ=0.067*USTAR*RH
      EX=0.1*EZ
      EY=0.1*EZ
      IF(W/D-100.) 81,82,82
81    EY=0.23*USTAR*RH
C  ** TRANSVERSE AND VERTICAL DISPERSION COEFFICIENTS
82    EV=6.*B*USTAR
      ET=0.011+0.025*(UT*T/B)**2
      TPV=T/(D**2/EZ)
      TPT=T/(B**2/EY)
      IF(TPV-1.) 83,83,84
83    GO TO 85
84    IF(ET/EV-1.) 85,85,86
85    E=EV
      GO TO 87
86    E=ET
87    RETURN
      END
```

FIGURE 3D-2 DISP.

```
      SUBROUTINE DLIN(IPLAG,XX,YY,ZZ,T,UF,UT,TP,DEL,W,D,XK,S,TMT,ZMDOT,
     1XL,XU,EPS,NDIM,FCT,Y,IER,AUX)
C
C ***************************************************************************
C *** THIS INTEGRATION SUBROUTINE RETURNS A VALUE ''Y'' WHLICH IS THE CO
C     OF THE POLLUTANT AT ANY INSTANT OF TIME  ''T'' AND POSITION XX,YY,
C     CONTINUOUS SPILL IN STILL OR OSCILLATING VELOCITY WATERS OF RIVERS
C ***************************************************************************
C
      DIMENSION AUX(1)
C     PREPARATIONS OF ROMBERG-LOOP
      AUX(1)=0.5*(FCT(IPLAG,XX,YY,ZZ,T,W,D,UF,UT,TP,DEL,XK,S,TMT,ZMDOT,
     1XL)+FCT(IPLAG,XX,YY,ZZ,T,W,D,UF,UT,TP,DEL,XK,S,TMT,ZMDOT,XU))
      H=XU-XL
      IF(NDIM-1)8,8,1
    1 IF(H)2,10,2
C     NDIM IS GREATER THAN 1 AND H IS NOT EQUAL TO 0.
    2 HH=H
      E=EPS/ABS(H)
      DELT2=0.
      P=1.
      JJ=1
      DO 7 I=2,NDIM
      Y=AUX(1)
      DELT1=DELT2
      HD=HH
      HH=.5*HH
      P=.5*P
      X=XL+HH
      SM=0.
      DO 3 J=1,JJ
      SM=SM+FCT(IPLAG,XX,YY,ZZ,T,W,D,UF,UT,TP,DEL,XK,S,TMT,ZMDOT,X)
    3 X=X+HD
      AUX(I)=.5*AUX(I-1)+P*SM
C     A NEW APPROXIMATION OF INTEGRAL VALUE IS COMPUTED BY MEANS OF
C     TRAPEZOIDAL RULE.
C     START OF ROMBERGS EXTRAPOLATION METHOD.
      Q=1.
      JI=I-1
      DO 4 J=1,JI
      II=I-J
      Q=Q+Q
      Q=Q+Q
    4 AUX(II)=AUX(II+1)+(AUX(II+1)-AUX(II))/(Q-1.)
C     END OF ROMBERG-STEP
      DELT2=ABS(Y-AUX(1))
      IF(I-5)7,5,5
    5 IF(DELT2-E)10,10,6
    6 IF(DELT2-DELT1)7,11,11
    7 JJ=JJ+JJ
    8 IER=2
    9 Y=H*AUX(1)
      RETURN
   10 IER=0
      GO TO 9
   11 IER=1
      Y=H*Y
      RETURN
      END
```

FIGURE 3D-3 DLIN.

```
      FUNCTION CNSPL(IFLAG,X,Y,Z,T,W,D,UP,UT,TP,DEL,XK,E,TMT,ZMDOT,TOW)
C ***  THIS FUNCTION IS CALLED BY THE DLIN INTEGRATION SUBROUTINE .
C      THIS FUNCTION RETURNS THE VALUES OF THE INTEGRAND IN THE INTEGRA
C      OBTAIN THE CONCENTRATION AT ANY POSITION AND TIME WHEN THE SPILL
C      CONTINUOUS.
      PI=3.14159265
      GO TO (10,20,30),IFLAG
C *** CONTINUOUS SPILL IN STILL WATER
10    IF(T-TOW) 11,11,12
11    CNSPL=0.
      RETURN
12    P1=(2.*ZMDOT)/(4.*PI*E)**1.5
      P2=EXP(-((X**2+Y**2+Z**2) /(4.*E*(T-TOW)))-XK*(T-TOW)) /(T-TOW)**
     1.5
      CNSPL=P1*P2
      RETURN
20    RETURN
C ***  TIDAL RIVER AND ESTURINE CONTINUOUS SPILL MODELS
30    IF(T-TOW) 31,31,32
31    CNSPL=0.
      RETURN
32    TT=T-TOW
      SIG=2.*PI/TP
      P1=ZMDOT/(W*D*SQRT(4.*PI*E))
      P2=(((X-UP*TT+(UT/SIG)*(COS(SIG*(TT-DEL))-COS(SIG*DEL)))/SQRT(4.*
     1*TT))**2+XK*TT)
      P3=EXP(-P2)/SQRT(TT)
      CNSPL=P1*P3
      RETURN
      END
```

FIGURE 3D-4 CNSPL.

```
      SUBROUTINE DILUN
      COMMON /MOP/ IFLAG,ICOND, ZMAS,ZMDOT, X,Y,Z,TIME, DIFCO,
     1 D,W,A, UF,UT,TP,DEL, XK,RF, C, T,TMT,TU, EX,EY,EZ,E, PI
      DATA PI /3.14159265/
C
C ***************************************************************************
C***   THIS SUBROUTINE GIVES THE CONENTRATION OF A WATER MISCIBLE LIQUID
C     AT A SPECIFIED POINT AND TIME. ALL THE LIQUID SPILLED IS ASSUMED
C     TO GO INTO SOLUTION IN WATER. THE SAME PROGRAM CAN ALSO BE USED
C     FOR DISPERSION OF SOLIDS WHICH ARE NEUTRALLY BUOYANT OR WHOSE
C     SETTLING TIMES ARE LARGE.
C
C     THIS SUBROUTINE CAN NOT BE USED WITH ACCURACY FOR THOSE FLUIDS
C     WHICH REACT WITH WATER OR WHOSE BOILING POINT IS LESS THAN THAT
C     OF THE AMBIENT WATER TEMPERATURE.
C
C ***************************************************************************
C
C **********  INPUT ARGUMENTS. **********
C ***  IFLAG = A FLAG WHICH INDICATES WHERE THE SPILL OCCURS. ( 1 FOR
C              SPILL IN STILL WATER, 2 FOR SPILL IN  NON-TIDAL RIVER,
C              3 FOR SPILL IN TIDAL RIVER)
C ***  ICOND = SPILL RATE FLAG. ( 0 FOR INSTANTANEOUS SPILL,
C              1 FOR CONTINUOUS SPILL )
C ***  ZMAS  = TOTAL MASS OF LIQUID SPILLED                    GMS
C ***  ZMDOT = RATE OF MASS SPILL ( NEEDED ONLY IF ICOND .NE. 1 )
C ***  X,Y,Z = COORDINATES OF POINT AT WHICH CONCENTRATION IS TO BE
C              CALCULATED. +X IS DOWNSTREAM, +Z IS DOWNWARDS.   CMS
C ***  TIME  = TIME ( T=0 AT TIME SPILL STARTS )               SEC
C ***  DIFCO = DIFFUSION COEFF. FOR THE LIQUID IN WATER        CM*CM/SEC
C ***  D     = MEAN RIVER DEPTH                                CM
C ***  W     = MEAN RIVER WIDTH                                CM
C ***  A     = Y-COORD. OF THE POINT OF SPILL ON WATER SURFACE   CM
C ***  UF    = STREAM VELOCITY ( TO BE GIVEN IF IFLAG = 2 OR 3 ) CM/SEC
C ***  UT    = TIDAL VELOCITY AMPLITUDE  ( FOR IFLAG = 3 )       CM/SEC
C ***  TP    = TIDAL PERIOD                                    SEC
C ***  DEL   = PHASE LAG-- ESSENTIALLY THE TIME TO THE NEXT HIGH
C              WATER SLACK FROM THE INSTANT OF SPILL.          SEC
C ***  XK    = DECAY COEFF. ( TO BE GIVEN ONLY IF THE POLLUTANT
C              OBEYS THE FIRST ORDER DECAY EQUATION ) .        1/SEC
C ***  RF    = MANNING ROUGHNESS FACTOR FOR RIVERS             NON-DIM
C
C **********  OUTPUT ARGUMENTS  **********
C ***  C     = CONCENTRATION OF THE POLLUTANT                  GMS/CM**3
C
C ***************************************************************************
C
C
      C = 0.0
      B = W * .5
      T = TIME
      IF ( ICOND .EQ. 0 ) GO TO 20
      TMT = ZMAS / ZMDOT
      IF ( T .GT. 5.*TMT ) ICOND = 0
      IF(IFLAG .EQ. 2 .AND. (X .LE.-1.E3 .OR. X .GE. UF*T+1.E5)) RETURN
```

FIGURE 3D-5 DILUN (modified for sensitivity analysis).

```
 20   IF ( IFLAG .GE. 2 ) CALL DISP(W,D,IFLAG, UF,UT,RF,TP,E,EX,EY,EZ)
      IF ( ICOND .EQ. 1 ) GO TO 100
C
C     INSTANTANEOUS SPILLS
      GO TO (60,70,80),IFLAG
C     SPILL IN STILL WATER
 60   F1 = 2.* ZMAS / (4.*PI *T *DIFCO )**1.5
      F2 = - ( X**2 + Y**2 + Z**2 ) / ( 4.* DIFCO * T) - XK * T
      PRINT 9060,T,DIFCO,F1,F2,ZMAS
 9060 FORMAT(*0DILUN 60 T DIFCO F1 F2 ZMAS *,5G12.4)
      IF ( F2 .LT. -46. ) RETURN
      C = F1 * EXP( F2 )
      RETURN
C
C     NON-TIDAL RIVER  INSTANTANEOUS SPILL
C     NEAR FIELD APPROXIMATION
 70   IF ( T .GT. 0.3*B*B/EY ) GO TO 75
      F1 = ( 2.*ZMAS) / ( (4.*PI*T)**1.5 * SQRT(EX*EY*EZ) )
      F2 = -XK*T - (X-UF*T)**2 / (4.*EX*T)
      DE = 4.*EY*T
      F3 = -(Y - A)**2 / DE
      F4 = -(Y + A + W)**2 / DE
      F5 = -(Y + A - W)**2 / DE
      DE = 4.*EZ*T
      F6 = -Z**2 / DE
      F7 = -( Z - 2.*D )**2 / DE
      DE = F2 + AMAX1(F3,F4,F5) + AMAX1(F6,F7)
      XD = X - UF*T
      SI = SQRT( 4.*EX*T )
      TC = 0.3 * B * B / EY
      PRINT 9070,F1,F2,F3,F4,F5,F6,F7,EX,EY,EZ,T,ZMAS,XD,SI,TC
 9070 FORMAT(*0DILUN 70 F VALUES EX EY EZ T ZMAS XD SI TC*,7G12.4,
     ) /,9G12.4)
      IF ( DE .LT. -46. ) RETURN
      C = F1 * EXP(F2) * ( EXP(F3) + EXP(F4) + EXP(F5) ) *
     1 ( EXP(F6) + EXP(F7) )
      RETURN
C     FAR FIELD APPROXIMATION
 75   F1 = ZMAS / A / SQRT( 4.*PI*E*T )
      F2 = - XK*T - ( X-UF*T )**2 / 4. / E / T
      XD = X - UF*T
      SI = SQRT( 4. * E * T )
      TC = 0.3 * B * B / EY
      PRINT 9075,E,F1,F2,XD,SI,TC
 9075 FORMAT(*0DILUN 75 E F1 F2 XD SI TC *,6G12.4)
      IF ( F2 .LT. -46.) RETURN
      C = F1 * EXP(F2)
      RETURN

C     TIDAL RIVER INSTANTANEOUS SPILL
C     SPILL INTO TIDAL REGIONS OF A RIVER
 80   SIG = 2. * PI / TP
C     THE CROSS SECTIONAL MEAN CONCENTRATION IS CALCULATED ASSUMING
C     THE RIVER OSCILLATION VELOCITY TO BE SINUSOIDAL.
      F1 = ZMAS / (W * D * SQRT( 4.*PI*E*T ) )
```

FIGURE 3D-5, continued DILUN (modified).

```
      F2 = UT/SIG * ( COS(SIG*(T-DEL) ) - COS(SIG*DEL) )
      F3 = -XK*T - (X - UF*T + F2)**2 / (4.*E*T)
      XD = X - UF*T + F2
      SI = SQRT( 4. * E * T )
      PRINT  9080,  E,F1,F2,F3, X,UF,T,UT,SIG, DEL,XD,SI
 9080 FORMAT (*0DILUN 80.   E F1 F2 F3 *, 4G12.4/* X UF T UT SIG DEL*,
     1 * XD SI *,8G12.4)
      IF ( F3 .LT. -46. ) RETURN
      C = F1 * EXP(F3)
      RETURN
C
C     CONTINUOUS SPILLS
  100 IF ( IFLAG .EQ. 2 ) GO TO 120
C     INTEGRATE FOR STILL WATER AND TIDAL RIVER
      TU = AMIN1(T , TMT)
      EPS = 0.10
      IF ( IFLAG .EQ. 3 ) EPS = 0.01
      CALL DLIN ( EPS )
      RETURN
C
C     NON-TIDAL RIVER   CONTINUOUS SPILL
  120 IF ( T .GT. 0.3 * B*B / EY ) GO TO 123
C     NEAR FIELD APPROXIMATION
      IF ( X .LT. 0. .OR. X .GT. UF*T ) RETURN
      IF ( T .GT. TMT .AND. X .LT. UF*(T-TMT) ) RETURN
      F1 = ZMDOT /2./PI/X / SQRT( EY*EZ )
      TU = X / UF
      F2 = -( Y**2 / EY + Z**2 / EZ ) / 4. / TU  - XK * TU
      PRINT  9120,   EY,EZ, T,TU,TMT, F1,F2
 9120 FORMAT (*0DILUN  120   EY EZ T TU TMT  F1 F2*, 7G12.4 )
      IF ( F2 .LT. -46. ) RETURN
      C = F1 * EXP ( F2 )
      RETURN
C     FAR FIELD APPROXIMATION
  123  OMG = SQRT( UF**2 + 4.*XK*E )
      F1 = ZMDOT / (W*D*OMG*2. )
      G1 = 1.
      G2 = 1.
      IF ( T .LE. TMT ) GO TO 125
  124  G1 = ERF( ( X + OMG * (T-TMT) ) / SQRT( 4. * E * (T-TMT) ) )
      G2 = ERF( ( X - OMG * (T-TMT) ) / SQRT( 4. * E * (T-TMT) ) )
  125 F2 = (ERF((X + OMG*T)/SQRT(4.*E*T)) - G1) * EXP((X*.5/E)*(UF+OMG))
      F3 = (ERF((X - OMG*T)/SQRT(4.*E*T)) - G1) * EXP((X*.5/E)*(UF-OMG))
      C = F1 * (F2 + F3)
      PRINT  9125,   UF,E,OMG, T,TMT, G1,G2, F1,F2,F3, C                    912
 9125 FORMAT (*0DILUN  125   UF E OMG T TMT*, 5G12.4 /                       912
     1     * G1 G2 F1 F2 F3 C*, 6G12.4 )                                    912
  126 RETURN
      END
```

FIGURE 3D-5, continued DILUN (modified).

```
      SUBROUTINE DISP(W,D,IFLAG,UF,UT,RF,TP,E,EX,EY,EZ)
C  ***************************************************************
C     CALLED BY DILUN AND EVAMX. DISPERSION AND TURBULENT DIFFUSION
C     COEFFICIENTS ARE RETURNED.
      DATA PI/3.14159265/
      B=W/2.
      RH = W*D / (2.*D + W)
      GO TO (60,70,80),IFLAG
 60   E = 0.
      RETURN

C     SPILL INTO A NON-TIDAL RIVER
 70   USTAR = 6.716 * RF * UF / RH**(1./6.)
      EZ = 0.067 * USTAR * RH
      EX = 0.1 * EZ
      IF ( W/D - 100.) 72,71,71
C     WIDE RIVER
 71   EY = 0.1 * EZ
      E = 77. * RF * UF * RH **(5./6.)
      GO TO 75
C     NARROW RIVER
 72   EY = 0.23 * USTAR * RH
      E = 225. * USTAR * RH
C75   RETURN
   75 PRINT  9075,  RH,USTAR, EX,EY,EZ,E                          907
 9075 FORMAT (*0DISP  NON-TIDAL   RH USTAR EX EY EZ E*, 6G12.4 )  907
      RETURN

C     TIDAL RIVER
 80   USTAR = 3.9 * RF * (2.*UT / PI) / RH**(1./6.)
C     USTAR IS BASED ON THE MEAN OSCILLATING FLOW VELOCITY.
      EZ = 0.067 * USTAR * RH
      EX = 0.1 * EZ
      EY = 0.1 * EZ
      IF ( W/D - 100.) 81,82,82
 81   EY = 0.23 * USTAR * RH
C     TRANSVERSE AND VERTICAL DISPERSION COEFFICIENTS
 82   EV = 6. * D * USTAR
C     NOTE  TP IS TIDAL PERIOD
C     .000275 = .011 * .025
      F = .000275 * ( UT * TP / B )**2
      TPV = TP/ (D**2 / EZ)
      IF ( TPV .LE. 1.) GO TO 85
      IF ( F .LE. 1. ) GO TO 85
      E = F * EV
      IF ( F .GT. 11.) E = 11.*EV
      GO TO 89
 85   E = EV
   89 PRINT  9089,  RH,USTAR, EX,EY,EZ,EV, F, TPV                 908
 9089 FORMAT (*0DISP  TIDAL   RH USTAR EX EY EZ EV F TPV*, 8G12.4 )  908
      RETURN
      END
```

FIGURE 3D-6 DISP (modified for sensitivity analysis).

```
      SUBROUTINE DLIN(EPS)
      COMMON /MOP/ IFLAG,ICOND, ZMAS,ZMDOT, X,Y,Z,TIME, DIFCO,
     1 D,W,A, UF,UT,TP,DEL, XK,RF, C, T,TMT,TU, EX,EY,EZ,E, PI
      REAL AUX(25)
      DATA NDIM/25/
C
      AUX(1) = 0.5 * ( CNSPL(0.0) + CNSPL(TU) )
      EP = EPS / TU
      DELT2 = 0.
      HH = TU
      P = 1.
      JJ = 1
      DO 7 I=2,NDIM
      C = AUX(1)
      DELT1 = DELT2
      HD = HH
      HH = .5 * HH
      P = .5 * P
      TX = HH
      SM = 0.
      DO 3 J=1,JJ
      SM = SM + CNSPL( TX )
.3    TX = TX + HD
      AUX(I) = .5 * AUX(I-1) + P * SM
C     A NEW APPROXIMATION OF INTEGRAL VALUE IS COMPUTED BY MEANS OF
C     TRAPEZOIDAL RULE.
C     START OF ROMBERGS EXTRAPOLATION METHOD.
      Q = 1.
      JI = I-1
      DO 4 J=1,JI
      II = I-J
      Q = 4. * Q
 4    AUX(II) = AUX(II+1) + (AUX(II+1) - AUX(II)) / (Q-1.)
C     END OF ROMBERG STEP
      PRINT 9004,I,AUX(1)
 9004 FORMAT(* DLIN 4 I AUX(1) *,I4,G12.4/)
      DELT2 = ABS(C - AUX(1))
      IF ( I .LT. 5 ) GO TO 7
      IF ( DELT2 .LE. EP ) GO TO 9
      IF ( DELT2 .GE. DELT1 ) GO TO 11
 7    JJ = JJ + JJ
 9    C = TU * AUX(1)
      RETURN
 11   C = TU * C
      RETURN
      END
```

FIGURE 3D-7 DLIN (modified for sensitivity analysis).

```
      FUNCTION CNSPL (TOW)
      COMMON /HOP/ IFLAG,ICOND, ZMAS,ZMDOT, X,Y,Z,TIME, DIFCO,
     1 D,W,A, UF,UT,TP,DEL, XK,RF, C, T,TMT,TU, EX,EY,EZ,E, PI
      CNSPL = 0.0
      TT = T - TOW
      IF ( IFLAG .EQ. 2 .OR. TT .LE. 0.0 ) RETURN
      IF ( IFLAG .EQ. 3 ) GO TO 32
C  STILL WATER
 12   F1 = 2.* ZMDOT / (4.*PI*DIFCO*TT)**1.5
      F2 = -( X**2 + Y**2 + Z**2 ) / (4.*DIFCO*TT) - XK*TT
      PRINT 9012,ZMDOT,DIFCO,T,TOW,TT,F1,F2
 9012 FORMAT(* CNSPL 12 ZMDOT DIFCO T TOW TT F1 F2 *,7G12.4)
      IF ( F2 .LT. -46. ) GO TO 41
      CNSPL =  1 * EXP(F2)
      GO TO 4
C  TIDAL RIVER
 32   SIG = 2. * PI / TP
      F1 = ZMDOT /W/D / SQRT( 4.*PI*E*TT )
      F3 = X - UF*TT + UT/SIG *( COS(SIG*(T-DEL)) - COS(SIG*(TOW-DEL)))
      F2 = XK*TT + F3**2 / 4. / E / TT
      S1 = 2 * SQRT( E * TT )
      PRINT 9032,SIG,TOW,TT,E,F1,F2,F3,SI
 9032 FORMAT(* CNSPL TIDAL    SIG TOW TT E F1 F2 F3 SI *,8G11.3)
      IF ( F2 .GT. 46. ) GO TO 41
      CNSPL = F1 * EXP(-F2)
 41   RETURN
      END
```

FIGURE 3D-8 CNSPL (modified for sensitivity analysis).

APPENDIX 3E

SENSITIVITY COEFFICIENTS

PRECEDING PAGE BLANK-NOT FILMED

XN = 120000. X = 117500.RIVER WIDTH = 4000.

OUTPUT IS POINT CONCENTRATION NORMAL VALUE IS .260E-03

INDEX	VARIABLE	SENS COEFF	V NORMAL	REFERENCE	V CHANGED	OUTPUT	FRACTION
1	SPILL MASS	1.000	.150E+09	.150E+09	.157E+09	.273E-03	1.050
2	SPILL RATE	0.000	.500E+06	.500E+06	.525E+06	0.	0.000
3	RIV DEPTH	-1.214	660.	600.	840.	.244E-03	.939
4	RIV WIDTH	-1.156	.400E+04	.400E+04	.420E+04	.246E-03	.947
5	SPILL Y	0.000	.250E+04	.250E+04	.263E+04	.260E-03	1.000
6	DELTA X	-.026	.100E+05	.100E+05	.105E+05	.26[illegible]E-03	.999
7	POINT Y	0.000	0.	[illegible]0E+04	100.	.260E-03	1.000
8	POINT Z	0.000	10.0	10.0	10.5	.260E-03	1.000
9	POINT TIME	-1.027	600.	600.	630.	.247E-03	.949
10	DECAY COEF	-.166	.270E-03	.270E-03	.292E-03	.258E-03	.992
11	RIVER FLOW	-.500	200.	200.	210.	.249E-03	.957
12	TIDAL FLOW	0.000	300.	300.	315.	0.	0.000
13	TIDAL PER	0.000	.432E+05	.432E+05	.454E+05	0.	0.000
14	TIDAL LAG	0.000	.130E+05	.432E+05	.151E+05	0.	0.000
15	ROUGHNESS	0.000	.500E-01	.500E-01	.525E-01	0.	0.000
16	WATER TEMP	0.000	10.0	283.	24.[illegible]	0.	0.000

FIGURE 3E-1 Results for NH_3, non-tidal river, instantaneous spill, river width = 4000.

X1 = 1200.0 X = 117500.RIVER WIDTH = 4000.

OUTPUT IS POINT CONCENTRATION NORMAL VALUE IS .407E-03

INDEX	VARIABLE	SENS COEFF	V NORMAL	REFERENCE	V CHANGED	OUTPUT	FRACTION
1	SPILL MASS	.898	.150E+09	.150E+09	.157E+09	.425E-03	1.045
2	SPILL RATE	.050	.500E+06	.500E+06	.525E+06	.408E-03	1.002
3	RIV DEPTH	-1.150	800.	800.	840.	.384E-03	.943
4	RIV WIDTH	-1.031	.400E+04	.400E+04	.420E+04	.386E-03	.948
5	SPILL Y	0.000	.250E+04	.250E+04	.263E+04	.407E-03	1.000
6	DELTA X	.036	.100E+05	.100E+05	.105E+05	.407E-03	1.001
7	POINT Y	0.000	0.	.200E+04	100.	.407E-03	1.000
8	POINT Z	0.000	10.0	10.0	10.5	.407E-03	1.000
9	POINT TIME	-.383	590.	600.	630.	.399E-03	.981
10	DECAY COEF	.149	.278E-03	.278E-03	.292E-03	.410E-03	1.007
11	RIVER FLOW	-.504	200.	200.	210.	.397E-03	.975
12	TIDAL FLOW	0.000	300.	300.	315.	0.	0.000
13	TIDAL PER	0.000	.432E+05	.432E+05	.454E+05	0.	0.000
14	TIDAL LAG	0.000	.130E+05	.432E+05	.151E+05	0.	0.000
15	ROUGHNESS	0.000	.500E-01	.500E-01	.525E-01	0.	0.000
16	WATER TEMP	0.000	10.0	283.	24.2	0.	0.000

END OF LOOP FOR NH3

FIGURE 3E-2 Results for NH_3, non-tidal river, continuous spill, river width = 4000.

XN = 120000. X = 117500.RIVER WIDTH = 50000.

OUTPUT IS POINT CONCENTRATION NORMAL VALUE IS .142E-03

INDEX	VARIABLE	SENS COEFF	V NORMAL	REFERENCE	V CHANGED	OUTPUT	FRACTION
1	SPILL MASS	0.000	.150E+09	.150E+09	.157E+09	.142E-03	1.000
2	SPILL RATE	1.000	.500E+06	.500E+06	.525E+06	.149E-03	1.050
3	RIV DEPTH	-.231	800.	800.	840.	.140E-03	.986
4	RIV WIDTH	-.007	.500E+05	.500E+05	.525E+05	.142E-03	1.000
5	SPILL Y	-1.421	.250E+04	.250E+04	.263E+04	.132E-03	.929
6	DELTA X	.039	.100E+05	.100E+05	.105E+05	.142E-03	1.002
7	POINT Y	14.286	0.	.250E+05	.125E+04	.243E-03	1.715
8	POINT Z	-.000	10.0	10.0	10.5	.142E-03	1.000
9	POINT TIME	0.000	600.	600.	630.	.142E-03	1.000
10	DECAY COEF	-.152	.278E-03	.278E-03	.292E-03	.141E-03	.992
11	RIVER FLOW	-.813	200.	200.	210.	.136E-03	.959
12	TIDAL FLOW	0.000	300.	300.	315.	0.	0.000
13	TIDAL PER	0.000	.432E+05	.432E+05	.454E+05	0.	0.000
14	TIDAL LAG	0.000	.130E+05	.432E+05	.151E+05	0.	0.000
15	ROUGHNESS	0.000	.500E-01	.500E-01	.525E-01	0.	0.000
16	WATER TEMP	0.000	10.0	283.	24.2	0.	0.000

FIGURE 3E-3 Results for NH_3, non-tidal river, continuous spill, river width = 50000.

XN = -53399. X = -55899.RIVER WIDTH = 50000.

OUTPUT IS POINT CONCENTRATION NORMAL VALUE IS .425E-04

INDEX	VARIABLE	SENS COEFF	V NORMAL	REFERENCE	V CHANGED	OUTPUT	FRACTION
1	SPILL MASS	1.000	.150E+09	.150E+09	.157E+09	.447E-04	1.050
2	SPILL RATE	0.000	.500E+06	.500E+06	.525E+06	0.	0.000
3	RIV DEPTH	-1.290	800.	800.	840.	.398E-04	.936
4	RIV WIDTH	-.950	.500E+05	.500E+05	.525E+05	.405E-04	.952
5	SPILL Y	0.000	.250E+04	.250E+04	.263E+04	.425E-04	1.000
6	DELTA X	-.131	.100E+05	.100E+05	.105E+05	.423E-04	.993
7	POINT Y	0.000	0.	.250E+05	.125E+04	.425E-04	1.000
8	POINT Z	0.000	10.0	10.0	10.5	.425E-04	1.000
9	POINT TIME	-.009	600.	600.	630.	.425E-04	1.000
10	DECAY COEF	-.166	.278E-03	.278E-03	.292E-03	.422E-04	.992
11	RIVER FLOW	-1.907	200.	200.	210.	.385E-04	.905
12	TIDAL FLOW	.790	300.	300.	315.	.442E-04	1.040
13	TIDAL PER	.764	.432E+05	.432E+05	.454E+05	.442E-04	1.036
14	TIDAL LAG	-9.558	.130E+05	.432E+05	.151E+05	.222E-04	.522
15	ROUGHNESS	-.422	.500E-01	.500E-01	.525E-01	.416E-04	.979
16	WATER TEMP	0.000	10.0	283.	24.2	0.	0.000

FIGURE 3E-4 Results for NH_3, tidal river, instantaneous spill, river width = 50000.

XN = -53399. X = -55849.RIVER WIDTH = 50000.

OUTPUT IS POINT CONCENTRATION NORMAL VALUE IS .323E-04

INDEX	VARIABLE	SENS COEFF	V NORMAL	REFERENCE	V CHANGED	OUTPUT	FRACTION
1	SPILL MASS	.367	.150E+09	.150E+09	.157E+09	.329E-04	1.018
2	SPILL RATE	.563	.500E+06	.500E+06	.525E+06	.332E-04	1.028
3	RIV DEPTH	-.990	800.	800.	840.	.307E-04	.951
4	RIV WIDTH	-.952	.500E+05	.500E+05	.525E+05	.307E-04	.952
5	SPILL Y	0.000	.250E+04	.250E+04	.263E+04	.323E-04	1.000
6	DELTA X	-.373	.100E+05	.100E+05	.105E+05	.317E-04	.981
7	POINT Y	0.000	0.	.250E+05	.125E+04	.323E-04	1.000
8	POINT Z	0.000	10.0	10.0	10.5	.323E-04	1.000
9	POINT TIME	1.789	600.	600.	630.	.351E-04	1.089
10	DECAY COEF	-.131	.276E-03	.276E-03	.292E-03	.321E-04	.993
11	RIVER FLOW	-3.265	200.	200.	210.	.270E-04	.837
12	TIDAL FLOW	4.150	300.	300.	315.	.390E-04	1.207
13	TIDAL PER	1.771	.432E+05	.432E+05	.454E+05	.351E-04	1.089
14	TIDAL LAG	-11.607	.130E+05	.432E+05	.151E+05	.135E-04	.420
15	ROUGHNESS	-.046	.500E-01	.500E-01	.525E-01	.322E-04	.998
16	WATER TEMP	0.000	10.0	283.	24.2	0.	0.000

END OF LOOP FOR NH3

FIGURE 3E-5 Results for NH_3, tidal river, continuous spill, river width = 50000.

XN = 120000. X = 117500.RIVER WIDTH = 4000.

OUTPUT IS POINT CONCENTRATION NORMAL VALUE IS .133E-03

INDEX	VARIABLE	SENS COEFF	V NORMAL	REFERENCE	V CHANGED	OUTPUT	FRACTION
1	SPILL MASS	1.000	.768E+08	.768E+08	.807E+08	.140E-03	1.053
2	SPILL RATE	0.000	.256E+06	.256E+06	.269E+06	0.	0.000
3	RIV DEPTH	-1.218	800.	800.	840.	.125E-03	.939
4	RIV WIDTH	-1.058	.400E+04	.400E+04	.420E+04	.126E-03	.947
5	SPILL Y	0.000	.250E+04	.250E+04	.263E+04	.133E-03	1.000
6	DELTA X	-.028	.100E+05	.100E+05	.105E+05	.133E-03	.999
7	POINT Y	0.000	0.	.200E+04	100.	.133E-03	1.000
8	POINT Z	0.000	10.0	10.0	10.5	.133E-03	1.000
9	POINT TIME	-1.027	600.	600.	630.	.127E-03	.949
10	DECAY COEF	-.169	.273E-03	.273E-03	.292E-03	.132E-03	.992
11	RIVER FLOW	-.868	200.	200.	210.	.128E-03	.957
12	TIDAL FLOW	0.000	300.	300.	315.	0.	0.000
13	TIDAL PER	0.000	.432E+05	.432E+05	.454E+05	0.	0.000
14	TIDAL LAG	0.000	.130E+05	.432E+05	.151E+05	0.	0.000
15	ROUGHNESS	0.000	.500E-01	.500E-01	.525E-01	0.	0.000
16	WATER TEMP	0.000	10.0	283.	24.2	0.	0.000

FIGURE 3E-6 Results for MAL, non-tidal river, instantaneous spill, river width = 4000.

XN = 120000. X = 117500.RIVER WIDTH = 4000.

OUTPUT IS POINT CONCENTRATION NORMAL VALUE IS .209E-03

INDEX	VARIABLE	SENS COEFF	V NORMAL	REFERENCE	V CHANGED	OUTPUT	FRACTION
1	SPILL MASS	.898	.768E+08	.768E+08	.807E+08	.214E-03	1.043
2	SPILL RATE	.050	.256E+06	.256E+06	.269E+06	.209E-03	1.002
3	RIV DEPTH	-1.150	800.	800.	840.	.197E-03	.943
4	RIV WIDTH	-1.031	.400E+04	.400E+04	.420E+04	.198E-03	.948
5	SPILL Y	0.000	.250E+04	.250E+04	.263E+04	.209E-03	1.000
6	DELTA X	.016	.100E+05	.100E+05	.105E+05	.209E-03	1.001
7	POINT Y	0.000	0.	.200E+04	100.	.209E-03	1.000
8	POINT Z	0.000	10.0	10.0	10.5	.209E-03	1.000
9	POINT TIME	-.383	600.	600.	630.	.205E-03	.981
10	DECAY COEF	.149	.278E-03	.278E-03	.292E-03	.210E-03	1.007
11	RIVER FLOW	-.504	200.	200.	210.	.203E-03	.975
12	TIDAL FLOW	0.000	300.	300.	315.	0.	0.000
13	TIDAL PER	0.000	.432E+05	.432E+05	.454E+05	0.	0.000
14	TIDAL LAG	0.000	.130E+05	.432E+05	.151E+05	0.	0.000
15	ROUGHNESS	0.000	.500E-01	.500E-01	.525E-01	0.	0.000
16	WATER TEMP	0.000	10.0	283.	24.2	0.	0.000

END OF LOOP FOR MAL

FIGURE 3E-7 Results for MAL, non-tidal river, continuous spill, river width = 4000.

XN = 120000. X = 117500.RIVER WIDTH = 50000.

OUTPUT IS POINT CONCENTRATION NORMAL VALUE 15 .727E-04

INDEX	VARIABLE	SENS COEFF	V NORMAL	REFERENCE	V CHANGED	OUTPUT	FRACTION
1	SPILL MASS	0.000	.768E+04	.768E+04	.807E+04	.727E-04	1.000
2	SPILL RATE	1.000	.256E+06	.256E+06	.269E+06	.763E-04	1.050
3	RIV DEPTH	-.231	800.	800.	840.	.716E-04	.985
4	RIV WIDTH	-.067	.500E+05	.500E+05	.525E+05	.727E-04	1.000
5	SPILL Y	-1.421	.250E+04	.253E+04	.263E+04	.675E-04	.929
6	DELTA X	.039	.100E+05	.100E+05	.105E+05	.728E-04	1.002
7	POINT Y	14.296	0.	.250E+05	.125E+04	.125E-03	1.715
8	POINT Z	-.000	10.0	10.0	10.5	.727E-04	1.000
9	POINT TIME	0.000	600.	600.	630.	.727E-04	1.000
10	DECAY COEF	-.152	.276E-03	.276E-03	.292E-03	.721E-04	.992
11	RIVER FLOW	-.213	200.	200.	210.	.697E-04	.959
12	TIDAL FLOW	0.000	300.	300.	315.	0.	0.000
13	TIDAL PER	0.000	.432E+05	.432E+05	.454E+05	0.	0.000
14	TIDAL LAG	0.000	.130E+05	.432E+05	.151E+05	0.	0.000
15	ROUGHNESS	0.000	.500E-01	.500E-01	.525E-01	0.	0.000
16	WATER TEMP	0.000	10.0	283.	24.2	0.	0.000

FIGURE 3E-8 Results for MAL, non-tidal river, continuous spill, river width = 50000.

XN = -53399. X = -55499.RIVER WIDTH = 50000.

OUTPUT IS POINT CONCENTRATION NORMAL VALUE IS .218E-04

INDEX	VARIABLE	SENS COEFF	V NORMAL	REFERENCE	V CHANGED	OUTPUT	FRACTION
1	SPILL MASS	1.000	.768E+08	.768E+08	.807E+08	.224E-04	1.030
2	SPILL RATE	0.000	.256E+06	.256E+06	.269E+06	0.	0.000
3	RIV DEPTH	-1.296	800.	800.	840.	.204E-04	.936
4	RIV WIDTH	-.959	.500E+05	.500E+05	.525E+05	.208E-04	.952
5	SPILL Y	0.000	.250E+04	.250E+04	.263E+04	.218E-04	1.000
6	DELTA X	-.131	.100E+05	.100E+05	.105E+05	.217E-04	.993
7	POINT Y	0.000	0.	.250E+05	.125E+04	.218E-04	1.000
8	POINT Z	0.000	10.0	10.0	10.5	.218E-04	1.000
9	POINT TIME	-.009	600.	600.	630.	.218E-04	1.000
10	DECAY COEF	-.166	.278E-03	.278E-03	.292E-03	.218E-04	.992
11	RIVER FLOW	-1.907	200.	200.	210.	.197E-04	.905
12	TIDAL FLOW	.790	300.	300.	315.	.227E-04	1.040
13	TIDAL PER	.764	.432E+05	.432E+05	.454E+05	.228E-04	1.037
14	TIDAL LAG	-9.556	.130E+05	.432E+05	.151E+05	.114E-04	.522
15	ROUGHNESS	-.422	.500E-01	.500E-01	.525E-01	.213E-04	.979
16	WATER TEMP	0.000	10.0	283.	24.2	0.	0.000

FIGURE 3E-9 Results for MAL, tidal river, instantaneous spill, river width = 50000.

XN = -53399. X = -55499.RIVER WIDTH = 50000.

OUTPUT IS POINT CONCENTRATION NORMAL VALUE IS .165E-04

INDEX	VARIABLE	SENS COEFF	V NORMAL	REFERENCE	V CHANGED	OUTPUT	FRACTION
1	SPILL MASS	.367	.768E+06	.768E+06	.807E+06	.168E-04	1.018
2	SPILL RATE	.563	.256E+06	.256E+06	.269E+06	.170E-04	1.028
3	RIV DEPTH	-.990	800.	800.	840.	.157E-04	.951
4	RIV WIDTH	-.952	.500E+05	.500E+05	.525E+05	.156E-04	.945
5	SPILL Y	0.000	.250E+04	.250E+04	.263E+04	.165E-04	1.000
6	DELTA X	-.573	.100E+05	.100E+05	.105E+05	.162E-04	.981
7	POINT Y	0.000	0.	.250E+05	.125E+04	.165E-04	1.000
8	POINT Z	0.000	10.0	10.0	10.5	.165E-04	1.000
9	POINT TIME	1.789	600.	600.	630.	.180E-04	1.089
10	DECAY COEF	-.131	.278E-03	.278E-03	.292E-03	.164E-04	.993
11	RIVER FLOW	-3.265	200.	200.	210.	.136E-04	.827
12	TIDAL FLOW	4.150	300.	300.	315.	.200E-04	1.207
13	TIDAL PER	1.771	.432E+05	.432E+05	.454E+05	.180E-04	1.089
14	TIDAL LAG	-11.607	.130E+05	.432E+05	.151E+05	.694E-05	.420
15	ROUGHNESS	-.048	.500E-01	.500E-01	.525E-01	.165E-04	.998
16	WATER TEMP	0.000	10.0	283.	24.2	0.	0.000

END OF LOOP FOR MAL

FIGURE 3E-10 Results for MAL, tidal river, continuous spill, river width = 50000.

CHAPTER 3 - LIST OF SYMBOLS

A = cross-sectional area (cm^2)

b = half-width of the river (cm)

c = local concentration of a pollutant (g/cm^3)

C = cross-sectional area averaged concentration (g/cm^3)

d = depth of flow (cm)

e_y, e_z = turbulent diffusion coefficients in y and z directions (cm^2/s)

$E(x,t)$ = dispersion coefficient (local value) (cm^2/s)

E_L = longitudinal dispersion coefficient (cm^2/s)

E_T = dispersion coefficient for the fresh water or well-mixed region of the estuary (cm^2/s)

g = acceleration due to gravity (cm/s^2)

h = depth of flow (or average depth) (cm)

k = decay rate coefficient (1/s)

M = mass of pollutant released (g)

$\dot{M}$ = rate of mass release of the pollutant (g/s)

n = Manning roughness factor $0.01 < n < .04$

R_h = hydraulic radius = cross-sectional flow area/wetted perimeter (cm)

S_i = i^{th} sensitivity coefficient for the i^{th} normal input variable

t = time (s)

t_{MT} = time at which tank is empty and venting stops (s)

T = tidal period (s)

T_c = horizontal dispersion time (s)

T_{cz} = vertical dispersion time (s)

T_v' = characteristic vertical mixing time ratio (s)

T_t' = characteristic transverse mixing time ratio (s)

PRECEDING PAGE BLANK-NOT FILMED

u = instantaneous velocity (cm/s)

u^* = shear velocity = $\sqrt{\tau_0/\rho}$ = 3.115 n $U/R_h^{1/6}$ (cm/s)

U = average velocity of cross section (cm/s)

U_T = peak oscillating velocity (amplitude) (cm/s)

W = width of river (cm)

x = longitudinal coordinate (cm)

X_{ci} = i^{th} changed input variable

X_{ni} = i^{th} normal input variable

X_{ri} = i^{th} reference variable

y = lateral coordinate (cm)

Y_n = normal output

Y_{ci} = i^{th} changed output

z = depth-wise coordinate (cm)

Greek symbols:

δ = phase lag (to the next high-water slack) (s)

ρ = density of fluid (g/cm^3)

ρ_w = density of water (g/cm^3)

Subscripts:

c = changed value of i^{th} variable

i = i^{th} variable; i = 1 to m

m = number of variables (m = 16 for Mixing and Dilution Model)

n = normal value of i^{th} variable; normal value of output

r = reference value of i^{th} variable

CHAPTER 3 - REFERENCES

[1] Department of Transportation, U.S. Coast Guard, Assessment Models in Support of the Hazard Assessment Handbook (CG-446-3), CG-D-65-74, January 1974.

[2] Arthur D. Little, Inc., Hazard Assessment Computer System, User Manual (HACS), Cambridge, Mass., December 1974.

[3] Holley, E. R., D. R. F. Harleman, and H. B. Fischer, "Dispersion in homogeneous estuary flow," Am. Soc. Civil Eng., J. Hydraulics Div. 96:1691-1709, 1970.

[4] Eisenberg, N. A., C. J. Lynch, and R. J. Breeding, Vulnerability Model: A Simulation System for Assessing Damage Resulting from Marine Spills, CG-D-136-75, NTIS AD-A015245, June 1975.

[5] Csanady, G. T., Water Res. 4:79, 1970.

[6] Stakgold, I., Boundary Value Problems of Mathematical Physics, vol. 1, MacMillan, New York, 1967.

[7] Hodgman, C. D. (ed.), C.R.C. Standard Mathematical Tables, 11th ed., Chemical Rubber Co., Cleveland, Ohio, 1957.

[8] Abramowitz, M., and I. Stegun (eds.), Handbook of Mathematical Functions, National Bureau of Standards, Applied Mathematics Series Number 55, U. S. Government Printing Office, 1964.

CHAPTER 4

THE FLAME GEOMETRY MODEL

INTRODUCTION

The models comprising the Flame Geometry Model are documented in Chapter 6 of AMSHAH [1] as well as in the HACS [2] subroutines MODB1, MODE1, MODE2, FLJET, FLMHT, and FLMAN. The purpose of these models is to predict the size and orientation of a flame, so that subsequent models may predict the thermal radiation hazard presented to a nearby receptor. Two types of flames are treated: (1) a flame originating from a burning pool of flammable cargo in the liquid state on the water surface, and (2) a flame originating from a cargo tank from which a jet of flammable cargo is issuing as a gas. For the pool burning flame, the geometric parameters determined by the model are the flame height and flame tilt angle from the vertical. For the jet burning flame, the model determines the length and diameter of a cylinder equivalent to the conical flame.

For these models there is virtually complete agreement between the documentation in AMSHAH and the computerized subroutines in HACS. The models rely primarily on empirically derived formulas, so there are no consequential assumptions or derivations subject to question. For empirically based models what can be questioned is whether the results of laboratory or controlled experiments can be extrapolated to predict actual field occurrences. For this particular set of models such extrapolation seems reasonable. The symbols and references are listed at the end of this chapter.

ASSUMPTIONS AND APPROXIMATIONS

There are actually three distinct models under consideration:

1. Shape and size of a flame from a burning gas jet
2. Height of a flame from a burning liquid pool
3. Angle of pool burning flame in a wind.

The assumptions and approximations inherent in each of these models will be considered separately.

---

[1] Department of Transportation, U.S. Coast Guard, Assessment Models in Support of the Hazard Assessment Handbook (CG-446-3), CG-D-65-74, January 1974.

[2] Arthur D. Little, Inc., Hazard Assessment Computer System, User Manual (HACS), Cambridge, Mass., December 1974.

Gas Jet

The following assumptions are stated explicitly in AMSHAH for the model describing the size and shape of a flame from a burning jet of gas:

1. The flame is turbulent.

2. The flame is shaped like a cone with a constant angle.

3. Buoyancy does not affect the flame in any way.

4. Wind has little effect on bending the flame.

Some implicit assumptions include:

5. The venting hole is circular or approximately so.

6. An equivalent cylindrical flame for heat transfer calculations can be obtained by equating the area of the cone to that of a cylinder of identical height.

7. Data obtained from laboratory scale experiments may be extrapolated to predict larger scale occurrences in the field.

A[illegible]ns stated explicitly in the computer program are:

8. The semiangle of the conical jet is 5.4 degrees.

9. The ambient temperature is 300°K.

The equation describing flame length is taken from a paper of Hawthorne, Weddell, and Hottel [3] who obtained the equation by comparing theoretical considerations with experimental data obtained for nozzle diameters between 3.05 cm and 7.60 cm and for a variety of fuels. It should be noted that the flame length given by equation (6.1) in AMSHAH is independent of the flow rate; flame length independence of flow rate does not hold if the flow in the jet is laminar. The most hazardous spill situations will be those in which the venting rate is large; in such cases the flow will be turbulent and the analysis will apply.

---

[3] Hawthorne, W. R., D. S. Weddell, and H. C. Hottel, "Mixing and combustion in turbulent gas jets," pp. 266-280, in Third Symposium on Combustion, Flame and Explosion Phenomena, William and Wilkins, Baltimore, 1949.

Simarily, if the flow is turbulent, then the second assumption will also generally be valid.

The third assumption involves the effects of buoyancy upon the venting jet of cargo vapor. For homogeneous flow problems where the jet has the same density as the fluid into which it is flowing, the importance of gravitational effects is indicated by the Froude number: $F = v^2/gD$. This number may be interpreted physically as the ratio of the inertial forces to gravitational forces acting on the jet. If the Froude number is large, gravitational effects may be ignored. When the jet consists of a fluid with a different density from the fluid into which the jet is flowing, the gravitational effects will depend on the density difference as well. In general, however, if the flow is large enough so that the flow is choked and the jet is fully turbulent, then the gravitational effects will be small. Similarly the effect of side winds on a high flow turbulent jet will be negligible; thus the fourth assumption is valid for the expected spill scenario.

The experiments and analyses upon which the formula for flame length is based are for jets issuing from circular orifices. Substantial departures from this shape of venting hole will produce flames whose lengths are not accurately predicted by the formula. Furthermore, if the hole shape is greatly different from circular, the issuing jet will not be conically shaped nor will its radiation characteristics be accurately represented by an equivalent cylinder. An extreme example of a departure from a circular vent hole is a long, narrow slit. Since it would appear more likely that "punctures" rather than "cuts" would produce tank venting, the fifth assumption, that the vent hole is nearly circular, is probably acceptable.

Once the ratio of the length of the conical flame (L) to the diameter of the hole (D) from which the jet issues is known, AMSHAH uses equation (6.3) to find D_e, which is the diameter of a right circular cylinder which has the same surface area as the truncated cone:

$$\frac{D_e}{D} = \left(\sec\frac{\theta}{2} + \frac{L}{D}\sin\frac{\theta}{2}\sec^2\frac{\theta}{2}\right) \qquad \text{AMSHAH (6.3)}$$

This equation is correct, and the derivation of it will be presented below. The radiation from a flame does of course depend upon the shape of the flame. The shape of the cone and a cylinder will not be too different if the cone angle is small and the length is not large. For other conditions, however, the radiation characteristics of the two different shapes, as manifested by the view factor, are significantly different. For some situations, then, the modeling of thermal radiation from a conical flame by radiation from a cylinder will be inexact. The validity of the sixth assumption is therefore subject to question.

The seventh assumption appears to be valid. For the high Reynolds number flows expected to occur, the laboratory experiments and field occurrences should be dynamically similar.

The eighth assumption is based on the work of Hottel [4]. Data on a wide variety of flames with different combustion gases were correlated by a length to width rate of 10.6; this implies a cone semiangle of 5.4 degrees. Various boundary criteria for noncombusting jets will yield semiangles between 4 and 15 degrees. Thus this assumption is well founded.

The ninth assumption is reasonable, although 300°K (~ 80°F) is somewhat high for an average ambient temperature in the expected region of interest. A lower value of ambient temperature would yield more conservative damage estimates, but not significantly so.

Flame Height

There are no assumptions stated in AMSHAH for this model. The relation describing the length of the flame, equation (6.4), is taken from Thomas [5] who obtained it from the analysis of experimental burning of wooden cribs in still air. The use of (6.4) implies that the following assumptions are valid:

1. The flame from a burning pool of liquid is very similar to the flame from a burning wooden crib.

2. The wind has a negligible effect.

3. The pool diameter does not change appreciably during the time in which the pool is burning.

4. The burning rate of the pool is independent of whether the pool is upon land or water, and is independent of the pool size.

No additional assumptions, implied or stated, are incorporated in the computerized version of the model.

It might not appear that flames from pools and wooden cribs would behave similarly; however, the behavior is similar, as has been demonstrated by correlation of data from both types of fires [5,6,7]. In general, for large fires of both types, the burning rate is limited by the amount of thermal radiation downward from the flame to the unburnt fuel [8]. In the case of cryogenic fuels, however, heat transfer from

---

[4] Hottel, H. C., "Burning in laminar and turbulent fuel jets," pp. 97-113, in 4th International Symposium on Combustion, 1953.

[5] Thomas, R. H., "The size of flames from natural fires," pp. 844-859, in 9th Symposium (International) on Combustion, Academic Press, New York, 1963.

the substrate beneath the pool may play a significant role in the phenomenology of the fire. In such a case, the two types of fires, solid and liquid fueled, may behave differently, and the nature of the substrate (especially whether it is solid or liquid, as discussed below) may be significant. Although this thermal radiation causes evaporation of fuel in the case of pool fires and pyrolysis in the case of wood fires, the processes are grossly similar in the sense that heat is used to produce vaporized fuel. Thus it appears that the first assumption is reasonable.

For about the same reasons, the second assumption also appears to be acceptable. The wind could affect the combustion process in two ways, (a) wind could increase the mixing of fuel and air, or (b) wind could increase the evaporation of fuel. Neither is likely to occur. The turbulent mixing, limiting the flame size, is generated by the combustion process itself. Atmospheric and wind-generated turbulence will be small compared to flame-generated turbulence, except perhaps in extreme weather conditions, e.g., a hurricane. The vaporization of fuel is dominated by the thermal radiation from the flame. Thus, the wind will not significantly increase the amount of fuel in air, unlike the case for a pool not burning.

The third assumption, that the pool diameter is constant during burning, is not a good assumption. For pools ignited at the beginning of their spread, this assumption will cause unrealistic answers. The burning time will be long because of the small pool diameter for the amount of fuel present. In that long a time, the pool will continue to spread. For pools ignited after reaching a moderate size (at least beyond the gravity-inertia spread regime), this assumption will not be as bad, because the burning of the fuel will decrease the mass in the spill and thereby decrease the spreading rate.

The fourth assumption appears to be reasonable. Burning rate is a function of pool size but approaches a limit as the pool size increases. For the pool sizes of interest (over 1 meter), the limiting value of burning rate will have been attained. As for differences in behavior between pools on land or in water, differences could arise because of different heat transfer rates between the fuel and substrate. Heat transfer between a pool and water will be greater than that between a pool and solid (e.g., earth). The increased heat transfer in water could result in a decreased flame height by dissipation of energy radiated from the flame. Alternatively, the increased heat transfer in water might increase the flame height by preheating cryogenic fuels such as has been noted with LNG.

---

[6] Atallah, S., and D. S. Allan, "Safe separation distance from liquid fuel fires," Fire Technol. 7(1):47-56, 1971.

[7] Welker, J. R., H. R. Wesson, and C. M. Sliepcevich, "LNG spills - to burn or not to burn," paper presented at Distribution Conference, Operating Section, American Gas Association, Philadelphia, May 12-15, 1969.

[8] Hertzberg, Martin, "The theory of free ambient fires. The convectively mixed combustion of fuel reservoirs," Combust. Flame 21:195-209, 1973.

Angle of Pool Burning Flame in a Wind

There are no assumptions stated in AMSHAH for this model. The model is essentially that developed by Welker and Sliepcevich [9] using dimensional analysis. The use of a dimensional analysis implies that the following assumptions were made:

1. No variables other than those included in the set chosen are significant in determining the outcome of the experiment.

2. The formula derived on the basis of flame behavior in wind tunnel experiments is applicable to flame behavior under field conditions.

No additional assumptions, implicit or stated, are incorporated in the computerized version of the model.

A danger in performing analyses based on dimensional considerations is that all significant variables may not have been included in the analysis [10]; however, in this case the agreement between data and analysis appears to validate the choice of variables. Likewise, the reasonable agreement between field data and the formulas based on wind tunnel data indicates no major difference between the two settings.

ERRORS AND INCONSISTENCIES

For this set of models, the typographical, analytical, and coding errors as well as the inconsistencies between CHRIS and HACS are minor. Typographical errors are given in Appendix 4A. Since the models are primarily empirical, there can be and are essentially no analytical errors. Coding errors are minor and are primarily concerned with values of parameters; these errors are detailed in Appendix 4B.

ACCURACY ASSESSMENT

As before, the assumptions for each of the three models will be discussed separately.

Gas Jet

The first assumption, that the flame is turbulent, is acceptable. This analysis assumes that the length to diameter ratio, L/D, of a flame is not a function of jet velocity as indicated in equation (6.1) of AMSHAH. In

---

[9] Welker, J. R., and C. M. Sliepcevich, The Effect of Wind on Flames, Technical Report No. 2, Contract OCD-OS-62-89, University of Oklahoma Research Institute, Norman, Oklahoma, November 1965.

[10] Thompson, P. A., Compressible-Fluid Dynamics, ch. 3, McGraw-Hill, New York, 1972.

order that jet velocity not influence L/D, the jet must be fully turbulent. The turbulence of the jet is assured if the jet Reynolds number

$$Re = \frac{UD}{\nu}$$

where

U is the jet velocity
D is the jet diameter
ν is the kinematic viscosity of the flame

is sufficiently high. For a given gas, the jet Reynolds number is directly proportional to jet velocity. Thus, as shown in Figure 4-1, the L/D ratio is constant for sufficiently high jet velocities. From these data, it appears that the flame will be fully turbulent if the jet Reynolds number is greater than 10^4

It is instructive to take a specific example to examine the validity of this assumption. Let us consider the venting tank which was discussed in Chapter 2. There, the loss of one metric ton of LNG from a tank which initially contained 83 metric tons is considered. For the diameter of the hole through which the gas is escaping equal to 50 cm, the outflow rate, w_o, and escape speed, v_o, are:

$$w_{o_1} = 92{,}000 \text{ g/sec}$$

$$w_{o_2} = 84{,}750 \text{ g/sec}$$

$$v_{o_1} = 13{,}580 \text{ cm/sec}$$

$$v_{o_2} = 12{,}500 \text{ cm/sec}$$

where the subscript 1 refers to the initial condition and the subscript 2 to the condition after the loss of one metric ton of LNG. The Reynolds number of this flow is on the order of 10^7, so the flow will be fully turbulent and any resulting flame will also be turbulent. However, even near the end of the venting when the internal tank pressure is nearly down to ambient pressure due to the temperature drop and the flow from the vent is laminar, the flame may still be turbulent because the combustion process itself tends to generate turbulence. Although not directly related, in his discussion of flames from tanks with no tops, Seeger [11] states that the flame becomes turbulent a short distance from the bottom due to the strong buoyant forces within the flame. And Seeger goes on to state that it may

---

[11] Seeger, P. G., "On the combustion and heat transfer in fires of liquid fuels in tanks," ch. 3, p. 101, P. L. Blackshear (ed.), Heat Transfer in Fires, Scripta Book Co., Washington, D.C., 1974.

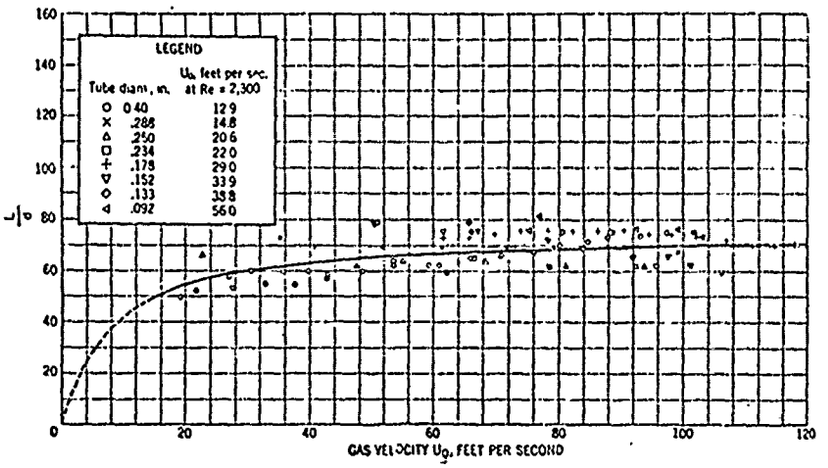


FIGURE 4-1 Constancy of ratio L/d (flame length/port diameter) in turbulent flames. Mixture of 50% Newark, Delaware, city gas and 50% air. U_0, gas velocity at the nozzle. Flames burning free in air. [12]

---

[12] Lewis, B., and G. Von Elbe, Combustion, Flames and Explosions of Gases, p. 550, Academic Press,

be assumed that the length to diameter ratio can be assumed to depend only on the Froude number. Thus, it would appear that the jet of escaping gas will be turbulent in itself for most of the time that gas is escaping and that the flame itself will be turbulent even when the jet may not be. Thus, the first assumption for a burning jet seems to be generally valid.

The second assumption, that the flame is shaped like a cone with a constant angle, also appears to be quite valid. The shape of a turbulent gas flame is not a very well defined concept. The fact that the flow is turbulent makes it difficult to define the edge of the flame sharply. Furthermore, the criterion for determining the edge of the jet can be based on a variety of factors. For example, the edge could be considered to be the locus of points where the temperature radial distance profile attains its peak. Alternatively, the jet edge could be considered to be the locus of points where the unburned fuel concentration is some fraction of the centerline concentration (say 0.1, 0.05, 0.01, etc.). Despite these limitations, whatever criterion is used to define the edge of the flame, a similarity principle seems to hold which indicates that the flame can, in general, be considered to be a cone with a constant angle. For example, consider the similarity profiles obtained for a hydrogen flame as shown in Figure 4-2. The conventional theories of the turbulent flame [3; 4; 13, ch. 7] consider the flame to be a constant angle cone, and experiment has verified these theories. Furthermore, the theory of turbulent jets [14], which is very pertinent since flames of this type are diffusion-limited, supports this view. The wide acceptance of the concept is illustrated by the following comment about direct and shadow photographs of a turbulent flame: "The luminous boundary as well as the outer shadow outline take the form of a small-angle inverted cone typical of a turbulent jet" [12, p. 30]. In summary, if the flame is turbulent it can be treated as a constant angle cone.

The third assumption, that the effect of buoyancy on the flame is negligible, is valid again for sufficiently high flow rates. In an analysis of turbulent gas jets, it was determined that buoyancy effects could be neglected provided the modified Froude number, Fr', is very large. By definition,

$$Fr' = \frac{V^2 \tan \theta}{Rg} \qquad (4\text{-}1)$$

where

---

[13] Williams, F. A., Combustion Theory, ch. 7, Addison-Wesley Publ. Co., Reading, Mass., 1965.

[14] Schlichting, H., Boundary-Layer Theory, 6th ed., pp. 699-700, McGraw-Hill, New York, 1968.

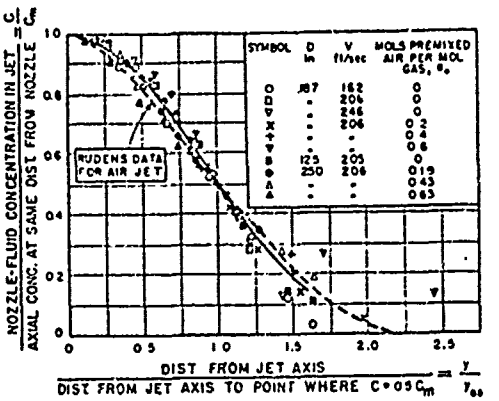


FIGURE 4-2 Correlation of radial concentration profiles in confined hydrogen flames. [3, p. 275]

R = nozzle radius

θ = half angle of spread of the jet

g = gravitational acceleration

V = jet velocity at the nozzle

This equation arises from the governing equation,

$$d\left\{\frac{(1/C^*)^2\,(1 - C^*)}{Y'^2}\right\} = C^* Y'^2\, dY' \qquad (4\text{-}2)$$

where

$$C^* = C(1 - \rho_N/\rho_S)$$

and

$$Y' = Y/(1 - \rho_N/\rho_S)^{2/5}$$

$$Y = \left(\frac{Rg}{V^2 \tan\theta}\right)^{1/5} \frac{y_b}{R},$$

y_b = value of y at edge of jet

C = time-mean mole fraction concentration of nozzle fluid in sample reduced to its unreacted constituents

ρ = fluid density

and subscripts S and N refer to surrounding and nozzle fluids, respectively.

In order to obtain the equation for flame length to diameter ratio, the right-hand side of this equation was considered negligible compared to the left-hand side. This will be true if either:

$$C^* \to 0$$

or

$$Y' \to 0$$

However, $C^* \to 0$ will occur only if

$$\rho_N \to \rho_S$$

For the fuel jets of interest here, the density of the fuel will be different from the density of air; hence

$$\rho_N \neq \rho_S$$

Thus, the only means for assuring that the right-hand side of (4-2) may be neglected is to require that Y' be small. Since

$$Y' = \frac{y_b}{R} (Fr')^{-1/5}$$

Y' will be small if Fr' is large. Performing the differentiation indicated in equation (4-2) shows that the right-hand side may be neglected if

$$Y'^5 << \left| \frac{2(1 - C^*)}{(C^*)^3} \right| \qquad (4\text{-}3)$$

Since C varies from zero to unity, a lower bound on the right-hand side of (4-3) may be found by taking $C = 1$. Thus, (4-3) becomes

$$Y'^5 << \left| \frac{2\ \rho_N/\rho_S}{(1 - \rho_N/\rho_S)^3} \right| \qquad (4\text{-}4)$$

A lower bound on the right-hand side of (4-4) is obtained by taking ρ_N/ρ_S as small as possible. For a hydrogen jet in air, $\rho_N/\rho_S \simeq .07$, the requirement of (4-4) may be taken to be,

$$Y'^5 << .17$$

or

$$\frac{1}{Fr'} \left(\frac{y_b}{R}\right)^5 << .17 \qquad (4\text{-}5)$$

From published data [3], a large value for y_b/R may be taken to be 50. Therefore, the criterion (4-5) becomes,

$$\frac{1}{Fr'} << 5.4 \times 10^{-10}$$

or

$$Fr' >> 1.8 \times 10^9$$

or

$$\frac{V^2 \tan \theta}{Rg} >> 1.8 \times 10^9$$

If we take θ to be 5.4 degrees (a suitable choice as demonstrated below), then the criterion becomes,

$$\frac{V^2}{Rg} >> 1.9 \times 10^{10} \qquad (4\text{-}6)$$

This, of course, is an extreme criterion, derived by taking limiting values.

For any given fuel and venting situation, the criterion for the neglect of buoyancy will in general be less severe. For releases of cargoes carried in marine transport, the buoyancy effects will generally be negligible. The importance of buoyancy effects, if they are of consequence, lies in the differences produced in the entrainment rate of the burning jet.

The fourth assumption is that the effect of the wind on flame bending may be neglected. To assess the validity of this assumption, the kinetic energy density of the wind and the gas in the burning jet need to be compared. With a wind speed of 5 m/s, the kinetic energy density of air is 306 g/(cm-s). To compute the kinetic energy density of the gas in the jet, the density of this gas will be needed. If complete combustion is assumed, one mole of CH_4 will react with two moles of O_2 to give two moles of H_2O and one mole of CO_2. Thus, where we originally had one mole of CH_4, one mole of O_2, and about 7.5 moles of N_2, the combustion products are two moles of H_2O, one mole of CO_2, and 7.5 moles of N_2. (In actuality, the flame temperatures will generally be hot enough to produce some oxides of nitrogen, but this is ignored for this simple example.) The average molecular weight of this mixture is 27.6 and, at ambient pressure and at an average flame temperature of 900°C, the burned gas will have a density of 0.29×10^{-3} g/cm^3.

Taking velocity to be sonic and approximately equal to 670 m/s at 900°C, the kinetic energy per unit volume is 129×10^4 g/(cm-s). This value is about 4.2×10^3 times the kinetic energy of the wind. If the velocity of the jet is 1/4 the sonic velocity, the kinetic energy of the jet would still be about 250 times the kinetic energy of the wind.

Let us now consider the bending effect when the kinetic energy of the jet is 300 times the kinetic energy of the wind. For jet deflection, Douglas and Neve [15] give the following equation:

$$\tan \theta = \frac{M_c}{M_p} * C$$

where C, an empirical constant, equals 1.6.

---

[15] Douglas, J. F., and R. S. Neve, "Investigation into the behavior of a jet interaction proportional amplifier," paper C3, pp. C3-29 to C3-50, Proceedings of 2nd Cranfield Conference on Fluidics, B.H.R.A., Cranfield, January 1967.

In this case,

$$M_c = (\rho v^2)_{wind}$$

$$M_p = (\rho v^2)_{jet}$$

$$\theta = \text{angle of deflection}$$

$$\tan\theta = \frac{1.6}{300} = .00533$$

which gives: $\theta \simeq 0.3$ deg. This can be safely ignored.

The fifth assumption, that the venting hole is approximately circular, would appear to be reasonable for most marine collisions resulting in gas venting; however, venting through a long, narrow hole (a slit) may cause a significant departure from the formula used to describe flame size. The production by a maritime accident of a long, narrow slit at a high enough level for gas venting to occur seems unlikely. Nevertheless, gas venting though a slit is better characterized as a two-dimensional planar jet, instead of as the circular jet contained in the present analysis.

A flame produced by a gas jet issuing from a slit will have a gross difference in appearance from a gas jet issuing from an approximately circular hole. The two-dimension planar jet will produce a flame shaped like a triangular prism (wedge) instead of the cone-shaped flame produced by an almost circular hole (see Figures 4-3a and 4-3b). In addition, the spreading rates of the two flames will differ. Circular jets spread much more rapidly than two-dimensional jets. This is because in a two-dimensional jet, momentum can be lost in only two directions; while in a circular jet, momentum is lost "all around." The fact that circular jets spread more rapidly than two-dimensional jets is demonstrated by the observed properties of these jets. For example, in a turbulent circular jet the centerline velocity decay is proportional to x^{-1}, where x is distance measured along the jet axis; for two-dimensional jets, the centerline velocity decays proportional to $x^{-1/2}$. That is, circular jets decay more rapidly.

The differences in spreading rate will cause the cone angle of the conical flame to be less than the wedge angle of the wedge-shaped flame. Consider the equation describing the turbulent circular jet [14, ch. 24]

$$U = U_c \frac{1}{(1 + \frac{\eta^2}{4})^2} \qquad (4\text{-}7)$$

$$\eta = \frac{1}{4}\sqrt{\frac{3}{\pi}}\ \frac{\sqrt{K}}{\varepsilon_0}\ \frac{r}{x} \qquad (4\text{-}8)$$

$$U_c = \frac{3}{8\pi}\frac{K}{x\varepsilon_0} \qquad (4\text{-}9)$$

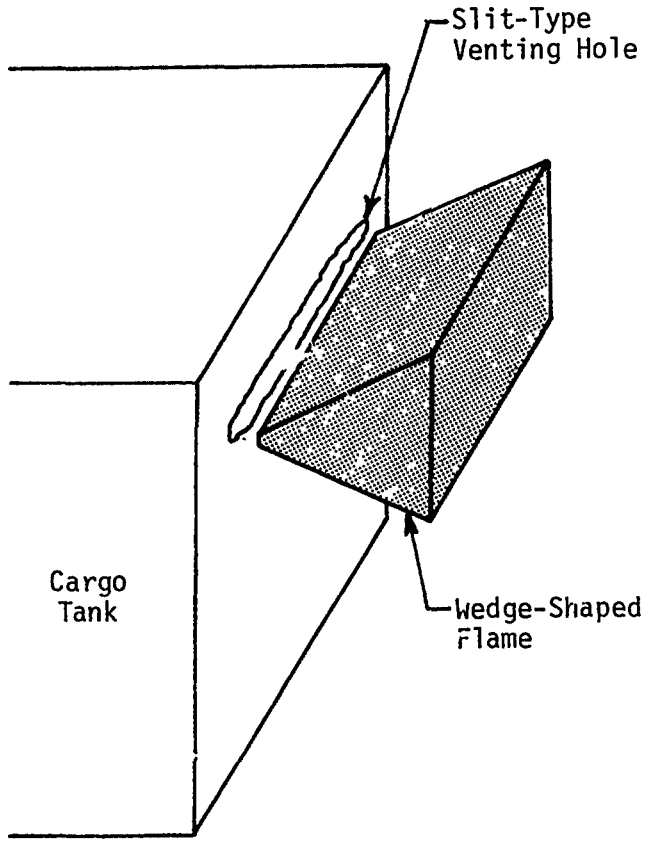


FIGURE 4-3a Wedge-shaped flame resulting from a long, narrow venting hole (slit). The magnitude of the wedge angle has been exaggerated for illustrative purposes.

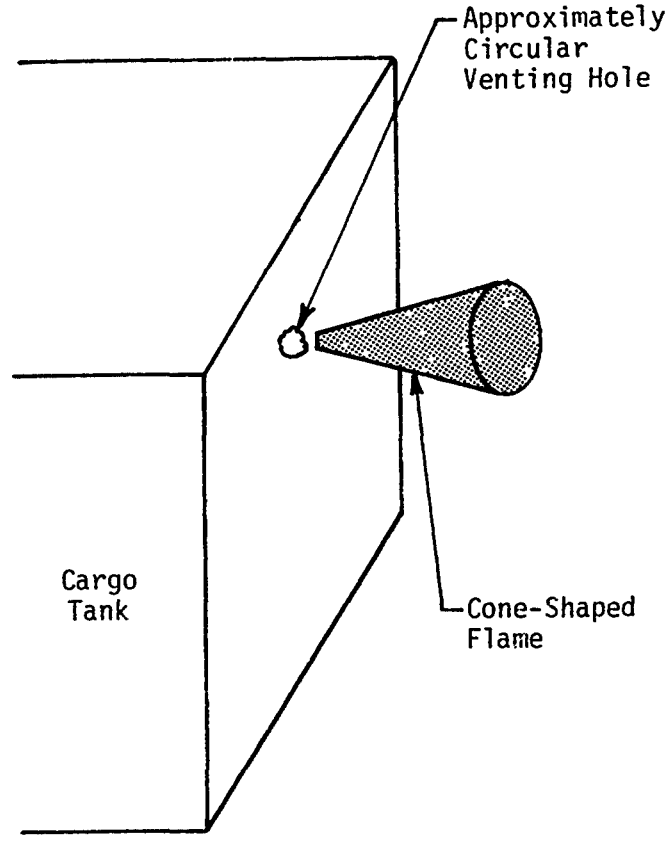


FIGURE 4-3b Cone-shaped flame resulting from an approximately circular venting hole. The magnitude of the cone angle has been exaggerated for illustrative purposes.

where

K is the kinematic momentum, a measure of the strength of the jet

$\frac{\varepsilon_0}{\sqrt{K}} = 0.0161$

U_c is the centerline velocity

r is the radial distance measured from the jet axis

x is distance along the jet axis

Now, from experiments on turbulent gas flames [4], the length of a flame, L, is related to half the width of the cone base, y_f, by

$$\frac{L}{D} = 5.3 \frac{y_f}{R} \tag{4-10}$$

where D and R are, respectively, the diameter and radius of the hole. Thus,

$$\frac{y_f}{L} = \frac{1}{10.6} \tag{4-11}$$

since $D = 2R$.

In the terminology of the equations describing the circular jet, equation (4-11) becomes,

$$\frac{r}{x} = \frac{1}{10.6} = .09434 \tag{4-12}$$

Thus, using (4-8),

$$\eta = 1.4315 \tag{4-13}$$

Placing this value for η into equation (4-7) yields,

$$\frac{U}{U_c} = 0.437 \tag{4-14}$$

Now, let us assume that in the case of the two-dimensional flame, the flame edge will be defined by the same velocity ratio as is given by (4-14). Since the concentration profiles follow the same similarity laws as the velocity profiles, this is an acceptable first approximation for comparing the behavior of the two types of jets. The equations describing the two-dimensional jet are

$$U = U_c (1 - \tanh^2 \xi) \tag{4-15}$$

$$\xi = \sigma \frac{y}{x} \tag{4-16}$$

$$U_c = \frac{\sqrt{3}}{2} \sqrt{\frac{K\sigma}{x}} \tag{4-17}$$

where

$$\sigma = 7.67$$

and

y is the distance measured normal to the jet axis

Now, applying the criterion stated in equation (4-14) implies that

$$(1 - \tanh^2 \xi) = 0.437$$

or

$$\tanh^2 \xi = 0.563$$

or

$$\tanh \xi = 0.75$$

or

$$\xi \simeq 0.97 \tag{4-18}$$

Thus,

$$\frac{y}{x} = \frac{\eta}{\sigma} = \frac{0.97}{7.67} = 0.126$$

or

$$\tan \theta = 0.126 \tag{4-19}$$

Then the spread angle is given by

$$\theta \simeq 7.2^\circ \tag{4-20}$$

instead of the 5.4° obtained for the circular jet. Thus, because the circular jet spreads more rapidly, the contour where enough air has mixed with fuel to allow combustion is closer to the jet axis than in the case of a two-dimensional jet. Thus, the spread angle on the cone is smaller than that of the wedge. The gas flame will begin to show two-dimensional, rather than circular, behavior whenever the largest dimension of the hole is about ten times its hydraulic radius or larger.

The sixth assumption, that the conical flame may be treated as an equivalent cylinder, also appears to be reasonable. This assumption may be considered in two parts. (1) On what basis is an equivalent cylinder obtained? (2) Is this equivalence valid for heat transfer purposes?

The cylinder equivalent to the conical flame is obtained by equating the surface area of the conical flame to the surface area of a cylinder of the same length. The fact that this is the criterion for finding an equivalent cylinder is not stated in AMSHAH, so it must be verified. That this is the manner by which the equivalent cylinder is obtained is shown in Appendix 4C; equation (6.3) in AMSHAH is derived by equating areas of a flame and cylinder of equal lengths. To determine the validity of the assumptions, however, it is necessary to find whether this type of equivalence is sufficient for heat transfer purposes.

As mentioned previously, data indicate [4] that for turbulent flames the cone length is related to the base radius by,

$$\frac{r}{L} = \frac{1}{10.6}$$

and the resulting cone semiangle is 5.4°. Let us assume

$$\frac{L}{D} = 10$$

then from Appendix 4C,

$$\frac{D_e}{D} = \sec \frac{\theta}{2} \left[1 + \frac{L}{D} \tan \frac{\theta}{2}\right] \tag{4-21}$$

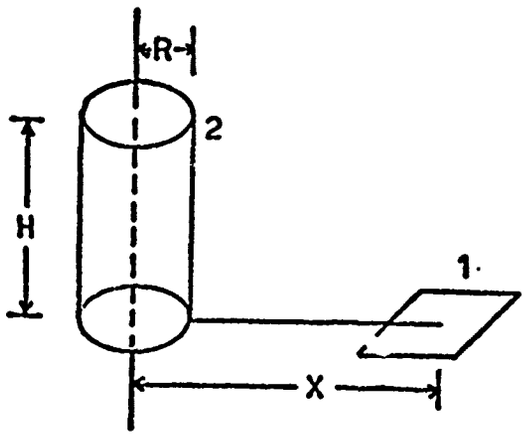
and since $\frac{\theta}{2} = 5.4°$,

$$\frac{D_e}{D} = 1.9539 \tag{4-22}$$

Now let us compare view factors for the cone and an equivalent cylinder. Consider the receptor to be a horizontal unit area located at a distance from the axis equal to the flame length. Then, for the cylinder, the general formulation given by Blackshear [16] is,

---

[16] Blackshear, Perry L. (ed.), Heat Transfer in Fires, Wiley, New York, 1974.



$$F_{12} = \frac{1}{\pi}\left[\tan^{-1}\sqrt{\frac{X' + R'}{X' - R'}} - \frac{(1.0 + X'^2 - R'^2)}{(1.0 + X'^2 + R'^2)} \tan^{-1}\sqrt{\frac{X' - R'}{X' + R'}}\right]$$

$$X' = \frac{X}{H}$$

$$R' = \frac{R}{H}$$

and for this problem,

$$R = D_e/2 = D \cdot 0.97695$$

$$X = H = L$$

hence,

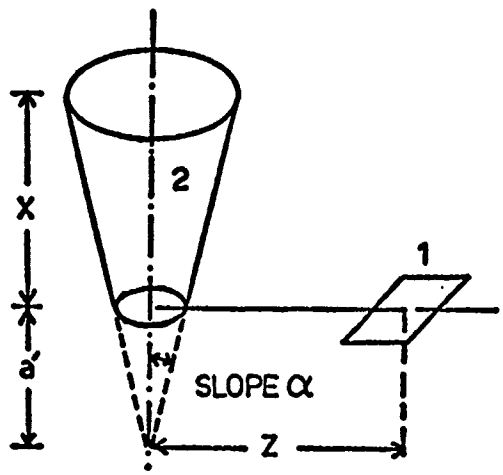
$$X' = 1$$

$$R' = 0.97695 \quad \frac{D}{L} = 0.097695$$

and

$$F_{12} = \frac{1}{\pi}[0.105] \qquad (4\text{-}23)$$

For the cone, we have the general formulation,



$$F_{12} = \frac{1}{\pi}\left\{\tan^{-1}\sqrt{\frac{Z' + \alpha A'}{Z' - \alpha A'}} - \frac{1.0 + Z'^2 - P'^2}{\sqrt{A'^4 - C'^4}} \tan^{-1}\sqrt{\frac{(A'^2+C'^2)(Z'-\alpha A')}{(A'^2-C'^2)(Z'+\alpha A')}}\right.$$
$$\left. + \frac{\alpha}{\sqrt{1+\alpha^2}} \tan^{-1}\sqrt{\frac{1+\alpha^2}{Z'^2 - \alpha^2 A'}}\right\}$$

$$A^2 = X^2 + Z^2 + 2(X+A)$$

$$B = \alpha(X+A)$$

$$C^2 = 2Z\alpha(X+A)$$

$$A' = A/X$$

$$Z' = Z/X$$

$$A' = A/X$$

$$B' = B/X$$

$$C' = C/X$$

However, this formulation taken from Blackshear is evidently in error. As an alternative, let us approximate the view factor on the basis of a small cone angle. The base of the cone will have a radius given by,

$$r_b = \frac{D}{2} \qquad (4\text{-}24a)$$

For a cone semiangle of ψ, the radius at the top will be

$$r_t = \frac{D}{2} + L \cdot \tan\psi$$

For a semiangle of 5.4°

$$r_t = \frac{D}{2} + \frac{L}{10.6}$$

and from above,

$$r_t = \frac{D}{2} + \frac{10.0}{10.6}$$

$$= D\ (1.44) \qquad (4\text{-}24b)$$

Let us compute the view factors for cylinders with height, L, and radii, r_b and r_t. For the cylinder of radius, r_b,

$$R = r_b = 0.5\ D$$

$$X = H = L$$

hence,

$$X' = 1$$

$$R' = \frac{1}{2}\ \frac{D}{L} = \frac{1}{20} = 0.05$$

Thus,

$$F_{12} = \frac{1}{\pi}\ [0.092\ ] \qquad (4\text{-}25a)$$

For the cylinder of radius, r_t,

$$R = r_t = 1.44\ D$$

$$X = H = L$$

hence,

$$X' = 1$$

$$R' = \frac{1.44\ D}{L} = 0.144$$

Thus,

$$F_{12} = \frac{1}{\pi}\ [0.503\ ] \qquad (4\text{-}25b)$$

The view factor for the cone will be bounded by these view factors modified to account for the inclined surface of the cone. The cone will radiate more directly toward the receiving surface because of the incline. The effect is approximately measured by the factor $1/\cos\psi$, where ψ is the cone semiangle. Thus, we expect the cone to have a view factor between the bounds.

$$\frac{(0.503)}{\cos\psi\,\pi} > F_{12\,\text{cone}} > \frac{(0.092)}{\cos\psi\,\pi}$$

or

$$\frac{0.50}{\pi} > F_{12\,\text{cone}} > \frac{0.092}{\pi} \qquad (4\text{-}26)$$

Thus, the view factor for the cone will be comparable to that of the equivalent cylinder, primarily because the cone semiangle is small. The sixth assumption, therefore, is acceptable.

The seventh assumption, that laboratory data may be extrapolated for field use, is apparently reliable. Differences between laboratory and field events could arise because of:

1. the presence in the laboratory of solid boundaries near the jet, whereas such boundaries would be absent in the field

2. differences in the scale and magnitude of turbulence of the ambient fluid into which the jet flows.

The presence of nearby boundaries will influence the spread of the jet, its direction (the jet may bend under the influence of nearby boundaries), and to some extent even the net flow rate of the jet. Nevertheless, the experiments performed to obtain these relationships [3,4] seem to have been done with sufficient care to exclude, or at the very least minimize, the effects of boundaries that are unavoidable in the laboratory setting. The scale and magnitude of turbulence in the laboratory will in general differ from that in the field. Laboratory turbulence will generally be of a lower level than in the field, and large-scale eddies will be absent. These differences in turbulence of the ambient fluid are important in determining the behavior of transition flames. However, for the fully turbulent flames considered here, the turbulence generated locally by the flame itself predominates and the turbulence characteristics of the ambient fluid are unimportant. Thus, the results of the laboratory experiments may be extrapolated for field use.

The eighth assumption, that the semiangle of the conical jet is 5.4 degrees, is a good one. Referring back to equations (4-7) through (4-9) which describe the behavior of a turbulent jet, we can examine the cone angles obtained for various conditions defining the jet boundary. As discussed above, one criterion for the jet boundary that can be used is that the ratio of jet velocity to centerline velocity be fixed; i.e.,

$$\frac{U}{U_c} = \text{const.} = A \tag{4-27}$$

For each value of the constant, A, a different cone angle will be defined. From equations (4-7), (4-9), and (4-27), we have

$$\frac{1}{(1 + \frac{\eta^2}{4})^2} = A \tag{4-28}$$

and from (4-8), we have

$$\tan \theta = \frac{r}{x} = B\eta \tag{4-29}$$

where

θ is the jet semiangle

and

$$B = \frac{4}{\sqrt{K}} \frac{\varepsilon_0}{} \sqrt{\frac{\pi}{3}} = 0.0659 \tag{4-30}$$

By choosing various values for A, different semiangles are thus obtained. For A = 0.04 , η = 4, and tan θ = 0.264; thus, θ = 14°46'. For A = 1/2, η = .828, tan θ = 0.0546; thus, θ = 3°8'. For A = 0.01, η = 6, and tan θ = .3954; thus, θ = 21°34'. It is certainly expected that the flame boundary be obtained for values of A between 0.01 and 0.5. The values chosen in the program and those alluded to in AMSHAH fall within these limits. As for the particular value of 5.4°, this is obtained from laboratory data [3, 4]. Figure 4-4 shows the correlation of flame spread data with jet analysis. As discussed above, the curve of flame length normalized by nozzle diameter versus flame width normalized by nozzle radius has a slope of approximately 5.3. This implies a cone semiangle of 5.4°. As can be seen from the figure, various gases depart somewhat from the average slope; for example, hydrogen and acetylene flames are lower and city gas flames are higher than the average. Nevertheless, for a wide variety of fuels, a cone semiangle of 5.4° is a good choice.

Assumption nine, that the ambient temperature is 300°K, is an acceptable assumption. The absolute temperature of the air is seldom, if ever, expected to exceed the range of 230°K to 320°K (about -40°F to 120°F). Equation (6.1) of AMSHAH may be written in the form,

$$f = \frac{L}{D} = K_1 \sqrt{K_2 + \frac{K_3}{T_0}} \tag{4-31}$$

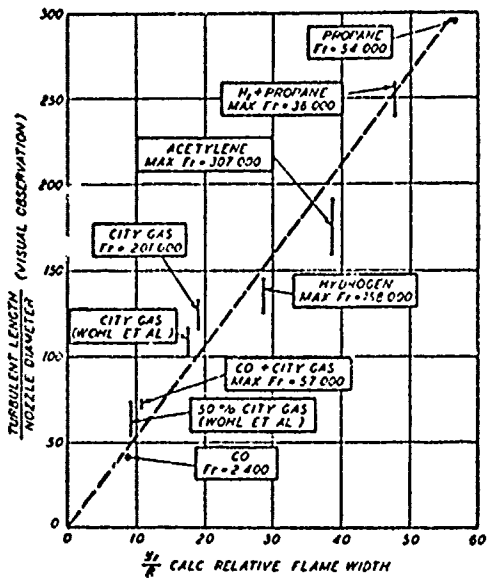


FIGURE 4-4 Correlation of turbulent free flame lengths with simplified jet theory. Abscissa is calculated jet width at point of completion of combustion, ignoring buoyancy. [4]

where, in the notation of AMSHAH,

$$K_1 = \frac{K_f}{C}$$

$$K_2 = C$$

$$K_3 = \frac{(1-C)}{\alpha} \frac{M_a T_f}{M_f}$$

$$C = \frac{1}{[1 + r\ (\frac{M_f}{M_a})]}$$

Differentiating (4-31) with respect to T_0 gives,

$$df = \frac{1}{2} K_1\ (K_2 + \frac{K_3}{T_0})^{-1/2}\ \ (\frac{-K_3 dT_0}{T_0^2})$$

Then the sensitivity coefficient for T_0 is given by,

$$S = \frac{df/f}{dT/T} = \frac{-1}{2\ (\frac{T_0 K_2}{K_3} + 1)} \qquad (4\text{-}32)$$

Since $T_0 \simeq 300°K$, $T_f \simeq 2100°K$, $C \simeq 1/2$, $\alpha \simeq 1$, $M_a/M_f \simeq 2$, $S \simeq -1/50$. Thus, changes in ambient temperature can probably be safely ignored. Nevertheless, it would be very simple to include ambient temperature as an input to this model.

Thus, it has been shown that the underlying assumptions of the gas jet model are quite reasonable.

Flame Height

With regard to the first assumption, Thomas [5] has attempted to fit his equation, equation (6.4) of AMSHAH,

$$\frac{L}{D} = 42 \left[\frac{\dot{m}''}{\rho_a \sqrt{gD}}\right]^{0.61} \qquad \text{AMSHAH (6.4)}$$

to the data of Yokoi [17] with some success. Atallah and Allan [6] and Welker, Wesson, and Sliepcevich [7] have used the Thomas correlation for calculating L/D for flames from a variety of industrial and high-boiling-point organic liquid fuels.

---

[17] Yokoi, S., Japan Ministry of Construction, Building Research Institute, Report No. 29, 1959.

Atallah and Raj [18] have presented an alternative equation for predicting the flame size for pool burning. We have compared the results of the equation and the data on LNG fires of May and McQueen [19] as well as the data on gasoline of Hertzberg [8] in Appendix 4D.. The Thomas equation predicted the results within 40%, while the deviations were up to 238% with the equation proposed by Atallah and Raj [18]. Welker [20] found that Thomas' correlation is adequate while correlating the field measurements on LNG fires made by the University Engineers [21]. It can be seen from his paper [20] that L/D can vary by an amount as much as 100% during the course of burning in a given experiment. In view of the nature of the data, predictions by the Thomas equation are quite reasonable.

With regard to the second assumption, Thomas [5] has stated that the effect of wind on the flame size is small. Over a range of 4.5 in $U/(gD)^{1/2}$, L varied by 37% in his experiments. He indicates that a small decrease in flame length with increasing wind speed is presumably a result of better mixing. Atallah and Raj [18] mention that increase in wind speed slightly increases the L/D ratio. Since L/D as obtained from the Thomas equation is quite approximate, the error introduced by neglecting the effect of the wind on L/D ratio is not likely to worsen the situation significantly.

The third assumption is that the pool size will not change during the burning from the pool. AMSHAH equation (6.4) could be applied for different values of D during the burning of the pool, but when the subroutines which are involved are examined, it is seen that D is the diameter of the pool at the time at which the pool is ignited and that D is not changed during the fire. Equation (6.4) may be rearranged to give

$$L = 42 \left| \frac{\dot{m}''}{\rho_a \sqrt{g}} \right|^{0.61} (D)^{0.695}$$

where $\dot{m}''$ is the burning rate.

We know that $\dot{m}''$ increases with the diameter. Therefore, increase in diameter will increase L both because $\dot{m}''$ will increase and because D will increase. Therefore, it would be preferable to take the change in diameter during the course of burning into account.

---

[18] Atallah, S., and P. P. K. Raj, "Radiation from LNG fires," LNG Safety Program Interim Report on Phase II Work, American Gas Association Project IS-3-1, July 1, 1974.

[19] May, W. G., and W. McQueen, "Radiation from large natural gas fires," Combust. Sci. Technol. 7:51-56, 1973.

[20] Welker, J. Reed, "Radiant heating from LNG fires," LNG Safety Program Interim Report on Phase II Work, American Gas Association Project IS-3-1, July 1, 1974.

[21] University Engineers, Inc., Radiant Heating from LNG Fires, Report to Battelle Columbus Laboratories, August 1973.

In order to calculate the increase in pool diameter accurately, either the spreading models or mixing models would have to be rederived taking into account the loss of mass by burning. Such a reformulation is not a trivial undertaking. Nevertheless, the errors induced by not considering the continued spread of the pool can lead to large errors, especially if the pool is ignited before it has been allowed to spread very much.

The fourth assumption concerns the heat transfer rate to the pool of fuel from beneath the pool. In general, the heat transfer characteristics of common types of ground and water are quite different. The mixture of fuel vapor and air which is combusting just above the pool surface must be constantly replenished. The air will come from the atmosphere outside the burning region, and the fuel vapor from the pool below the flame. The rate of fuel vaporization will depend directly upon the heat flow into the pool, and the bulk of this heat flow will come from the water or land upon which the pool rests. Atallah and Raj [18] state that the heat flux is derived from two sources for pools of LNG maintained by earthen dikes: 1) radiation from the flame, and 2) heat conducted from the floor and sidewalls of the impounding area. The burning rate of an LNG pool for which the sidewall effects are small (large diameter to depth ratio) can be given as

$$\dot{m}''_{total} = \dot{m}''_{flame} + \dot{m}''_{ground}$$

Initially, the ground contribution to burning rate is large, but it drops off roughly with square root of time because of the progressive cooling of the ground. Atallah and Raj [18] attempted to separate the ground heat conduction from the flame contribution. Judging from the lack of agreement between the values of heat flux due to radiation obtained from the burning rate data (which were, in turn, derived from depth gauge data) and the heat flux calculated from the radiometer data, this attempt at separation was not particularly successful.

In this experiment, the thermal conductivity of water was found to be 60,560 ergs/(cm-sec-°K) (0.35 Btu/(hr-ft-°F))and the thermal conductivity of the soil was 13,840 ergs/(cm-sec-°K) (0.08 Btu/(hr-ft-°F)). The contribution of the ground falls off with time, while this may not occur for a pool on water since the convection currents may be set up. Further, the specific heat of water is about five times the specific heat of most types of rock and earth. Another source of heat may be from an exothermic reaction. Burgess, Biordi, and Murphy [22] report that G. J. Boyle's preliminary interpretations of experiments in which LNG and liquid methane were poured on water is: "The LNG and liquid methane do not derive their heat of vaporization entirely from the water in the usual sense, but also by forming hydrate, the exothermicity of which is available at the interface." In view of these items, the burning rate of a pool on the water surface

---

[22] Burgess, D., J. Biordi, and J. Murphy, Hazards of Spillage of LNG into Water, p. 3, App. I, NTIS AD 754-498, September 1972.

could be several times that of a similar pool on the ground under similar conditions. The error induced would be the same type as that induced by errors in measurements of burning rate.

Thus, although some errors result by departing from strict adherence to the assumptions, the level of accuracy is assessed to be acceptable.

Flame Angle

AMSHAH gives two equations for the angle, θ, that the axis of the flame makes with the vertical:

$$\cos\theta = 0.7\left[\frac{U}{(\frac{\dot{m}''}{\rho_a}gD)^{1/3}}\right]^{-0.49} \qquad \text{AMSHAH (6.5)}$$

$$\frac{\tan\theta}{\cos\theta} = 3.3\,(\frac{DU}{\nu_a})^{0.07}(\frac{U^2}{gD})^{0.8}(\frac{\rho g}{\rho_a})^{-0.6} \qquad \text{AMSHAH (6.6)}$$

The angle, θ, is also denoted as the tilt angle. Equation (6.6) is taken from Welker and Sliepcevich [9] and is the one used in the subroutine FLMAN. Equation (6.5) is taken from Thomas [5].

Each equation fits best the data of the author(s) who developed the equation, and no independent source of data with which to test these two equations for the tilt angle was discovered. It should be mentioned that the two equations depend on different parameters, and in some experiments insufficient measurements are made so that only one equation of the two can be tested against the data. The physical reasoning behind the model of flame bending discussed by Welker and Sliepcevich appears to be specious. The view presented is one in which the flame is subject to wind drag and bends accordingly. Actually, the bending is caused by the relative convection rates of fluid particles by the wind and by the induced upward natural convection in the flame. Fortunately, the validity of the dimensional analysis is not compromised by the explanatory reasoning accompanying it.

The agreement between the formula obtained from dimensional analysis confirms the validity of the variable set chosen. Since the variable set used in AMSHAH equation (6.6) is larger than that of AMSHAH equation (6.5) and since the variables used in (6.6) are fundamental rather than derived (e.g., $\dot{m}''$ in (6.5)), equation (6.6) is preferred as stated in AMSHAH. Thus, the first assumption is acceptable.

The effect of turbulence scale in the field as opposed to that found in the laboratory is expected to have a minimal effect. Since the action of the wind is primarily to convect the fluid particles in the flame, the primary determination of bending will be the mean wind velocity; the instantaneous wind velocity, as measured to some degree by the turbulence level and scale, will be at best a second-order effect.

Thus, the assumptions underlying this model are acceptable, and deviations from the assumptions in the field need not be considered.

SENSITIVITY ANALYSIS

The sensitivity analysis for the Flame Size Model is carried out on the same principles as discussed in earlier chapters. Various variables and parameters are initially selected to describe the model. Normal values and reference values (usually equal to the normal values) are assigned to the variables and the parameters. The normal output is determined from the computer simulation of the model, utilizing the normal values of the variables and the parameters. The variables and the parameter are changed, one at a time, and the changed output is used to determine the sensitivity coefficient of the changed variable or parameter. When a second variable or parameter is being changed for a second sensitivity coefficient, all the other variables and parameters are brought back to their normal values.

The Flame Size Model is subdivided into three submodels and the sensitivity analysis is carried out separately for each of these three submodels. The submodels are:

1. Shape and size of flame from a burning gaseous fuel jet

2. Height of a flame from a pool of burning liquid fuel

3. Inclination from vertical (because of wind) of a flame from a pool of burning liquid fuel

Discussion of the sensitivity coefficients for each of the submodels is presented below.

1. Shape and size, gaseous fuel jet. The basic equations used for this submodel are equations (6.1) and (6.2) of AMSHAH. Various variables and parameters are selected to describe this submodel. These variables and parameters are:

Variable: V1, diameter of jet hole

Parameters: P1, molecular weight of fuel
P2, adiabatic flame temperature
P3, molar ratio of reactants to products of combustion
P4, stoichiometric air-fuel ratio

The normal and reference values of the variables and parameters were chosen for the venting of gaseous methane (e.g. from ruptured LNG containers) from a circular hole of 10.0 cm diameter; having a molecular weight of 16.0; an adiabatic flame temperature of 2010°C; with a molar ratio of 1.00 between reactants (methane and total moles of oxygen) and the total moles of products of combustion (carbon dioxide, carbon monoxide, and water vapor); and a stoichiometric air-fuel ratio of 17.2. With these normal values of the variables and parameters, the submodel simulation predicted a normal output

for the flame length as 201 cm. The first variable is now made larger than its absolute normal value by 5%, hence, the new diameter of the jet hole is 10.5 cm. With all the other variables and parameters at their normal values, the computer simulation of the submodel gives a changed output of 211 cm for the flame length. Hence, the sensitivity coefficient is determined by:

$$\text{sensitivity coefficient} = \left[\frac{(\text{changed output}) - (\text{normal output})}{(\text{normal output})}\right] \div \left[\frac{(\text{changed variable or parameter}) - (\text{normal variable or parameter})}{(\text{reference value of variable of parameter})}\right]$$

$\therefore$ sensitivity coefficient (for diameter of jet hole)

$$= \frac{211 - 201}{201} \div \frac{10.5 - 10.0}{10.0} = 1.000$$

These values are shown in Figure 4-5. The sensitivity coefficients for the other parameters are determined in a similar manner.

Along with a computer simulated prediction for the flame length from a burning gaseous fuel jet, another computer simulated prediction is also made for the diameter of the base of the conical shaped flame, based on empirical relations between the diameter of the conical base and the length of the flame from a burning gaseous jet. The sensitivity coefficients for the flame diameter are based on the same variables and parameters and are shown in Figure 4-6.

The physical significance of the sensitivity coefficients for this submodel is discussed in the following:

The sensitivity coefficient, as predicted by the computer simulation, for the diameter of the hole is 1.000. This implies that the length of the flame from a burning jet is sensitive to the diameter of the hole from which the gas is venting. This is also evident from equation (6.1) of AMSHAH, wherein the length of the flame is directly proportional to the diameter of the venting hole. The molecular weight of the gaseous fuel affects the flame length in a complex manner, thereby giving a moderate sensitivity of 0.425. The "heavier" gases of higher molecular weight would give longer flame lengths, probably because the rate of diffusion (required for combustion) is slightly slower and the gases would travel further before combustion is completed. This may only apply for fuels of molecular weights near the normal value used in the simulation (the highest value

RESULTS FOR CH_4 FLAME JET

OUTPUT IS FLAME LENGTH

NORMAL VALUE IS 201.

INDEX	VARIABLE	SENS COEFF	V NORMAL	REFERENCE	V CHANGED	OUTPUT	FRACTION
1	HOLE DIA	1.000	10.0	10.0	10.5	211.	1.050

INDEX	PARAMETER	SENS COEFF	P NORMAL	P CHANGED	OUTPUT	FRACTION
1	MOLEC WT	.425	16.0	16.8	205.	1.021
2	FLAME TEMP	.414	.201E+04	.211E+04	205.	1.021
3	PROD/REACT	-.458	1.00	1.05	196.	.977
4	AIR/FUEL	.879	17.2	18.0	209.	1.044

FIGURE 4-5 Sensitivity coefficients, flame length from gaseous jet

RESULTS FOR CH4 FLAME JET

OUTPUT IS FLAME DIAMETER

NORMAL VALUE IS .202E+04

INDEX	VARIABLE	SENS COEFF	V NORMAL	REFERENCE	V CHANGED	OUTPUT	FRACTION
1	HOLE DIA	1.000	10.0	10.0	10.5	.212E+04	1.050

INDEX	PARAMETER	SENS COEFF	P NORMAL	P CHANGED	OUTPUT	FRACTION
1	MOLEC WT	-.447	16.0	16.8	.207E+04	1.022
2	FLAME TEMP	.436	.201E+04	.211E+04	.206E+04	1.022
3	PROD/REACT	-.482	1.00	1.05	.197E+04	.976
4	AIR/FUEL	.925	17.2	18.0	.211E+04	1.046

FIGURE 4-6 Sensitivity coefficients, flame diameter from gaseous jet

used by Hottel [4] to verify the model appears to be a molecular weight of 26). In reality, the increase in the flame length with increase in molecular weight of gaseous fuel may have a limit and any further increase of the molecular weight may not increase the flame length. The next parameter is the adiabatic flame temperature of the flame. This parameter has moderate sensitivity of 0.414, slightly less than the molecular weight. In the analytical expression in AMSHAH, the flame length is proportional to the square root of the absolute adiabatic flame temperature (in degrees Kelvin), and hence, the sensitivity of about a half seems to be correct. The variation of the sensitivity from one half is because the normal value of the parameter for the adiabatic flame temperature is in degrees Centigrade and the analytic expression uses the temperature in degrees Kelvin. The next parameter, molar ratio of reactants to products of combustion, has a moderate negative sensitivity of -0.458. This negative sensitivity of about one-half is also evident from the analytical expression, where the flame length is inversely dependent on the square root of the molar ratio of reactants to products of combustion. The last parameter in this submodel is the stoichiometric air-fuel ratio. The flame length is sensitive to the air-fueld ratio (sensitivity coefficient of 0.879). The relationship is very complex and can be seen from two equations in AMSHAH, equations (6.1) and (6.2). Increasing the air-fuel ratio by changing the fuel would increase the length of the flame.

The second part of the sensitivity analysis for this submodel was for the diameter of the base of the conical flame. As mentioned earlier, the diameter is obtained from empirical correlations with flame length. The ratio of the flame diameter to the flame length has been determined empirically as 1.0: 10.6. The simulation for the diameter of the conical base of the flame uses the same model as that for the length of the flame, with the additional empirical relation. The variables and the parameters selected are the same as before, and the normal and reference values are also the same. The sensitivity coefficients, determined in the standard manner, are shown in Figure 4-6. It can be seen that the sensitivity coefficients for the flame diameter are close to those of the flame length. The physical reasoning is the same as indicated earlier.

2. Flame height, pool burning. The submodel for the flame height prediction is based on the correlations of Thomas [5], equation (6.4) of AMSHAH and the variables and parameters required for the model are:

Variable: V1, pool diameter for the burning liquid fuel

Parameters: P1, density of liquid fuel
P2, burning rate

The computed sensitivity coefficients are given in Figure 4-7. The wind velocity was found not to change the height of the flame.

RESULTS FOR CH_4 FLAME JET

OUTPUT IS FLAME HEIGHT

NORMAL VALUE IS 157. cm

INDEX	VARIABLE	SENS COEFF	V NORMAL	REFERENCE	V CHANGED	OUTPUT	FRACTION
1	POOL DIA	.690	183.	183.	192.	163.	1.034

INDEX	PARAMETER	SENS COEFF	P NORMAL	P CHANGED	OUTPUT	FRACTION
1	DEN LIQ	.604	.415	.436	162.	1.030
2	BURN RATE	.604	.208E-02	.219E-02	162.	1.030

FIGURE 4-7 Sensitivity coefficients, flame height from pool fires

The normal and reference values of these variables and parameters were chosen for the pool burning in a circular pool of 183 cm diameter. The fuel was liquefied natural gas of liquid density 0.415 g/cm^3 and burning at the rate of 0.00208 cm/s. These normal and reference values of the variables and parameters gave a normal output for flame height as 157 cm. From the computer simulation, it can be seen that the pool diameter, density of the liquid fuel and the burning rate have moderate sensitivities on the height of the flame. The values of the sensitivity coefficients are close to the expected values from the relationship given in AMSHAH. The pool diameter has slightly more sensitivity to the flame height when compared to the two parameters.

3. Flame inclination, pool burning. The submodel for the flame inclination is based on the correlations of Welker and Sliepcevich [9], equation (6.6) of AMSHAH, and the variables and parameters required for the model are:

Variables: V1, pool diameter for the burning liquid fuel
V2, wind velocity

Parameters: P1, molecular weight of fuel
P2, temperature of fuel vapor

The computed sensitivity coefficients are given in Figure 4-8.

The normal and reference values of these variables and parameters were chosen for the pool burning in an experimental circular pool of 10 cm diameter with a wind velocity of 4 cm/s. The molecular weight of the liquefied natural gas was 17.0 and the temperature of the vapor just above the pool was -160°C. The correlations of this small experimental fire are also applicable to large fires because the correlation was derived in terms of nondimensional constants, using dimensional analysis. The normal output for the flame inclination from the vertical was obtained from the predictions of the computer simulation. This predicted flame inclination was 0.0223 radians (≃ 1°15'). The values of the sensitivity coefficients give moderate to high sensitivities for the variables and the parameters. The pool diameter is related in a complex manner to the flame inclination, and the relationship is an inverse relationship. This implies that increasing the pool diameter would decrease the flame angle from the vertical and hence the moderately negative sensitivity coefficient of -0.699. The flame inclination is very sensitive to the wind velocity (sensitivity coefficient, 1.696). This can be seen from the analytical expression where there is a strong dependence of the flame angle on the equivalent Reynolds number of the wind. The parameter of the molecular weight has a moderate negative sensitivity coefficient (-0.577) and the parameter of temperature of vapor also has a moderate sensitivity coefficient (0.837). The values of the sensitivity coefficients for all of these submodels are close to the

RESULTS FOR CH4 FLAME ANGLE

OUTPUT IS FLAME ANGLE

NORMAL VALUE IS .223E-01

INDEX	VARIABLE	SENS COEFF	V NORMAL	REFERENCE	V CHANGED	OUTPUT	FRACTION
1	POOL DIA	-.699	10.0	10.0	10.5	.215E-01	.965
2	VELOC WIND	1.696	4.00	4.00	4.20	.242E-01	1.085

INDEX	PARAMETER	SENS COEFF	P NORMAL	P CHANGED	OUTPUT	FRACTION
1	MOLEC WT	-.577	17.0	17.8	.216E-01	.971
2	TEMP VAPOR	.837	-160.	-152.	.232E-01	1.042

FIGURE 4-8 Sensitivity coefficients, flame inclination from pool fires

values that can be expected for the normal values of the variables and parameters. A different set of normal values would change the sensitivities, but the changes would not be large.

SUMMARY AND RECOMMENDATIONS

In summary, the Flame Geometry Models are quite acceptable. Most departures from conditions specified by the underlying assumptions need not be considered important. The Flame Height Model for pool burning could be improved somewhat by considering (1) continued spreading or mixing while burning takes place, and (2) the differences in behavior of pool fires on water as compared to pool fires on land. In any event, these models are among the best reviewed.

APPENDIX 4A

TYPOGRAPHICAL ERRORS

Page 64 - Equation (6.1) is incorrect:

$$\frac{L}{D} = \frac{K_f}{C}\left[C + (1-C)\frac{M_a}{M_f}\frac{T_f}{\alpha T_o}\right]^{1/2}$$

The equation given by Hawthorne, Weddell and Hottel [3], is

$$\frac{L}{D} = \frac{K_f}{C}\left[\{C + (1-C)\frac{M_a}{M_f}\}\frac{T_f}{\alpha T_o}\right]^{1/2}$$

Page 67 - The bottom line should be

$$P_a\sqrt{gD} = 1.3 * \sqrt{9.8} * 10 = 12.869 \text{ kg/m}^2\text{s}$$

Page 68 - The second line from the top should be

$$\frac{L}{D} = 42\left[\frac{.07083}{12.869}\right]^{0.61} = 1.76$$

The brackets have been omitted in the text.

Page 70 - The eighth line from the top contains Equation (4.6); this should be Equation (6.6).

PRECEDING PAGE BLANK-NOT FILMED

APPENDIX 4B

CODING ERRORS

EXPRESSION FOR EQUIVALENT DIAMETER FLJET

An equivalent form of equation 6.3 in AMSHAH is programmed in HACS subroutine FLJET by assuming the semiangle of the jet to be 5.4 degrees. For that semiangle the exact expression for equivalent diameter should read:

$$DE = HOLED * 1.00446 + XLEN/10.53$$

The corresponding equation in the delivered version of FLJET is:

$$DE = HOLED + XLEN/10.6$$

The expression as programmed will give consistently lower values for the equivalent diameter than would be obtained with the exact expression; however, the differences are negligible (less than one per cent).

VALUE FOR FUEL DENSITY ON FLMAN

The subroutine FLMAN calculates the flame angle of a burning pool using the formulation of Welker and Sliepcevich. In their model the quantity, ρ_g, is the density of the fuel vapor at the boiling point of the fuel. Although this point is not stated in the clearest way in the original [9] or subsequent [20] papers, a telephone conversation with Dr. Welker's associates confirmed that this is indeed the case, MODE2 acquires the data necessary to call FLMAN. It contains the following two statements.

```
CALL FRCL (1003, TB, IS, IR)
IF (TB.GT.15.) CALL FRCL (2004, TB, IS, IR)
```

Thus if the boiling point of the fuel is greater than 15°C, the program replaces the boiling temperature (1003 in the state file) by the cargo temperature (2004 in the state file). For some conditions this could lead to an error in flame angle by as much as 5° or 6°. For slightly tilted flames such deviations are significant. Obviously the error becomes more serious for substances with higher boiling points.

ADIABATIC FLAME TEMPERATURE IN FLJET

There appears to be an error in the value used for adiabatic flame temperature as required by Hottel's model of flame size. Hottel [4] clearly states that the flame temperature required is "the theoretical

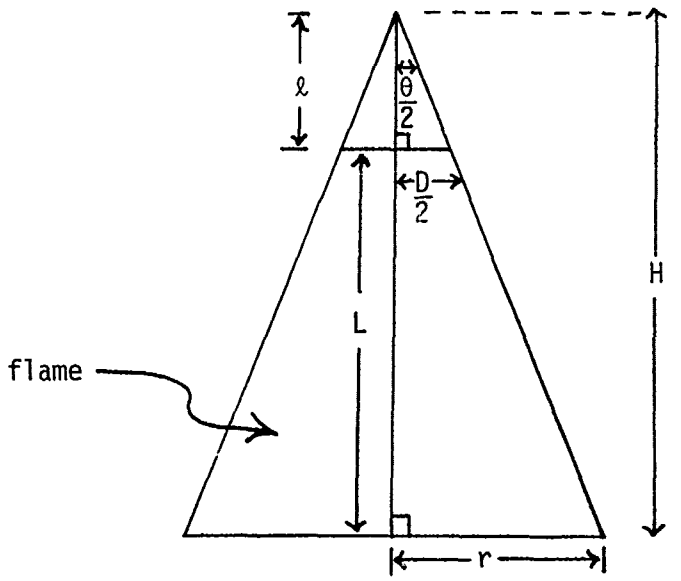
PRECEDING PAGE BLANK-NOT FILMED

flame temperature of stoichiometric mixtures." The values appearing in the properties files, used in subroutine FLJET, appear to be experimental values, which are generally 100°C to 300°C less than the theoretical values called for. For example for LNG the properties file contains ADFLM = 1875, while the theoretical adiabatic flame temperature for methane is 2012°C (experimental is 1885°C).

APPENDIX 4C

DERIVATION OF EQUIVALENT CYLINDER

The derivation of AMSHAH equation (6.3) is given below.



Surface area of the total cone $= \pi r\sqrt{r^2 + H^2}$

$= \pi r H \left[1 + \frac{r^2}{H^2}\right]^{1/2}$

$= \pi r H \left[1 + \tan^2 \frac{\theta}{2}\right]^{1/2} = \pi r H \sec \frac{\theta}{2}$

Surface area of the flame $= \pi r H \sec \frac{\theta}{2} - \pi\left(\frac{D}{2}\right) \ell \sec \frac{\theta}{2}$ (4C-1)

Now, from geometric similarity,

$$\frac{r}{D/2} = \frac{L+\ell}{\ell}$$

and

$$\frac{D/2}{\ell} = \tan \theta/2$$

which implies that

$$\ell = (D/2)\text{Cot } \theta/2$$

This gives

$$\frac{r}{D/2} = \frac{L + (D/2)\text{Cot } \theta/2}{(D/2)\text{Cot } \theta/2}$$

or

$$r = \frac{L + (D/2)\text{Cot } \theta/2}{\text{Cot } \theta/2} \qquad (4C\text{-}2)$$

Also,

$$H = L + \ell = L + D/2 \text{ Cot } \theta/2 \qquad (4C\text{-}3)$$

Thus, substituting (4C-2) and (4C-3) into (4C-1) gives

$$\text{Surface area of flame} = \pi \sec \theta/2 \left[(L + (D/2)\text{Cot } \theta/2)\right.$$
$$\left.(L \tan \theta/2 + D/2) - D/2 \cdot D/2 \text{ Cot } \theta/2\right] \qquad (4C\text{-}4)$$

This is to be equated to the surface area of an equivalent cylinder. We have,

$$\text{Surface area of cylinder} = \pi D_e L \qquad (4C\text{-}5)$$

where D_e is the diameter of the equivalent cylinder. Equating the right-hand sides of (4C-4) and (4C-5) gives:

$$\frac{D_e}{D} = \sec \theta/2 \left[(1/D + 1/2L \text{ Cot } \theta/2)(L \tan \theta/2 + D/2)\right.$$
$$\left. - D/2 \cdot 1/2L \text{ Cot } \theta/2\right]$$
$$= \sec \theta/2 \left[L/D \tan \theta/2 + 1/2 + 1/2 + D/4L \text{ Cot } \theta/2\right.$$
$$\left. - D/4L \text{ Cot } \theta/2\right]$$
$$= \sec \theta/2 \left[1 + L/D \tan \theta/2\right] \qquad (4C\text{-}6)$$

or

$$\frac{D_e}{D} = [\sec \theta/2 + L/D \sin \theta/2 \sec^2 \theta/2] \qquad (4C\text{-}7)$$

which is AMSHAH equation (6.3).

This indicates that an equivalent diameter of the cylinder is calculated by equating the surface area of the cylinder (with the height equal to the height of cone) and that of the cone.

APPENDIX 4D

COMPARISON OF THE FLAME HEIGHT MODEL TO FIELD DATA

The following discussion pertains to pool burning. The measurements of May and McQueen [19], as given in their Table V, along with L/D ratios calculated with AMSHAH equation (6.4) are tabulated below. The calculations for one observation (burning rate, 16,300 BBL/D) are also given. The measurements were made on LNG fires.

Burning rate, BBL/D	Height, ft $(L)_{exp}$	Length, ft $(D)_{exp}$	$(\frac{L}{D})_{exp}$	$(\frac{L}{D})_{cal}$	% Deviation
16,300	80	70	1.1428	0.917675	19.7
19,000	79	79	1.000	0.83795	16.2
40,000	88	92	0.9565	1.046	9.35

% Deviation = ABS $[(\frac{(L/D)_{exp} - (L/D)_{cal}}{(L/D)_{exp}}) \times 100]$, where ABS means the absolute value

The percent deviations go up to about 20%. May and McQueen have stated that the values of L and D actually varied somewhat above and below the values listed by them. No quantitative estimate of this variation in flame size is given by them.

The measurements of May and McQueen [19] were also correlated by the equations (G-7) or (G-8) (whichever was applicable) of Atallah and Raj [18]. The equations are:

$$\frac{L}{D} = \left(\frac{\dot{m}''}{\rho_a\sqrt{gD}}\right)^{-0.19} U^{*0.06} \qquad \text{for } U^* \geq 1 \qquad \text{(G-7)}$$

$$\frac{L}{D} = \left(\frac{\dot{m}''}{\rho_a\sqrt{gD}}\right)^{-0.19} \qquad \text{for } U^* \leq 1 \qquad \text{(G-8)}$$

where

$U^* = U/U_C$ and

U = wind velocity

U_C = characteristic velocity = $\left[\frac{\dot{m}''}{\rho} gD\right]^{1/3}$

D = diameter of dike

$\dot{m}''$ = burning rate in mass units

The results of applying these equations are tabulated below:

Wind mph	Burning rate, BBL/D	Height, ft, $(L)_{exp}$	Length, ft, $(D)_{exp}$	$(L/D)_{exp}$	$(L/D)_{cal}$	% Deviation
9	16,300	80	70	1.1428	3.29	187
5	19,000	79	79	1.000	3.385	238.5
12	40,000	88	92	0.9565	3.212	235.8

Obviously, Thomas' correlation yields better results.

The following data about the pool burning of gasoline have been taken from Hertzberg [8]. The flame sizes are given in his Table 2, while the burning rates have been read from his Figure 3. It is not possible to read L/D values corresponding to the pool diameter of 1 cm x 300 cm. L/D has been calculated using Thomas' equation.

Burning rate cm/min	Pool diameter cm $(D)_{exp}$	Flame height, cm $(L)_{exp}$	$(L/D)_{exp}$	$(L/D)_{cal}$	% Deviation
	1	13			
.15	10	50	5	3.192	36
.25	30	97.5	3.25	3.108	4.3
.42	100	210	2.10	2.95	40.4
	300	520			

The results that are given below use the same observed data as above, but the values of $(L/D)_{cal}$ have been obtained with the equation taken from Atallah and Raj.

Burning rate, cm/min	Pool diameter, cm $(D)_{exp}$	Flame height, cm $(L)_{exp}$	$(L/D)_{exp}$	$(L/D)_{cal}$	% Deviation
	1	13			
.15	10	50	5	2.23	55.4
.25	30	97.5	3.25	2.25	30.8
.42	100	210	2.10	3.40	61.9
	300	520			

Once again, the better fit provided by Thomas' equation is verified.

CHAPTER 4 - LIST OF SYMBOLS

$A = \frac{U}{U_c}$

B = defined by equation (4-30)

$C = \frac{1}{\left[1+r\left(\frac{Mf}{Ma}\right)\right]}$

C = time-mean model concentration of nozzle fluid in sample reduced to its unreacted constituents; empirical constant

$C^* = C\,(1-\rho_n/\rho_s)$

d = port diameter (cm)

D = jet diameter (cm)

D_e = equivalent diameter of right cylindrical flame envelope (cm)

f = L/D

F_r' = Froude number

g = gravitational acceleration (cm/s^2)

K = kinematic momentum (cm^4/s^2)

$K_1 = \frac{K_f}{C}$

$K_2 = C$

$K_3 = \left(\frac{1-C}{\alpha}\right)\frac{Ma\ Tf}{Mf}$ (°K)

K_f = factor depending on Froude number

ℓ = axial length along cone (cm)

L = length of conical flame; length of equivalent cylindrical flame (cm)

$\dot{m}''$ = burning rate ($g/s\ cm^2$)

PRECEDING PAGE BLANK-NOT FILMED

M_a = molecular weight of air (amu)

M_c = $(\rho v^2)_{wind}$ (g/cm s^2)

M_f = molecular weight of fuel (amu)

M_p = $(\rho v^2)_{jet}$ (g/cm s^2)

r = radial distance measured from jet axis (cm)

R = nozzle radius (cm)

R_e = Reynolds number

S = sensitivity coefficient

T_f = adiabatic flame temperature (°K)

T_o = ambient air temperature (°K)

U = jet velocity; defined in equation (4-7); wind velocity (cm/s)

U_c = centerline velocity (cm/s)

U_o = gas velocity (cm/s)

U^* = U/U_c

v_o = escape speed (cm/s)

V = jet velocity at the nozzle (cm/s)

w_o = rate of outflow (g/s)

x = distance along jet axis (cm)

y = distance measured normal to jet axis (cm)

y_b = value of y at edge of jet (cm)

y_f = half-width of cone base (cm)

$$Y = \left(\frac{Rg}{v^2 \tan \theta}\right)^{1/5} \frac{y_b}{R}$$

$$Y' = Y/(1-\rho_n/\rho_s)^{2/5}$$

Greek symbols:

α = stoichiometric ratio of moles of reactants to moles of products

ε_o = $0.0161\sqrt{K}$ (cm^2/s)

η = $\frac{1}{4}\sqrt{\frac{3}{\pi}}\frac{\sqrt{K}}{\varepsilon_o}\frac{r}{x}$

θ = half angle of conical flame envelope (degrees)

ν = kinematic viscosity of the flame (cm^2/s)

ξ = $\sigma\frac{y}{x}$

ρ = fluid density (g/cm^3)

ρ_a = density of air (g/cm^3)

σ = 7.67

Subscripts:

S = surrounding fluid

N = nozzle fluid

CHAPTER 4 - REFERENCES

[1] Department of Transportation, U.S. Coast Guard, Assessment Models in Support of the Hazard Assessment Handbook (CG-446-3), CG-D-65-74, January 1974.

[2] Arthur D. Little, Inc., Hazard Assessment Computer System, User Manual (HACS), Cambridge, Mass., December 1974.

[3] Hawthorne, W. R., D. S. Weddell, and H. C. Hottel, "Mixing and combustion in turbulent gas jets," pp. 266-280, in Third Symposium on Combustion, Flame and Explosion Phenomena, William and Wilkins, Baltimore, 1949.

[4] Hottel, H. C., "Burning in laminar and turbulent fuel jets," pp. 97-113, in 4th International Symposium on Combustion, 1953.

[5] Thomas, R. H., "The size of flames from natural fires," pp. 844-859, in 9th Symposium (International) on Combustion, Academic Press, New York, 1963.

[6] Atallah, S., and D. S. Allan, "Safe separation distance from liquid fuel fires," Fire Technol. 7(1):47-56, 1971.

[7] Welker, J. R., H. R. Wesson, and C. M. Sliepcevich, "LNG spills - to burn or not to burn," paper presented at Distribution Conference, Operating Section, American Gas Association, Philadelphia, May 12-15, 1969.

[8] Hertzberg, Martin, "The theory of free ambient fires. The convectively mixed combustion of fuel reservoirs," Combust. Flame 21:195-209, 1973.

[9] Welker, J. R., and C. M. Sliepcevich, The Effect of Wind on Flames, Tech. Rep. No. 2, Contract OCD-OS-62-89, University of Oklahoma Research Institute, Norman, Oklahoma, November 1965.

[10] Thompson, P. A., Compressible-Fluid Dynamics, ch. 3, McGraw-Hill, New York, 1972.

[11] Seeger, P. G., "On the combustion and heat transfer in fires of liquid fuels in tanks," ch. 3, p. 101, P. L. Blackshear (ed.), Heat Transfer in Fires, Scripta Book Co., Washington, D.C., 1974.

[12] Lewis, B., and G. Von Elbe, Combustion, Flames and Explosions of Gases, p. 550, Academic Press, New York, 1951.

[13] Williams, F. A., Combustion Theory, ch. 7, Addison-Wesley Publ. Co., Reading, Mass., 1965.

PRECEDING PAGE BLANK-NOT FILMED

[14] Schlichting, H., Boundary-Layer Theory, 6th ed., pp. 699-700, McGraw-Hill, New York, 1968.

[15] Douglas, J. F., and R. S. Neve, "Investigation into the behavior of a jet interaction proportional amplifier," paper C3, pp. C3-29 to C3-50, Proceedings of 2nd Cranfield Conference on Fluidics, B.H.R.A., Cranfield, January 1967.

[16] Blackshear, Perry L. (ed.), Heat Transfer in Fires, Wiley, New York, 1974.

[17] Yokoi, S., Japan Ministry of Construction, Building Research Institute, Report No. 29, 1959.

[18] Atallah, S., and P. P. K. Raj, "Radiation from LNG fires," LNG Safety Program Interim Report on Phase II Work, American Gas Association, Project IS-3-1, July 1, 1974.

[19] May, W. G., and W. McQueen, "Radiation from large natural gas fires," Combust. Sci. Technol. 7:51-56, 1973.

[20] Welker, J. Reed, "Radiant heating from LNG fires," LNG Safety Program Interim Report on Phase II Work, American Gas Association, Project IS-3-1, July 1, 1974.

[21] University Engineers, Inc., Radiant Heating from LNG Fires, Report to Battelle Columbus Laboratories, August 1973.

[22] Burgess, D., J. Biordi, and J. Murphy, Hazards of Spillage of LNG into Water, p. 3, App. I, NTIS AD 754-498, September 1972.

CHAPTER 5

THERMAL RADIATION FROM FLAMES MODEL

INTRODUCTION

The Thermal Radiation from Flames Model is designed to compute the total direct thermal radiation flux from a burning cargo to any exposed area which is near the fire. This model corresponds to the documentation in Chapter 7, Thermal Radiation from Flames, of the Assessment Models in Support of the Hazard Assessment Handbook (AMSHAH) [1]. The corresponding computer code in the Hazard Assessment Computer System (HACS) [2] is under the executive subroutine MODB2 which utilizes the following computational subroutine: JHHRF.

The factors influencing the total direct thermal radiation flux from a cargo fire to an adjacent area are the type and quantity of the cargo, the total flame area and height, the wind velocity, the atmospheric conditions at the site of the fire, and the orientation and distance of the area directly exposed to the flame. A fundamental assumption in modeling the flame is to treat the flame as a cylindrical inclined radiator of uniform temperature. The model will compute the total direct thermal radiation flux of fires for particular types of cargo by using estimated values of individual fire emission coefficients. Engineering estimates of flame temperatures are also utilized by the model along with the outputs of other models which give flame length, diameter and inclincation and the view factor between the radiator and the receptor. The atmospheric conditions at the site of the fire, in terms of the surrounding air temperature and relative humidity of water vapor, are used to determine the transmissivity of the intervening space between the fire and the exposed area. The symbols and references are listed at the end of this chapter.

A major problem encountered while trying to use the computer codes in HACS for the models developed in AMSHAH was that the methods developed in AMSHAH for the determination of flame emissivity and atmospheric transmissivity were not the same as those coded in HACS. The values utilized in HACS were oversimplifications, using a constant value equal to unity when, in reality, the flame emissivity and atmospheric transmissivity are variable quantities dependent on the flame and atmospheric characteristics.

ASSUMPTIONS AND APPROXIMATIONS

Various assumptions and approximations, both explicit and implicit, have been made in the modeling and calculations of the Thermal Radiation

---

[1] Department of Transportation, U.S. Coast Guard, Assessment Models in Support of the Hazard Assessment Handbook (CG-446-3), CG-D-65-74, January 1974.

[2] Arthur D. Little, Inc., Hazard Assessment Computer System, User Manual (HACS), Cambridge, Mass., December 1974.

from Flames Model developed in AMSHAH and in HACS.

The assumptions in AMSHAH are:

1. The shape of the flame is cylindrical.

2. The flame is at a uniform temperature.

3. The burning rate of the flame is constant over the total duration of the fire.

4. The radiation processes are invariant.

5. Flame shape, temperature, burning rate, radiant thermal flux, emissivity, and atmospheric transmissivity are invariant for the duration of the burn.

6. The radiant heating of the receptor is only due to the direct radiation from the flame and radiant heating by reflections is negligible.

Additional implicit assumptions in HACS are:

7. The emissivity of the flame is at its maximum attainable value of unity.

8. The transmissivity of the intervening atmosphere is at its maximum attainable value of unity.

9. The incident radiant flux and not the absorbed heat flux is calculated.

10. The amount of solar thermal energy flux on the receptor is constant at 300 Btu hr^{-1} ft^{-2}.

In the following a brief discussion of the implications and physical realism of these assumptions is presented.

1 Cylindrical Flame Shape Assumption. The shape of the flame is dependent on the source of the flame, the turbulence within the flame, the wind velocity, the type of fuel, the products of combustion, and the rate of fuel consumed. When the flame is due to an expanding jet of fuel from a hole, the shape of the flame is approximately conical with the vertex at the source. The conical shaped flame is approximated to an equivalent cylindrical shaped flame - in terms of the radiating surface area - of the same length as the cone but of an equivalent diameter. The equivalent diameter is computed on the basis of the derivation in the appendix of Chapter 4 of this report. When the flame is due to a spill and when there is a pool of burning fuel, the shape of the flame is dependent on the shape of the spill.. A cylindrical shape is assumed for fires whose dimensions are "reasonably regular," i.e. if the ratio of the longest dimension along

a straight side of the fire is not more than about four times the shortest side. The equivalent diameter of these fires is the hydraulic diameter which is

$$\text{Hydraulic Diameter} = \frac{4 \times (\text{area of base of fire})}{\text{perimeter of base of fire}}$$

Flames that are not "reasonably regular" are not analyzed in AMSHAH.

The assumption of a cylindrical flame shape has additional implicit assumptions. One of these is that the view factor between the actual flame and the receptor is the same as the view factor between the equivalent cylindrical flame and the receptor, for any angle of inclination of the flame and for any distance of the receptor from the flame. In reality the view factor between two surfaces is dependent on the true shape of the radiator, different shapes of the radiators having different characteristic curves for view factors versus distance of receptor from radiator. The assumption of the equivalent cylinder would give the same view factor at a particular distance - when the view factor characteristics of the true flame and the equivalent cylindrical flame are matched - but the equivalent cylinder approach would change the characteristic curve of the actual flame to that of a cylindrical flame. It is to be noted that at distances far away from the flame, the asymptotic behavior of most flame shapes for the view factor versus distance of receptor from radiator would be identical for equal total projected surface areas.

2. Uniform Flame Temperature Assumption. Throughout the extent of the flame, the temperature is not constant and large temperature gradients exist both radially and vertically within a flame. When modeling the flame in AMSHAH, a constant flame temperature has been used and the variations in the temperature are neglected. For large fires, this assumption of constant flame temperature can approximate reality quite closely.

3. Constant Burning Rate Assumption. The fuel burning rate of liquid fuel had been measured experimentally [3] for fuel in soil dikes with heat transfer to the fuel from the ground and from the flame. The experiments had indicated a fairly constant fuel regression rate over a large portion of the total burning time (Figure 5-1). The data during the period of constant regression rate were further analyzed and the regression rates were plotted against the average wind speed. No significant effect of wind speed on the burning rate was determined (Figure 5-2). In experiments conducted

---

[3] American Gas Association, LNG Safety Program, Interim Report on Phase II Work, Project IS-3-1, July 1974.

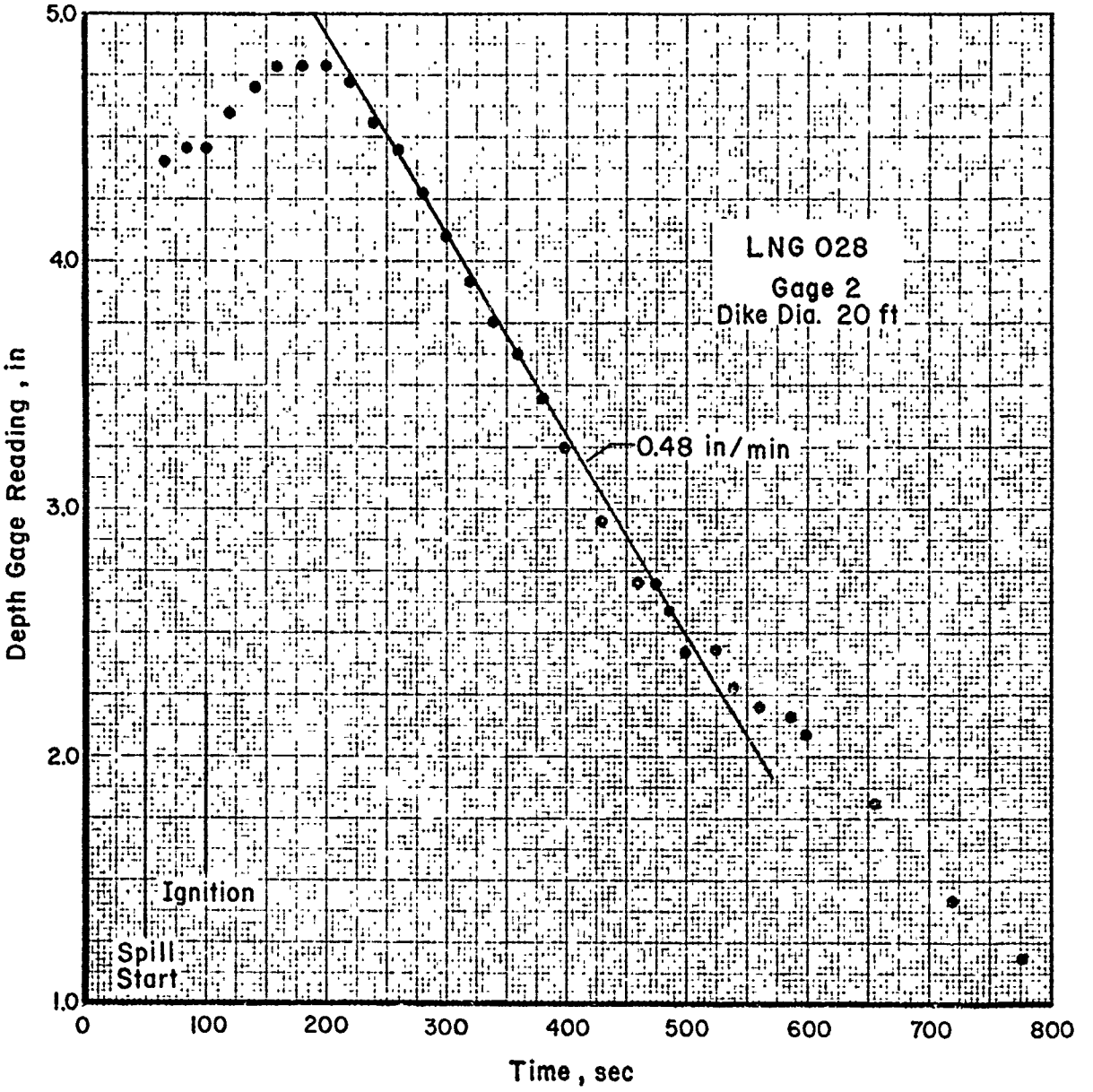


FIGURE 5-1 Typical depth gage record [3].

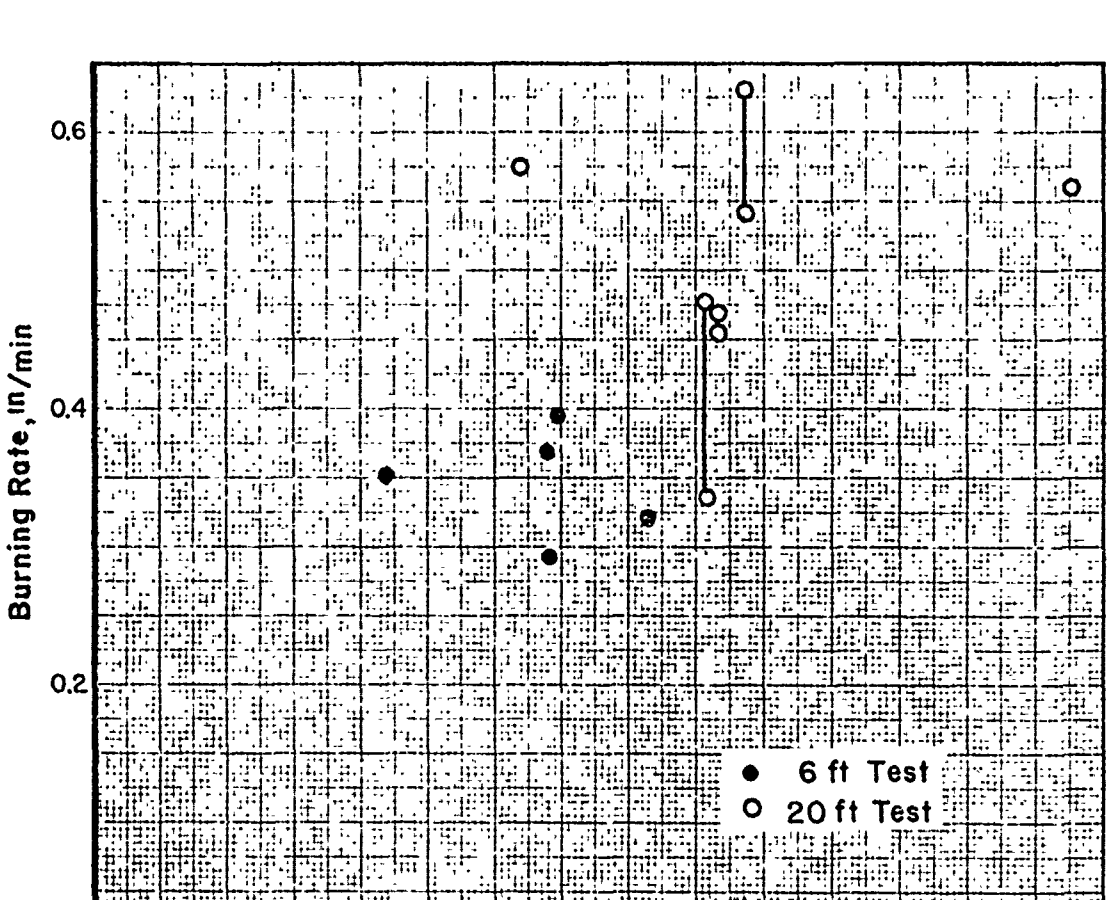


FIGURE 5-2 Effect of wind on burning rate [3].

separately, Burgess et al. [4, 5] had also come to the conclusion that there was not significant correlation between the wind speed and the regression rate of the fuel. From these experimental results, the constant burning rate assumption in AMSHAH appears to be valid.

4. Temporal Invariance of Radiation Processes Assumption. The thermal radiation flux from the flame is constantly changing with time, being dependent on the type of fuel, the amount of mixing and turbulence, the gustiness of the winds, and the particular distillation fraction being burnt. The model in AMSHAH for the total thermal radiation flux does not consider these variables and it computes a constant value for the flux when a flame of a particular temperature, size, and inclination to the vertical are specified.

5. Temporal Invariance of Flame Shape, Temperature, etc. The shape of the flame is constantly changing with time because the shape is dependent, at any location, on changing quantities such as the fuel-air mixture variations, the wind gustiness, the turbulence, the shape of the spill, etc. While modeling the flame shape, AMSHAH utilizes an equivalent flame shape which would be of constant shape, when the spill shape and the wind velocity are known.

6. Negligible Reflections Assumptions. The model developed in AMSHAH considers only direct heating of the receptor from the radiations of the flame. The receptor could also receive thermal radiation from large neighboring objects which might be heated directly by the flame and may therefore reradiate thermal energy. The amount of indirect thermal radiation flux received by the receptor would depend to a large extent on the surroundings of the fire and the receptor. For flat terrain and especially for fires over water, this component of radiant thermal flux would appear to be negligible.

7. Unit Emissivity Assumption. AMSHAH models the emissivity by utilizing κ, the emission coefficient, and the thickness dimension of the flame. This formulation is based on the work done by Love [6] on laminar diffusion flames utilizing the gradient of monochromatic radiation intensity

---

[4] Burgess, D., and M. G. Zabetakis, Fire and Explosion Hazards Associated with Liquefied Natural Gas, Bureau of Mines, U.S. Department of the Interior, RI 6099, 1962.

[5] Burgess, D., and M. Hertzberg, "Radiation from pool flames," pp. 413-430, in N. H. Afgan and J. M. Beer (eds.), Heat Transfer in Flames, John Wiley & Sons, New York, 1974.

[6] Love, T. J., Radiative Heat Transfer, Merrill Publishing Co., Columbus, Ohio, 1968.

at a point with respect to the length of travel within the flame, and the ratio of J_λ, the monochromatic volumetric emission coefficient to β_λ, the monochromatic extinction coefficient at a particular wave length, λ. These coefficients are dependent on the fuel composition which is burning at that particular time. The fuel composition for liquid fuels changes as burning continues because different fractions of the fuel burn at different rates and hence are consumed at various rates thereby continuously changing the composition of the fuel. The overall expression for κ is dependent on the flame shape and the monochromatic flux radiated over all wave lengths and the ratio of J_λ to β_λ. The last ratio is assumed constant for all sizes of flames of any particular fuel in AMSHAH and this gives the constant value for κ for a particular type of fuel. In the actual computer code for the flame emissivity the value of unity is assigned to the emissivity of all flames, unity being the maximum value that the emissivity can attain; hence computed heat flames from the flame are expected to be higher than what would be expected from experimental measurements of the heat fluxes.

8. Unit Transmissivity Assumption. The thermal radiation flux from the flame is partially attenuated before reaching the receptor by absorption and scattering along the intervening path by water vapor, carbon dioxide, dust, and aerosol particles. This reduction of the thermal radiation flux is expressed by the transmissivity of the intervening medium. In AMSHAH only the attenuation due to water vapor is considered. An average transmissivity coefficient was developed by utilizing the transmissivity and emissive power of the source at wave numbers from zero to infinity. This value of the transmissivity depends on the partial pressure of water vapor, the line intensity of the radiant flux, the line attenuation coefficient, the separation distance of the spectral lines, and the line half-width at wave number ω. The values of the above parameters are nearly constant for particular environmental conditions and these are assumed not to change when the flame is burning. HACS uses the maximum possible value of the transmissivity, unity, in the computer coding of the subroutine. This maximum value for the transmissivity would give a higher simulated value of the thermal radiant flux received by the receptor, when compared with what would be expected with correct values of transmissivities.

9. Incident Radiation Flux Assumption. The absorptivity of a surface is the fraction of the incident radiation absorbed by the receptor and this ratio is dependent on the surface characteristics of the receptor. The model developed in AMSHAH utilizes the absorptivity of the receptor and uses it with its maximum possible value of unity. Hence the simulation in AMSHAH would give a higher absorbed radiant thermal flux than what would be measured. It should be noted that in the computer coding of HACS, the Incident Thermal Radiant Flux, is computed and not the Absorbed Thermal Radiant Flux; hence HACS does not use absorptivity in its computations.

10. Constant Solar Heating Assumption. The solar thermal energy flux on any receptor is dependent on the orientation of the receptor with respect to the sun, the time of the day, the day of the year, the location of the receptor on earth (latitude) and the environment at the time of the fire. The effects of solar radiation on the model in AMSHAH are not considered. HACS adds 300 Btu hr^{-1} ft^{-2} to the total thermal radiation flux received by the receptor to account for solar radiation. The solar constant is 442 Btu hr^{-1} ft^{-2}, this being the rate at which solar energy impinges upon a surface of unit area placed normal to the sun at the outer fringes of the earth's atmosphere. The value of 300 Btu hr^{-1} ft^{-2} for the solar radiation is reasonable as this is the solar radiation that would be expected on the latitudes of most of North America on clear summer days.

ERRORS AND INCONSISTENCIES

Differences Between AMSHAH and HACS

There are many differences in the documentation of the models presented in AMSHAH and the computer code of HACS. Models which were developed at length in the documentation of AMSHAH for computing the variable values of parameters are not computer coded in HACS. Instead HACS generates internal constant values - in one computer statement - for the variable valued parameters. These parameters are the flame emissivity and the transmissivity of the intervening medium. In one of the models - for the transmittance of the environment - the method discussed at length in the text is different from the method outlined in the flow chart accompanying the description.

The following are specific methods developed in AMSHAH. The emissivity of the flames from a burning cargo is computed by utilizing the flame emission coefficient for the particular cargo and the characteristic flame diameter, assuming the flame to be cylindrical in shape. This model is developed in the documentation of AMSHAH where the equation for the emissivity is:

$$\varepsilon_f = 1 - \exp\,[-\kappa D]$$

where

ε_f = flame emissivity
κ = attenuation coefficient
D = diameter of flame

The analysis shown above for determining the flame emissivity, which is documented in AMSHAH, is not utilized in the computer coding (subroutine JHHRF) of HACS. HACS just has one computer statement stating that the flame emissivity is unity. The implication of making the flame emissivity a constant at unity would be to make the flame emissivity independent of

the attenuation of the thermal radiant flux within the flame and also independent of the flame diameter.

The transmissivity of the intervening space between the flame and the receptor is dependent on the attenuation of the thermal heat flux by absorption and scattering by water vapor, carbon dioxide and dust particles. Only the attenuation caused by water vapor is considered in AMSHAH. The model developed in AMSHAH determines the transmissivity, τ_ω, of water vapor for a thermal radiation of wave number, ω, from the mean integrated line intensity s_ω; the mean distance of separation of spectral lines of wave number ω, d_ω; the mean line half width at wave number ω, b_ω; the integral U of partial pressure of water vapor along the length of travel between the flame and receptor; and the attenuation coefficient for a single line centered at ω, κ_ω. This relationship is given in AMSHAH for the transmissivity for a radiation of wave number ω by the following equation:

$$\tau_\omega = \exp\left[\frac{-\left(\frac{s_\omega}{d_\omega}\right) U}{\sqrt{1 + \left(\frac{s_\omega}{4\ b_\omega}\right) U}}\right]$$

The model in AMSHAH uses τ_ω and the emission power E_ω of the source at wave number ω to determine an average transmittance τ_{avg} given by:

$$\tau_{avg} = \frac{\int_o^\infty \tau_\omega\ E_\omega\ d\omega}{\int_o^\infty E_\omega\ d\omega}$$

where

$$E_\omega = C_1 \left(\frac{\omega}{T_f}\right)^3 \Big/ \left[e^{\left(\frac{C_2\omega}{T_f}\right)} - 1\right]$$

C_1 = First Planck constant = 3.7418×10^{-16} w/m

C_2 = Second Planck constant = 1.4388×10^{-2} m°K

T_f = Flame temperature, °K

It should be noted that the average transmittance as developed in the AMSHAH model utilizes an integration of the expression for wave number variation from zero to infinity.

Unfortunately the method in HACS (subroutine JHHRF) does not use the elaborate model developed in AMSHAH. The transmissivity is made equal to unity by a statement in the computer program.

AMSHAH also has a flow chart for determining the water vapor transmissivity in which a completely different method is developed, using the partial pressure of water vapor, the temperature of the flame, the atmospheric temperature, and the absorptivity - obtained from Lagrangian interpolation from a water vapor absorption table. This flow chart in AMSHAH is not documented in the text of AMSHAH and is not used in the computer coding for the transmissivity. The procedure for calculations of the water vapor transmissivity as indicated in the flow chart is first to calculate the water vapor partial pressure with the distance from the flame to the receptor X, to obtain the product Y. The value of Y is then utilized in a table lookup (using Lagrangian interpolation) to determine the standard absorptivity α'. Then the actual absorptivity, α, is calculated by [7]

$$\alpha = \alpha' \left(\frac{T_a}{T_s}\right)^{0.45}$$

where

T_a = air (ambient) temperature, absolute
T_s = flame (source) temperature, absolute

The transmissivity τ, is given by:

$$\tau = 1 - \alpha$$

In the computer coding of HACS, the effect of solar heating has been incorporated at a constant value of 300 Btu hr^{-1} ft^{-2}. This has not been documented in the text of AMSHAH.

The Thermal Radiation from Flames Model computes the radiant heat flux from a flame to the surface of a receptor. Not all the radiant energy on a surface is absorbed by the receptor as some of the energy is reflected or scattered. The model developed in AMSHAH does take into account the effect of the absorptivity of the receptor but no mention is made in the computer coding in HACS of the absorptivity of the receptor. Hence the model developed in AMSHAH would compute the total radiant heat transfer to the receptor, whereas the computer coding of HACS would compute only the total radiated heat flux incident on the receptor. This omission of the absorptivity in determining the total radiant thermal flux absorbed by a receptor does not affect the damage criteria because the damage criteria are based on the incident flux on a receptor and not the absorbed flux of the receptor. If the absorbed thermal flux is to be determined by HACS,

---

[7] Hottel, H. C., and A. F. Sarofim, Radiative Transfer, p. 231, McGraw-Hill, New York, 1967.

the absorptivities of various types of receptors can be incorporated in the computer coding in HACS and the absorbed thermal flux can then be computed.

Coding Errors

Our review did not uncover any coding errors in the subroutine JHHRF, which is used to compute the thermal radiation from flames.

Typographical Errors

Typographical errors are listed in Appendix 5A.

Error in Analysis Model for AMSHAH

The transmissivity of water vapor is determined by two methods in AMSHAH. The method depicted in the flow chart on page 78 of AMSHAH, seems to be in error.

The method in the flow chart first calculates the partial pressure of water vapor, p_{H_2O}. This partial pressure is then multiplied by the distance of thermal radiation travel in the gas medium, during which the thermal radiation is attenuated to give the product Y, where $Y = X \cdot p_{H_2O}$. Then the modified absorptivity, α', is obtained by Lagrangian interpolation from the Water Vapor Absorption Table for the Y value calculated above. This absorptivity is further modified to obtain the true absorptivity α of the medium by water vapor, by utilizing the ratio of the temperature of the atmosphere T_a, and the temperature of the source T_s. The relation given in the flow chart of AMSHAH is:

$$\alpha = \alpha' \left[\frac{T_a}{T_s}\right]^{0.45} \tag{5-1}$$

Finally the transmissivity τ of the medium is calculated by:

$$\tau = 1 - \alpha \tag{5-2}$$

The method developed in [6] is different from the method in AMSHAH. The main difference is that the relationship given in (5-1) is not between absorptivities but is the relation for converting the gas emissivity ε into the gas absorptivity α. The equation (5-1) should have read:

$$\alpha = \varepsilon \left[\frac{T_a}{T_s}\right]^{0.45} \tag{5-3}$$

Another difference is that the emissivity ε should be determined from the temperature of the source, T_s, and from the product $[p_{H_2O}X(T_s/T_a)]$. The product Y of AMSHAH is different from the product shown above.

ACCURACY ASSESSMENT

The accuracy of the simulation of the Thermal Radiation from Flames can be estimated by first investigating the accuracy of any analytical or empirical constants used in the modeling, then investigating how close the model is to experimental results when the conditions for both the model and the experiment are as close as possible, and finally investigating the realism of the model when the assumptions of the model are not adhered to in actuality.

The only physical constant that is used in HACS for the model is the Stefan-Boltzmann constant σ and this is known precisely. The value of σ correct to four significant figures [8] is 5.669×10^{-8} w/m^2 °K^4 or 0.1712×10^{-8} Btu hr^{-1} ft^{-2} R^4 and hence any error due to the value of σ would be of a low order of magnitude.

The exponent of 0.45 for the conversion of the emissivity of water vapor into the absorptivity of water vapor has been based on the experimental correlations done by Hottel [7], wherein the correlations have been substantiated by theoretical relations for the general structure of the relation between the absorptivity and the emissivity.

The following discusses how close the simulation is to experimental testing when the assumptions in the model are satisfied as closely as possible in the experiment.

The results computed by the existing subroutine JHHRF in the HACS will now be compared with the experimentally measured values for the total thermal radiant flux when the inputs to HACS are as close to the experimental conditions as is possible. The data used for comparison were developed in experiments carried out by University Engineers (UE) [3] and by May and McQueen (MMQ) [9]. Table 5B-1 of Appendix 5B gives the measured values of the radiant heat flux and the heat flux calculated by HACS for fires from LNG. The experiment was performed with a continuous metered flow of LNG to the burning pool and no wind blowing. The equivalent pool diameter for the input into HACS was obtained by utilizing an average fuel regression rate of 0.38 in/min. The values of the Heat Flux in the last column of the table are 16.4% of the Total Flux, as suggested by MMQ. It

---

[8] Siegel, R., and J. R. Howell, Thermal Radiation Heat Transfer, p. 738, McGraw-Hill, New York, 1972.

[9] May, W. G., and W. McQueen, "Radiation from large liquefied natural gas fires," Combust. Sci. Technol. 7:51-56, 1973.

should be noted that the time of the day when the experiments were carried out was either late in the evening or at night and hence the solar radiation of 300 Btu hr^{-1} ft^{-2} which is automatically added in the computer results of HACS has been subtracted and the modified calculated radiant heat flux is shown in the table. It should also be noted that the values of the flame emissivity and the transmissivity of the intervening space are taken as unity in the computer coding of HACS.

Comparison of the measured and calculated radiant heat flux shows that there is close agreement in the values of the model simulation and experimental measurements.

Based on values of the flame emissivity and medium transmissivity being their respective maximum values, we would expect that the simulated values of the thermal radiation flux would be greater than the measured values. The calculated fluxes are seen to be nearly equal to the experimental fluxes rather than greater than the experimental fluxes. On checking the subroutine SVIEW for the view factor determination, for vertical flames (no wind velocity), the results are equivalent to the analytical equation for the view factor given by Blackshear [10].

The flame emissivity, ε_f is given by:

$$\varepsilon_f = 1 - e^{-\kappa D}$$

where

κ = attenuation coefficient
D = flame diameter

From the values of κ given in Table 7-2 of AMSHAH for Alcohol and Gasoline, the values of the flame emissivities for 6-ft diameter pools and 20-ft diameter pools can be calculated to give:

	6-ft pool	20-ft pool
Alcohol flame emissivity	0.492	0.895
Gasoline flame emissivity	0.974	0.99999

As can be seen clearly from these calculated results, the flame emissivity is very close to unity for large fires of gasoline or other fuels with high values of the attenuation coefficient κ and for fuels of small values of the attenuation coefficient, the flame emissivity would approach the value of unity at very large fire dimensions. The experimental fires

---

[10] Blackshear, P. L. (ed.), Heat Transfer in Fires, p. 424, John Wiley & Sons, 1974.

were very large and hence taking the flame emissivity as unity would be approximately correct. The distance between the flame and the receptor is large (300 ft to 600 ft) and the transmissivity of the intervening medium would not be unity. For a relative humidity of 0.80 with a distance of 492 ft (150 meters) between the flame and the receptor and a flame temperature of 800°C, the absorptivity of water vapor in the intervening medium can be calculated to be 0.54 by first finding the product $p_{H_2O} \times (T_s/T_a)$, at which the emissivity of the water vapor is determined and then the emissivity is multiplied by $(T_a/T_s)^{0.45}$ to give the absorptivity. The transmissivity was calculated to be 0.46. The flame temperature used in HACS was 800°C and it is suggested that HACS should use a flame temperature for LNG of 900°C which would increase the thermal radiation flux from the flame by about 43%. This would bring the model closer to the experimental results and the model would also utilize the transmissivity of the intervening medium.

The effects of violating the assumptions of the model for thermal radiant flux from fires will now be determined. We note that in comparing the View Factor Model of AMSHAH and the view factors from analytical results, for the 6-ft and 20-ft fires, the view factors calculated from SVIEW do not agree with the view factors obtained from Rein, Sliepcevich and Welker [11]. The results are tabulated in Table 5B-2 of Appendix 5B of this chapter. In the calculations, for flame inclinations of 61.4° and 55.9°, the analytical results from Figure 5-3, for 60° inclination was used; for flame inclination of 45.1°, Figure 5-4, for 45° inclination was used; and for flame inclination of 32°, Figure 5-5 for 30° inclination was used. Good agreement for view factors cannot be expected under windy conditions between the calculated and analytical results because the calculated view factors from JHHRF are for inclined receptors inclined at the same angle as the flame whereas the analytical results are for receptors which are vertical. In all the tests for which the view factors were computed, the view factors obtained from SVIEW were less than the analytical values of the view factors.

The simulated data are compared with the experimental results of UE in what follows. The experiments conducted by UE were with LNG fires having diameters of 6 feet, 20 feet, and 80 feet; and LNG pools having dimensions of 20 feet square and 30 feet x 40 feet with the radiant thermal flux being measured at locations downwind, crosswind, and upwind to the flame. The computer coding of HACS calculated the thermal radiant flux

---

[11] Rein, R. G., C. M. Sliepcevich, and J. R. Welker, "Radiation view factors for tilted cylinders," J. Fire Flammability 1:140-153, 1970.

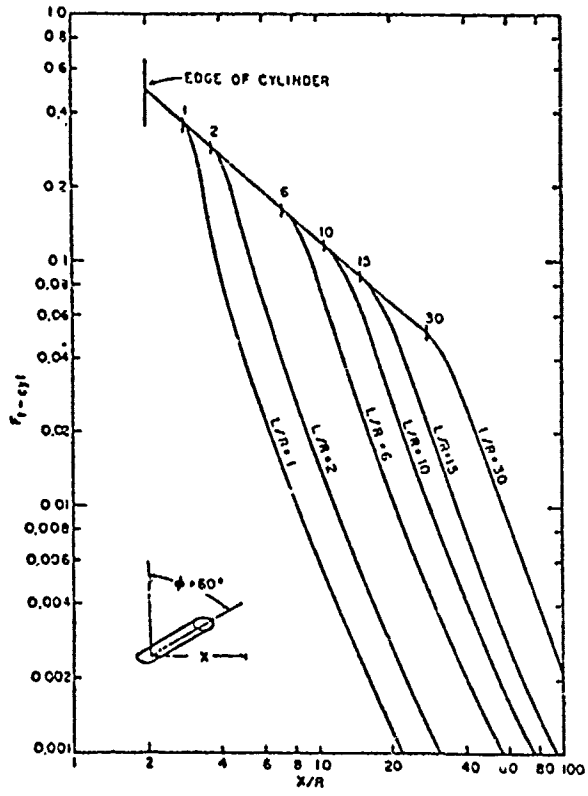


FIGURE 5-3 View factors for tilted cylinders: $\Phi = 60$ degrees [11].

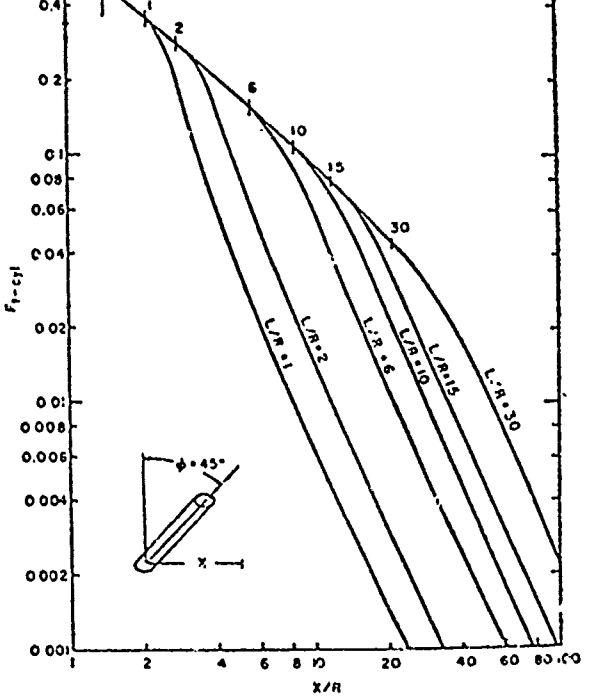


FIGURE 5-4 View factors for tilted cylinders: Φ = 45 degrees [11].

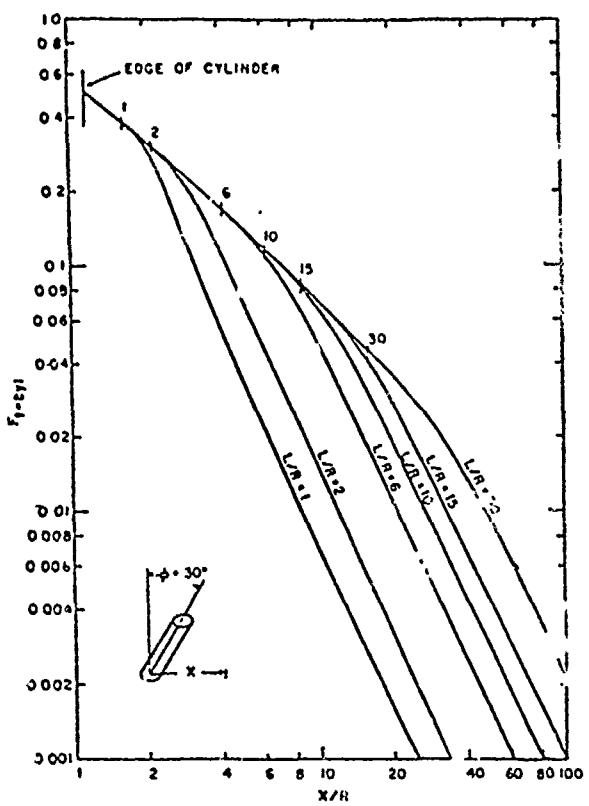


FIGURE 5-5 View factors for tilted cylinders: Φ = 30 degrees [11].

at positions only downwind of the flame. HACS also assumed the flame emissivity and atmospheric transmissivity as unity, whereas these would not be the values for the UE experiments. The distances and orientations of the radiometers with respect to the fire are given in Figure 5-6; the numeral stands for the distance in feet of the radiometer from the center of the flame and the letter denotes the position of the radiometer with respect to the wind direction. For example,24.00 D would stand for a radiometer situated 24 feet downwind from the LNG flame.

The experimental and the simulated results are tabulated in Tables 5B-3, 5B-4, 5B-5, and 5B-6. The values of the heat flux from the experiments are arithmetic average values for Tables 5B-5 and 5B-6. These tables are in Appendix 5B of this chapter.

For the 20-ft fire, the agreement between the calculated and observed values appears to be better; however, this agreement would be misleading if the values of the view factors are incorrect - at least, they do not agree with the view factors obtained from Rein, Sliepcevich and Welker.

For the 20-ft square pool, the calculated values of heat flux are less than the measured values in most of the tests. For the 30 x 40 ft pool, the calculated values are also less than the measured values in most of the tests.

The predicted values of the radiant heat flux for the 6-ft fire are in general greater than the experimentally measured values of the radiant heat flux.

In order to analyze further the data for the 6-ft and 20-ft fires, Tables 5B-7 and 5B-8 are calculated,

$$\% \text{ Error} = \left| \frac{\text{Value of ratio - Mean value of ratio}}{\text{Mean value of ratio}} \right| * 100$$

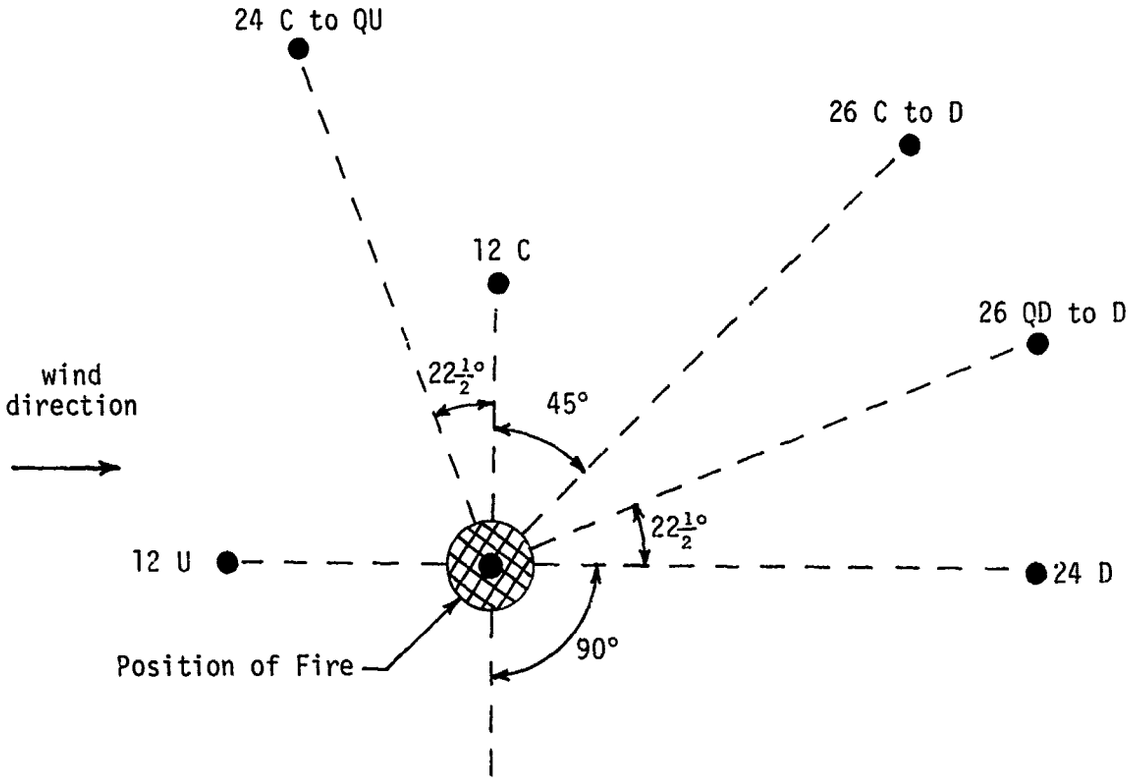
$$\% E_{max} = \text{Maximum of all \% Errors for a given column}$$

Under the subcolumn "Ratio," each value is a ratio of the calculated heat flux to the measured heat flux. The equation for the heat flux is

$$Q = F \tau \varepsilon \sigma T_f^4$$

The model in HACS assumes $\tau=1$, and $\varepsilon=1$. Therefore, this equation reduces to

$$Q = F \sigma T_f^4$$



C = Crosswind
D = Downwind
U = Upwind
C to D = Crosswind to Downwind
C to QU = Crosswind to Quartering Upwind
QD to D = Quartering Downwind to Downwind

FIGURE 5-6 Radiometer positions with respect to flame center and wind direction.

Let the subscripts p and c denote the predicted and the correct values of the quantitites. Then

$$\frac{Q_p}{Q_c} = \frac{F_p}{F_c} \left[\frac{T_{fp}}{T_{fc}}\right]^4 \times \frac{1}{\varepsilon_c \times \tau_p}$$

σ is the Stefan-Boltzman constant and it cancels out. If the view factor is correct, $F_p = F_c$ then we have,

$$\frac{Q_p}{Q_c} = \left[\frac{T_{fp}}{T_{fc}}\right]^4 \times \frac{1}{\varepsilon_c \times \tau_c}$$

For a flame of a given diameter, it is reasonable to assume that T_{fc} and ε_c remain constant for various test runs. Further, if changes in transmissivity are neglected for various runs for a given diameter of flame, Q_p/Q_c should be approximately constant. The measured values of heat flux for Q_c are used.

These tests were done during the day time and at different dates. Therefore the solar contribution to the measured heat flux is not known. Since some of the measured values are very small, the solar contribution in those cases were certainly less than 300.0 Btu hr^{-1} ft^{-2}. Because of solar contribution and the fact that heat flux at a given location does vary during the test, it is not possible to expect Q_p/Q_c to be a constant. However, Table 5B-7 shows that % E_{max} is much less if the view factors from Rein, Sliepcevich and Welker are used rather than when the heat flux is calculated using view factors obtained from the subroutine SVIEW. The same is true for the 20-ft fire in Table 5B-8, although the difference is pronounced for the 6-ft fire. For tests 023 and 026 the view factors were obtained using Figures 5-4 and 5-5, respectively. For tests 029, 030, and 032, Figures 5-4, 5-5, and 5-6 were used respectively for calculating the heat flux.

Q_p/Q_c is much greater for the 6-ft fire than for the 20-ft fire. This suggests that for the 6-ft fire the flame emissivity should be much less than unity. In addition, use of transmissivity of 1.0 may be an error since distances up to 150 ft are involved.

In order to determine the effect of variations in the heat flux radiated from a fire, the following analysis is carried out.

An average steady heat flux, A is assumed to exist - averaged over time - and a superimposed sinusoidal flux variation with time, of amplitude B, is applied to the steady flux. Hence the instantaneous total heat flux at any time can be expressed as the sum

$$A + B \sin z,$$

where z = dummy time variable.

The damage criteria I can be expressed as [12]

$$I = \frac{1}{\omega} \int_0^{2\pi} [A + B \sin z]^{4/3} \, dz$$

where ω = the frequency of the superimposed sinusoidal heat flux.

The damage criteria are determined by an integration of the total heat flux raised to the exponent (4/3), the integration interval being over a full cycle of the superimposed sinusoidal heat flux. The integration process is carried out by using a binomial expansion of the integrand and for a small amplitude of the superimposed sinusoidal heat flux as compared to the amplitude of the instantaneous total heat flux, that is for $|B| < |A|$. An approximate value of the integral is evaluated in Appendix 5C.

From the analysis, the relative change in the damage criteria is dependent on

$$\left[\frac{1}{9} \left(\frac{B}{A}\right)^2\right]$$

This expression was computed for the experimental values of heat fluxes and these are tabulated in Tables 5B-9 and 5B-10 of Appendix 5B for the 20-ft square fire and the 30 ft x 40 ft fire. The value of A was shown to be the average value of the incident radiant flux and the value of B was the maximum variation of this average value from the values of the incident radiant flux. As can be seen from the tabulated results, the maximum relative change in the damage criteria is 0.09 for the 20-ft square pool with the receptor at a distance of 40 ft from the flame edge and 0.02 for the 30 ft x 40 ft pool with the receptor at 107 ft from the flame edge. These variations are small and hence would give a maximum variation of 9% for the 20-ft square pool and a maximum variation of only 2% for the 30 ft x 40 ft pool. The lower values of these variations are 0.8% for the 20-ft square pool with the receptor at a distance of 26 ft from the flame edge and 0.04% for the 30 ft x 40 ft pool with the receptor at a distance of 101 ft from the flame edge. From the above analysis it is evident that the average radiant flux from a fire is a good estimate to use for the damage criteria.

SENSITIVITY ANALYSIS

For the Thermal Radiation from Flames Model, the relationship between the radiant heat flux Q (output), and the flame temperature, T_f,

---

[12] Eisenberg, N. A., C. J. Lynch, and R. J. Breeding, Vulnerability Model: A Simulation System for Assessing Damage Resulting from Marine Spills, CG-D-136-75, NTIS AD-A015245, Department of Transportation, U.S. Coast Guard, June 1975.

flame emissivity, ε_f, media transmissivity τ, and view factor F (inputs) is given by the relation:

$$Q = F\ \varepsilon_f\ \tau\ \sigma\ T_f^4$$

where σ is the Stefan-Boltzman constant. Differentiating the above equation, we obtain:

$$dQ = \varepsilon_f\ \tau\ \sigma\ T_f^4\ dF + F\ \tau\ \sigma\ T_f^4\ d\varepsilon_f + F\ \varepsilon_f\ \sigma\ T_f^4\ d\tau + 4T_f^3\ F\ \varepsilon_f\ \tau\ \sigma\ dT_f$$

$$\therefore\ \frac{dQ}{Q} = (1)\ \frac{dF}{F} + (1)\ \frac{d\varepsilon_f}{\varepsilon_f} + (1)\ \frac{d\tau}{\tau} + (4)\ \frac{dT_f}{T_f}$$

In the above equation, the relative change in Q (the output) is dependent on the relative change of each of the (input) factors on which Q is dependent and the effect on Q of each of the factors taken singly determines the sensitivity coefficient of that factor. These sensitivity coefficients are the coefficients of the relative change of the factors in the above equation and they are:

Sensitivity Factor	Theoretical Sensitivity Coefficient	Computer Sensitivity Coefficient
F	1	0.987
ε_f	1	0.987
τ	1	0.987
T_f	4	3.207

In HACS the equation for Q has insolation added to it as

$$Q = F\ \varepsilon_f\ \tau\ \sigma\ T_f^4 + 300\ \text{Btu hr}^{-1}\ \text{ft}^{-2}$$

Hence the sensitivity coefficients are modified and values obtained on the computer program are less than the theoretical values. The change of input flame temperature from °C to °R also affects the sensitivity coefficient for T_f and makes the sensitivity coefficient smaller.

Most of the variables have the same order of magnitude effect on the total sensitivity of the model but the flame temperature, T_f, has four times the influence of the other variables. Relative errors of the order of 10% in the flame temperature cause relative errors of about 40% in the predicted radiant heat flux. Since the sensitivity coefficients are of the order of magnitude of ~1 forall the variabies hence large errors in

the input variables should be avoided. The program as it now stands does not avoid these errors. The sensitivity coefficients as computed by a separate computer program are as expected.

In summary, this model is not exceptionally sensitive to any particular input variable, but the sensitivity coefficients are all of the same order of magnitude, thus large errors in input variables will be directly reflected in the output.

SUMMARY AND RECOMMENDATIONS

In summary, the model gives reasonable agreement with experimental data when the conditions of the experiment are close to the conditions assumed for model development; however, for the set of experimental data used here the close agreement between model and experiment may be the result of fortuitously compensating inaccuracies. In general, the inaccuracies of the modeling and the inaccuracies of the parametric values which are inputs to the model cannot be counted on to combine in an ameliorative manner; on the contrary, in general, these inaccuracies will add together to produce an inexact output. Consequently realistic results can only be assured if as many as possible of the inaccuracies in modeling and data input are eliminated. Among the refinements that should be incorporated into the computerized version of the model are:

- Calculation of flame emissivity based on flame size.
- Calculation of atmospheric transmissivity as a function of humidity.
- Supplying flame temperatures in the Chemical Properties File where they are currently missing.

APPENDIX 5A

TYPOGRAPHICAL ERRORS IN CHAPTER 7 OF ASSESSMENT MODELS (AMSHAH)

TERMS MISSING IN EQUATIONS

1. Page 74, equation (7.3). Subscript ω is missing with d in the equation for τ_ω, which should read:

$$\tau_\omega = \exp\left[\frac{-\left(\frac{s_\omega}{d_\omega}\right) U}{\sqrt{1+\left(\frac{s_\omega}{4b_\omega}\right)U}}\right]$$

2. Page 75, line 2. ω is missing at the end of the statement for τ_ω, which should read:

   τ_ω = transmissivity for a radiation of wave number ω.

3. Page 75, line 3. Subscript ω is missing with κ in the equation for s_ω which should read:

$$s_\omega = \int_{\omega' = -\infty}^{\infty} \kappa_\omega (\omega, \omega')\, d\omega'$$

4. Page 79, statement block for $S_f(I)$. π is missing in the denominator and the expression should be:

$$SF(I) = \left(\frac{\text{Cos } \theta_1 \text{ Cos } \theta_2}{\pi\, r^2}\right) dA_2$$

SYMBOLS NOT DEFINED IN LIST OF SYMBOLS, SECTION 7.11

1. ε used on pages:

   a. 74, equation (7.1)

   b. 74, first line after equation (7.1)

   c. 74, first line of section 7.5.1

   d. 74, equation (7.2)

   ε should be ε_f, the flame emissivity.

PRECEDING PAGE BLANK-NOT FILMED

2. T used on pages:

   a. 75, first explanation of E_ω after equation (7.4)

   b. 75, last equation

   c. 76, line 6 of section 7.7

   d. 77, second statement block

   e. 77, last output block

   In (c) and (e) T should be T_f, the flame black body temperature.

3. d used on page 74, equation (7.2)

4. τ_ω used on page 74, equation (7.3)

5. s_ω used on page 74, equation (7.3)

6. U used on page 74, equation (7.3)

7. ω' used on page 75, line 3 in the equation for s_ω

8. $\kappa(\omega,\omega')$ used on page 75, line 3 in the equation for A_ω

9. x used on page 75, line 7 in the equation for U

10. τ_{avg} used on page 75, equation (7.4)

11. A_2 used on page 76, equation (7.5)

12. $\overline{A}_2$ used on page 76, equation (7.5)

13. RH used on page 80, line 5

14. K used on page 81, line 3

15. Most symbols used in the flow charts on pages 78 and 79 are undefined.

APPENDIX 5B - TABLES

TABLE 5B-1 Radiant Heat Fluxes, Computed vs. Measured (no wind)

Time	Observed			Calculated		Modified Heat Flux. (Calc. Heat Flux-300.0) Btu/hr*ft^2	Heat Flux Measured, Btu/hr*ft^2
	Flow Rate BBL/D	Distance from Pool Center, ft	Wind Speed, mph	View Factor	Heat Flux, Btu/hr*ft^2		
2225	15,100	500	0	0.005666	437	137	137.6
2346	15,900	400	0	0.009221	524	224	222.9
0123	16,300	300	0	0.016546	702	402	403.8
1751	23,000	600	0	0.005636	437	137	141.5

TABLE 5B-2 View Factors, Computed vs. Measured

Test #	Observed		Calculated		L/R	X/R	View Factor (11)
	Distance from Pool Center, ft*	Wind Speed, mph	Angle, deg	View Factor from Subroutine SVIEW			
022	45.00D	6.80	61.372	0.014425	7.00	15	0.004
028	80.00D	9.20	55.87	0.063312	4.87	8	0.13
029	80.00D	6.36	45.07	0.065660	4.87	8	0.08
029	150.00D	6.36	45.07	0.011998	4.87	15	0.023
032	150.00D	4.30	32.04	0.014428	4.87	15	0.019

*The D's after the distances indicate a position downwind of the fire; refer to Figure 5-6.

TABLE 5B-3 Radiant Heat Fluxes, Computed vs. Measured.
Diameter = 6.0 ft; Height = 21.0 ft.

Test	Observed		Calculated		Heat Flux Calculated, $Btu/hr*ft^2$	Heat Flux Measured, $Btu/hr*ft^2$
	Distance from Pool Center, ft.	Wind Speed, mph	Angle, deg	View Factor		
022	24.00D	6.80	61.372	0.142451	3758	810
022	45.00D	6.80	61.372	0.014425	650	260
022	12.00U	6.80	61.372	0.393405	9851	500
022	12.00C	6.80	61.372	0.393405	9851	470
023	24.00D	4.42	50.074	0.115706	3109	910
023	45.00D	4.42	50.074	0.019814	781	300
023	12.00U	4.42	50.074	0.310712	7843	910
023	12.00C	4.42	50.074	0.310712	7843	920
024	24.00D	8.13	65.187	0.154804	4058	860
024	45.00D	8.13	65.187	0.012046	592	250
024	12.00U	8.13	65.187	0.429832	10735	---
024	12.00C	8.13	65.187	0.429832	10735	730
025	24.00D	4.67	51.683	0.118899	3186	720
025	45.00D	4.67	51.683	0.019216	766	260
025	12.00U	4.67	51.683	0.320742	8087	720
025	12.00C	4.67	51.683	0.320742	8087	910
026	24.00D	6.47	60.221	0.139149	3678	880
026	45.00D	6.47	60.221	0.015095	666	320
026	12.00U	6.47	60.221	0.383436	9609	860
026	12.00C	6.47	60.221	0.383436	9609	800
027	24.00D	6.95	61.865	0.143918	3794	1,000
027	45.00D	6.95	61.865	0.014130	643	300
027	12.00U	6.95	61.865	0.397804	9958	720
027	12.00C	6.95	61.865	0.397804	9958	630

TABLE 5B-4 Radiant Heat Fluxes, Computed vs. Measured.
Diameter = 20 ft; Height = 48.49 ft.

Test	Observed		Calculated		Heat Flux Calculated, Btu/hr*ft^2	Heat Flux Measured, Btu/hr*ft^2
	Distance from Pool Center, ft	Wind Speed, mph	Angle, deg	View Factor		
028	80.0D	9.20	55.87	0.063312	1837	1630
028	150.0D	9.20	55.87	0.008732	512	440
028	40.0U	9.20	55.87	0.332889	8382	690
028	40.0C	9.20	55.87	0.332889	8382	360
029	80.0D	6.36	45.07	0.065660	1894	1640
029	150.0D	6.36	45.07	0.011998	591	480
029	40.0U	6.36	45.07	0.266879	6779	910
029	40.0C	6.36	45.07	0.266879	6779	440
030	80.0D	9.66	57.14	0.062525	1818	1510
030	150.0D	9.66	57.14	0.008295	501	400
030	40.0U	9.66	57.14	0.342382	8612	600
030	40.0C	9.66	57.14	0.342382	8612	360
031	80.	14.53	66.25	0.052131	1566	1220
031	150.0D	14.53	66.25	0.005044	422	410
031	40.0U	14.53	66.25	0.427680	10669	590
031	40.0C	14.53	66.25	0.427080	10669	360
032	80.0D	4.30	32.04	0.062043	1806	1250
032	150.0D	4.30	32.04	0.014428	650	380
032	40.0U	4.30	32.04	0.209949	5397	1480
032	40.0C	4.30	32.04	0.209949	5397	---
033	80.0D	9.37	56.35	0.063030	1830	---
033	150.0D	9.37	56.35	0.008568	580	430
033	40.0U	9.37	56.35	0.336433	8468	670
033	40.0C	9.37	56.35	0.336433	8468	240

TABLE 5B-5 Radiant Heat Fluxes, Computed vs. Measured.
20-ft Square Pool; Height = 48.49 ft

Observed		Angle Used for Calculations, deg	View Factor	Heat Flux Calculated, Btu/hr*ft^2	Average Heat Flux Measured, Btu/hr*ft^2
Distance From Edge, ft	Approximate Flame Angle, deg				
24.0D	40 to 60	50.0	0.351787	8841	12880
26.0CtoD	15 to 45	30.0	0.230137	5887	12457
38.0D	40 to 60	50.0	0.227007	5881	7000
20.0CtoD	15 to 45	30.0	0.281279	7129	10[illegible]
40.0D	40 to 60	50.0	0.211584	5437	894
118.0U	60	60.0	0.011732	585	400
154.0U	60	60.0	0.005650	437	200
210.0U	15 to 45	30.0	0.006146	449	450-650

TABLE 5B-6 Radiant Heat Fluxes, Computed vs. Measured.
30 ft X 40 ft Pool; Height = 70.54 ft

Observed		Angle Used for Calculations, deg	View Factor	Heat Flux Calculated, Btu/hr*ft^2	Average Heat Flux Measured, Btu/hr*ft^2
Distance From Edge, ft	Approximate Flame Angle, deg				
61.0D	30 to 45	37.50	0.17799	4621	9650
60.0C	up to 15	7.50	0.109371	2955	6300
74.0C	up to 15	7.50	0.085033	2364	4733
77.0D	30 to 45	37.50	0.124155	3314	7175
101.0D	30 to 45	37.50	0.07450	2109	1700
107.QC	up to 15	7.50	0.050443	1525	1000
114.0QDtoD	30 to 45	37.50	0.057874	1705	2550
114.0CtoQU	up to 15	7.50	0.045679	1409	2700
122CtoQU	up to 15	7.50	0.040965	1294	1650
126QDtoD	30 to 45	37.50	0.046555	1430	2375

TABLE 5B-7 % Error Analysis. 6-ft Fire.

Test	Distance from Pool center, ft	Angle	Heat Flux from JHHRF-300,0 Btu/hr*ft^2		Heat Flux from JHHRF, Btu/hr*ft^2		Heat Flux with View Factor from Ref(11) with Solar Contribution, Btu/hr*ft^2		Heat Flux with View Factor from Ref(11) w/o Solar Contribution, Btu/hr*ft^2		Heat Flux Measured, Btu/hr*ft^2
				ratio		ratio		ratio		ratio	
023	24.00	50.074	2809	3.1	3109	3.4	3100	3.4	2800	3.1	910
023	45.00	50.074	481	1.6	781	2.6	1100	3.7	800	2.7	300
026	24.00	60.221	3378	3.8	3678	4.2	4000	4.5	3700	4.2	880
026	45.00	60.221	366	1.1	666	2.1	1270	4.0	970	3.0	320
	% E_{max}		58		37		15		29		

TABLE 5B-8 % Error Analysis. 20-ft Fire.

Test	Distance from Pool center, ft	Angle	Heat Flux from JHHRF-300,0 Btu/hr*ft^2		Heat Flux from JHHRF, Btu/hr*ft^2		Heat Flux with View Factor from Ref(11) with Solar Contribution, Btu/hr*ft^2		Heat Flux with View Factor from Ref(11) w/o Solar Contribution, Btu/hr*ft^2		Heat Flux Measured, Btu/hr*ft^2
				ratio		ratio		ratio		ratio	
029	80.00	45.07	1594	0.97	1894	1.1	2260	1.4	1960	1.2	1640
029	150.00	45.07	291	0.6	591	1.2	810	1.7	510	1.1	480
030	80.00	57.14	1518	1.0	1818	1.2	3104	2.0	2804	1.86	1510
030	150.00	57.14	201	0.5	501	1.2	906	2.3	606	1.5	400
032	80.00	32.04	1506	1.2	1806	1.4	1800	2.3	1500	1.2	1250
032	150.00	32.04	350	0.92	650	1.7	761	2.0	461	1.2	380
	%E_{max}		42		31		28		39		

TABLE 5B-9 Effect of Time Variations in Radiant Heat Flux
20-ft Square Pool

Distance from Edge, ft	Incident Radiant Flux, Btu/hrxft^2	A	B	$\frac{B^2}{9A^2}$
24	19000	12880	6120	0.02508
	11000			
	15000			
	10000			
	9400			
26	14000	12457	3257	0.007596
	10000			
	13000			
	9200			
	13000			
	14000			
	14000			
38	11000	7000	4000	0.03628
	6500			
	7900			
	5200			
	4400			
20	10000	10828	3828	0.013887
	8800			
	>12000			
	7000			
	>12000			
	13000			
	13000			
40	1700	894	806	0.090313
	300			
	800			
	600			
	470			

TABLE 5B-10 Effect of Time Variations in Radiant Heat Flux
30 ft x 40 ft Pools

Distance from Edge, ft	Incident Radiant Flux, Btu/hrxft	A	B	$\frac{B^2}{9A}$
61	10000	9650	1350	0.002174
	8400			
	9200			
	11000			
60	8100	6300	2000	0.011198
	6500			
	4300			
74	6600	4733	1867	0.017289
	4700			
	2900			
77	8000	7175	1075	0.002494
	6100			
	6600			
	8000			
101	1700	1700	100	0.000384
	1800			
	1600			
107	1400	1000	400	0.017778
	1000			
	600			
114	2700	2550	650	0.007219
	3200			
	2300			
	2000			
122	2200	1650	550	0.012346
	1100			
126	2100	2375	725	0.010354
	3100			
	2300			
	2000			

APPENDIX 5C

DERIVATION OF RELATIVE DAMAGE CRITERIA FOR A SINUSOIDAL RADIANT FLUX AS COMPARED TO A STEADY HEAT FLUX

The damage criteria for thermal radiation from a steady source are given by:

$$I_0 = \int_0^{\tau} A^{4/3}\, dz, \text{ where } \tau = \frac{2\pi}{\omega}$$

$$I_0 = \int_0^{\frac{2\pi}{\omega}} A^{4/3}\, dz = \frac{2\pi}{\omega}\ A^{4/3}$$

where

I_0 = damage criteria for steady source of radiation

ω = frequency of superimposed sinusoidal radiant heat flux

A = value of the steady radiant heat flux

z = dummy variable for integration

$\tau = \frac{2\pi}{\omega}$ = time for completion of a complete cycle of the superimposed sinusoidal radiant heat flux

A sinusoidal radiant heat flux of amplitude B is superimposed on top of the steady radiant heat flux A. The total radiant heat flux can be expressed as:

$$A + B \sin z$$

where

B = amplitude of superimposed radiant flux.

The damage criteria for thermal radiant from a sinusoidally varying source are now given by:

$$I = \int_0^{\tau} (A + B \sin z)^{4/3}\, dz$$

$$I = \int_0^{\frac{2\pi}{\omega}} (A + B \sin z)^{4/3} dz$$

PRECEDING PAGE BLANK-NOT FILMED

$$\therefore I = A^{4/3} \int_0^{\frac{2\pi}{\omega}} \left(1 + \frac{B}{A} \sin z\right)^{4/3} dz$$

Expanding binomially, we have for $|B| < |A|$

$$I = A^{4/3} \int_0^{\frac{2\pi}{\omega}} \left[1 + \frac{4}{3}\left(\frac{B}{A} \sin z\right) + \frac{\frac{4}{3} \cdot \frac{1}{3}}{2!}\left(\frac{B}{A} \sin z\right)^2 - \ldots\right] dz$$

On integration, we have

$$I = A^{4/3} \left[z - \frac{4}{3} \frac{B}{A} \cos z + \frac{2}{9} \cdot \frac{B^2}{A^2}\left(\frac{z}{2} - \frac{\sin 2z}{4}\right) - \ldots\right]_0^{\frac{2\pi}{\omega}}$$

$$I = A^{4/3} \cdot \left[\frac{2\pi}{\omega} - 0 + \frac{2}{9}\left(\frac{B}{A}\right)^2 \cdot \frac{2\pi}{\omega \cdot 2} - \ldots\right]$$

$$\therefore I = \frac{2\pi}{\omega} A^{4/3} + \frac{2\pi}{9\omega}\left(\frac{B}{A}\right)^2 \cdot A^{4/3}$$

Hence the difference between I and I_0 is:

$$I - I_0 = \frac{2\pi}{\omega} A^{4/3} + \frac{2\pi}{9\omega}\left(\frac{B}{A}\right)^2 \cdot A^{4/3} - \frac{2\pi}{\omega} A^{4/3}$$

$$I - I_0 = \frac{2\pi}{9\omega}\left(\frac{B}{A}\right)^2 \cdot A^{4/3}$$

The relative change is given by:

$$\frac{I - I_0}{I_0} = \frac{\frac{2\pi}{9\omega}\left(\frac{B}{A}\right)^2 A^{4/3}}{\frac{2\pi}{\omega} A^{4/3}} = \frac{1}{9}\left(\frac{B}{A}\right)^2$$

$$\therefore \left[\frac{I - I_0}{I_0}\right] = \left[\frac{1}{9} \cdot \left(\frac{B}{A}\right)^2\right]$$

CHAPTER 5 - LIST OF SYMBOLS

A = average value of heat flux (cal/cm^2 s)

b_ω = mean line half-width at wave number ω (cm)

B = amplitude of superimposed sinusoidal change in f (cal/cm^2 s)

C_1 = first Planck constant (w/m)

C_2 = second Planck constant (m °K)

d_ω = mean distance of separation of spectral lines of wave number ω (cm)

D = diameter of flame (m or ft)

E_ω = emissive power of the source at wave number ω (cal/cm^2 s)

I = damage criteria due to sinusoidal superimposed heat flux ([cal/cm^2 s]$^{4/3}$)

I_0 = damage criteria due to steady heat flux ([cal/cm^2 s]$^{4/3}$)

p_{H_2O} = water vapor partial pressure (bar)

s_ω = $\int_{-\infty}^{\infty} \kappa_\omega (\omega,\omega') \, d_\omega'$ = mean integrated line intensity (1/cm)

T_a = atmospheric temperature (°K)

T_f = flame temperature (°K)

T_s = flame (source) temperature (°K)

U = $\int_0^X p \, dy$ = integral of partial pressure of water vapor along the length of travel between the flame and the receptor (bar cm)

X = distance from the flame to the receptor (m or ft)

Y = product of X and p_{H_2O} (bar cm)

z = dummy variable

Greek symbols:

α = standard absorptivity

α' = absorptivity for flame temperature T_s

ε_f = flame emissivity

κ = attenuation coefficient (1/cm)

κ_ω = attenuation coefficient for a single line centered at ω (1/cm)

σ = Stefan-Boltzman constant (Btu/m ft^2 $°R^4$ or cal/s cm^2 $°K^4$)

τ = transmissivity

τ_{avg} = average transmissivity

τ_ω = transmissivity for a radiation of wave number ω

ω = wave number

CHAPTER 5 - REFERENCES

[1] Department of Transportation, U.S. Coast Guard, Assessment Models in Support of the Hazard Assessment Handbook (CG-446-3), CG-D-65-74, January 1974.

[2] Arthur D. Little, Inc., Hazard Assessment Computer System, User Manual (HACS), Cambridge, Mass., December 1974.

[3] American Gas Association, LNG Safety Program, Interim Report on Phase II Work, Project IS-3-1, July 1974.

[4] Burgess, D., and M. G. Zabetakis, Fire and Explosion Hazards Associated with Liquefied Natural Gas, Bureau of Mines, U.S. Department of the Interior, RI 6099, 1962.

[5] Burgess, D., and M. Hertzberg, "Radiation from pool flames," pp. 413-430, in N. H. Afgan and J. M. Beer (eds.), Heat Transfer in Flames, John Wiley & Sons, New York, 1974.

[6] Love, T. J., Radiative Heat Transfer, Merrill Publishing Co., Columbus, Ohio, 1968.

[7] Hottel, H. C., and A. F. Sarofim, Radiative Transfer, McGraw-Hill, New York, 1967.

[8] Siegel, R., and J. R. Howell, Thermal Radiation Heat Transfer, McGraw-Hill, New York, 1972.

[9] May, W. G., and W. McQueen, "Radiation from large liquefied natural gas fires," Combust. Sci. Technol. 7:51-56, 1973.

[10] Blacksnear, P. L. (ed.), Heat Transfer in Fires, John Wiley & Sons, New York, 1974.

[11] Rein, R. G., C. M. Sliepcevich, and J. R. Welker, "Radiation view factors for tilted cylinders," J. Fire Flammability 1:140-153, 1970.

[12] Eisenberg, N. A., C. J. Lynch, and R. J. Breeding, Vulnerability Model: A Simulation System for Assessing Damage Resulting from Marine Spills, CG-D-136-75, NTIS AD-A015245, Department of Transportation, U.S. Coast Guard, June 1975.

CHAPTER 6

MIXING AND EVAPORATION MODEL

INTRODUCTION

The Mixing and Evaporation Model is designed to compute the mass of vapor liberated, the duration of evaporation, and the maximum spread of significant pollution when a highly water-soluble liquid cargo of high vapor pressure spills on water. This model corresponds to the documentation in Chapter 11, Mixing and Dilution of a High-Vapor-Pressure, Highly Water-Soluble Chemical, of the Assessment Models in Support of the Hazard Assessment Handbook (AMSHAH) [1]. The corresponding computer code in the Hazard Assessment Computer System (HACS) [2] is under the executive subroutine MODR which utilizes the following computational subroutines: EVAMX, DISP, QSF, VAPPR, and HMTC.

When a liquid cargo of high vapor pressure spills, vapors of the cargo will be released. This vapor formation process is simulated in order to predict the toxic and combustion hazards from spills. The Mixing and Evaporation Model predicts the total mass of vapor formed from a cargo spill when the cargo properties, mass of spill, and receiving water body properties are given to the model as inputs.

One of the major problems encountered in this model is that the predicted total mass of vapor liberated may be greater than the total mass of the spilled cargo. This is physically impossible. This problem occurs because the total mass of vapor liberated is computed on the basis of an incorrect assumption, that the evaporation rate is dependent on the original mass of the spill without any reduction in the current mass by evaporation. In reality, the current mass of spill in the receiving water body is the difference between the original mass of spill and the total mass evaporated. Accounting for the changed spill mass in the receiving water body would change the pollutant concentration predictions and make the concentrations more realistic.

Another major problem is that the input to this model - the concentration of the pollutant - is unrealistic for very short times of observation after spills in flowing water and is also unrealistic for very long times of observation after spills in still water. This problem is amplified by the fact that most of the spilled high vapor pressure cargo evaporates in

---

[1] Department of Transportation, U.S. Coast Guard, Assessment Models in Support of the Hazard Assessment Handbook (CG-446-3), CG-D-65-74, January 1974.

[2] Arthur D. Little, Inc., Hazard Assessment Computer System, User Manual (HACS), Cambridge, Mass., December 1974.

the first few minutes (i.e., when the input pollutant concentration is high). Another problem is that the formula used to determine the molar concentration of the pollutant is valid only for low concentrations of the pollutant; but when spills occur, the major portion of the evaporation occurs from regions of high concentrations, and using the formula of low concentrations would give inaccurate predictions.

A third major problem is in assuming that Raoult's law is valid for all spills, whereas the predictions of partial vapor pressures from Raoult's law can be different by an order of magnitude from experimental results for spills with either a very high or a very low affinity to the receiving water body. A modified law should be used in the model simulation. The symbols and references are listed at the end of this chapter.

ASSUMPTIONS AND APPROXIMATIONS

Various assumptions and approximations, both explicit and implicit, have been made in the model developed in AMSHAH and HACS.

Explicit Assumptions

1. The evaporation of the spill takes place only at the air-mixture interface.

2. The temperature of the spilled cargo instantly changes to the temperature of the receiving water body with no effect on cargo dispersion.

3. The partial vapor pressure above the spill is linearly dependent on the surface concentration and the saturated vapor pressure of the pollutant.

4. The cargo is infinitely soluble in the receiving water body.

5. The spill is an instantaneous spill and behaves as a point source.

Implicit Assumptions

6. The cargo is neutrally buoyant in the receiving water body.

7. The entire spill mixes completely with the receiving water body before evaporation begins. (This assumption is documented in AMSHAH but is not stated explicitly as an assumption.)

8. The major portion of the evaporation occurs from regions of high spill concentration.

9. The formula converting pollutant concentration into a concentration in mole fraction is applicable over all regions of the spill, even though the formula is strictly valid only for low concentrations.

A brief discussion of the explicit and implicit assumptions is presented below.

1. Evaporation only at air-cargo interface. The first explicit assumption is that the evaporation of the liquid cargo takes place only at the water surface and is primarily due to the difference between the concentration of the cargo vapor just above the water surface and the concentration in the atmosphere at points far away from the water surface. This assumption excludes substances whose boiling temperature is less than the ambient water temperature. This assumption is generally valid for a wide range of cargoes.

2. Spill temperature. The second explicit assumption is that the chemical spilled reaches the temperature of the water instantly. Since some cryogenic cargoes are considered in a separate submodel, the cargo's temperature will usually be within 10°C or 20°C of the water temperature, and this assumption is reasonable. If the temperature of the solution is incorrect by 5°C or so, the error introduced will not be significant with respect to the errors introduced by other assumptions and approximations. This assumption implies that any cooling due to evaporation of the spill is negligible. This is probably a good assumption for cargoes that are shipped in unpressurized and unrefrigerated containers.

3. Spill partial vapor pressure. The third explicit assumption is that the partial pressure of the cargo over the solution (p_C) is linearly related to the saturation vapor pressure of pure liquid cargo (p_V) and the molar fractional concentration (c_m). The equation is ($p_C = c_m p_V$). This equation expresses Raoult's law [3]. This relationship is quite accurate for many pairs of solvents and solutes. Departures from Raoult's law are not uncommon, but the departures are related in a complicated manner to other properties of the solutes and solvents.

4. Cargo solubility in water is infinite. The fourth explicit assumption is that all the cargo that is spilled is completely soluble in the receiving water body. This assumption is valid for most cargoes which have high affinity for water. For cargoes of finite solubility, the mechanism of dispersion (because of turbulent diffusion of neutrally buoyant spills) will be less accurate because the finite solubility will exaggerate the buoyancy effects.

5. Spill is instantaneous. The fifth and last explicit assumption is that the spill is instantaneous and behaves as a point source. Many types of spills were analyzed in the Mixing and Dilution Model but only one of these is considered in this model, namely, the instantaneous spill of a cargo in a non-tidal river. For spills which would occur after a rapid

---

[3] Moelwyn-Hughes, E. A., Physical Chemistry, pp. 758-760, 2nd rev. ed., Pergamon Press, Oxford, England, 1965.

release of cargo, the approximation of an instantaneous spill behaving as a point source seems to be a valid assumption. The Mixing and Evaporation Model, as available, would not be applicable to continuous spills.

After an instantaneous spill in a receiving water body of uniform velocity, U, the concentration of the pollutant is given by

$$c(x,y,z,t) = \frac{2\,M_{liq}}{(4\pi t)^{3/2}\sqrt{e_x e_y e_z}} \cdot \left[EXP - \left\{ \frac{(x-Ut)^2}{4e_x t} + \frac{y^2}{4e_y t} + \frac{z^2}{4e_z t} \right\} \right]$$

AMSHAH (11.1), (6-1)

6. Spill is neutrally buoyant. This and the remaining assumptions are implicit assumptions. The assumption of neutrally buoyant cargo is implicit in the expression for predicting the pollutant concentration. This assumption is also a limiting assumption for the model because most cargoes are not neutrally buoyant. This assumption would affect the predicted vaporization rate of the pollutant because, if the cargo is lighter than water and floats, nearly pure, on the water surface, the mass of vapor actually liberated may be underestimated. If the cargo is denser than water and sinks to the bottom of the channel while going into solution with water, then this assumption may overestimate the amount of vapor liberated.

7. Mixing followed by evaporation. The assumption is that all the spilled liquid cargo goes into solution immediately, so that any evaporation from a surface of pure liquid cargo may be ignored for the period in which the cargo goes into solution. In other words, this assumption states that the mixing and evaporation starts only after the mixing and dilution has been completed. This is a major limitation in the simulation of the combined mixing, dilution, and evaporation of spills because, while the initial mixing and dilution process is being completed, the high vapor pressure of the cargo would release significant amounts of vapor. It is to be noted that initial pollutant concentrations are high near the spill site and hence significant amounts of vapor can be released during the initial periods after a spill.

8. Major portion of evaporation from areas of high spill concentration. AMSHAH stipulates that "the evaporation from water surface regions, having a molar concentration less than c_m^*, is negligibly small (the value of c_m^* is quite arbitrary and may have to be chosen properly for different chemicals; however a value between 0.1 and 0.05 may be reasonable). By choosing a value of c_m^* we are actually limiting the area from which evaporation can occur." This assumption is necessary for the model because of the previous assumption, that the current mass of the spilled cargo in water is not reduced by evaporation of the cargo.

9. Conversion formula for dilute concentrations is applicable. AMSHAH utilizes a conversion formula to convert the pollutant concentration from density units to concentration as a molar fraction of the mixture of pollutant and spilled cargo. The formula is:

$$c_m(x,y,z,t) = \left[\frac{1}{1 + (\rho_w \mu_{liq}) / (c \mu_w)}\right] \qquad \text{AMSHAH (11.2), (6-2)}$$

This conversion formula is applicable only to dilute concentrations of the pollutant; but when spills occur, the concentrations of the pollutant are high where a major portion of the evaporation takes place. Hence, assuming that the concentration of the pollutant is dilute in the regions of interest is not realistic.

ERRORS

Only minor typographical errors were encountered in the documentation of this model. Appendix 6A contains a list of the typographical errors in AMSHAH.

ACCURACY ASSESSMENT

The accuracy assessment for the Mixing and Evaporation Model is presented below. The assessment is based on the assumptions - both explicit and implicit - which were used in developing the model.

1. When a high vapor pressure, high solubility liquid cargo is spilled in water, mixing and dilution of the spill will displace the pollutant not only on the surface of the water but also in the depths of the receiving water body. While the pollutant disperses in all directions within the receiving water body, the vapor formulation of the pollutant is assumed to occur at the pollutant-air interface (at the top of the receiving water body). This assumption appears to be valid when the cargo is not boiling. Some of the boiling spilled cargoes, when they occur, are simulated by other models.

2. The Mixing and Evaporation Model also assumes that, when the spill mixes with the water, the temperature of the spilled cargo is instantly brought to the temperature of the receiving water body. In reality, the temperature of the spilled cargo would take a finite time to be brought to the temperature of the receiving water body. This finite time would be less for cargoes of low specific heat and in receiving water bodies in which pollutant diffusion is very rapid. The effect of temperature on the turbulent diffusivities in the three coordinate directions can be considered of a second order when the mass of vapor formed is being simulated. Cooling of the receiving water body due to evaporation is also considered negligible. Hence, assuming that the temperatures of the spilled cargo and the receiving water body are equal appears to be a valid assumption.

3. The partial pressure of cargo and most solute-solvent relationships are based on the properties of pure substances, and the relationships for water are usually based on distilled or demineralized water. The receiving water bodies for spills do not generally contain pure water. Salt (NaCl) concentration is open sea is around 35 ppt (parts per thousand). Hence, salt concentrations of receiving water bodies can range from nearly zero to 35 ppt. These water bodies may contain significant concentrations of other substances, for example, sewage and industrial wastes. These substances may cause the properties of the resulting solution to differ from pure water. The partial pressure of the cargo is assumed to be directly proportional to the product of the partial pressure of the pure cargo and the molar fraction of cargo in the mixture of spilled cargo and the receiving water body. A detailed discussion of this assumption is presented below.

The basic criterion for phase equilibrium is

$$\bar{f}_k' = \bar{f}_k'' = \bar{f}_k''' = \bar{f}_k^{iv} \tag{6-3}$$

where

f is the fugacity
k is the k^{th} component, and the
primes are the different phases.

For liquid solutions, it is possible to develop the following equation starting from equation (6-3)

$$\ln\left[\frac{\bar{f}_k}{f_k x_k}\right] = \frac{1}{RT}\int_0^p (\bar{v}_k - v_k)\, dp \tag{6-4}$$

where

p is the pressure
R is the Universal Gas Constant
T is the temperature
v is the volume
x is the mole fraction

The term within the integral is the difference between the partial molal volume of component k and its molal volume in the pure state at the same temperature and pressure. It represents the change in the total volume when one mole of k is added to a mixture, i.e., the volume change on mixing.

If $\bar{v}_k = v_k$ at all pressures and compositions, equation (6-4) gives a simple relationship for the effect of composition on the fugacity of a gas, namely

$$\bar{f}_k = f_k x_k \tag{6-5}$$

This is the well-known Lewis and Randall Rule. The liquid phase fugacities can be replaced with gas phase fugacities by applying equation (6-3). Thus, the fugacity, $\bar{f}_k$, is equal to the fugacity of k in the gas phase, in equilibrium with the liquid solution. If the gas phase is assumed to be ideal, then $\bar{f}_k$ is equivalent to the partial pressure $\bar{p}_k$ of k in the gas phase. Similarly, for the liquid phase of pure k, f_k is equal to the vapor pressure p'_k of the ideal gas over the liquid. Only under these conditions, equation (6-5) may be written as

$$\bar{f}_k = \bar{p}_k = p'_k x_k \qquad (6\text{-}6)$$

This expression is known as Raoult's law.

Since we are considering situations where the gas phase is at atmospheric pressure, assuming the gas phase to behave as an ideal gas is valid. However, unless $\bar{v}_k = v_k$ for all pressures and compositions, the liquid phase would not be an ideal solution and equation (6-6) would not be applicable. When we are dealing with solutions, the components of which have identical properties like the solutions of benzene-toluene, heptane-octane, ethylene-bromide-propylene-bromide, $\bar{v}_k \cong v_k$ and the Raoult's law can be used justifiably. Figures 6-1 and 6-2 show the systems where equation (6-6) should not give major errors.

However, when $\bar{v}_k \neq v_k$ (that is, for solutions of dissimilar molecules) for all pressures and compositions, equation (6-6) would not apply, and the partial pressures calculated by Raoult's law may be in excess of or less than the actual values. Consider A and B to be the components of a binary solution. If the intermolecular forces between A-B are stronger than those which exist between A-A or B-B, the actual partial pressure p_A or p_B would be less than that calculated by Raoult's law i.e., the system would exhibit negative deviation from Raoult's law. However, when the intermolecular forces between A-B are weaker than those which exist between A-A or B-B, the system would exhibit positive deviation from Raoult's law.

In the case of spills of cargoes like NH_3, SO_2, C_2H_5OH, CH_3OH in water, use of Raoult's law for calculating the partial pressure at the surface of the pool is erroneous. Table 6-1 lists the experimental values of partial pressures of NH_3 as well as those obtained by Raoult's law at various concentrations of ammonia in water at 20°C. Table 6-2 lists the experimental values of the partial pressures of SO_2 as well as those obtained by Raoult's law at various concentrations of SO_2 at 30°C. Differences between the experimental and calculated results are significant.

On the other hand, Figure 6-3 shows that partial pressures calculated by Raoult's law can be several times lower than the experimental values for water-dioxane system at 35°C. The values corresponding to the dashed lines refer to the values obtained by Raoult's law.

Hence, predictions from Raoult's law have to be compared with experimental results in order to give more accurate predictions of the partial pressures of various spilled cargoes in receiving water bodies.

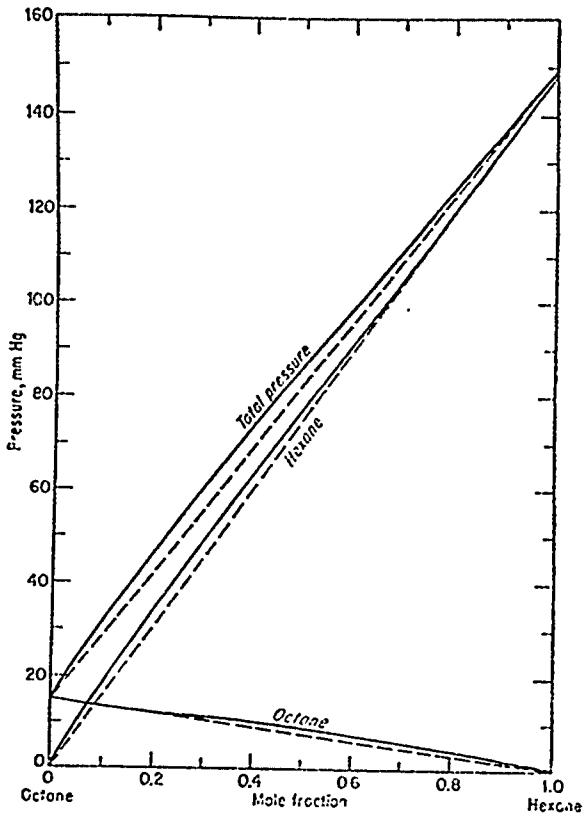


FIGURE 6-1 Vapor pressure of hexane-octane system at 23.9°C.

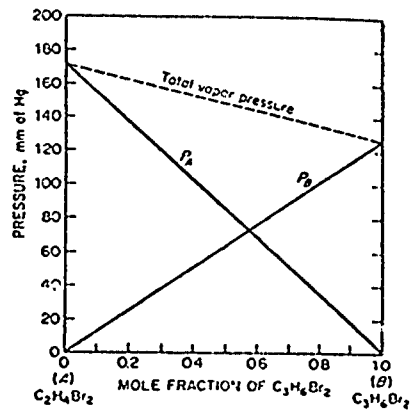


FIGURE 6-2 Pressures of vapors above solutions of ethylene bromide and propylene bromide at 85°C. The solutions follow Raoult's law.

TABLE 6-1

Mass NH_3 per 100 masses H_2O	PNH_3 from Foust et al. [4] at 20°C in mm Hg	PNH_3 from Raoult's law at 20°C in mm Hg
60	945	2424
50	686	2160
40	470	1856
30	298	1505
25	227	1306
20	166	1091
15	114	855
10	70	598
5	25	314
2	12	129

Vapor pressure can be determined from Weast [5]. For ammonia, the constants are, A = 6001.2 and B = 8.269901 for the temperature range -109.1 to 98.0°C. The equation is

$$\text{Log}_{10}P = (-0.2185\ A/K) + B$$

where P is the pressure in Torr, K is the temperature in degrees Kelvin. At 20°C, vapor pressure of ammonia is 6241 mm Hg by calculations.

---

[4] Foust, A. S., L. A. Wenzel, C. W. Clump, L. Maus, and L. B. Andersen, Principles of Unit Operations, p. 553, Wiley, New York, 1960.

[5] Weast, Robert C. (ed.), Handbook of Chemistry and Physics, 52nd ed., pp. D-171, Chemical Rubber Co., Cleveland, Ohio, 1971.

TABLE 6-2

Mass SO_2 per 100 masses H_2O	PSO_2 from Foust et al. [4] at 30°C in mm Hg	PSO_2 from Raoult's law at 30°C in mm Hg
7.5	688	66
5.0	452	44
2.5	216	22
1.5	125	13
1.0	79	9
0.7	52	6

For SO_2, A = 6398.1, B = 8.115603 for the temperature range -95.5 to 141.7°C. At 30°C, vapor pressure of SO_2 is 3180 mm Hg by calculations.

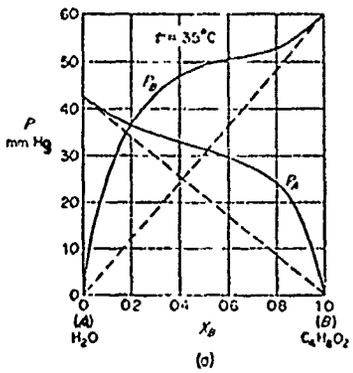


FIGURE 6-3 Positive deviation from Raoult's Law. Partial vapor pressures in water-dioxone system at 35°C.

4. The next assumption is that the solubility of the cargo in the receiving water body is infinite. This could be a valid assumption for those cargoes which do not have a saturation concentration in the receiving water body but go into solution in all concentrations. For these cargoes, the total diffusion is dependent on the rate of solubility of the cargo and the rate of turbulent diffusion due to turbulent eddy currents in the receiving water body. On the other hand, for those cargoes that do have a finite solubility, the pollutant concentration would change very sharply from regions within the pure cargo to regions where the concentration is below the saturation concentration. Qualitative descriptions of the pollutant concentrations for cargoes which are infinitely soluble and for cargoes with finite solubility are presented in Figures 6-4a and 6-4b. Cargoes which are lighter than water and are of finite solubility would be subjected to greater buoyancy forces as compared to lighter cargoes with infinite solubility. This is because of the formation of a pool of pure cargo, floating on the water surface. This in turn would change the diffusion predictions for cargoes of finite solubility. This change in the diffusion for cargoes of finite solubility is not modeled in the present simulation based on cargoes of infinite solubility.

5. Spills of cargo can be explosive, rapid, or slow, depending upon the cause of the spill. Spills can also occur so that the location of the spill can be fixed or moving. The model that was developed here simulates only one type of spill, namely, the instantaneous release of cargo at one point. Even though all spills cannot be simulated by the above assumption, this assumption would give quite good results for the instantaneous release of cargo.

6. Cargoes are normally not neutrally buoyant in the receiving water bodies in which spills may occur, and they may sink or float. This is also an assumption from the Mixing and Dilution Model, and the limitations mentioned in the discussion of that model also apply here.

7. In the simulation of evaporation of spilled cargo, it is assumed that the initial mixing and dilution occurs independent of any evaporation. The evaporation of the cargo begins after the mixing and dilution has been completed. This assumption is a major weakness in the simulation of the mixing and evaporation process. In reality, while the pollutant is dispersing, evaporation from the pollutant-air interface continues, thereby reducing the extent to which the spilled cargo would disperse in the receiving water body. The actual combined dispersion and evaporation would, in general, give a different amount of vapor formation as compared to only mixing followed by only evaporation. Hence, for a realistic estimate of the vapor released, the combined dispersion and evaporation of the pollutant must be simulated simultaneously.

The combined dispersion and evaporation may be simulated as follows. Using the basic dispersion equation for the dispersion of the pollutant in the receiving water body, we can modify it to include evaporation. Hence, we have:

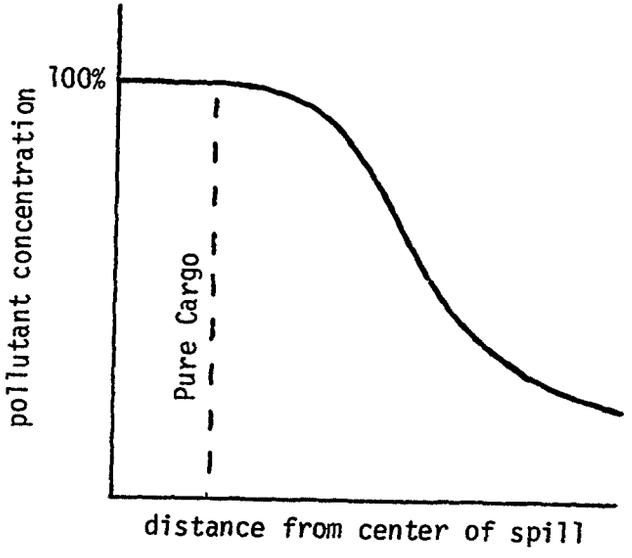


FIGURE 6-4a Pollutant of infinite solubility.

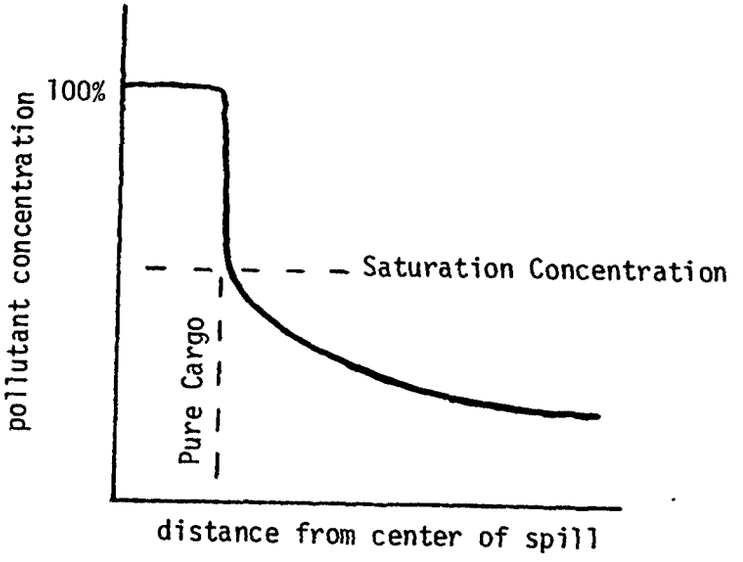


FIGURE 6-4b Pollutant of finite solubility.

$$\frac{\partial c(x,y,z,t)}{\partial t} = D\,\nabla^2 c(x,y,z,t) \qquad (6\text{-}7)$$

where

$c(x,y,z,t)$ = concentration of the pollutant

t = time variable

D = diffusion constant

∇^2 = Laplacian operator

For a spill into a semi-infinite body of water, the boundary conditions can be expressed as:

$$c = 0 \quad \text{at} \quad x = \pm\infty \qquad (6\text{-}8)$$

$$c = 0 \quad \text{at} \quad y = \pm\infty \qquad (6\text{-}9)$$

$$c = 0 \quad \text{at} \quad z = +\infty \qquad (6\text{-}10)$$

and

$$\frac{\partial c}{\partial z} = -Kc \quad \text{at} \quad z = 0 \qquad (6\text{-}11)$$

where K = a constant for evaporation. The above equation can be solved to give the concentration of the pollutant when both dispersion and evaporation are considered together.

8. The computation of the total mass of cargo evaporated was based on assuming that a major portion of the evaporation occurred in regions where the surface concentration of the pollutant was greater than a small critical value. It should be noted that as this critical pollutant concentration is made smaller, the area of the region over which the pollutant concentration is greater than the critical increases. This larger region would account for more of the total vapor formed. Hence by making the critical concentration small enough, the major portion of the vapor formed can be predicted. This assumption is necessary because of the previous assumption of no reduction of spilled material in the water by evaporation.

The derivation of an expression for the mass of vapor liberated, M_V, by using a first approximation for dilute solutions is presented below. It will be shown in the accuracy assessment of the next assumption that the first approximation of an accurate, solvent-solute-specific conversion between concentration in molar fraction and mass per unit volume is a better approximation than the second approximation for concentrated solutions. As the first approximation for concentration conversion is a simple expression, the approach taken in AMSHAH may be used to derive an analytic expression for M_V, the mass of vapor liberated. This derivation is instructive in that its results point up a limitation in this submodel.

Although the simple Gaussian expression in three dimensions has been shown to give unrealistically high values of the concentration for small values of t (time), for this derivation it will be used:

$$c^{max}(t) = \frac{2\,M_c}{(4\pi t)^{3/2}(e_x e_y e_z)^{1/2}} \qquad \text{AMSHAH (11.4), (6-12)}$$

$$c(x,y,z,t) = c^{max}(t)\,\exp\left[-\frac{(x-Ut)^2}{4e_x t} - \frac{y^2}{4e_y t} - \frac{z^2}{4e_z t}\right] \qquad (6\text{-}13)$$

where c^{max} is the concentration at the center of the distribution. The mass of the cargo spilled is denoted by M_c and by M_{liq} in AMSHAH. Equation 6-13 corresponds to AMSHAH (11.1)

c* is defined as the concentration such that the evaporation from the water surface where c is less than c* may be neglected, and $\hat{t}$ is defined as the time at which the concentration everywhere is less than c*, i.e., when $c^{max} = c^*$. Thus

$$c^* = \frac{2\,M_c}{(4\pi\hat{t})^{3/2}\,(e_x e_y e_z)^{1/2}} \qquad (6\text{-}14a)$$

$$\hat{t} = \frac{1}{4\pi}\left[\frac{2\,M_c}{c^*\,(e_x e_y e_z)^{1/2}}\right]^{2/3} \qquad \text{AMSHAH (11.5b), (6-14b)}$$

It should be noted that

$$c^{max}(t) = c^*\,\left(\frac{\hat{t}}{t}\right)^{3/2} \qquad (6\text{-}15)$$

holds without regard to any conversion between different units of concentration.

By Raoult's law and the definition of the mass transfer coefficient, we have

$$\dot{M}_v = h_p p_v \int c_m dA = h_p p_v\,\pi\,a(t)b(t)c_m^{mean} \qquad (6\text{-}16a)$$

where

$$c_m^{mean} = [c_m^{max} - c_m^*] \,/\, \ell n(c_m^{max}/\,c_m^*) \qquad \text{AMSHAH (11.9), (6-16b)}$$

and

$$a(t) = [4e_x t \ell n\{(\hat{t}/t)^{3/2}\}]^{1/2} \qquad (6\text{-}17a)$$

$$b(t) = [4e_y t \ell n\{(\hat{t}/t)^{3/2}\}]^{1/2} \qquad (6\text{-}17b)$$

Equation (6-16a) corresponds to (11.7a) and (11.8) in AMSHAH. The integral is over the area on the water surface where the concentration is greater than c_m^*. AMSHAH evaluates this integral in the Appendix to Chapter 11. Equations (6-17) are simplifications of AMSHAH (11.3). The vapor pressure here has been denoted p_v instead of p_{vap}^{sat}.

$\dot{M}_v$ is the rate of vapor liberation (mass/time) and equations (6-16) and (6-17) may be combined to give

$$\dot{M}_v = 4\pi h_p \, p_v \, (e_x e_y)^{1/2} t \, \ell n\{(\hat{t}/t)^{3/2}\} \, c_m^{mean} \qquad (6\text{-}18)$$

where h_p is the mass transfer coefficient.

A connection between c and c_m can be obtained from

$$c_m = \frac{\mu_w}{\mu_c \, \rho_w} c \qquad (6\text{-}19)$$

From AMSHAH (11.9),

$$c_m^{mean} = \left[\frac{\mu_w}{\mu_c \, \rho_w} c^{max} - \frac{\mu_w}{\mu_c \, \rho_w} c^*\right] / \ell n(c^{max}/c^*) \qquad (6\text{-}20a)$$

and

$$c_m^{mean} = c_m^* \, [(\frac{\hat{t}}{t})^{3/2} - 1] / \ell n [(\frac{\hat{t}}{t})^{3/2}] \qquad (6\text{-}20b)$$

If the second or third approximate conversions were being used, equation (6-18) would have to be integrated numerically, but in this case the integral may be evaluated analytically. From equation (6-18),

$$\dot{M}_v = 4\pi h_p \, p_v \, (e_x e_y)^{1/2} c_m^* \, t[(\frac{\hat{t}}{t})^{3/2} - 1] \qquad (6\text{-}21)$$

Following the method used by AMSHAH, a new variable, τ, is introduced:

$$\hat{t}/t = \tau \quad , \qquad t = \tau\hat{t} \qquad (6\text{-}22)$$

The mass of vapor liberated is the integral of the rate over the time during which vapor escapes:

$$M_v = \int_0^{\hat{t}} \dot{M}_v \, dt = \int_0^1 \dot{M}_v \, \hat{t} \, d\tau \qquad (6\text{-}23a)$$

The constants in this expression may be gathered together and denoted by M_{ch}:

$$M_{ch} = 4\pi h_p \, p_v \, (e_x e_y)^{1/2} (\hat{t})^2 \qquad \text{AMSHAH (11.10a), (6-23b)}$$

Hence, equation (6-23a) may be written as:

$$M_v = M_{ch} \, c_m^* \int_0^1 [(1/\tau)^{3/2} - 1]\tau \, d\tau \qquad (6\text{-}24)$$

This integral is readily evaluated and equals 3/2. Hence, the mass of vapor liberated is:

$$M_v = \frac{3}{2} M_{ch} \, c_m^* = (\tfrac{3}{2}) 4\pi h_p \, p_v \, (e_x e_y)^{1/2} \, (\hat{t})^2 \, c_m^* \qquad (6\text{-}25)$$

Because both t and c_m^* are expressions of c*,

$$c_m^* (\hat{t})^2 = \frac{\mu_w}{\mu_c \, \rho_w} (\frac{1}{4\pi})^2 \, [\frac{(2M_c)^2}{e_x e_y e_z}]^{2/3} \, (\frac{1}{c^*})^{1/3} \qquad (6\text{-}26)$$

and M_v may be written in more explicit terms as:

$$M_v = \frac{6 h_p \, p_v \, (e_x e_y)^{1/2} M_c^2 \, (\mu_w / \rho_w \, \mu_c)}{4\pi (e_x e_y e_z)^{2/3} \, (c^*)^{1/3}} \qquad (6\text{-}27)$$

It is interesting to note that the mass of cargo which evaporates is a function of the square of the mass spilled. This is because the area of the surface where c is greater than c* is proportional to M_c, and the time it takes for c^{max} to decrease to c* is also proportional to M_c.

The result from equation (6-27) is the inverse dependence of M_v on c*. This means that as c* approaches zero, the mass of vapor liberated approaches infinity. This, of course, is not physically possible. While all cargoes will have some affinity for water so that the concentration may never be identically zero, it is seen that by choosing c* too small the mass of vapor liberated, M_v, may exceed the mass of cargo spilled, M_c. Further, for the assumption that evaporation from regions where the concentration is less than c*, M_v must approach some limiting value which is less than M_c, as c* approaches zero. But in the equations derived, M_v does not approach a limiting value, which should be less than M_c, hence the model does not appear to be physically realistic.

Another related problem was the prediction of pollutant concentrations greater than those of the liquid cargo. We will investigate these predictions by using the example described in Section 11.7 of AMSHAH. The quantities given were recomputed.

It is interesting to note the consequences of the expression for the maximum density:

$$c^{max} = 8.996 \times 10^6 / t^{1.5}$$

with c^{max} in kg/m^3 and t in seconds. The density of diethylamine at 20°C is 705.6 kg/m^3. If c^{max} is set equal to this value, the above equation gives t = 546 seconds; however, t was found to be 1205 seconds. Thus, it is seen that the dispersion equation gives a concentration greater than the normal liquid density in the river for almost half the time that evaporation is supposed to be significant.

9. The conversion formula (for concentration of pollutant in density units into molar fraction) which is used in AMSHAH will be discussed below.

Equation (11.2) on page 156 of AMSHAH concerns the assumption of the applicability of the conversion between molar fraction, c_m, and concentration in terms of mass by unit volume, c, for liquids. The expression for determining mole fractions of solutes is more complex for liquids than for gases, because the total volume of a liquid-liquid mixture may not be equal to the sum of the volumes of the individual solutes and solvents. The total volume would be less than the sum of the volumes of the solute and solvent for liquid-liquid mixtures which have a high affinity for each other. The volume of M_W grams of solvent and M_C grams of solute is generally more than the volume of the solvent alone and less than the sum of the volume of the solvent and the volume of the solute prior to the formation of the solution. Further, the relationship between the final volume and the concentration of the solution is often nonlinear and depends upon the exact solvent and solute being used. A detailed description of this problem may be found in Moelwyn-Hughes [3].

Most of the standard formulas cannot be used for a general approximation which may be used for any given solvent and solute, because they require that the density of the solution be known, and this quantity is not known for the cargo-water mixtures of interest. Thus, expressions which do not depend upon the density of the solution are derived below from three different approximations.

Let us adopt the following nomenclature:

M = mass
V = volume
ρ = density
μ = molecular weight
N = number of moles

Let the solvent be water and the subscript w denote the solvent in pure state. Let the solute be the cargo and the subscript c denote the cargo in pure state. Quantities without subscripts will refer to the solution of the cargo in water.

By definition, we have

$$c_m = \frac{N_c}{N_c + N_w} \tag{6-28}$$

$$M_c = cV \tag{6-29}$$

$$M = M_c + M_w \tag{6-30}$$

$$M_w = N_w \mu_w \qquad M_c = N_c \mu_c \tag{6-31}$$

And in the pure state before the solution is formed, we have

$$M_w = \rho_w V_w \qquad M_c = \rho_c V_c \tag{6-32}$$

The three approximations are:

a) $N_c << N_w$ and $V \simeq V_w$

b) $V \simeq V_w$

c) $V \simeq V_w + V_c$

Each of the approximations will be discussed below.

a. <u>First Approximation</u>: $N_c << N_w$ and $V \simeq V_w$

By means of this approximation we neglect the N_c in the denominator of equation (6-28), and we assume that the volume of the solvent does not change upon the addition of the solute. These assumptions imply that the solution is a very dilute solution. Using the equation above, we have:

$$c_m = \frac{N_c}{N_w} = \frac{M_c \mu_w}{M_w \mu_c} = \frac{c\ V\ \mu_w}{\rho_w\ V\ \mu_c} = \frac{\mu_w\ c}{\mu_c\ \rho_w} \tag{6-33a}$$

which may be inverted to give

$$c = c_m\ \rho_w\ (\mu_c/\mu_w) \tag{6-33b}$$

Since the computer program does not test to prevent the application of the conversion between c and c_m for solutions which are not very dilute, it is of interest to see what these conversion equations give in the case of pure cargo (solute) where

$$c = \rho_c \quad , \quad c_m = 1.0 \tag{6-34}$$

Using equation (6-33b), we get

$$c = \rho_w \mu_c / \mu_w \quad \text{for} \quad c_m = 1 \tag{6-35a}$$

and this value of c is usually not close to ρ_c. Using equation (6-33a), we get

$$c_m = \frac{\rho_c \mu_w}{\rho_w \mu_c} \quad \text{for} \quad c = \rho_c \tag{6-35b}$$

and this value of c_m will not, in general, be 1.0. In fact it may be greater than one.

It should also be noted that equation (6-33) is the same expression as that used for gas mixtures, and that it is based upon the assumption that one mole of a substance occupies the same volume as one mole of any other substance.

b. Second Approximation: $V \simeq V_w$

In this case we assume that the volume does not change when the solute (cargo) is added as before, but we do not neglect the number of moles of solute in the denominator of equation (6-28). Clearly, this is a better approximation than the first, but the use of V_w for V clearly implies a dilute solution. From equation (6-28) through equation (6-32), we have

$$c_m = \frac{N_c}{N_c + N_w} = \frac{(cV/\mu_c)}{(cV/\mu_c) + (\rho_w V/\mu_w)} = \frac{1}{1 + \{(\rho_w \mu_c)/(c\mu_w)\}} \tag{6-36a}$$

and the inverse

$$c = \rho_w (\mu_c/\mu_w)\{(c_m)/(1 - c_m)\} \tag{6-36b}$$

Equation (6-36a) is identical to equation (11.2) of AMSHAH, however AMSHAH has assumed that the volume of the solvent does not change when the solute is added.

In the limit of pure cargo, we have from equation (6-36b)

$$c = \infty \quad \text{for} \quad c_m = 1.0 \tag{6-37a}$$

and from equation (6-36a)

$$c_m = [1 + \{(\rho_w \mu_c)/(\rho_c \mu_w)\}]^{-1} \tag{6-37b}$$

The value of c_m in this expression cannot be greater than one, but when c_m = 1.0, c is infinite.

c. Third Approximation: $V \simeq V_w + V_c$

In this case we assume that the volumes of solvent and solute are additive, so that the volume of the solution is the sum of the volumes before mixing. From the first five equations of these approximations, we have

$$c_m = \frac{N_c}{N_c + N_w} = \frac{(cV/\mu_c)}{\{(cV)/\mu_c\}+\{(\rho_w V_w)/\mu_w\}}$$

$$= \frac{1}{1+\{(\mu_c \rho_w)/(\mu_w c)\}\{1-(V_c)/(V)\}} \qquad (6\text{-}38)$$

where we have used $V_w = V - V_c$. Now, $V_c = M_c/\rho_c = cV/\rho_c$, so

$$c_m = [1+\{(\mu_c \rho_w)/\mu_w\}\{(1/c)-(1/\rho_c)\}]^{-1} \qquad (6\text{-}39a)$$

and the inverse of this is

$$c = [\{\mu_w/(\mu_c \rho_w)\}\{(1/c_m) - 1\} + (1/\rho_c)]^{-1} \qquad (6\text{-}39b)$$

In the limit of pure cargo, we see that equations (6-39) give the correct limiting values for c and c_m. Thus, this third approximation, while it may be less accurate than experimental results for those cargoes in which $[V < V_w + V_c]$ and for low pollutant concentrations, does give reasonable predictions when the solutions are concentrated.

Looking at the conversion equations which result from these three approximations, it can be noted that in the limit of very small concentrations, equations (6-36) and (6-39) reduce to equation (6-30). This is shown in Tables 6-3 and 6-4 for the case of methyl alcohol and water. It may be noted that the error in the conversion is of the order of the molar fractional concentrations. The results of the first approximation lie between those from the second and third approximations in every case.

The third approximation is more accurate for high concentrations. This may be shown for the case of ammonia in water directly. Moelwyn-Hughes [3] states that a solution which is 0.3550 ammonia, by weight, has 0.3123 grams of ammonia per milliliter. A weight fraction of 0.3550 converts to a molar fraction of 0.3631. Converting this to grams per cubic centimeter by equations (6-33b), (6-36b), and (6-39b), we have:

1st Approximation, $c = 0.3429$ g/cm^3
2nd Approximation, $c = 0.5385$ g/cm^3
3rd Approximation, $c = 0.3246$ g/cm^3

TABLE 6-3 Results of Converting from c (Concentration in Terms of Mass per Unit Volume of Solution) to c_m (Molar Fractional Concentration) for Methyl Alcohol in Water

c (g/cm^3)	c_m		
	1st Approx.	2nd Approx.	3rd Approx.
0.7900	0.44438	0.30766	1.00000
0.0790	0.04444	0.04255	0.04705
0.0079	0.004444	0.004424	0.004468
0.00079	0.0004444	0.0004441	0.0004446

Equations (6-33a), (6-36a), and (6-39a) have been used.

TABLE 6-4 Results of Converting from c_m to c for Methyl Alcohol in Water

c_m	c (g/cm^3)		
	1st Approx.	2nd Approx.	3rd Approx.
1.000	1.7778		0.7900
0.100	0.1778	0.1975	0.1580
0.010	0.01778	0.01795	0.01756
0.001	0.001778	0.001780	0.001775

Equations (6-33b), (6-36b), and (6-39b) have been used.

Thus we see that, in this case, the third approximation is the most accurate and the second approximation is the least accurate. Since the conversions are done numerically in the computer program, it would seem best to use the third approximation.

In the following, we will analyze the concentration conversions in the computer subroutine EVAMX (the computer program listings are in Appendix 6B).

Although the documentation in AMSHAH states that the second approximation is used, different approximations are used in the computer program of HACS. In an early operational step in EVAMX (Figure 6B-1 in Appendix 6B), C* (CSTAR) is computed from the input value of c_m^* (CSTM), and the first approximation is used (equation (6-33b)). Later on, in the DO loop, c_m^{max} (CMAXM) is computed from c^{max} (CMAX), and the second approximation is used (equation (6-36a)).

All three approximations are not valid for high pollutant concentrations. In reality, high pollutant concentrations can be expected. Two examples will illustrate the problems encountered. The computer submodel was run using each of the three approximate conversion schemes and the scheme of the original program. The results are shown in Table 6-5. The number of integration intervals was reduced from 100 to 50 for these tests. The values of c^{max} were printed out for the 51 points, and 8 of the 51 values of c^{max} were above ρ_c in the example for ammonia, and 11 of the 51 values were above ρ_c for methyl alcohol. In these cases, of course, c^{max} will be greater than one. In equation (6-39a) it may be noted that if c is greater than ρ_c, then c_m will be negative. But if c_m^{max} is negative, where c_m^{max} is given by,

$$c_m^{mean} = (c_m^{max} - c_m^*) \,/\, \{\ell n\, (c_m^{max}/c_m^*)\} \qquad \text{AMSHAH (11.9), (6-40)}$$

the logarithm is meaningless. Thus, some steps had to be taken to prevent c^{max} from exceeding ρ_c when the third approximation was being used. The expedient chosen was to set $c^{max} = \rho_c$ in these cases.

It may be seen from Table 6-5 that, for the four cases, the amounts of vapor liberated differ from one another. Further, in case 4 the conversion scheme used is that of the original program, and it gives the lowest estimate of vapor liberated. In a model which one would like to err in the direction of overestimating the damage potential, this is undesirable.

TABLE 6-5 Results of Using Different Concentration Conversions in EVAMX, for Ammonia and Methyl Alcohol

	NH_3				CH_3OH			
	Case 1	Case 2	Case 3	Case 4	Case 1	Case 2	Case 3	Case 4
THAT (sec)	205.1	211.8	208.5	205.1	86.15	89.00	89.62	86.15
ZMCHR (g)	1.178×10^6	1.258×10^6	1.219×10^6	1.178×10^6	4457	4756	4823	4457
ZMV (g)	77.90×10^3	50.48×10^3	64.79×10^3	48.28×10^3	295	191	279	183
ZM(N)	0.0661	0.0401	0.0532	0.0410	0.0661	0.0401	0.0578	0.0410
S (cm)	410.1×10^2	423.1×10^2	417.1×10^2	410.1×10^2	172.3×10^2	178.0×10^2	179.2×10^2	172.3×10^2
SIZMX (cm)	11.57×10^2	11.76×10^2	11.66×10^2	11.57×10^2	7.50×10^2	7.62×10^2	7.65×10^2	7.50×10^2

Case 1 refers to the use of the first approximation, case 2 to the use of the second, and case 3 to the use of the third. In case 4, the first approximation was used to calculate c* from c_m^*, and the second approximation was used to calculate c_m^{max} from c^{max}. This was the scheme used in EVAMX as it was delivered to ECI. For these calculations the following values of input variables were used: river width = 500 m, river depth = 15 m, roughness factor = 0.05, current = 2 m/s, water temperature = 10°C, and $c_m^* = 0.050$. The mass spilled was 150 metric tons for ammonia and 76.85 metric tons for methyl alcohol. Most of the output quantities listed in the left-hand column are defined in the comments in EVAMX. ZM(N) is the value of the integral in AMSHAH (11.11a):

$$m = -\frac{3}{2}\int_0^1 \tau \, \ell n(\tau) \, c_m^{mean}(\tau) d\tau \qquad \text{AMSHAH (11.11a)}$$

and ZMV = ZM(N)*ZMCHR. S = UF*THAT, where UF is the river current, and so is a direct function of THAT.

SENSITIVITY ANALYSIS

A sensitivity analysis for the Mixing and Evaporation Model would be based on the input variables to the subroutines EVAMX and COMPD and on the parameters which are built into the model. Some of the variables and parameters for the sensitivity analysis are:

1. Spilled mass of cargo.
2. Spilling rate of cargo (if continuous spills are considered).
3. The turbulent diffusion coefficients of the spill.
4. The limiting concentration of the pollutant; so that evaporation from regions of spill with lower concentrations is neglibile in comparison to the total mass of a vapor formed.
5. Water flow velocity.
6. The mass transfer coefficient.

The output variables of the sensitivity analysis would be the total mass of vapor liberated, the time for maximum area of spread, and the maximum area of spread. Each of the factors mentioned above would contribute to the total mass of vapor liberated, the time for maximum area of spread, and the maximum area of spread. Three sets of sensitivity coefficients would be determined on the basis of each of the three output variables. For a realistic sensitivity analysis, all of the above factors are to be analyzed in the complete model. Unfortunately, one of the inputs to the Mixing and Evaporation Model (the pollutant concentration prediction from the Mixing and Dilution Model) is unrealistic. Another problem was that the total vass of vapor liberated from the spill was predicted to be greater than the total mass of the spill, which is physically impossible. Because of the problems associated with the current version of the Mixing and Evaporation Model, a sensitivity analysis, if performed, would not give meaningful results. Hence, a sensitivity analysis for the Mixing and Evaporation Model was not performed.

SUMMARY AND RECOMMENDATIONS

The Mixing and Evaporation Model simulates the process of vapor formation when a liquid cargo spills on water. The model analytically considers the initial spread of a pollutant from an instantaneous spill of liquid cargo and the consequent evaporation. The concentration of the pollutant, obtained from the Mixing and Dilution Model, is utilized to compute the mass of vapor liberated. The present analysis of the vapor formation and the inputs to this analysis are not applicable to most spills of commonly transported cargoes. The following recommendations are made for improvement of the simulation process.

- The combined evaporation and dilution processes should be considered, rather than first considering the mixing and dilution without evaporation and then considering the evaporation of the pollutant. This would avoid the unrealistic prediction of the total mass of vapor formed being greater than the total mass of the spilled cargo.

- The pollutant concentration predictions from the Mixing and Dilution Model should be corrected to give physically meaningful values for all times after spills.

- The formula used for conversion of pollutant concentration in density units into molar fraction concentration should account for regions of high pollutant concentrations and not just regions of low pollutant concentration.

- Modifications of Raoult's law should be made to account for solute-solvent solutions of high affinity, and these are to be used in the simulation.

APPENDIX 6A

TYPOGRAPHICAL ERRORS

The following is a list of the typographical errors in AMSHAH.

1. Page 159, equation (11.9) and page 168, equation (A-5). c_m in the numerator should be c_m^*. The corrected equation would be (both equations are the same relationship):

$$c_m^{mean} = \frac{c_m^{max} - c_m^*}{\ln [c_m^{max}/c_m^*]} \qquad \text{AMSHAH (11.9), AMSHAH (A-5)}$$

2. Page 160, equation (11.11a). The last symbol should be $d\tau$ and and not just d. The correction equation would be:

$$m = \int_0^1 \dot{m}\, d\tau = -\frac{3}{2} \int_0^1 \tau \ln(\tau)\, c_m^{mean}(\tau)\, d\tau \qquad \text{AMSHAH (11.11a)}$$

3. Page 167. The units of the coordinates x, y, and z is to be mentioned, as meters (m).

PRECEDING PAGE BLANK-NOT FILMED

APPENDIX 6B

COMPUTER PROGRAM LISTINGS

PRECEDING PAGE BLANK-NOT FILMED

```
      SUBROUTINE EVAMX(ZML,XMOL,ACR,BCR,CCR,DIPVA,DENL,DIFLW,IFLAG,D,W,
     1US,XN,TW,CSTM,ZMV,S,SIZMX,THAT)
C*****************************************************************************
C
C  ***  THIS SUBROUTINE CALCULATES THE TOTAL MASS OF VAPOR PRODUCED WHEN
C       WATER MISCIBLE- HIGH VAPOR PRESSURE LIQUID IS SPILLED ON WATER AND
C       MIXES WITH THE WATER DUE TO TURBULENT DIFFUSION.
C
C  *************  INPUT ARGUMENTS  *************
C  ***    ZML   = MASS OF LIQUID SPILLED                                  GMS
C  ***    XMOL  = MOLECULAR WEIGHT OF THE LIQUID SPILLED
C  ***    ACR   = CONSTANTS IN THE VAPOR PRESSURE EQUATION  P=10**(ACR-BC
C  ***    BCR   =   ---------------'' -----------------------
C  ***    CCR   = ---------------------' ' ----------------------
C  ***    DIPVA = DIFFUSION COEFFICIENT OF VAPOR IN AIR AT AMBIENT TEMP
C  ***    DENL  = DENSITY  F LIQUID AT THE SPILL TEMPERATURE          GM/C
C  ***    DIPLW = DIFFUSION COEFFICIENT OF LIQUID IN WATER            CM*
C  ***    IFLAG = A FLAG INDICATING THE LOCATION OF SPILL (1=STILL WATER,
C  ***    D     = RIVER DEPTH  (TO BE GIVEN ONLY IF IFLAG=2)          CMS
C  ***    W     = RIVER WIDTH   -------- '' ------------              CMS
C  ***    US    = AVERAGE VELOCITY OF THE STREAM   ----  ''  ----     CM/
C  ***    XN    = STREAM ROUGHNESS FACTOR   ---  ''  -------
C  ***    TW    = WATER TEMPERATURE                                     DEG
C  ***    CSTM  = LIMITING VALUE OF THE MOLE FRACTION CONCENTRATION. SUCH THAT THE
C                 CONTRIBUTION TO EVAPORATION FROM WATER SURFACE REGIONS BEYOND
C                 THIS CONCENTRATION IS NEGLIGIBLE.
C
                                                  REAL DUMMY
C  *************  OUTPUT ARGUMENTS  ************
C  ***    ZMV   = MASS OF VAPOR LIBERATED                                 GMS
C  ***    S     = MAXIMUM DISTANCE IN THE STREAM DIRECTION BEYOND WHICH THE
C                 CONCENTRATION IS EVERYWHERE LESS THAN 'CSTM'.           CMS
C  ***    SIZMX = MAXIMUM SIZE (RADIUS) OF THE SPREAD       CMS
C  ***     THAT = TIME AT WHICH EVAPORATION IS COMPLETE      SEC
C
C*****************************************************************************
C
      DIMENSION  FX(200),ZM(200)
      PI=3.141592654
      TP=0.
      T=0.
      UT=0.
      VOLI=ZML/DENL
      CALL HMTC(DIPVA,XMOL,VOLI,HMP)
      GO TO (10,20),IFLAG
10    EX=DIPLW
      EY=DIPLW
      EZ=DIPLW
      GO TO 30
20    CALL DISP(W,D,IFLAG,T,US,UT,XN,TP,E,EX,EY,EZ)
30    CALL VAPPR(ACR,BCR,CCR,TW,PVAP)
      CSTAR=CSTM*(XMOL/18.)
```

FIGURE 6B-1 Subroutine EVAMX.

```
C  ***  CALCULATION OF THE CHARACTERISTIC CONSTANTS  *******
       THAT=(1./(4.*PI))*(2.*ZML/(CSTAR*SQRT(EX*EY*EZ)))**(2./3.)
       A=SQRT(4.*EX*THAT)
       B=SQRT(4.*EY*THAT)
       DZMCH=PI*A*B*HMP*PVAP
       ZMCHR =DZMCH *THAT
C  ***    INTEGRATION PREPARATION  ********
       N=101
       PX(1)=0.
       DO 40 I=2,N
       TOW=FLOAT(I-1)/FLOAT(N-1)
       CMAX=CSTAR/TOW**1.5
C  ***  'TOW' IS THE NON DIMENSIONAL TIME = TOME/THAT. CMAX IS THE MAXIMUM
C       CONCENTRATION AT ANY TIME IN GM/CM**3
       CMAXM=CMAX/(CMAX+XMOL/18.)
       IF(TOW-0.98) 50,50,60
50     CMENM=(CMAXM-CSTM)/ALOG(CMAXM/CSTM)
       GO TO 40
60     CMENM=CSTM
40     PX(I)=-1.5*TOW*CMENM*ALOG(TOW)
       PX(N)=0.
       DTOW=1./FLOAT(N-1)
C  ***    SIMPSON'S RULE INTEGRATION    **********
       CALL QSF(DTOW,PX,ZM,N)
       ZMV=ZMCHR*ZM(N)
       S=US*THAT
       SIZMX=W/2.
       IF(SIZMX.GT.SQRT(EY*THAT)) SIZMX=SQRT(EY*THAT)
       RETURN
       END
```

FIGURE 6B-1 , continued Subroutine EVAMX.

```
      SUBROUTINE QSF(H,Y,Z,NDIM)
C*****************************************************************
C  ***   SIMPSON=S RULE INTEGRATION ROUTINE . FOR DETAILS SEE THE IBM MANUAL
C
      DIMENSION Y(1),Z(1)
      HT=.3333333*H
      L1=1
      L2=2
      L3=3
      L4=4
      L5=5
      L6=6
      IF(NDIM-5) 7,8,1
C     NDIM IS GREATER THAN 5. PREPARATIONS OF INTEGRATION LOOP
    1 SUM1=Y(L2)+Y(L2)
      SUM1=SUM1+SUM1
      SUM1=HT*(Y(L1)+SUM1+Y(L3))
      AUX1=Y(L4)+Y(L4)
      AUX1=AUX1+AUX1
      AUX1=SUM1+HT*(Y(L3)+AUX1+Y(L5))
      AUX2=HT*(Y(L1)+3.875*(Y(L2)+Y(L5))+2.625*(Y(L3)+Y(L4))+Y(L6))
      SUM2=Y(L5)+Y(L5)
      SUM2=SUM2+SUM2
      SUM2=AUX2-HT*(Y(L4)+SUM2+Y(L6))
      Z(L1)=0.
      AUX=Y(L3)+Y(L3)
      AUX=AUX+AUX
      Z(L2)=SUM2-HT*(Y(L2)+AUX+Y(L4))
      Z(L3)=SUM1
      Z(L4)=SUM2
      IF(NDIM-6) 5,5,2
C     INTEGRATION LOOP
    2 DO 4 I=7,NDIM,2
      SUM1=AUX1
      SUM2=AUX2
      AUX1=Y(I-1)+Y(I-1)
      AUX1=AUX1+AUX1
      AUX1=SUM1+HT*(Y(I-2)+AUX1+Y(I))
      Z(I-2)=SUM1
      IF(I-NDIM) 3,6,6
    3 AUX2=Y(I)+Y(I)
      AUX2=AUX2+AUX2
      AUX2=SUM2+HT*(Y(I-1)+AUX2+Y(I+1))
    4 Z(I-1)=SUM2
    5 Z(NDIM-1)=AUX1
      Z(NDIM)=AUX2
      RETURN
    6 Z(NDIM-1)=SUM2
      Z(NDIM)=AUX1
      RETURN
```

FIGURE 6B-2 Subroutine QSF.

```
C       END OF INTEGRATION LOOP
      7 IF(NDIM-3) 12,11,8
C       NDIM IS EQUAL TO 4 OR 5
      8 SUM2=1.125*HT*(Y(L1)+Y(L2)+Y(L2)+Y(L2)+Y(L3)+Y(L3)+Y(L3)+Y(L4))
        SUM1=Y(L2)+Y(L2)
        SUM1=SUM1+SUM1
        SUM1=HT*(Y(L1)+SUM1+Y(L3))
        Z(L1)=0.
        AUX1=Y(L3)+Y(L3)
        AUX1=AUX1+AUX1
        Z(L2)=SUM2-HT*(Y(L2)+AUX1+Y(L4))
        IF(NDIM-5) 10,9,9
      9 AUX1=Y(L4)+Y(L4)
        AUX1=AUX1+AUX1
        Z(L5)=SUM1+HT*(Y(L3)+AUX1+Y(L5))
     10 Z(L3)=SUM1
        Z(L4)=SUM2
        RETURN
C       NDIM IS EQUAL TO 3
     11 SUM1=HT*(1.25*Y(L1)+Y(L2)+Y(L2)-.25*Y(L3))
        SUM2=Y(L2)+Y(L2)
        SUM2=SUM2+SUM2
        Z(L3)=HT*(Y(L1)+SUM2+Y(L3))
        Z(L1)=0.
        Z(L2)=SUM1
     12 RETURN
        END
```

FIGURE 6B-2, continued Subroutine OSF.

DISP

```
      SUBROUTINE DISP(W,D,IFLAG,T,UF,UT,XN,TP,E,EX,EY,EZ)
C ***********************************************************
C ****  THIS SUBROUTINE IS CALLED BY THE DILUN SUBROUTINE . DISPERSION
C       AND TURBULENT DIFFUSION COEFFICIENTS ARE RETURNED BY THIS SUBROUTINE
C
      PI=3.14159265
      B=W/2.
      RH=W*D/(2.*D+W)
      GO TO (60,70,80),IFLAG
60    E=0.
      RETURN
C *** SPILL INTO A NON TIDAL RIVER
70    USTAR=6.716*XN*UF/RH**(1./6.)
      EZ=0.067*USTAR*RH
      EX=0.1*EZ
      IF(W/D-100.) 72,71,71
71    EY=0.1*EZ
      E=77.*XN*UF*RH**(5./6.)
      GO TO 75
72    EY=0.23*USTAR*RH
      E=225.*USTAR*RH
75    RETURN
C ***  TIDAL RIVER   ******
80    USTAR=3.9*XN*(2.*UT/PI)/RH**(1./6.)
C  ***  USTAR IS BASED ON THE MEAN OSCILLATING FLOW VELOCITY.  ***
      EZ=0.067*USTAR*RH
      EX=0.1*EZ
      EY=0.1*EZ
      IF(W/D-100.) 81,82,82
81    EY=0.23*USTAR*RH
C  ** TRANSVERSE AND VERTICAL DISPERSION COEFFICIENTS
82    EV=6.*D*USTAR
      ET=0.011*0.025*(UT*T/B)**2
      TPV=T/(D**2/EZ)
      TPT=T/(B**2/EY)
      IF(TPV-1.) 83,83,84
83    GO TO 85
84    IF(ET/EV-1.) 85,85,86
85    E=EV
      GO TO 87
86    E=ET
87    RETURN
      END
```

FIGURE 6B-3 Subroutine DISP.

COMPD

```
      SUBROUTINE COMPD(AM,TA,DENLB,DIFCO)
C     THIS SUBROUTINE CALCULATES THE DIFFUSION COEFFICIENT OF A VAPOR IN
C     AND SHOULD BE THE DEFAULT VALUE IF THE DATA IS NOT PRESENT IN THE
C     MANUAL 2 DATA FILE.
C
C  ***INPUTS
C
C     AM       THE MOLECULAR WEIGHT OF THE CHEMICAL
C     TA       AMBIENT TEMPERATURE,DEGREES C
C     DENLB    THE DENSITY OF THE LIQUID AT ITS BOILING POINT,GM/CM**3.
C
C  ***OUTPUTS
C
C     DIFCO    THE DIFFUSION COEFFICIENT,CM**2./SEC
C
      VB=29.9**.33333
      WMO=29.0
      VA=AM/DENLB
      T=(TA+273.2)**1.5
      S1=((1./WMO)+(1./AM))**.50
      S2=((VA**.33333)+VB)**2.
      DIFCO=.0043*(T/S2)*S1
      RETURN
      END



      SUBROUTINE HMTC(DIFCO,XMOL,VOLI,HMP)
C
      ANU=0.15
      AL=VOLI**0.3333
      CUT=5.*10.**5
      TEMP= 293.
      RVAP=82.057/XMOL
      SCHM=ANU/DIFCO
      VELOC= 450.
      REYN=(VELOC*AL)/ANU
      IF(REYN-CUT)  1,1,2
    1 HBAR=(1.328*(REYN**.5)*DIFCO*(SCHM**.3333))/AL
      GO TO 3
    2 HBAR=(.037*DIFCO*(SCHM**.3333)*(REYN**0.8))/AL
    3 HMP=HBAR/(RVAP*TEMP)
      RETURN
      END
```

FIGURE 6B-3, continued Subroutine DISP.

CHAPTER 6 - LIST OF SYMBOLS

$a(t), b(t)$	=	Semi-axes for elliptical regions of pollutant concentration, within which the pollutant concentration is greater than the limiting concentration (cm or m)
c	=	concentration of pollutant (g/cm^3)
c_m	=	concentration of pollutant as a molar fraction
c_m^*	=	limiting molar concentration
$c_m max$	=	maximum pollutant concentration at any time
$c_m mean$	=	a theoretical mean concentration of pollutant
D	=	diffusion constant (cm^2/s)
e_x, e_y, e_z	=	turbulent diffusion coefficients (cm^2/s)
f	=	fugacity of gas ($dyne/cm^2$)
$\bar{f}$	=	fugacity of a component in solution ($dyne/cm^2$)
h_p	=	mass transfer coefficient (s/cm)
K	=	temperature (°K); constant for evaporation
m	=	total mass of vapor liberated (dimensionless)
$\dot{m}(\tau)$	=	rate of vapor liberated (dimensionless)
M	=	mass (g)
$\dot{M}$	=	rate of mass change (g/s)
N	=	number of moles
p	=	total pressures; partial vapor pressure of liquid at the water surface ($dyne/cm^2$)
$\bar{p}$	=	partial pressure ($dyne/cm^2$)
p'	=	vapor pressure ($dyne/cm^2$)
P	=	pressure in tanks ($dyne/cm^2$)
R	=	universal gas constant (erg/g-mole °K)
t	=	time (s)

PRECEDING PAGE BLANK-NOT FILMED

$\hat{t}$	=	time beyond which the pollutant concentration is less than the limiting concentration (s)
T	=	temperature (°K)
v	=	molal volume in pure state (cm^3)
$\bar{v}$	=	partial molal volume (cm^3)
V	=	volume (cm^3)
x	=	mole fraction (dimensionless); coordinate (cm)
y	=	coordinate (cm)
z	=	coordinate (cm)
∇^2	=	Laplacian operator $\equiv \frac{\partial}{\partial x^2} + \frac{\partial}{\partial y^2} + \frac{\partial}{\partial z^2}$ ($1/cm^2$)
ρ	=	density (g/cm^3)
μ	=	molecular weight (amu)
τ	=	modified time variable

Subscripts:

c	=	cargo
k	=	k th component in mixture, k = 1, 2, 3, ...
liq	=	liquid
v	=	vapor
w	=	water

CHAPTER 6 - REFERENCES

[1] Department of Transportation, U.S. Coast Guard, Assessment Models in Support of the Hazard Assessment Handbook (CG-446-3), CG-D-65-74, January 1974.

[2] Arthur D. Little, Inc., Hazard Assessment Computer System, User Manual (HACS), Cambridge, Mass., December 1974.

[3] Moelwyn-Hughes, E. A., Physical Chemistry, pp. 758-760, 2nd rev. ed., Pergamon Press, Oxford, England, 1965.

[4] Foust, A. S., L. A. Wenzel, C. W. Clump, L. Maus, and L. B. Andersen, Principles of Unit Operations, p. 553, Wiley, New York, 1960.

[5] Weast, Robert C. (ed.), Handbook of Chemistry and Physics, 52nd ed., p. D-171, Chemical Rubber Co., Cleveland, Ohio, 1971.

CHAPTER 7

RADIATION VIEW FACTOR MODEL

INTRODUCTION

The Radiation View Factor Model is designed to compute the view factor between a fire and a receptor. This model corresponds to the documentation in Chapter 13, Radiation View Factor between an Inclined Flame and an Arbitrarily Oriented Surface in Space, of the Assessment Models in Support of the Hazard Assessment Handbook (AMSHAH) [1]. The correspoinding computer code in the Hazard Assessment Computer System (HACS) [2] is under the executive subroutine MODB2 which utilizes the following computational subroutine: SVIEW.

The factors influencing the value of the view factor between any finite surface and an infinitesimal surface are the size and shape of the finite surface, and the position and relative orientation of the infinitesimal surface with respect to the finite surface. A fundamental assumption in modeling both jet flames and pool fires is to treat the envelope of the flame from the fire as a tilted right circular cylinder. Radiation flux incident on the receptor, rather than the total heat transfer, is of interest; hence the receptor is modeled as an infinitesimal receiving surface. The inclination is because of wind effects for pool fires and the angle of emission for gas jets. The radius, length, and inclination of the equivalent right circular cylindrical flame are obtained as inputs to this model from the outputs of other flame models of HACS. The view factor is based on calculations from analytical expressions derived for the view factor between an inclined right circular cylinder and a receptor placed downwind facing the flame directly, and inclined at the same angle as the flame. The Radiation View Factor Model should be designed so as not to give an underestimate of the view factor between a flame and a receptor so that damage estimates would be conservative.

A problem in the Radiation View Factor Model is that the general analytical expressions derived for the view factor - from an inclined right circular clyindrically shaped envelope of the flame to any arbitrary infinitesimal receptor at any position and in any orientation - in AMSHAH are not computer coded in the corresponding computer subroutine SVIEW of HACS. Instead, SVIEW utilizes a simplified version of the analytical results, with the limitations that the receptor be downwind of the flame and inclined at the same angle to the vertical as is the flame. These analytical limitations on the receptor position (downwind) and orientation (facing the flame and inclined at the same angle to the vertical as the flame) may not give the maximum value of the view factor between a flame and a receptor, for a given distance between the center of the base of

---

[1] Department of Transportation, U.S. Coast Guard, Assessment Models in Support of the Hazard Assessment Handbook (CG-446-3), (AMSHAH), CG-D-65-74, January 1974.

[2] Arthur D. Little, Inc., Hazard Assessment Computer System, User Manual (HACS), Cambridge, Mass., December 1974.

the flame and the receptor. Thus, contrary to a comment card in the HACS program, the maximum flux at a given location is not necessarily computed. The problems in the model would have given unrealistic sensitivity coefficients, hence a complete sensitivity analysis was not performed. The symbols and references are listed at the end of this chapter.

ASSUMPTIONS AND APPROXIMATIONS

There are various assumptions and approximations, both explicit and implicit, in the development of the Radiation View Factor Model used in AMSHAH and in HACS.

The assumptions in AMSHAH are:

1. The flame envelope is in the shape of a tilted right circular cylinder.

2. The view factor between the flame and the receptor may be computed only on the basis of the sides of the cylindrical envelope, since the contributions from the ends of the cylindrical envelope are small and hence negligible.

Additional implicit assumptions in HACS are:

3. The receptor is placed directly downwind from the flame.

4. The receptor is at the same level as the base of the flame.

5. The receptor and the flame are both inclined at the same angle to the vertical.

6. The receptor is oriented to face the flame, the normal to the receptor surface intersecting the axis of the flame.

The implications and physical realism of these assumptions are briefly discussed in the following.

1. Tilted Right Circular Cylindrical Flame Envelope. The assumptions of a tilted right circular cylindrical flame envelope, as shown in Figure 7-1, have been discussed in the Thermal Radiation from Flames Model, Chapter 5 of this report. In short, the assumption of a right circular cylindrical flame envelope is valid for fires that are "reasonably regular," i.e., if the longest dimension along a side of the fire is not more than about four times the shortest dimension. In such cases the equivalent diameter of these fires, as represented by the hydraulic diameter, will provide a reasonable representation of the fire.

2. Major Contributions to View Factor is from the Cylindrical Surfaces. The second major assumption in AMSHAH is that the major contribution to the view factor is from the cylindrical surface of the flame

envelope and the contribution from the top end surface is negligible. The contribution of the top end of a cylindrical flame to the view factor (between the cylindrical flame and an infinitesimal area of a receptor) is about a maximum of one-hundredth of the contribution from the cylindrical surface (for the ratio of 1/6 between the radius and the length of a cylindrical flame). Hence this assumption seems valid.

3. Receptor is Downwind from the Flame. The analytical derivation in AMSHAH is a general derivation and in HACS a limitation was placed of positioning the receptor in the downwind direction only. For positions of the receptor near a fire, the maximum heat flux received by a receptor on the same level as the base of the flame is in the downwind direction, as the flame would be to the side of the receptor and also above the receptor. Hence this approximation seems valid for positions near inclined flames.

4. The Receptor is at the Same Level as the Base of the Flame. This is another implicit assumption made in the computer coding in HACS and hence limiting the generality of the analytic derivations of AMSHAH. This would be a good assumption for large fires that break out on water and for receptors on the surface of the water.

5. Receptor Inclination Equal to the Flame Inclination. Another limitation imposed on the general analytical expressions of AMSHAH is that the angle at which the receptor is inclined to the vertical is always equal to the inclination of the flame with the vertical. This assumption would not normally give the maximum heat flux received by the receptor and hence is a limitation on the predictions of maximum heat received by receptor.

6. Receptor Orientation to Directly Face Flame Envelope. An implicit assumption of HACS is that the receptor directly faces the flame; that is, the normal to the surface of the receptor would intersect the axis of the right circular cylindrical flame envelope. This particular orientation is a limitation on the general orientation of the receptor in the analytical analysis of AMSHAH. It is the orientation in which the maximum possible radiant thermal flux would be intercepted by the receptor, for a particular distance of the receptor from the center of the base of the flame envelope (the receptor being downwind).

ERRORS AND INCONSISTENCIES

Differences Between AMSHAH and HACS

The main differences between AMSHAH and HACS are that there are many limitations assumed implicitly in HACS which are not mentioned in AMSHAH and these limitations give different expressions for the view factors. These new expressions for the view factors are computer coded but are not expressed explicitly in the corresponding documentation of AMSHAH. One particular serious limitation is keeping the receptor inclination with the vertical equal to the inclination of the flame envelope with the vertical. This would, in general, not give the maximum view factor between

the flame envelope and the radiator. Another limitation in the computer coding of HACS is the implicit assumption of positioning the receptor in the downwind position. For inclined flames, the view factors at positions that are crosswind may be greater than for positions downwind--for equal large distances from the center of the base of the flame--as the crosswind locations have a larger projected area of the flame envelope as compared to the positions downwind of the flame envelope. In Appendix 7C (Figure 7C-7) is a flow chart of the subroutine SVIEW of HACS and comparing the subroutine with the documentation of Chapter 13 and Appendix to Chapter 13 of AMSHAH, we note that the general analytical procedure developed in AMSHAH is not computer coded in the corresponding subroutine SVIEW of HACS. Subroutine VRCYL mentioned in the flow chart of AMSHAH is not called and does not exist in the corresponding computer coding of HACS that is currently available.

Coding Errors

Some variables, e.g., PF, are defined in the computer coding but are not used subsequently. Some other variables, e.g., RT and XM, are defined twice in the same set of computer statements without having any intermediate branching points which might have revalued these variables selectively.

Typographical Errors

The typographical errors in AMSHAH are listed in Appendix 7D.

ACCURACY ASSESSMENT

The following is an accuracy assessment for the View Factor Model. An assessment is made for each of the assumptions in AMSHAH and HACS.

The tilted right circular cylindrical flame envelope assumption is for fires that are "reasonably regular." For such fires, the equivalent diameter is represented by the hydraulic diameter, which is given by

$$\text{Hydraulic Diameter} = \frac{4 \times (\text{area of base of fire})}{(\text{perimeter of base of fire})}$$

As stated earlier, the assumption of a cylindrical flame envelope has an additional implicit assumption that the view factor characteristic curve (view factor versus distance of receptor from center of base of flame) would be the same for the real fire and the assumed cylindrical envelope. This would not be correct at points other than at which the actual flame view factor characteristic and the cylindrical flame envelope view factor characteristic are matched. The differences between the modeled view factor prediction and the actual view factors would be expected to vary more for the same variation of distances when the receptor is closer to the flame. When the receptor is far from the flame, it is expected that the matching of the characteristics would be such as to obtain identical asymtotic behavior for the predicted view factors and for the actual view factors, because, when the receptor is at a large distance from the flame, the geometric details of radiating objects becomes relatively unimportant. Cylinders, rectangular prisms, and cones will all appear to be line sources.

Rein, Sliepcevich and Welker [3] have taken the flame envelope as an inclined circular cylinder with the top and bottom ends horizontal, as shown in Figure 7-2. In the modeling of the inclined flame as a cylinder with horizontal ends, the top and base become ellipses with semi-minor axis equal to the radius R of the cylinder and the semi-major axis being (R sec θ), where θ is the angle of inclination of the flame envelope to the vertical. As the flame tilts more due to greater wind velocities, the angle of inclination, θ , with the vertical increases and the semi-major axis (R sec θ), also increases. Rein et al. mention that the increase in the base length causes this cylindrical model to approximate the flame-receptor situation more closely than if the base length were not increased because the flame actually trails downwind from the fuel source due to the action of the wind. Hence modeling with horizontal ends will give more realistic view factors than the AMSHAH model.

In order to evaluate the contribution of the cylindrical surfaces to the total view factor between a flame and a receptor, Table 7A-1 of Appendix 7A is constructed. This table presents a tabulation of the view factors of cylindrical surfaces for flame inclination of 45° for (R/L) = (1/6). The tabulated results are from calculations done by the computer program SVIEW, the analytical procedure of AMSHAH, and the results of Rein et al, and because of the differences of the different methods used, the values for the view factors are slightly different. To be able to assess the effect of the top end surface of the flame envelope on the view factor, an analysis is presented in Appendix 7B of this chapter wherein an approximation of the maximum possible view factor is determined from the total area at the top end of an inclined right circular cylindrical surface to a receptor inclined such that the normal to the receptor passes through the center of the top end surface. Values of the view factors for different inclinations of the flame and for different distances from the base of the flame are tabulated in Table 7B-1 for ratios of cylindrical flame envelope radius (R) to length (L) of (1) and (1/6). Comparison of the view factors from Tables 7A-1 and 7B-1 are given in Table 7A-2 for (R/L) = (1/6), and this shows that for the same equivalent distances of the receptor from the flames, the contribution of the top end is about a maximum of one-hundredth of the contributions of the cylindrical surfaces and this ratio further decreases as the distance between the receptor and the flame increases, for flames inclined at 45° to the vertical. The actual ratio of the contribution is expected to be lower than the one-hundredth value mentioned above for the case of maximum view factor for a given receptor-to-flame distance. This is because the contribution to the receptor from the top end will decrease when the receptor is inclined to give the maximum overall view factor from the cylindrical surface as well as the top end surface of the inclined right circular cylindrical flame envelope. From the above analysis, it seems reasonable to neglect the effect of the top end surface on the view factor.

---

[3] Rein, R. G., C. M. Sliepcevich, and J. R. Welker, "Radiation view factors for tilted cylinders," J. Fire Flammability 1:140-153, 1970.

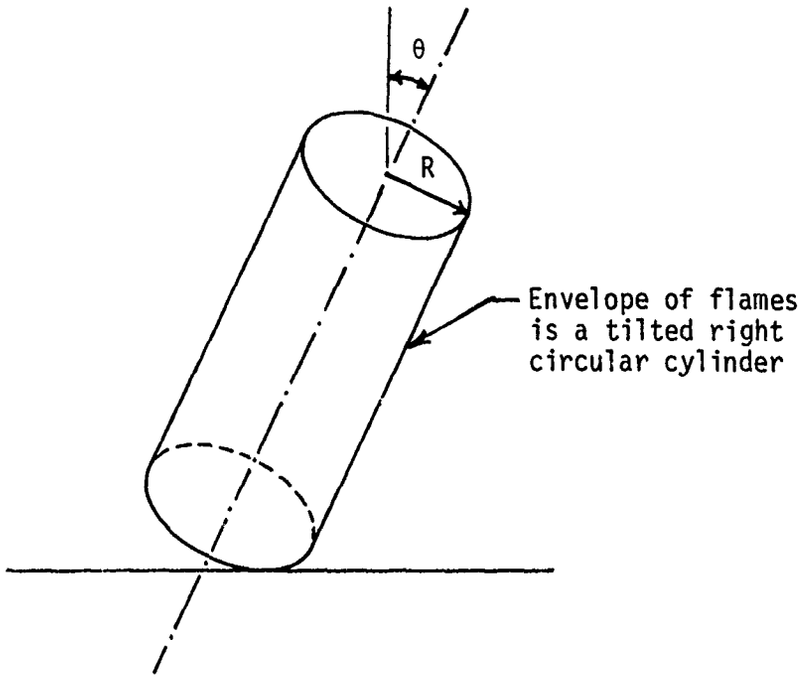


FIGURE 7-1 Flame envelope, A.

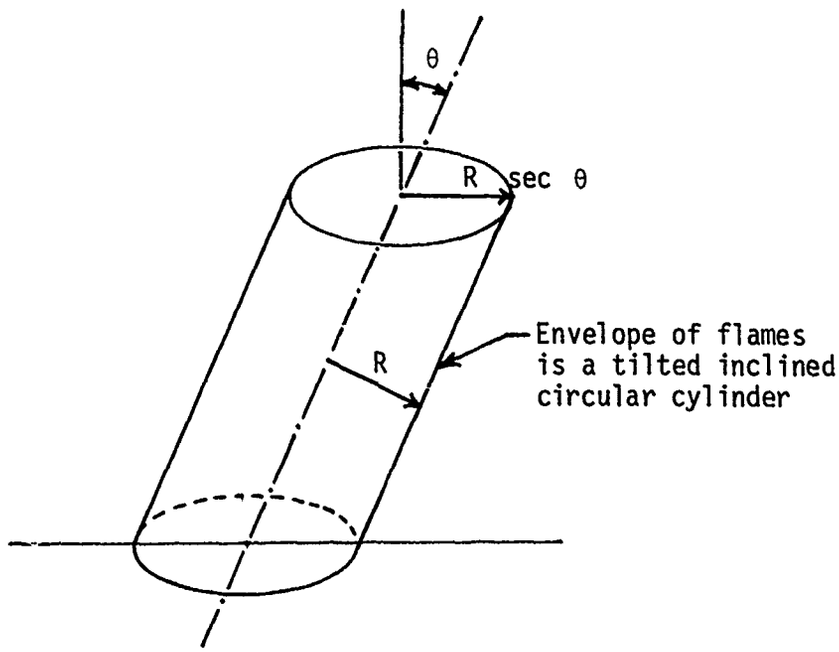


FIGURE 7-2 Flame envelope, B.

Locating the receptor downwind from the flame is a limitation on the analytical derivation in AMSHAH for any general location of the receptor. At distances close to the flame, positions of the receptor which are downwind are expected to receive the maximum radiant heat flux because these positions would be closest to the entire flame length, but for flames that are inclined and for positions that are distant from the flame base, positions crosswind may give greater view factors because positions that are at crosswind locations "see" a larger projected area of the flame as compared to positions that are downwind. The general analytical expressions of AMSHAH, if computer coded into HACS, would give the precise view factors for locations that are crosswind for relatively large distances between the surfaces. The ability to treat crosswind locations should be incorporated into the modeling, since conservative estimates of damage are not assured by considering only downwind positions.

The receptor being at the same level as the bases of the flame is a good assumption for tall fires because in general, most receptors are at only a small height above the base of the flame. It should also be noted that for small distances of receptors from the base of inclined flames, any increase in the height of the receptor from the base of the flame would bring the receptor closer to the flame and would hence make the view factor larger and hence the estimates of SVIEW would not be conservative estimates. This is because there is no provision in SVIEW to account for a receptor being higher than the base of the flame. There could be instances of nearby cargo vessels and harbor structures that would not be at the same level as the flames burning on the water and HACS would not give accurate predictions of radiant thermal flux to such receptors.

The assumption of the receptor inclination being equal to the flame inclination is a severe limitation on the View Factor Model because at only one particular distance of the receptor from the base of the flame will the receptor, having the same inclination as the flame, receive the maximum radiant heat flux (because the maximum view factor for different inclinations, at that particular distance, would be at the same receptor inclination as the inclination of the flame). Even for vertical flames (when there is no wind) a receptor inclined at the same angle as the flame (i.e., the receptor is vertical) would not receive the maximum radiant thermal flux. The radiant flux received by a vertical receptor would approach asymptotically the maximum flux that can be received at any particular distance only as the distance from the receptor to the flame increases.

The radiant thermal flux received by a receptor inclined at the same inclination as the flame - as computed by HACS - can be compared to the maximum radiant thermal flux received by a receptor inclined to receive the maximum radiant thermal flux. The comparison can be as a ratio of the HACS computation to the maximum value. This ratio would change in value as the distance of the receptor from the flame is increased. The ratio would be unity for a receptor at the surface of the flame envelope. As the distance between the receptor and the flame increases this ratio would decrease from unity to some lower value, then increase to the maximum of unity and then finally decrease asymptotically to a value of approximately the cosine of the angle of inclination of the receptor. This behavior is clearly seen in Figure 7-3.

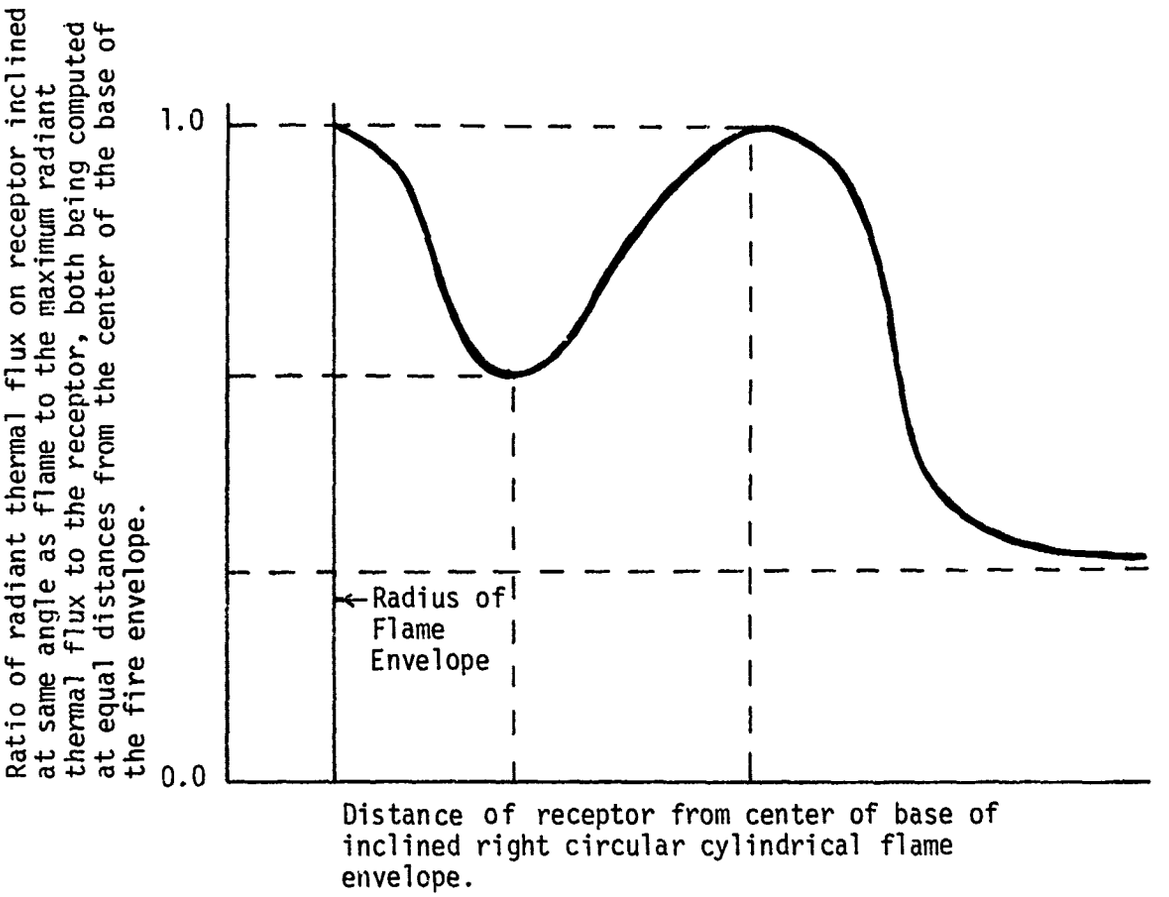


FIGURE 7-3 Ratio of actual radiant thermal flux received by a receptor inclined at the same angle as the flame to the maximum radiant thermal flux to the receptor. Flame angle non-zero.

In the computations for Table 7A-1, the model used by SVIEW has the receptor inclined at the same angle to the vertical as the flame envelope is inclined to the vertical. The analytical results of AMSHAH and the numerical results of Rein et al. are the view factors between the inclined cylindrical flame envelope and a vertical receptor. A comparison of the results shows that the values of the view factors as predicted by SVIEW are larger than the analytical results for small distances between the receptor and the flame envelope - up to $(X/R) \leq 6$. For greater distances between the receptor and the flame envelope the model from SVIEW gives lower values of the view factors, up to 30% lower than those of Rein et al. This is to be expected because the inclination of the receptor to the vertical is the same as the inclination of the flame envelope to the vertical and for small distances between the inclined flame and the receptor, the receptors "see" more of the flame as compared to the vertical receptors. The model in SVIEW does not consider locations which are crosswind where the view factors can be greater than for locations downwind for the same distances between the receptor and radiator. Because the values given by SVIEW for the view factors for a given distance from the receptor to the radiator are not the maximum; hence using SVIEW without receptor modifications would not give consistent conservative results.

The assumption of the orientation of the receptor to be such that the normal to the receptor - placed downwind - would intersect the axis of the cylindrical flame envelope is valid to obtain the maximum view factor between a flame and a receptor. Any variation of the orientation of the receptor would decrease the view factor between the flame and the receptor. This lower value would then not be a conservative estimate.

SENSITIVITY ANALYSIS

For a complete sensitivity analysis to be performed for determining the view factor from the flame envelope to a receptor, not only the inputs to the subroutine SVIEW but also other factors would have to be considered. The inputs to the subroutine SVIEW are:

1) The length of the flame envelope, L;

2) The radius of the flame envelope, R;

3) The inclination of the flame envelope, θ, with the vertical;

4) The distance of the receptor from the center of the base of the flame envelope.

In addition to the above, some more factors have to be considered as these are the implied assumptions and would affect the view factor that would be computed. The additional factors in the sensitivity of the view factor model are:

5) The inclination of the receptor;

6) The orientation of the receptor;

7) The position of the receptor at a position other than a downwind location;

8) The level of the receptor compared to the level of the base of the flame envelope;

9) The shape of the flame envelope.

Each of the above factors would contribute to the view factor between the flame envelope and the receptor. For a realistic sensitivity analysis to be performed, all of the above factors are to be analysed in the complete model. Any coefficients obtained from a sensitivity analysis for view factors as modeled in HACS with many limitations would not consider the more critical coefficients of receptor inclination for maximum radiant thermal flux received by the radiator and for crosswind positions of the receptor and hence the sensitivity coefficients would not be realistic. For these reasons, a sensitivity analysis for the subroutine SVIEW was not performed.

SUMMARY AND RECOMMENDATIONS

The general model developed in AMSHAH would give the view factor between a receptor, which can be located anywhere and oriented in any direction, and a flame, its envelope being modeled in the shape of an inclined right circular cylinder. The effect of the top end surface on the view factor was analyzed for a flame length to radius ratio of six, with 45° inclination of the flame; the contribution of the top end surface was less than one hundredth of the contribution from the cylindrical surfaces. This shows that the assumption of neglecting effects of top end surface on the view factor seems to be justified. Limitations on the position and orientation of the receptor were made in the corresponding computer coding of HACS (subroutine SVIEW). The major limitations being that the receptor is inclined to the vertical at the same angle as the flame envelope is inclined to the vertical. Another limitation is that the receptor is only in a downwind position from the base of the flame. Because of these limitations, consistent conservative estimates of the radiated thermal flux from the fire to the receptor cannot be obtained. It is recommended that variations in the receptor inclination be taken into account to give a local maximum view factor. It is also recommended that positions of the receptor other than downwind locations - especially crosswind locations - be investigated to enable the computation of the maximum values of view factors for a given distance from the receptor to the center of the base of the flame envelope.

APPENDIX 7A

TABLES OF VIEW FACTORS

TABLE 7A-1 View Factor, $\frac{L}{R} = 6$, $\theta = 45°$, Receptor Vertical

$\frac{X}{R}$	SVIEW [1]	AMSHAH (Analytical) [2] Figure 13.6	Rein et al. [3]
2	0.518	0.39	0.40
5	0.213	0.18	0.18
6	0.1619	0.13	0.155
8	0.0890	0.088	0.10
10	0.0501	0.055	0.065
14	0.0200	0.024	0.03
17	0.01198	0.016	0.017
20	0.00790	0.010	0.012
28	0.00347	0.0046	0.005
40	0.00152	0.0021	0.0021

R = radius of cylindrical flame
X = distance of receptor from nearest edge of flame base
L = axial length of the flame
θ = inclination of flame with vertical by wind

Different methods were used by SVIEW, AMSHAH and Rein et al. [3] for obtaining the view factors. Because of the differences in the methods, the values for the view factors are slightly different.

TABLE 7A-2 Comparison of View Factors from Cylindrical Surface and from Top End Surface of Inclined Right Circular Cylindrical Flame Envelope to Receptor at Same Level as Base of Flame (Flame Inclination 45°, R/L = 1/6)

$\frac{S}{R}$	View Factor from Cylindrical Surfaces			Approximate View Factor from Top End Surface
	SVIEW [1]	AMSHAH [2]	Rein, et al. [3]	
2	0.518	0.39	0.40	0.0036
5	0.213	0.18	0.18	0.00086
10	0.0501	0.055	0.065	0.00021
20	0.0079	0.010	0.012	0.000051
40	0.0015	0.0021	0.0021	0.000012

APPENDIX 7B

EFFECT OF TOP END OF RIGHT CIRCULAR INCLINED CYLINDRICAL FLAME ENVELOPE ON VIEW FACTOR

The effect of including the top of a right circular cylindrical flame envelope on the model for the view factor to a receptor on the ground is investigated on the basis of projected areas. This investigation would give close to the maximum effect on the view factor as it assumes the receptor to be oriented in such a manner that the normal to the receptor passes through the center of the top end surface of the inclined right circular cylindrical flame envelope. The projected area in any direction is given by equation 7B-1, see Figure 7B-1.

$$(\text{Projected Area}) = (\text{Actual Area}) \times (\cos \gamma) \qquad (7B\text{-}1)$$

where γ = angle between the normal to the area and a line drawn from the center of the area to the receptor

The receptor is placed on the ground, as at C in Figure 7B-2 and for the receptor to see the top surface of the inclined flame AB, AC has to be greater than AD, where $A\hat{B}D$ is a right angle. From trignometrical relations applied to Figure 7B-2, the following expressions are obtained.

$$X_1 = AD = AB \operatorname{cosec} \theta = L \operatorname{cosec} \theta \quad ; \quad \text{let} \quad n_1 = X_1/L \,.$$

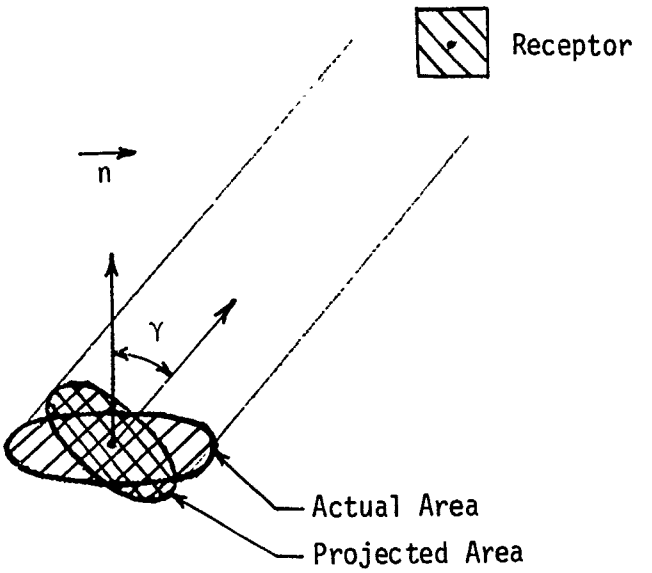
$$BC = M = \sqrt{AB^2 + AC^2 - 2\,(AB)\,(AC)\,(\cos B\hat{A}C)}$$

$$\therefore \quad M = \sqrt{L^2 + X^2 - 2\,(L)\,(X)\,(\sin \theta)} \qquad (7B\text{-}2)$$

$$M = L\sqrt{1 + (X/L)^2 - 2\,(1)\,(X/L)\sin \theta}$$

$$\therefore \quad M = L\sqrt{1 + n^2 - 2\,n \sin \theta}, \text{ where } n \equiv X/L$$

$$n_2 \equiv \left[\frac{M}{L}\right] = \sqrt{1 + n^2 - 2\,n \sin \theta}$$

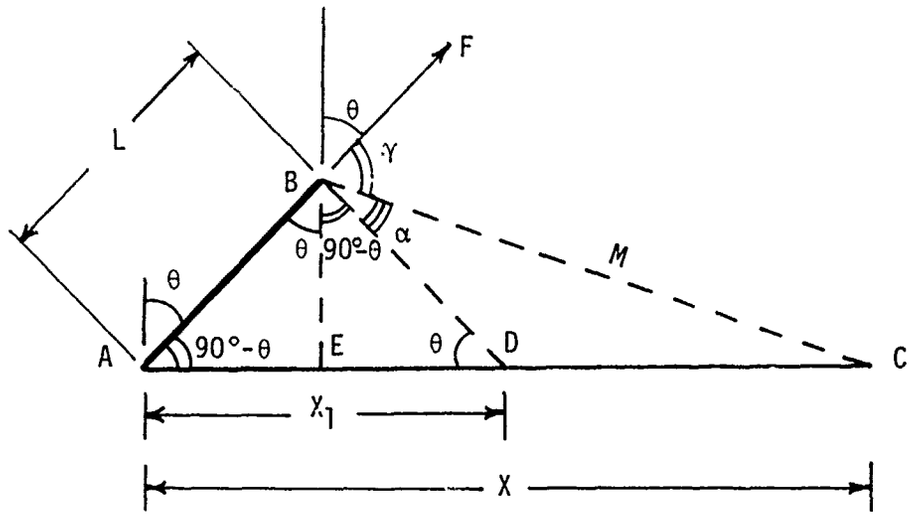


Actual area

Projected area

Receptor

FIGURE 7B-1 Projected area.



$\overline{AB} \equiv L$ = Axial length of flame

$\overline{BC} \equiv M$ = Distance of receptor from top surface of inclined right circular cylindrical flame

$\overline{CA} \equiv X$ = Distance of receptor from base of flame

$\overline{AD} \equiv X_1$ = Distance of receptor from base of flame, beyond which the top surface of cylindrical flame starts contributing to view factor from flame to receptor

$\hat{ABE} \equiv \theta$ = Inclination of flame to the vertical, due to wind

$\hat{FBC} \equiv \gamma$ = Angle between normal to top surface of inclined right circular cylindrical flame envelope and a line joining the center of the top surface to the receptor

$\hat{ABC} \equiv \beta$

$\hat{ABD} = 90°$

$\hat{DBC} \equiv \alpha = \beta - 90°$

$\alpha = 90° - \gamma$

$n \equiv X/L$

$n_1 \equiv X_1/L$

$n_2 \equiv M/L = BC/AB$

FIGURE 7B-2 Effect of top surface on view factor.

From ΔABD,

$$X_1 = AD = AB \operatorname{cosec} A\hat{D}B = L \operatorname{cosec} \theta$$

$$\therefore n_1 \equiv \frac{X_1}{L} = \operatorname{cosec} \theta \qquad (7B\text{-}3)$$

From ΔABC,

$$\left[\frac{\sin A\hat{B}C}{AC}\right] = \left[\frac{\sin B\hat{A}C}{BC}\right]$$

$$\therefore \sin A\hat{B}C = \left[\frac{AC}{BC}\right] \sin B\hat{A}C$$

i.e. $\sin \beta = \frac{X}{M} \sin (90-\theta) = \frac{X}{M} \cos \theta$, but $\sin \beta = \sin (180-\beta) = \sin \gamma$

$$\therefore \sin \gamma = \frac{n L \cos \theta}{L\sqrt{1 + n^2 - 2 n \sin\theta}}$$

$$\sin \gamma = \frac{n \cos \theta}{\sqrt{1 + n^2 - 2 n \sin \theta}}$$

$$\cos \gamma = \sqrt{1 - \sin^2 \gamma}$$

$$= \sqrt{1 - \frac{n^2 \cos^2 \theta}{1 + n^2 - 2 n \sin \theta}}$$

$$= \sqrt{\frac{1 + n^2 - 2 n \sin \theta - n^2 \cos^2 \theta}{1 + n^2 - 2 n \sin \theta}}$$

$$= \sqrt{\frac{1 - 2 n \sin \theta + n^2 (1 - \cos^2 \theta)}{1 - 2 n \sin \theta + n^2}}$$

$$\therefore [\cos \gamma] = \left[\sqrt{\frac{1 - 2 n \sin \theta + n^2 \sin^2 \theta}{1 - 2 n \sin \theta + n^2}}\right] = \left[\frac{\text{Projected Area}}{\text{Actual Area}}\right] \qquad (7B\text{-}4)$$

The view factor $F_{dA_1 \rightarrow A_2}$ from a surface A_2 to an elemental surface dA_1 is given by equation[1](7B-1).

$$F_{dA_1 \rightarrow A_2} = \frac{1}{\pi} \int_{A_2} \frac{\cos \theta_1 \cos \theta_2}{r^2} \, dA_2 \qquad (7B\text{-}5)$$

where

A_1 = area of receptor

A_2 = area of radiating surface

θ_1 = angle between the normal to the receptor A_1 and the line joining the receptor to the elemental area dA_2 on the radiating surface

θ_2 = angle between the normal to the elemental radiator dA_2 and the line joining the receptor to the elemental area dA_2 on the radiating surface

r = distance of the receptor from the radiator

R = radius of inclined right circular cylindrical flame envelope

The top surface of the right circular cylindrical flame envelope is flat and for obtaining our results, we have assumed that the receptor is oriented in such a manner that the normal to the receptor passes through the center of the top surface of the flame, thereby giving the maximum view factor from the top surface of the flame. The total area of the top surface ($A_2 = \pi R^2$) is considered and the values of the angles are based on fixed orientation for the normal to the top of the flat flame surface (dependent on θ) and for the normal to the receptor pointing to the center of the top surface of the flame (dependent on θ and x). This gives, as an approximation, constant values of θ_1, θ_2 and r and hence the equation (7B-5) is simplified for the total area of radiator and unit area of receptor. Since $\theta_1 = 0$ and $(\cos \theta_1) = 1$,

$$F_{dA_1 \rightarrow A_2} \simeq \frac{1}{\pi} \left[\frac{\cos \theta_2}{r^2} \right] \times \pi R^2 \qquad (7B\text{-}6)$$

Here r is equivalent to BC which is M; θ is equivalent to γ of Figure 7B-2. The expression for the view factor can now be expressed in terms of the symbols of Figure 7B-2 to obtain

$$F_{dA_1 \to A_2} \simeq R^2 \frac{\cos \gamma}{M^2} = \left[\sqrt{\frac{1 - 2\,n \sin\theta + n^2 \sin^2\theta}{1 - 2\,n \sin\theta + n^2}}\right]$$

$$\times \left[\frac{1}{L^2\,(1 - 2\,n \sin\theta + n^2)}\right] \times R^2$$

$$\simeq \frac{1}{L^2} \left[\frac{(1 - 2\,n \sin\theta + n^2 \sin^2\theta)^{1/2}}{(1 - 2\,n \sin\theta + n^2)^{3/2}}\right] \times R^2$$

$$F_{dA_1 \to A_2} \simeq \left(\frac{R}{L}\right)^2 \left[\frac{1 - 2\,n \sin\theta + n^2 \sin^2\theta}{(1 - 2\,n \sin\theta + n^2)^3}\right]^{1/2} \qquad (7B\text{-}7)$$

The values of n_1, n_2, cos γ and $F_{dA_1 \to A_2}$ (for R/L = 1 and 1/6) are tabulated in Table 7B-1 for different values of θ and n. From the equations and from the tabulated results it can be seen that for a given flame inclination, the view factor first increases with the distance of the receptor from the base of the flame (and $X > X_1$) reaches a maximum, and then decreases. This is because of the initial rapid increase of the projected area. Then, the rate of increase of the projected area decreases and the reduction in the view factor by the square of the distance between the surfaces becomes larger and the view factor first levels off and then starts decreasing, asymptotically approaching the value of zero for large distances between the two surfaces.

TABLE 7B-1 View Factors of Top Surface of Inclined Right Circular Cylindrical Flames

Angle of Inclination to Vertical	Minimum "Distance" of Receptor from Base of Flame to See Top Surface of Inclined Right Circular Cylindrical Flame Envelope	"Distance" of Receptor from Base of Flame	"Distance" of Receptor from Top Surface of Inclined Right Circular Cylindrical Flame Envelope	$\left[\frac{\text{Projected Area}}{\text{Actual Area}}\right]$	Approximate View Factor from Top End Surface of Inclined Right Circular Cylindrical Flame Envelope to Receptor (R/L)=(1)	Approximate View Factor from Top End Surface of Inclined Right Circular Cylindrical Flame Envelope to Receptor (R/L)=(1/6)
θ	n_1 (eq. 7B-3)	n	n_2 (eq. 7B-2)	$\cos\gamma$ (eq. 7B-4)	$F_{dA_1 \to A_2}$ [(R/L)=1] (eq. 7B-7)	$F_{dA_1 \to A_2}$ [(R/L)=1/6] (eq. 7B-7)
30°	2.0	2	1.732	0.0000	0.0000	0.0000
		5	4.583	0.3273	0.0156	0.00043
		10	9.539	0.4193	0.0046	0.00013
		20	19.519	0.4611	0.0012	0.000034
		40	39.509	0.4809	0.00031	0.0000086
45°	1.41	1.5	1.062	0.0571	0.0506	0.0014
		2	1.474	0.2811	0.1294	0.0036
		5	4.351	0.5828	0.0308	0.00086
		10	9.320	0.6514	0.0075	0.00021
		20	19.306	0.6807	0.0018	0.000051
		40	39.299	0.6943	0.00045	0.000012
60°	1.15	1.2	0.6013	0.0652	0.1805	0.0050
		1.5	0.8074	0.3704	0.5681	0.0158
		2	1.239	0.5907	0.3846	0.0107
		5	4.164	0.7997	0.0461	0.0013
		10	9.148	0.8374	0.0100	0.00028
		20	19.141	0.8527	0.0023	0.000065
		40	39.137	0.8596	0.00056	0.000016

APPENDIX 7C

SUBROUTINE SVIEW

The computations of the subroutine SVIEW of HACS are documented in this Appendix. These are used for computing the view factor between an inclined or vertical right circular cylindrical flame envelope and a receptor placed on the same level as the base of the cylindrical flame envelope; the receptor being downwind from the flame, facing the flame, and the receptor being inclined to the vertical at the same angle as the flame is inclined to the vertical. This documentation is not in AMSHAH because the analytical model developed in AMSHAH is not computer coded in HACS.

The subroutine SVIEW calculates the view factor from a receptor on the same level as the cylinder base to the cylinder, the cylinder being either vertical (Figure 7C-1) or tilted toward the target. However, when the cylinder is tilted toward the target, the analysis is correct only when the target is also tilted to the same extent as the cylinder so that it is parallel to the axis of the cylinder. SVIEW considers three major cases for the location of the receptor in the case of the tilted cylinder:

1. (S-RT) negative, where S is the distance of the target from the center of the base, with the cylinder being upright, and RT is the radius of the cylinder
2. (S-RT) zero
3. (S-RT) positive

Neither case 1 nor 2 is considered by the HACS program. Case 3 is programmed correctly.

The three conditions for the flame angle are analyzed in the following:

A. <u>No Wind: Angle $\theta = 0°$</u>

When there is no wind, the flame inclination θ is zero, and control passes to statement number 42 after initially defining some constants and determining some variables. In the following, the right hand sides of the expression have been modified for $\theta = 0°$.

```
42      EXC = S
        D   = S/RT
        HF1 = 0.0
        HF2 = HF
        GO TO 95
```


THIS PAGE IS BEST QUALITY PRACTICABLE FROM COPY FURNISHED

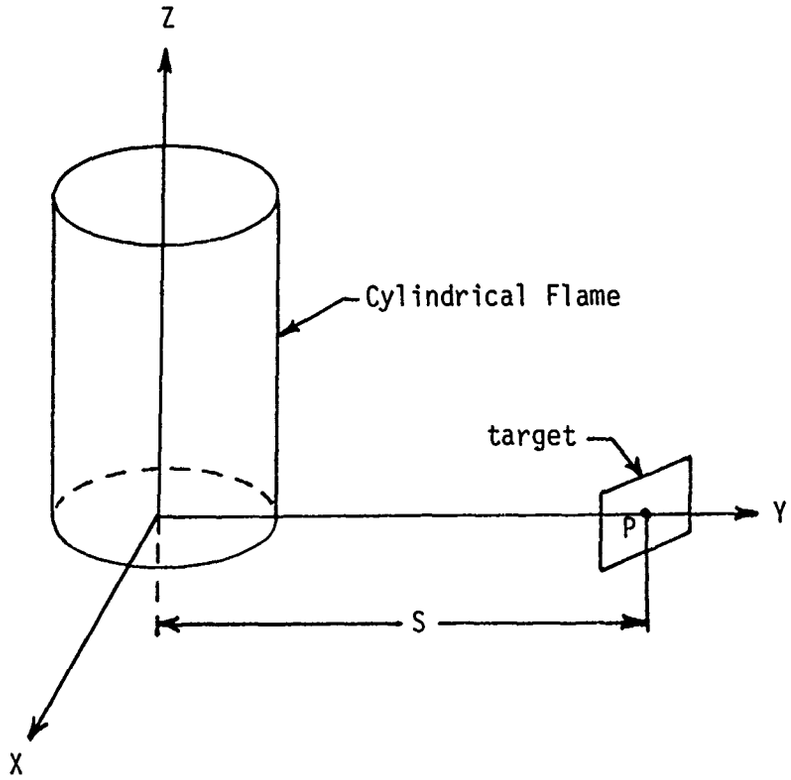


FIGURE 7C-1 Equivalent vertical cylindrical flame envelope and inclined receptor.

95 ELV1 = 0.0.

ELV2 = HF/RT

A1 = $(D+1)^2$

A2 = $(D+1)^2 + (HF/RT)^2$

B1 = $(D-1)^2$

B2 = $(D-1)^2 + (HF/RT)^2$

ARGA1 = 0.0.

ARGA2 = $\dfrac{HF/RT}{\sqrt{D^2-1}}$

ARGB1 = $\sqrt{\dfrac{(D+1)^2 \times (D-1)}{(D-1)^2 \times (D+1)}}$

ARGB2 = $\sqrt{[(D+1)^2 + (HF/RT)^2] \times (D-1)} \;/\; \sqrt{[(D-1)^2 + (HF/RT)^2] \times (D+1)}$

ARGC = $\sqrt{(D-1)/(D+1)}$

F1 = $\dfrac{1}{3.1416*D} \tan^{-1} 0.0 + 0.0 = 0.0$

F2 = $\dfrac{1}{3.1416*D} \tan^{-1} \dfrac{HF/RT}{\sqrt{D^2-1}} + \dfrac{(HF/RT)}{3.1416} *$

$$\left\{\left[\frac{\{(D+1)^2 + (HF/RT)^2 - 2D\}}{D*\sqrt{\{(D+1)^2 + (HF/RT)^2\}\{(D-1)^2 + (HF/RT)^2\}}}\right] * \right.$$

$$\left. \tan^{-1}\left|\sqrt{\frac{\{(D+1)^2 + (HF/RT)^2\}(D-1)}{\{(D+1)^2 + (HR/RT)^2\}(D+1)}}\right| - \frac{1}{D} \tan^{-1}\sqrt{\frac{D-1}{D+1}}\right\}$$

Then control passes to statement number 117

117 VF = F2+F1

Since F1 = 0.0, VF=F2.

Blackshear [4] has different symbols which are related to those in SVIEW by:

SVIEW		Blackshear
S/RT	=	D
HF/RT	=	L
$(D+1)^2 + (HF/RT)^2$	=	A
$(D-1)^2 + (HF/RT)^2$	=	B
VF	=	F_{12}
3.1416	=	π

Therefore,

$$F_{12} = \frac{1}{\pi D}\tan^{-1}\left(\frac{L}{\sqrt{D^2-1}}\right) + \frac{L}{\pi}\left[\frac{A-2D}{D\sqrt{AB}}\tan^{-1}\sqrt{\frac{A(D-1)}{B(D+1)}} - \frac{1}{D}\tan^{-1}\sqrt{\frac{D-1}{D+1}}\right]$$

This is the same expression as given in Blackshear [4].

B. Windy: Angle $\theta < 0°$

For THETA <0, the program will calculate the view factor as for THETA = 0.0. However, THETA is an input to the subroutine SVIEW from the subroutine FLMAN and the latter subroutine computes only positive or zero values of the flame tilt angle. Therefore THETA <0 would not occur. A better programming method would be to report an error for inputs of THETA<0.

C. Windy: Angle $\theta > 0°$

For THETA >0, control passes to statement number 43.

XC = (S-RT)COS θ
EXC = RT+(S-RT)COS θ
D = 1+((S-RT)/RT)COS θ
HFA = (S-RT)SIN θ
HFB = HF-(S-RT)SIN θ

Depending on (S-RT) being negative, zero, or positive, control transfers to statement number 105, 205, or 305 respectively, to calculate HF1 and HF2.

---

[4] Blackshear, P.L. (ed.), Heat Transfer in Fires, John Wiley and Sons, New York, 1974.

Case C.1: (S-RT) is negative

105 HF1 = -(S-RT)Sin θ
HF2 = HF-(S-RT)Sin θ

From Figure 7C-2 it can be seen that HF1 = -PN and HF2 = HF-PN. Once HF1 and HF2 have been determined, control passes to statement number 95. Then the variables needed for determining F1 and F2 are calculated as above. For a vertical cylinder, D is the dimensionless distance (S/RT) of the differential area from the axis of the cylinder. The same value for the tilted cylinder (for this case) would be (QP/RT).

$$QP = OR-NR$$

$$= RT + (S-RT)\cos\theta$$

$$\left[\frac{QP}{RT}\right] = 1 + \frac{(S-RT)\cos\theta}{RT}$$

where RT is the radius of the cylinder. The expression for [QP/RT] here, is identical to D in the computer coding. F1 and F2 are calculated after the calculation of HF1, HF2, and D by using the same equations which hold good for the vertical cylinder with the differential area being vertical and normal to the y axis (Figure 7C-1). For Figure 7C-2, the analytic equations for the case in Figure 7C-1 would not apply. The analytical expressions to determine the view factor are for X>0. The model in HACS was not designed to compute view factors when the receptor is inside the flame. When X is negative, the computer program would try and determine a real root of a negative number, resulting in an error. Hence only positive values of X are simulated in the View Factor model. After the calculation of F1 and F2, control passes to statement number 118.

$\therefore$ VF = F2-F1

= (view factor due to height HF+PN)-(view factor due to height PN)

Case C.2: (S-RT) is zero

$\therefore$ D = 1
HF1 = 0.0
HF2 = HF

Control then passes to statement number 95, to evaluate the variables to be used in F1 and F2. Then control passes to statement number 116 according to which

VF = F2

= (view factor due to the height HF)

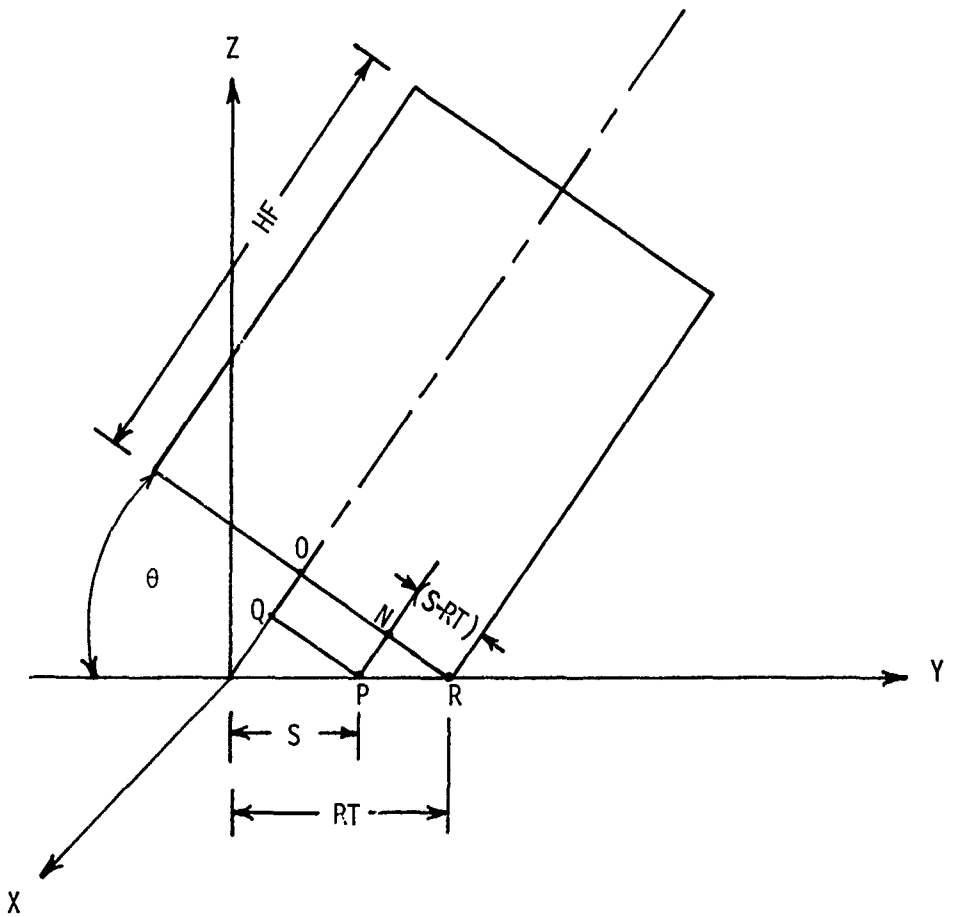


FIGURE 7C-2 Case C.1: (S-RT) is negative.

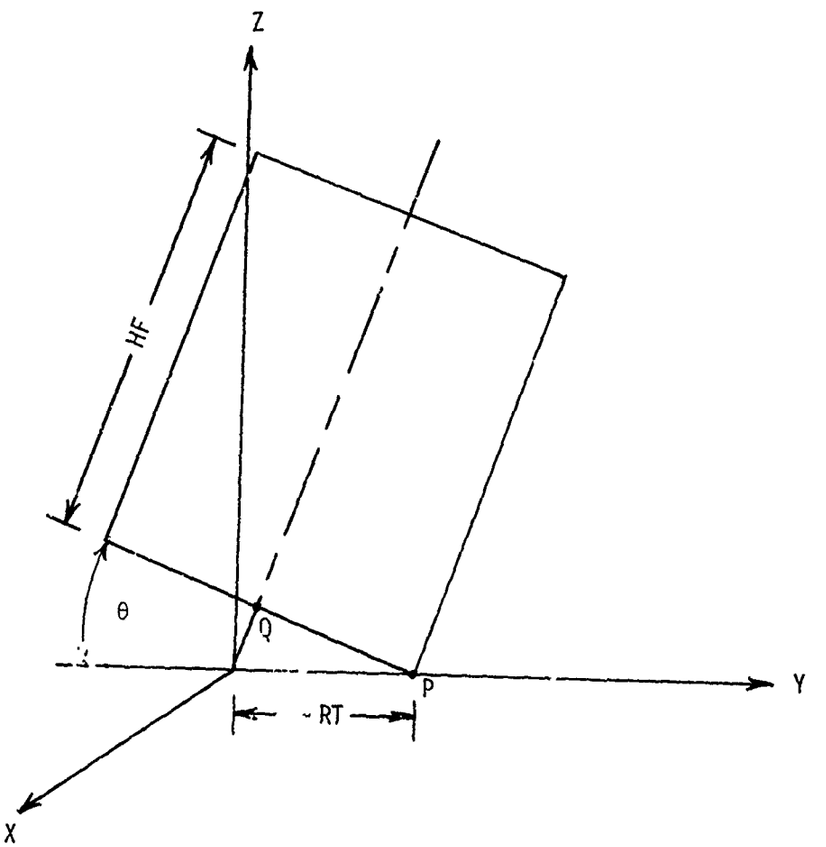


FIGURE 7C-3 Case C.2: (S-RT) is zero.

It should be noted that the view factor should approach 0.5 for a vertical cylinder as (S-RT) → 0, and when (S-RT) = 0, the computer coding tries to determine a real root of a negative number, resulting in an error.

Case C.3: (S-RT) is positive

Three cases arise under this according to the program:

1. ((S-RT)-HF/Sin θ)<0 (Figure 7C-4). Control passes to statement number 405.

   HF1 = HFA = (S-RT)Sin θ
   HF2 = HFB = HF-(S-RT)Sin θ
   GO TO 95

   The parameters for calculation of F1 and F2 are evaluated and then F1 and F2 are calculated. Then control passes to 45; since (S-RT) >0, control branches to statement number 90. For (X-XF) <0, which is identical to((S-RT)-HF/Sin θ) less than zero, we have

   VF = F2+F1, (statement number 117),
   = (view factor due to height OQ) + (view factor due to height QT)

2. ((S-RT)-HF/Sin θ) = 0 (Figure 7C-5). Control passes to statement number 605. We have from the subroutine SVIEW

   HF2 = HF
   HF1 = 0.0

   After F1 and F2 are calculated as in case 1, we have by statement number 116.

   VF = F2
   = (view factor due to height HF)

3. ((S-RT)-HF/Sin θ) >0 (Figure 7C-6). Control passes to statement number 705. Accordingly

   HF1 = (S-RT)Sin θ
   HF2 = HF + (S-RT) Sin θ

   Finally, from statement number 119,

   VF = F1-F2
   = (view factor due to height OQ) - (view factor due to height TQ)

The calculation procedure in HACS is shown in Figure 7C-7, where a complete flow chart is presented. The computer listing for subroutine SVIEW is presented in Figure 7C-8.

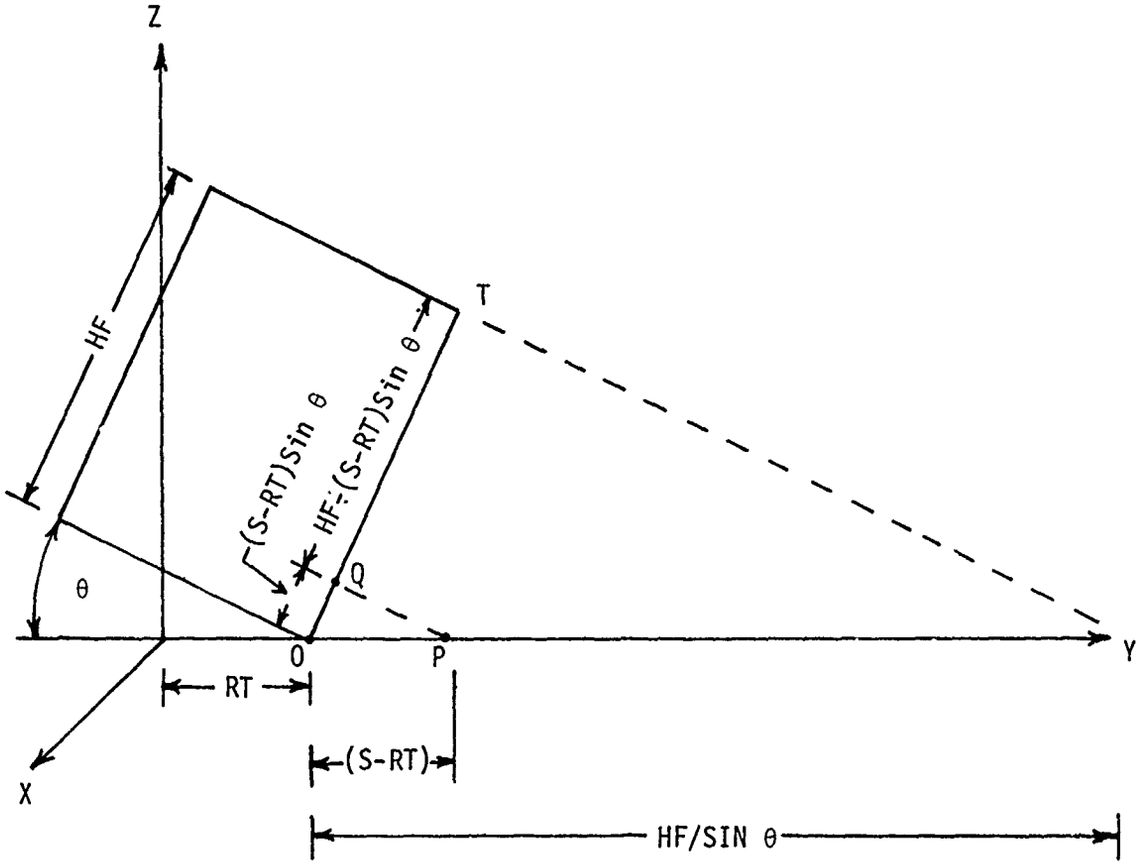


FIGURE 7C-4 Case C.3: (S-RT) is positive; ((S-RT)-HF/Sin θ) <0.

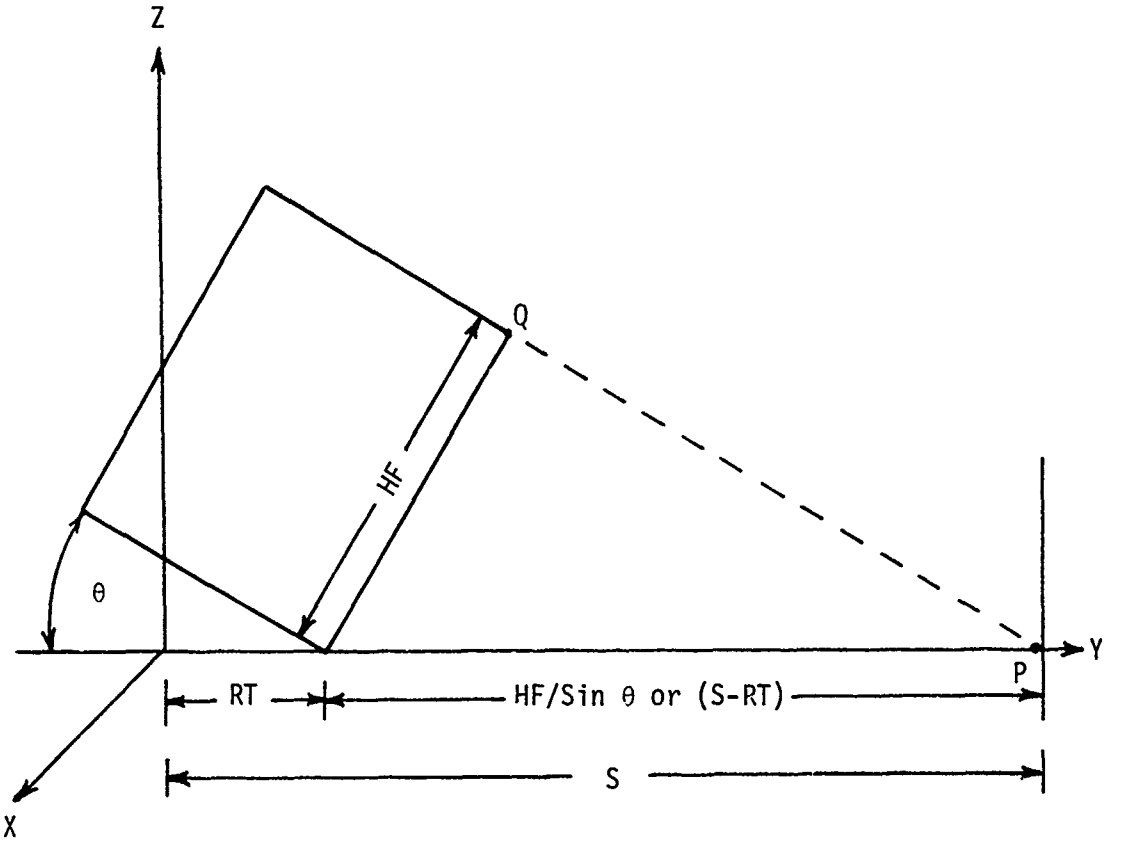


FIGURE 7C-5 Case C.3: (S-RT) is positive; ((S-RT)-HF/Sin θ) = 0.

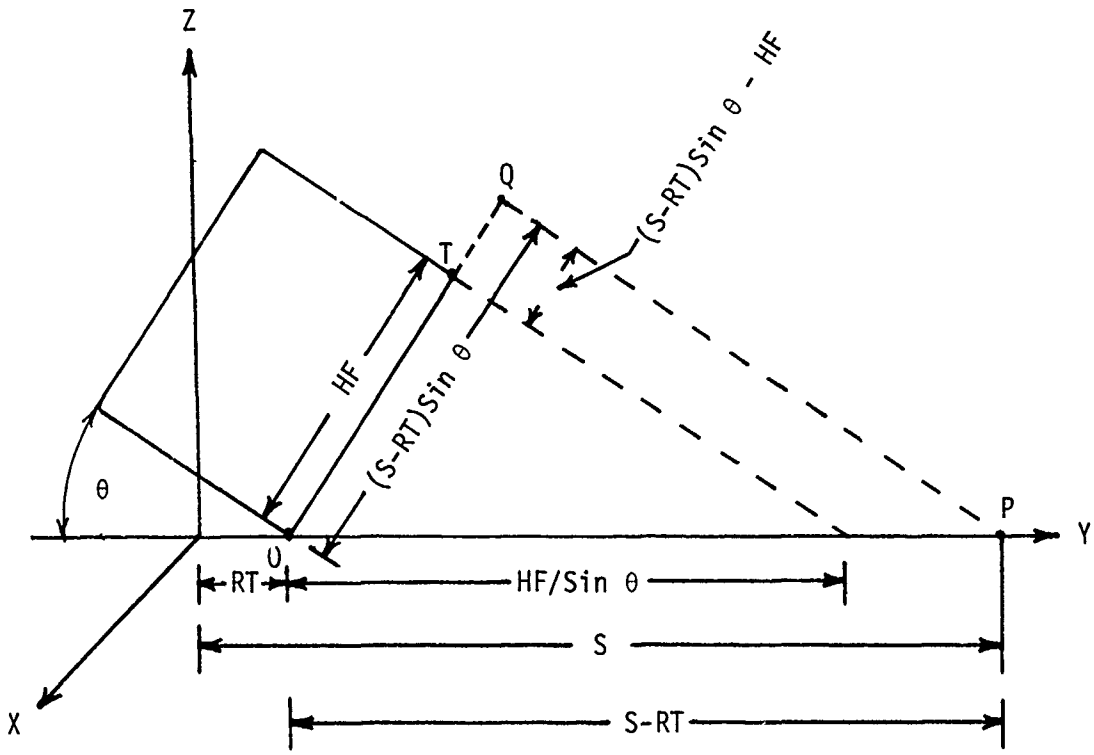


FIGURE 7C-6 Case C.3: (S-RT) is positive; ((S-RT)-HF/Sin θ) > 0.

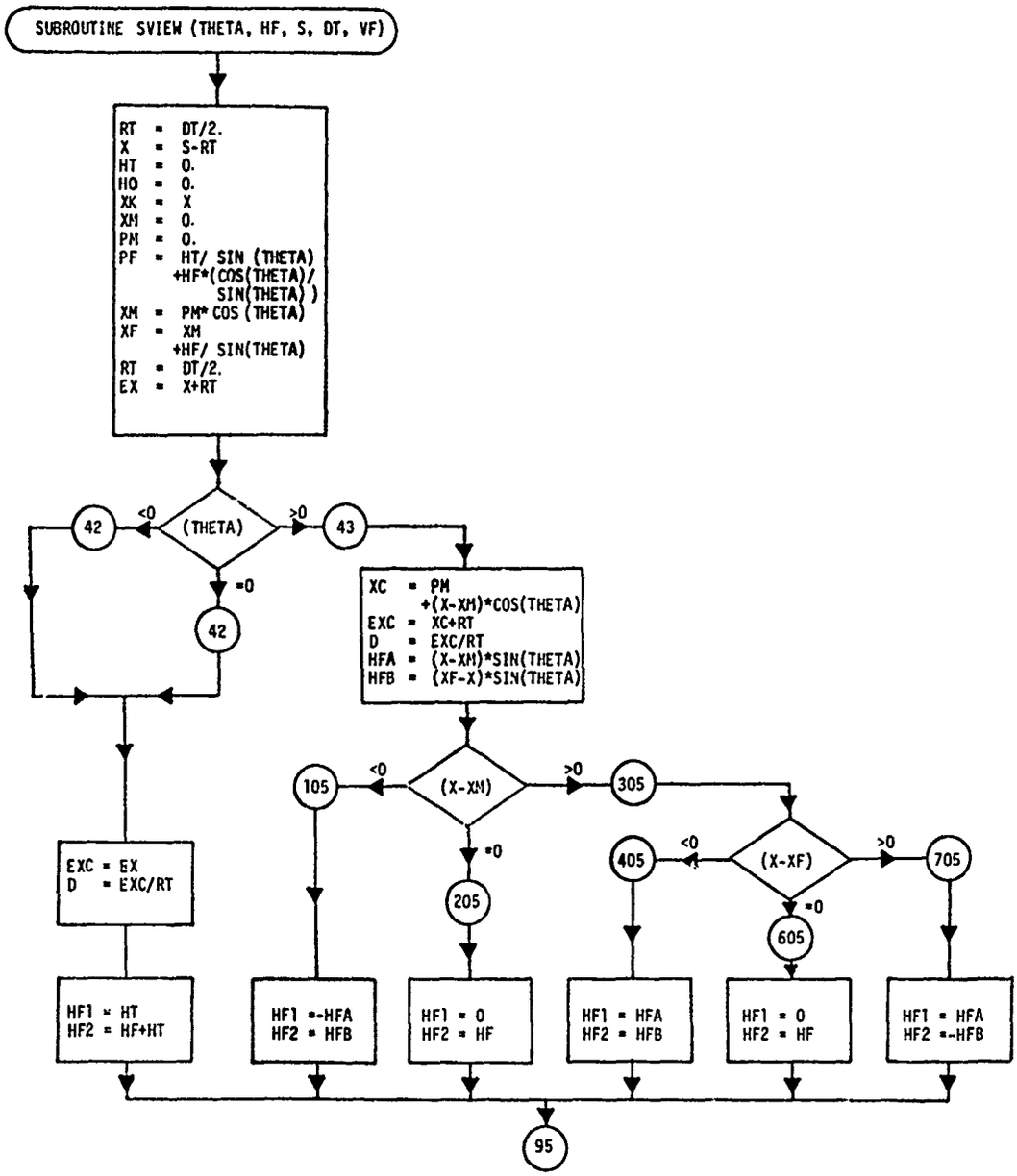


FIGURE 7C-7 Flow Chart for Subroutine SVIEW.

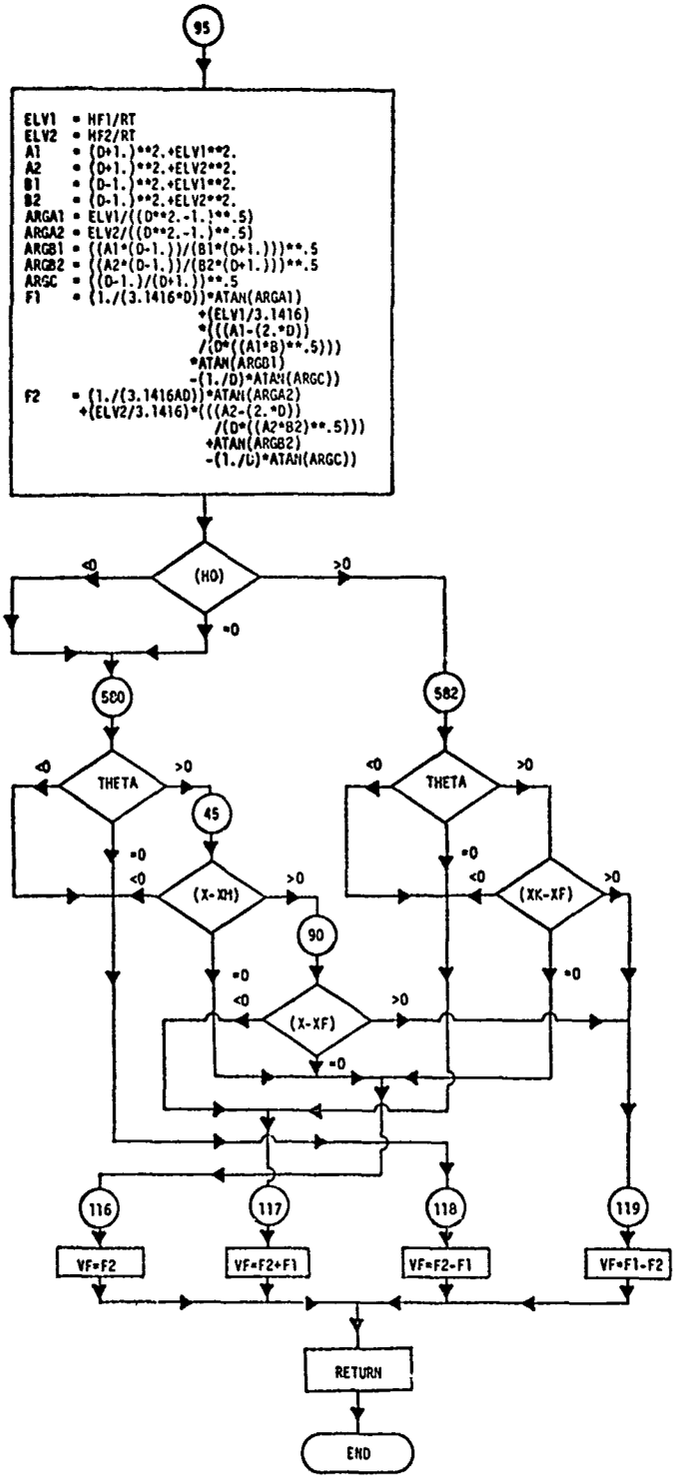


Figure 7C-7 Continued.

```
FORTRAN IV G1 RELEASE 2.0            SVEIW            DATE = 75083        15/46/29          PAGE 0001

0001                  SUBROUTINE SVEIW(THETA,HF,S,DT,VF)                                    0005
                C     THIS SUBROUTINE IS USED BY THE RADIATION FLUX SUBROUTINE.             0006
                C     NO SPECIAL INPUTS ARE REQUIRED BEYOND THOSE LISTED IN SUBROUTINE J    0007
0002                  RT=DT/2.                                                              0008
0003                  X=S-RT                                                                0009
0004                  HT=0.0                                                                0010
0005                  HO=0.0                                                                0011
0006                  XK=X                                                                  0012
0007                  XM=0.0                                                                0013
0008                  PM=0.0                                                                0014
0009                  PF = HT/SIN(THETA) + HF*COS(THETA)/SIN(THETA)                         0015
0010                  XM = PM*COS(THETA)                                                    0016
0011                  XP = XM + HF/SIN(THETA)                                               0017
0012                  RT=DT/2.                                                              0018
0013                  EX = X+RT                                                             0019
0014                  IF(THETA) 42,42,43                                                    0020
0015              43  XC = PM + (X-XM)*COS(THETA)                                          0021
0016                  EXC = XC + RT                                                         0022
0017                  D = EXC/RT                                                            0023
0018                  HFA = (X-XM)*SIN(THETA)                                               0024
0019                  HFB = (XP-X)*SIN(THETA)                                               0025
0020                  GO TO 44                                                              0026
0021              42  EXC = EX                                                             0027
0022                  D = EXC/RT                                                            0028
0023                  HF1=HT                                                                0029
0024                  HF2 = HF + HT                                                         0030
0025                  GO TO 95                                                              0031
0026              44  IF (X-XM) 105,205,305                                                0032
0027             105  HF1 = -HFA                                                           0033
0028                  HF2 = HFB                                                             0034
0029                  GO TO 95                                                              0035
0030             205  HF2 = HF                                                             0036
0031                  HF1 = 0.0                                                             0037
0032                  GO TO 95                                                              0038
0033             305  IF (X-XP) 405,605,705                                                0039
0034             405  HF1 = HFA                                                            0040
0035                  HF2 = HFB                                                             0041
0036                  GO TO 95                                                              0042
0037             605  HF2 = HF                                                             0043
0038                  HF1 = 0.0                                                             0044
0039                  GO TO 95                                                              0045
0040             705  HF1 = HFA                                                            0046
0041                  HF2 = -HFB                                                            0047
0042                  GO TO 95                                                              0048
0043              95  ELV1 = HF1/RT                                                        0049
0044                  ELV2 = HF2/RT                                                         0050
0045                  A1 = (D+1.)**2. +ELV1**2.                                             0051
0046                  A2 = (D+1.)**2. +ELV2**2.                                             0052
0047                  B1 = (D-1.)**2. + ELV1**2.                                            0053
0048                  B2 = (D-1.)**2. + ELV2**2.                                            0054
0049                  ARGA1 = ELV1/((D**2.-1.)**.5)                                         0055
0050                  ARGA2 = ELV2/((D**2.-1.)**.5)                                         0056
0051                  ARGB1 = ((A1*(D-1.))/(B1*(D+1.)))**.5                                 0057
0052                  ARGB2 = ((A2*(D-1.))/(B2*(D+1.)))**.5                                 0058
0053                  ARGC = ((D-1.)/(D+1.))**.5                                            0059
0054                  F1 = (1./(3.1416*D))*ATAN(ARGA1) + (ELV1/3.1416)*(((A1-(2.*D))/       0060
                     1(D*((A1*B1)**.5)))*ATAN(ARGB1) - (1./D)*ATAN(ARGC))                   0061
0055                  F2 = (1./(3.1416*D))*ATAN(ARGA2) + (ELV2/3.1416)*(((A2-(2.*D))/       0062
```

Figure 7C-8 Subroutine SVIEW.

```
FORTRAN IV G1  RELEASE 2.0          SVEIN          DATE = 75083        15/46/29          PAGE 0002

                    1(D*((A2*B2)**.5)))*ATAN(ARGB2) - (1./D)*ATAN(ARGC))                  4463
0056                IF (RO) 580,580,582                                                   4464
0057           580  IF(THETA) 118,118,45                                                  4465
0058           582  IF (THETA) 117,117,581                                                4466
0059           581  IF (XK - XP) 117,116,119                                              4467
0060            45  IF (X-XM) 118,116,90                                                  4468
0061            90  IF (X-XP) 117,116,119                                                 4469
0062           116  VP = P2                                                               4470
0063                GO TO 96                                                              4471
0064           117  VP = P2 + P1                                                          4472
0065                GO TO 96                                                              4473
0066           118  VP = P2-P1                                                            4474
0067                GO TO 96                                                              4475
0068           119  VP = P1 - P2                                                          4476
0069            96  RETURN                                                                4477
0070                END                                                                   4478
```

Figure 7C-8 Continued.

APPENDIX 7D

TYPOGRAPHICAL ERRORS IN
CHAPTER 13 OF ASSESSMENT MODELS (AMSHAH)

Typographical errors in Chapter 13 of AMSHAH are listed below:

1. Figure 13.1, page 192 of AMSHAH, the coordinates of point Q should be (O,V,W) instead of (O,U,W). The same error is repeated in Figure 13.2 on page 195.

2. Capital X as well as lower case x have been used to indicate cross product of vectors on page 194.

3. The sixth line on page 194 has $r_{PQ}Xr_{Q}$. It should be $\vec{r}_{PQ}X\vec{r}_{Q}$.

4. The first line on page 197 states "point Q is beyond the top of the cylinder (i.e. point T), i.e. $W > (H+R\tan\alpha)\cos\alpha$." Because of the inequality contained in $W \geq (H+R\tan\alpha)\cos\alpha$, this should be rewritten as "point Q is at or beyond the top of the cylinder...." Similarly the third line on this page should be "Q is at or below the bottom of cylinder...."

5. On page 197, section on view factor calculation case a, it is stated $W \geq (H\cos\alpha+R\tan\alpha)$. It should be $W \geq (H\cos\alpha+ R\sin\alpha)$. The equality sign is introduced so that this equation is consistent with the first line on page 197 and, in addition, $\tan\alpha$ needs to be replaced by $\sin\alpha$, and $H_2 = H_1-H$ and not $H_2= H-H_1$.

6. On page 222, the equation (3) is

$$F_{ABEF} = \sum_{l,m,n} \ell\ \phi \quad (-----)$$

$$= \Sigma\ \ell\{\int_{AB}(---)+\int_{BE}(---)+\int_{EA}(---)+\int_{FA}(---)\}$$

The R.H.S. of this equation should be

$$= \Sigma\ell\{\int_{AB}(--)+\int_{BE}(--)+\int_{EF}(---)+\int_{FA}(---)\}$$

In addition to the typographical errors, the following anamolies exist.

AMSHAH Chapter 13

1. On page 197, line 13, "the observation plane is S away from the axis of the cylinder." Actually S is the distance between the

PRECEDING PAGE BLANK-NOT FILMED

observation plane and the center of the base of the cylinder when the cylinder is vertical.

2. The flowchart given in Figure 13.5, on page 216, does not correspond to the subroutine SVIEW.

Handwritten Appendix to Chapter 13

1. In this Appendix several relations are derived for the evaluation of view factor for different contours. On page A4, one of the integrals is

$$\int_{\text{line QS}} \frac{(z_2-z_1)\,dx_2}{\rho^2} \to 0$$

It should be

$$\int_{\text{line RS}} \frac{(z_2-z_1)\,dx_2}{\rho^2} \to 0$$

2. On page A5, the integral

$$A \int_0^{\nu_1} \frac{d\nu_1}{A-\cos\nu} \quad \text{is evaluated to be}$$

$$\frac{A}{\sqrt{A^2-1}} \left[\left\{ \tan^{-1}\frac{(A+1)\tan^{-1}\frac{\nu}{2}}{\sqrt{A^2-1}} \right\} \Bigg|_0^{\nu} \right]$$

but should be

$$\frac{2A}{\sqrt{A^2-1}} \left[\left\{ \tan^{-1}\frac{(A+1)\tan\frac{\nu}{2}}{\sqrt{A^2-1}} \right\} \Bigg|_0^{\nu_1} \right]$$

On the same page

$$\frac{h}{s} \left[-\nu_1 + A \int_0^{\nu_1} \frac{d\nu}{A-\cos\nu} \right]$$

$$= \frac{h}{s} \left[-\nu_1 + \frac{A}{\sqrt{A^2-1}} \left\{ \tan^{-1}\frac{(A+1)\tan^{-1}\frac{\nu}{2}}{\sqrt{A^2-1}} \right\} \Bigg|_0^{\nu_1} \right]$$

the factor multiplying $\tan^{-1}$ (---) should be

$$\frac{2A}{\sqrt{A^2-1}} \quad \text{and not} \quad \frac{A}{\sqrt{A^2-1}} .$$

However, the expression is correct in the next line.

$$= \frac{h}{s} \left[-\nu_1 + \frac{2A}{\sqrt{A^2-1}} \tan^{-1} \left(\sqrt{\frac{A+1}{A-1}} \tan^{-1} \frac{\nu_1}{2} \right) \right]$$

The substitution is made

$$\nu_1 = \text{Cos}^{-1} \left(\frac{1}{S}\right) = \tan^{-1} \sqrt{S^2-1}$$

$$\therefore \tan \nu_1 = \frac{2 \tan^1(\nu_1/2)}{1-\tan^2(\nu_1/2)} \qquad \therefore (\nu_1/2) = \sqrt{\frac{S-1}{S+1}}$$

Instead of substituting for $\tan^{-1}(\nu_1/2)$, the expression derived above for $\tan (\nu_1/2)$ is substituted, and hence this mistake is also not propogated.

3. On page A5, the substitution $\nu = \Phi - \pi/2$ and $\nu_1 = \pi/2 - \alpha$ is made, while on page A7 another substitution $-\nu = \pi/2 - \Phi$ and $-\nu_1 = \pi/2 - \alpha$ is made. The later is inconsistent with the former substitution. No error is propogated, but it is better to be consistent.

CHAPTER 7 - LIST OF SYMBOLS

A_1, A_2 = areas of receptor and radiator, respectively (cm^2)

$F_{dA_1 \to A_2}$ = view factor of radiating surface A_2 to infinitesimal receptor dA_1

L = axial length of the circular cylindrical flame envelope (cm,m,or ft)

M = distance of receptor from top surface of inclined right circular cylindrical flame envelope (cm)

n, n_1, n_2 = ratios of lengths, refer to Figure 7B-2

R = radius of cylindrical flame envelope (cm)

r = distance between the receptor and radiator (cm)

X = distance of the receptor from the nearest edge of the base of the cylindrical flame envelope (cm)

X_1 = distance of the receptor from the base of the flame, beyond which the top surface of the right circular cylindrical flame envelope starts contributing to the view factor from the flame to the receptor (cm)

α, β, γ = angles, refer to Figure 7B-2 (degrees)

θ = angle of inclination of the cylindrical flame envelope axis to the vertical (degrees)

θ_1, θ_2 = angle between the line joining infinitesmal areas on the receptor and radiator, and the normal to the receptor; and the normal to the radiator, respectively (degrees)

CHAPTER 7 - REFERENCES

[1] Department of Transportation, U.S. Coast Guard, Assessment Models in Support of the Hazard Assessment Handbook (CG-446-3), (AMSHAH), CG-D-65-74, January 1974.

[2] Arthur D. Little, Inc., Hazard Assessment Computer System, User Manual (HACS), Cambridge, Mass., December 1974.

[3] Rein, R. G., C. M. Sliepcevich, and J. R. Welker, "Radiation view factors for tilted cylinders," J. Fire Flammability 1:140-153, 1970.

[4] Blackshear, P. L. (ed.), Heat Transfer in Fires, John Wiley and Sons, New York, 1974.

GPO 912-420